CZECH TECHNICAL UNIVERSITY IN PRAGUE

Faculty of Civil Engineering
Department of Steel and Timber Structures

The impact of corrosion on the fatigue life of steel bridges

Vliv koroze na únavovou životnost ocelových mostů

DOCTORAL THESIS

Ing. Martin Macho

Doctoral study programme: Civil Engineering

Branch of study: Structural and Transportation Engineering

Doctoral thesis tutor: prof. Ing. Pavel Ryjáček, Ph.D.
M.Sc. José Campos e Matos, Ph.D.

Prague, 2022

DECLARATION

Ph.D. student's name: Ing. Martin Macho

Title of the doctoral thesis: The impact of corrosion on the fatigue life of steel bridges

I hereby declare that this doctoral thesis is my own work and effort written under the guidance of the tutor prof. Ing. Pavel Ryjáček, Ph.D. and tutor specialist M.Sc. José Campos e Matos, Ph.D.
All sources and other materials used have been quoted in the list of references.

The doctoral thesis was written in connection with research on the project:
LD-COST CZ (č. 15127) "Pokročilé metody posuzování degradovaných ocelových konstrukcí"
SGS15/141/OHK1/2T/11 "Vliv degradace na únosnost a životnost ocelových mostů"
SGS17/126/OHK1/2T/11 " Změny v únavovém chování korozí oslabených ocelových mostních konstrukcí"
DG18P02OVV033 "Metody pro zajištění udržitelnosti ocelových mostních konstrukcí industriálního kulturního dědictví"

In Prague on   31.7.2022   _____
                                                                    signature

Abstract

Decades-old steel bridges have to endure an unfavourable environment that causes the ageing and deterioration of material properties. Moreover, railway bridges in particular are exposed to a large number of stress ranges that may lead to fatigue damage. The combination of both phenomena has a significant impact on the condition of bridges and their remaining service life. However, there is no relevant background information that can be used in assessment of this phenomenon. There are almost no recommendations for civil engineers how to take into account the corrosion weakening for the assessment of bearing capacity and fatigue strength of riveted members. For this reason, the subject of the doctoral thesis was to analyse and describe the relation between corrosion and fatigue. The research was based on experimental fatigue tests performed on corrosion-weakened specimens taken from a bridge structure more than 120 years old. The relationships between various parameters characterizing the corroded surface of the specimens and the fatigue life were investigated.

Subsequently, a methodology was developed to predict the remaining service life of existing steel riveted bridges considering the effects of fatigue and corrosion. The derived relationships were implemented in the methodology. In the next phase, using MATLAB® software, an analytical software tool (called FALCom) for the prediction of the remaining fatigue life has been developed. The results of experimental research were integrated into this tool. Various scenarios regarding the future maintenance of bridges were included in the program, thus making it possible to calculate the remaining service life of bridges, including corresponding costs. The application of the developed methodology and the use of the program is shown in the doctoral thesis through a case study aimed at the assessment of the residual life of a railway bridge.

Key words: fatigue, corrosion, steel bridges, stress spectrum, bridge maintenance.

Abstrakt

Ocelové mosty staré desítky let musí odolávat nepříznivému prostředí, které způsobuje stárnutí a zhoršování vlastností materiálu. Zejména železniční mosty jsou navíc vystaveny velkému namáhání od dopravy, které může vést k únavovému poškození. Kombinace obou jevů má významný vliv na stav mostů a jejich zbývající životnost. Neexistují však žádné relevantní podklady, které by bylo možné využít při posuzování tohoto jevu. Neexistují téměř žádná doporučení pro stavební inženýry, jak zohlednit korozní oslabení při posuzování únosnosti a únavové pevnosti nýtovaných prvků. Z tohoto důvodu bylo předmětem disertační práce analyzovat a popsat vztahy mezi korozí a únavou. Výzkum byl založen na experimentálních únavových zkouškách provedených na korozně oslabených vzorcích odebraných z mostní konstrukce staré více než 120 let. Byly zkoumány vztahy mezi různými parametry charakterizujícími zkorodovaný povrch vzorků a únavovou životností.

Následně byla vypracována metodika pro predikci zbytkové životnosti stávajících ocelových nýtovaných mostů s ohledem na únavové a korozní účinky. Odvozené vztahy byly implementovány do metodiky. V další fázi byl s využitím softwaru MATLAB® vyvinut analytický softwarový nástroj (nazvaný FALCom) pro predikci zbývající únavové životnosti. Do tohoto nástroje byly integrovány výsledky experimentálního výzkumu. Do programu byly dále zahrnuty různé scénáře týkající se budoucí údržby mostů, což umožňuje vypočítat zbývající životnost mostů včetně odpovídajících nákladů. Aplikace vyvinuté metodiky a využití softwarového nástroje je v disertační práci ukázáno na případové studii zaměřené na posouzení zbytkové životnosti ocelového železničního mostu.

Klíčová slova: únava, koroze, ocelové mosty, spektrum napětí, údržba mostů.

Acknowledgement

I would like to warmly thank my supervisor Prof. Pavel Ryjaček, Ph.D. for his professional guidance and supervision during my research and doctoral thesis writing as well as throughout my doctoral studies. I greatly appreciate his advice, suggestions and recommendations, which were based on his vast knowledge and experience.

Many thanks also to my supervisor specialist M.Sc. Jose Campos e Matos, Ph.D. for his valuable advice during the writing of my doctoral thesis and for his expert guidance during my study stay at University of Minho in Portugal.

Thanks also go to the members of the Department of Steel and Timber Structures for the valuable advice and suggestions received during the seminars of the PhD students. In particular, I thank to Assoc. Prof. Tomáš Rotter, Ph.D. for valuable advice and consultation during the study.

I would also like to thank the members of the Experimental Centre of the Faculty of Civil Engineering of CTU for the opportunity to carry out experimental tests in dynamic testing laboratory and for their help in arranging the experiments.

I would like to thank the Railway Administration of the Czech Republic for providing the material from the railway bridge in Holubov for the production of test samples.

Last but not least, I would like to thank my family for their support and especially my girlfriend Šárka, who was a great support and motivation during the writing of my doctoral thesis.

Poděkování

Velmi moc děkuji svému školiteli prof. Ing. Pavlovi Ryjáčkovi, Ph.D. za odborné vedení a dohled při mém výzkumu a psaní disertační práce i během celého doktorského studia. Velice si cením jeho rad, námětů a doporučení, které vycházeli z jeho obrovských znalostí a zkušeností.

Děkuji moc také svému školiteli specialistovi M.Sc. Josemu Camposovi e Matosovi, Ph.D. za cenné rady při psaní disertační práce a za odborné vedení během mého studijního pobytu na Universidade do Minho v Portugalsku.

Poděkování také patří členům katedry ocelových a dřevěných konstrukcí za cenné rady a náměty obdržené při seminářích doktorandů. Zejména děkuji doc. Ing. Tomáši Rotterovi, CSc. za cenné rady a konzultace během mého studia.

Také děkuji členům Experimentálního centra fakulty stavební ČVUT za možnost provést experimentální zkoušky v prostorách dynamické zkušebny a za pomoc s uspořádáním experimentů.

Za poskytnutí materiálu z železničního mostu v Holubově pro výrobu zkušebních vzorků děkuji Správě železnic České republiky.

V neposlední řadě moc děkuji za podporu svým rodičům a zejména své přítelkyni Šárce, která pro mě byla při psaní disertační práce velikou oporou a motivací.

Content

1. Motivation

The combined effects of corrosion and fatigue have become a topic issue in recent times. In particular, steel bridges are exposed to adverse weather conditions that initiate their subsequent degradation and corrosion, while the effects of rail traffic in particular can result in fatigue damage to cyclically stressed details. Decades-old steel bridges that are still in service need to be reassessed. However, there is no relevant background information that can be used to assess the above-mentioned phenomena to which these bridges are exposed. There are only few recommendations for structural engineers on how to take corrosion weakening into account when assessing the bearing capacity and fatigue strength of riveted elements.

Fatigue Load Effects

The service life of many steel bridges in the Czech Republic, and in many other countries, is close to their expected lifetime and therefore assessment of the current state of such bridges needs to be carried out. In particular, railway bridges, which are known for their permanent resistance to heavy movable loads, are exposed to large stress ranges that may lead to fatigue damage (see Fig. 1). However, diagnostic methods for existing riveted bridges are limited. Several documents containing background to the assessment of fatigue life of riveted bridges are available. Assessment procedures and detail categories for riveted connections of steel bridges are stated in the International Union of Railways publication IRS 77802 [35]. This document considers three groups of significant fatigue-sensitive details of riveted connections. Fatigue strengths of the most common riveted construction details are also available in [58].
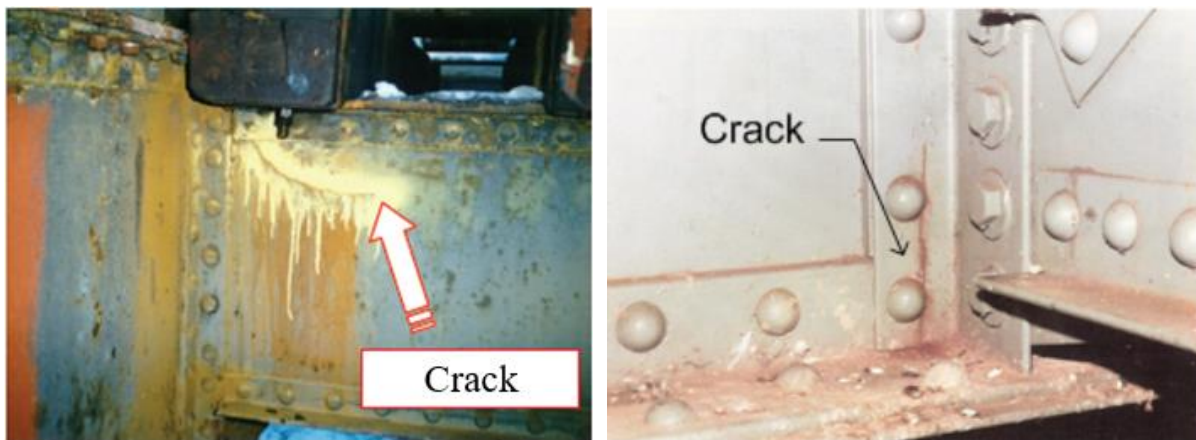
Fig. 1 Examples of fatigue cracks on riveted steel bridges - Left: Fatigue crack in the riveted connection of stringer to crossbeam [62], Right: Fatigue crack in the riveted connection of cross-bracing element [63]

Corrosion Effects

The corrosion process of steel is affected by many factors, such as the kind of steel and surface protection; environmental impact; and the presence of pollutants, cracks and stresses. The loss of material may result in a reduction in the cross-sectional area and thereby increase the stress level for a given load or increase the stress range for cycling loads. In addition, it can lead to a reduction in the buckling resistance of elements or the initiation of fractures. In general, the loss of cross-sectional area results in a decrease in geometric parameters such as the moment of inertia and radius of inertia. For the assessment of existing steel members, the loss of material may be taken into account using corrosion models. Corrosion models depict the dependence of corrosion loss on time. Many types of models have been developed [48]. Individual types of corrosion models differ according to the various mathematical

functions that describe the development of corrosion loss over time, the various corrosive environments that are considered (rural, urban, etc.) and the various types of steel material.

Combination of Fatigue and Corrosion Damage

At present, there are not enough methods available for assessing steel bridge structures affected by degradation and corrosion. The methods used for the assessment of bearing capacity are based on the methods used to assess new constructions. Consideration of corrosion is not sufficiently defined in structural analysis, for either static or fatigue capacity. To solve this problem, only a small amount of background is available to structural engineers. For example, the approach set out in IRS 77802 [35] is based on the application of a partial safety factor, the value of which depends on the state of the components in terms of corrosion. The consideration of degradation for assessing bridges is also stated in Standards Council of Canada code CAN/CSAS6- 06 [60]. Chapter 14 of this bridge design code, together with [60], recommends how to take into account the effects of corrosion on fatigue resistance, using a pitting factor K_p, whereby the pitting factor is analogous to notch factor.

If an existing structure needs to be assessed for load capacity, an inspection of the structure is always carried out, focusing on defects and failures, and a corrosion survey of the structure is also carried out. During the corrosion survey, the cross-sections of all structural elements are carefully measured and the corrosion weakening value is determined. This corrosion weakening is taken into account in the load-bearing capacity assessment by reducing the cross-sectional area of the weakened elements and the associated cross-sectional characteristics. The weakened cross-sections are also fed into the numerical models to take into account their stresses (depending on the static certainty of the structure and the possible redistribution of internal forces between the elements). By reducing the cross-sectional area, we are therefore able to take into account the increase in stress in the element, the greater susceptibility to buckling of the element and to buckling of parts of the cross-sections. However, we are not yet able to account satisfactorily for the possible effect of corrosion on the fatigue strength. Therefore, it is important to understand whether and what effect corrosion weakening, whatever the extent, has on the fatigue behaviour and fatigue life of steel structural members. If we know the relationship between the level of corrosion weakening and fatigue strength, then we can safely and effectively assess existing bridge structures in terms of fatigue life.

A study of available literature shows that the effects of corrosion loss on the behaviour of steel structural elements have been the subject of many research projects. The studies were in most cases focused on the behaviour of individual steel sheets.

Many studies conducted in the past was based on the accelerated corrosion method to achieve the desired corrosion. However, the effects of real corrosion and "artificially" created corrosion may not be identical. For this reason, it is important to focus more on research in the field of real structures and to carry out experiments and measurements directly on real structures and their individual elements. This is the best way to understand the behaviour of structures and to understand their response to different loading patterns under different types of loads.

On the basis of the above, the aim of the doctoral thesis is to analyse and describe the relation between corrosion and fatigue. To determine the relationship between corrosion loss and fatigue life, experimental fatigue tests will be performed on elements taken from a real bridge structure weakened by corrosion. Parameters, influencing corrosion and fatigue will be analysed. Subsequently, a methodology will be developed to account for both fatigue and corrosion phenomenon. The methodology will be usable for the fatigue assessment of existing steel riveted bridge structures affected by corrosion. Moreover, various scenarios related to maintenance will be taken into account for the remaining service life calculation.

2. State of the art

The chapter gives an overview of the practical and theoretical knowledge of the above-mentioned issues. A summary of knowledge resulting from the previously conducted experiments, measurements, numerical analysis, or analytical calculations has been made. The recapitulation of the main findings from the research and the available literature is divided into several basic parts.

The key part is Chapter 2.2 which describes the effects of corrosion on the properties and behaviour of steel structural elements. The first part of this chapter focuses in detail on the effects of corrosion on the load-bearing capacity of steel elements (see Chapter 2.2.1). The second part gives an overview of the effects of corrosion on the fatigue behaviour of steel structural elements (see Chapter 2.2.2). Section three analyses the findings of the behaviour of corroded weakened riveted joints (see Chapter 2.2.3). Chapter 2.3 briefly summarizes the approaches of current codes and standards how to take into account the effect of corrosion weakening of structural elements.

2.1. Corrosion as a degradation process of steel structures

Material corrosion can be understood as the spontaneous deterioration of materials. Corrosion is caused by the interaction between the material and the environment. It is manifested by: changes in material structure, appearance, strength, weight and dimensional loss. All this affects the operational reliability and safety of structures.

Corrosion damage is a comprehensive group of failures caused by the environment, especially on the surface of metals. Depending on the extent of the damage, we distinguish between general (surface) corrosion, which occurs more or less uniformly over the entire surface exposed to the corrosive environment, and non-uniform - local (localised) corrosion, which is significantly more intense only in some parts of the exposed metal surface, while the corrosion is acceptable on the rest of the surface. The classification of the types of corrosion has different aspects [1], [2]:

A) Corrosion by mechanism of corrosion:
- Uniform corrosion
- Non-uniform corrosion
  - o Pitting corrosion
  - o Point corrosion
  - o Crevice corrosion
  - o Intergranular corrosion
  - o Selective corrosion
  - o Stress Corrosion cracking
  - o Corrosion fatigue
  - o Erosion corrosion

B) Corrosion according to the type of corrosion processes:
- Chemical corrosion
- Electrochemical corrosion
- Other types of corrosion

C) Corrosion according to reaction environment:
- Corrosion in electrically non-conductive media - liquid, gaseous
- Corrosion in electrically conductive media - electrolyte solutions and melts, ionised gases
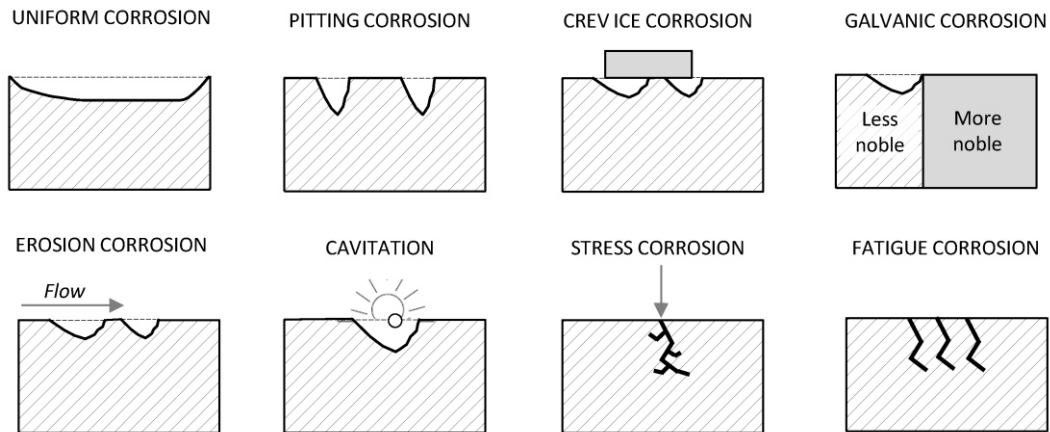
Fig. 2 Types of corrosion according to the corrosion mechanism [1]

We will look in more detail at the types of corrosion according to the mechanism of corrosion:

1. Surface (uniform) corrosion

Surface corrosion occurs at approximately the same rate over the entire metal surface. Uniform surface corrosion occurs especially when the entire metal surface is in a passive state - uniform material loss over the entire surface. In the case of uniform corrosion, the rate of material loss can be relatively easily determined and taken into account. This is the type of corrosion that is most common in atmospheric conditions.

2. Non-uniform corrosion

In the case of non-uniform corrosion, only a certain part of the surface or even the interior of the material is attacked. Non-uniform attack is caused by heterogeneity in the properties of the metals, the environment or composition of corrosion products in different parts of the surface. This is a dangerous type of corrosion because it may not be visible. Types of non-uniform corrosion:

   2.1 Pitting corrosion

If the non-uniform attack on the surface of the metal or alloy is manifested by a relatively small depth-to-width ratio and this ratio is maintained during further corrosion, it is pitting or pitting corrosion. Pitting corrosion is manifested by larger or smaller pits on the surface of the material. It is most common in passivated materials at the points where the passivation layer is broken. The ratio of the depth to the width of the affected area is small.

   2.2 Point corrosion

Pitting corrosion is a localised corrosion process in which deep pits are formed on the metal surface and the surrounding surface remains free from observable attack. This type of attack occurs on a wide range of passivable metals, and is typical not only of stainless steels and aluminium, but also of iron and copper.
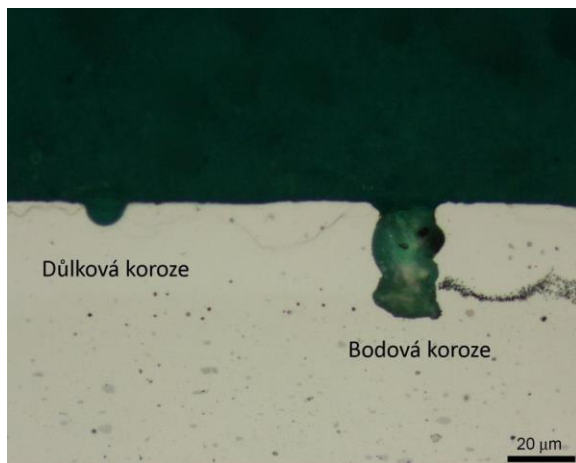
4

Fig. 3 Comparison of pitting and point corrosion [2]   Fig. 4 Appearance of crevice corrosion

2.3 Crevice corrosion

In narrow crevices or gaps between a metal surface and another surface (metallic or non-metallic), localised corrosion often occurs. Usually, one dimension of the gap mouth is very small. This situation occurs in the case of structural crevices, in threaded joints, in weld pores, in flanged and riveted joints, under sealing surfaces at joints, or under coatings that have lost adhesion to the metal. The crevice effect is also manifested in cracks and other non-solids (pores, folds) of the metal that leak at the surface. This effect accompanies many other types of corrosion such as corrosion cracking, corrosion fatigue, intergranular and pitting corrosion.

2.4 Intercrystalline corrosion

Intercrystalline corrosion is the most important example of the effect of structural changes in a metal on its corrosion resistance. The cause of intercrystalline corrosion is the structural and chemical inhomogeneity of the metal at grain boundaries, which is most common in stainless steels and occurs mainly during welding. In the vicinity of welds, chromium-depleted areas occur at grain boundaries due to the formation of chromium-rich carbides. Metal material that corrodes intercrystalline loses mechanical strength without any observable change in appearance. This is due to the fact that under certain conditions it preferentially corrodes only in a narrow zone at the depleted grain boundary.

2.5 Selective corrosion

In selective corrosion, corrosion processes remove one component of the alloy. A typical representative of this type of corrosion is the dezincification of brass, where part of the original copper-zinc alloy material is converted into spongy copper. This occurs either throughout the layer near the surface or locally. The spongy copper has no strength and gradually perforates the wall. Zinc plating also plays a role in the corrosion cracking of brasses.

Another example of selective corrosion is spongiosis (graphitization) of gray cast iron with flake graphite. Spongiosis of grey cast iron occurs in waters and in soil under a massive layer of rust. The flake graphite is continuous in the structure of grey cast iron and forms a very noble phase against iron, which in some conditions leads to galvanic cell activity and selective corrosion of the iron matrix. The original cast iron becomes a non-metallic material in which the iron is completely converted to corrosion products and has practically no strength.

2.6 Corrosion cracking

Corrosion cracking occurs when static tensile stresses are applied to a metallic material exposed in a specific environment (at specific temperatures and concentrations). Cracks propagate in the metal structure either along grain boundaries - intercrystalline or across grains - transcrystalline. The corrosion cracking mechanism of many metallic materials is explained by active dissolution at the crack front, which also acts as a stress concentrator. External mechanical stresses are not always necessary for corrosion cracking to occur, but only internal stresses are sufficient, e.g. after cold forming or at welded joints. The more homogeneous the material, the less susceptible it is (pure metals are the most resistant). Materials with high tensile strength are more susceptible. Cracks grow mainly in the direction perpendicular to the tensile stress. Intercrystalline attack is more common than transcrystalline. Transcrystalline corrosion is common for stainless steel or special steels, not for old steels.
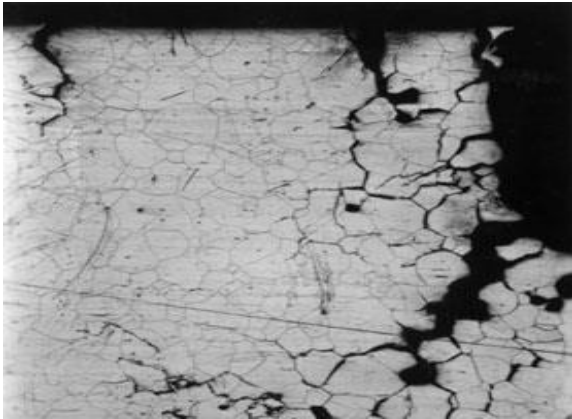
Fig. 5 Intercrystalline corrosion cracking [2]
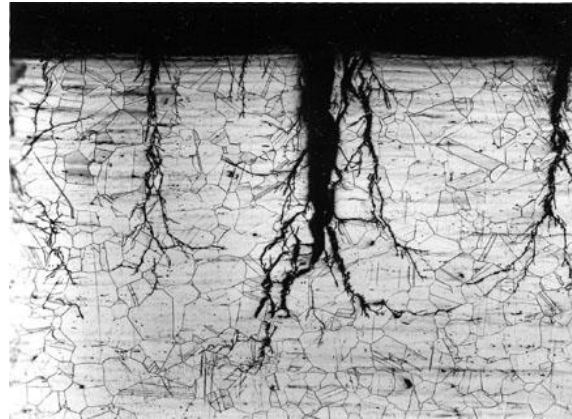
Fig. 6 Transcrystalline corrosion cracking [2]
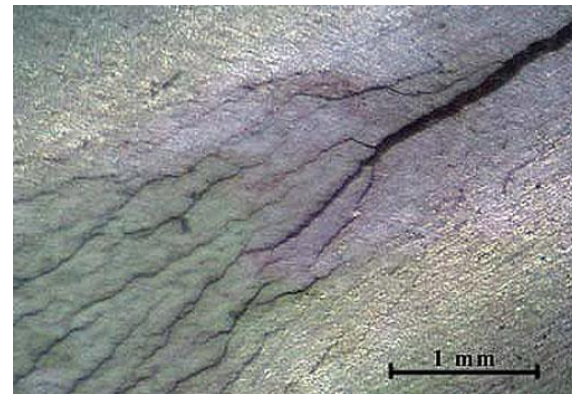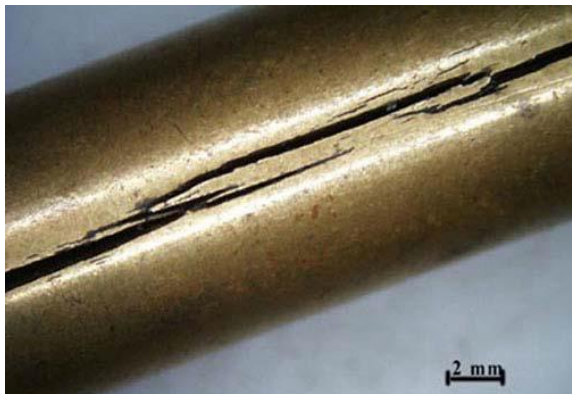
Fig. 7 Corrosion cracking of brass due to internal stress [2]

2.7 Corrosion fatigue

Corrosion fatigue is a type of attack that requires the interaction of a corrosive environment and cyclic mechanical stresses with a tensile component.

Under cyclic loading, integrity is compromised by cracking even in the absence of a corrosive environment when the load is above the fatigue limit. Corrosion fatigue is characterised by the absence of a fatigue limit under cyclic loading in an aggressive environment. That is, the largest repeated stress change that a material can theoretically withstand for an infinite number of cycles without failure. A crack in corrosion fatigue is trans-cystal, has a blunt face, and propagates discontinuously (resulting in the formation of shear bands). The frequency of loading has a great influence on the rate of crack

propagation, the lower the frequency, the greater the increase in crack length per cycle. In cracks that close and open rapidly, corrosion attack is not sufficient and the mechanical effect is dominant. Corrosion fatigue failure is often already evident at a relatively low number of load cycles. Similar to corrosion cracking, the crack propagates from areas of surface inhomogeneities (indentations, inclusions, grain boundaries, extrusions, intrusions). The fracture is covered with corrosion products.

2.8 Erosion corrosion

Of the various types of purely mechanical wear (abrasive, adhesive, erosive, cavitation), erosive corrosion is of the greatest importance in combination with the corrosive effects of the environment. Purely mechanical deterioration of the metal material can occur when a fast-flowing liquid or gas is in contact. Damage is further increased if the flowing medium contains particles, solid or liquid in the gas, solid or gas in the liquid (bubbles).

Corrosion of steel on building structures is generally caused by aggressive environments and lack of maintenance. The consequence of corrosion is a reduction in the cross-sectional area of the members and consequently reduced load-bearing capacity and safety of the structure.

Note that this study does not aim to describe in detail the origin and process of corrosion of steel (or metals in general), but focuses on the effects of corrosion loss on the properties and behaviour of steel structural elements.

For example, an analysis of the condition of existing railway bridges in Vietnam by Tuan Hai (2006) [3] shows that for many bridges older than 10 years, the extent of corrosion damage is quite significant. Here, corrosion is one of the most common and critical deficiencies of steel railway bridges along with fatigue damage and functional obsolescence.

The main cause of the above is mainly the unfavourable climate (wide temperature range and high atmospheric humidity), which creates suitable conditions for the occurrence of corrosion on steel elements.

However, the absence of proper surface protection can also be declared a cause of corrosion, as degraded protective coatings are not replaced in time or at all due to lack of funds. Unfortunately, the fact of lack of funds for the necessary maintenance is also a matter for other countries.

2.2. Effects of steel corrosion

In most of the experiments carried out on corrosion effects, corrosion on the elements was induced artificially. This means that the test specimens were not obtained from a real structure that would have been exposed to adverse weathering over many years. Corrosion was thus achieved by an accelerated process whereby the steel elements were exposed to an adverse aggressive environment in laboratory conditions. Corrosion pitting was achieved, for example, by the constant temperature and humidity method with prior immersion in a saturated NaCl solution, or by methods based on a similar principle. This is how, for example, Beaulieu, Legeron and Langlois (2010) [4] or Shan-hua Xu and You-de Wang (2015) [5] proceeded in their scientific work.

One of the documents where the procedure for artificial corrosion is described in detail is ASTM G85 [6] or the technical standard EN ISO 9227 [7], which deals with corrosion tests in artificial atmospheres. This international standard provides a procedure for testing metallic materials in salt spray, which is generally suitable for testing corrosion protection. The standard specifies the type of apparatus, the chemicals and the procedure for testing in neutral sodium chloride solution (NSS), acidified sodium chloride solution (AASS) and acidified sodium chloride and copper chloride solution (CASS) mists to

determine the corrosion resistance of metallic materials, both unprotected and with protective coatings or temporary corrosion protection.

The standard also mentions a method used to determine the corrosion aggressiveness of the test chamber environment, which was used in their study, for example, by Caprili and Salvatore (2014) [8].

The advantage of the method with achieving corrosion in salt spray is obvious. First of all, it is the reduction of the exposure time (between 10 and 90 days) and the possibility to simulate different environmental conditions, i.e. to vary different pH. On the other hand, the disadvantage remains that the result is not a real corroded weakened element obtained from a corroded bridge or other structure.

The second way of corrosion of metals is the natural way. Experiments on samples taken from old corroded steel structures (century-old railway bridges or others) have been carried out, for example, by Appuhamy et al. (2011) [9], Saad-Elden, Garbatov and Guedes Soares (2013) [10], Garbatov et al. (2014) [11] or Rahgozar and Sharifi (2009) [12].

There are many factors that can influence the extent of steel corrosion, and at the same time there is not enough statistical data available to formulate analytical models.

For this reason, corrosion rates are very difficult to predict accurately. It can only be estimated on the basis of approximate empirical formulas.

The behaviour of different types of steel exposed to different types of environments such as urban, rural, industrial and marine was the subject of a study by Albrecht and Naeemi (1984) [13]. The results showed that there is a high variation in corrosion rate. However, this could be due to the small size of the test elements which only approximated the behaviour of the actual structure during the study. Other researchers have also observed a high variation in the rate of corrosion development (Townsend et al (1982) [14]). There is a common agreement that the time dependence of corrosion rate is best represented by an exponential function as reported by Komp (1987) [15]:

$$C = A \cdot t^B \tag{1}$$

where: C is the corrosion loss after t years of exposure of the structure to corrosion,
  A is the corrosion loss after 1 year of exposure,
  B is the regression coefficient numerically equal to the slope of the curve.

The values of the coefficients for carbon steel without surface protection and for weathering steel and 3 different types of environments are shown in Tab. 1. For other types of steel and different environments the values of the coefficients A and B can be found in [13].

Tab. 1 Coefficients for the calculation of corrosion loss over time

Type of steel		Carbon steel		Weathering steel	
	Coefficient	A	B	A	B
Environment	Rural	34.0	0.65	33.3	0.50
	Urban	80.2	0.59	50.7	0.57
	Marine	70.6	0.79	40.2	0.56

Obviously, the values obtained from the above relationship are only indicative. Moreover, this model assumes that corrosion starts as soon as the structure is put into service, and thus does not take into account the application of the anti-corrosion coating.

Other, more complex mathematical relationships also take into account the concentration values of the most significant corrosion agents (SO2, Cl, relative humidity, ...). See for example [13].

The corrosion of steel is affected by several factors, such as the type of steel and the type of surface protection, the influence of the environment, the presence of pollutants, cracks and stresses. Loss of material can result in a reduction in cross-sectional area, and thus can increase the stress level for a given load or increase the stress range for cyclic loading (thus affecting fatigue life). In addition, it can lead to a reduction in the buckling capacity of the members. In general, a reduction in cross section results in a reduction in geometric parameters such as moment of inertia and radius of inertia.

2.2.1. Effects of corrosion on bearing capacity of steel members

Corrosion is one of the most common causes of deterioration of steel bridges, affecting their long-term mechanical properties, serviceability and durability. The lack of information on the load capacity and limiting behaviour of corroded elements makes it difficult for structural engineers to assess their residual capacity.

Corrosion of steel structures occurs when they are exposed to aggressive environments and when they are not adequately maintained. The load capacity of corroded elements is reduced and the result is a reduction in load-bearing capacity of the bridge. As corrosion increases, the level of uncertainty of the input values decreases and thus the level of safety decreases. In practice, if a corroded element is found during an inspection, it is necessary to estimate the residual capacity of such elements in order to decide whether to replace them, repair them or just remove the corrosion and protect the damaged element again.

In order to obtain the relationships between the corrosion weakening of an element and its load capacity, studies were carried out on steel plate, pipe or angle specimens. Ahmad Rahbar-Ranji (2012) [16] studied the ultimate capacity of corroded steel plates with irregular surfaces subjected to plane compression (in-plane plate). He used the nonlinear finite element method to determine the ultimate load capacity. A reduction factor was introduced which gives the ratio of the reduced ultimate capacity of corroded plate with irregular surfaces to the ultimate capacity of corroded plate with uniform thicknesses. A study of the significant parameters found that the reduction in ultimate capacity of the plate due to corrosion is very sensitive to the value of the plate slenderness, but less sensitive to the ratio of the plate side sizes, the degree of steel strengthening and the direction of in-plane loading. As the yield strength increases, the reduction factor increases, and as the plate slenderness increases, the reduction factor of the ultimate capacity increases. The ultimate capacity is reduced by up to 3.5% for rectangular plates and 3% for square plates under transverse compression loading if buckling is the dominant mode of collapse. Although these values are small, it appears that corroded plates with irregular surfaces have a lower ultimate capacity, which may be significant for structural elements. It should be noted, however, that the results obtained using the finite element method have not been experimentally verified and thus it cannot be said with certainty whether the actual behaviour of such corroded elements is close to the expected behaviour.

Research on the load carrying capacity of corroded steel plates has also been carried out by Appuhamy et al. (2011) [9]. His work is based on experimental tensile tests on specimens of larger widths (70-180 mm), which makes it a much more accurate reflection of the actual effects of corrosion. Indeed, under real corrosion conditions, severe corrosion damage with extremely large corrosion pits even 30 mm in diameter are observed on old steel bridges. The test specimens were taken from a steel girder of a railway bridge. Based on the thickness measurements of the corroded specimens, 3 corrosion types were defined: (i) overall corrosion, (ii) pitting corrosion and (iii) local corrosion. According to the test results, the estimation of the residual tensile capacity of the degraded plate can be determined with high accuracy based on the representative effective thickness, which is defined as:

$$t_{eff} = t_0 - 3.3 \cdot \sigma_{st} \hspace{4cm} (2)$$

where: t_0 is the initial thickness of the plate,

σ_{st} is the standard deviation of the thickness of the weakened plate, determined from a set of measured average thickness values.

Nakai, Matsushita, and Yamamoto (2006) [17] developed a series of analyses of the effect of pitting corrosion on the bearing capacity of steel plates using the finite element method. The subject of their study was to investigate the effect of rotating cone-shaped corrosion pits, which are frequently observed on structures. For plates subjected to a combination of compressive force and bending moment in the plane of the member, it is necessary to distinguish whether the loss of material due to corrosion is uniform or whether pitting corrosion is present. For plates with corrosion pits the value of the ultimate load is less than for uniformly corroded plates, taking into account the average loss in thickness of the plate. On the other hand, in terms of the average thickness loss at the minimum cross-section, the ultimate load in compression and bending moment for corroded plates is greater than for uniformly corroded plates. The ultimate tensile strength decreases due to pitting corrosion more than the compressive and flexural strength. Thus, the key fact is that tensile capacity is reduced the most as a result of corrosion pitting of conical shape.

Steel pipes are a common structural element. In the case of internal corrosion, varying degrees of degradation of the inner wall of the element can be expected depending on the type and aggressiveness of the material being transported. If we assume the presence of internal pressure and axial force and the mode of failure by full plasticization, then the flexural capacity of corroded steel pipes with random corrosion shape can be determined by a set of generalized solutions according to Yanfei Chen et al. (2010) [18]. However, for practical use, one can proceed to simplify and determine the bending capacity by using approximate closed-form equations for an idealized constant, elliptical or parabolic corrosion shape (see Fig. 8). These simplifications provide a good comparison of the results with the general solution and with experiments carried out on pipes with different corrosion depths and widths. Pipes with an idealized elliptical or parabolic corrosion shape have a higher bending capacity than those with a constant corrosion depth. This difference is mainly significant for deep corrosion. Thus, simplifying the actual corrosion geometry to a corrosion loss of constant thickness underestimates the bending capacity of pipes, especially those with deep corrosion.

constant-depth corrosion   elliptical corrosion   parabolic corrosion
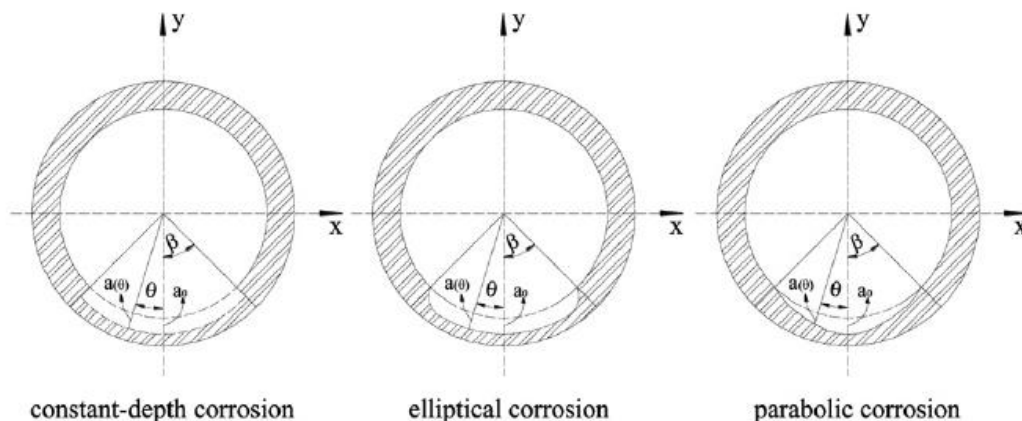
Fig. 8 Idealized corrosion loss shapes inside steel tubes [18]

A widely used structural element of steel structures are members with an angular cross-section. These elements most often act as bracing for the structures and form the infill members of the trusses of older

10

railway bridges. As already mentioned in the introduction of the study, material loss can lead, among other things, to a reduction in the buckling capacity of the members. In order to investigate this issue, Beaulieu, Legeron and Langlois (2010) [4] carried out compression tests on corrosion affected and unaffected specimens of an isosceles cross section, with boundary conditions set so that the specimen attachment simulated the actual type of connection carried out in practice. The tested elements of the angular cross-section were attached to the contact plate at both ends by a trio of bolts with one leg (the bolts were positioned consecutively in the direction of the longitudinal axis of the element). The specimen thus attached was part of the frame, where it formed a bracing compression diagonal. Subsequent comparisons of the results with analytical methods considering weight loss, led to relationships for the approximate estimation of the residual capacity (see below for the meaning of the symbols):

$$F_a = \left[1 - \frac{1}{2} \cdot \left(\frac{KL/r}{C_c}\right)\right] \cdot F_y \qquad \text{for: } \frac{KL}{r} \leq C_c \qquad (3)$$

$$F_a = \frac{\pi^2 \cdot E}{\left(\frac{KL}{r}\right)^2} \qquad \text{for: } \frac{KL}{r} > C_c \qquad (4)$$

$$\text{where: } \quad C_c = \pi \sqrt{\frac{2 \cdot E}{F_y}} \qquad (5)$$

Add the value of the effective yield strength Fcr to equations *(3)* to (5) after the yield strength Fy, which is calculated as:

$$F_{cr} = \left[1.667 - 0.667 \cdot \frac{w/t}{(w/t)_{lim}}\right] \cdot F_y \qquad \text{for: } \left(\frac{w}{t}\right)_{lim} \leq \frac{w}{t} \leq \frac{144 \cdot \psi}{\sqrt{F_y}} \qquad (6)$$

$$F_{cr} = \frac{0.0332 \cdot \pi^2 \cdot E}{(w/t)^2} \qquad \text{for: } \frac{w}{t} \geq \frac{144 \cdot \psi}{\sqrt{F_y}} \qquad (7)$$

$$\text{where: } \quad \left(\frac{w}{t}\right)_{lim} = \frac{80 \cdot \psi}{\sqrt{F_y}} \qquad (8)$$

$$\frac{KL}{r} = 60 + 0.5 \cdot \frac{L}{r} \qquad \text{for: } 0 \leq \frac{L}{r} \leq 120 \qquad (9)$$

$$\frac{KL}{r} = 46.2 + 0.615 \cdot \frac{L}{r} \qquad \text{for: } 120 \leq \frac{L}{r} \leq 250 \qquad (10)$$

where: b is leg width of the angle,
       E is Young's modulus of elasticity,
       F_a is ultimate compressive stress,
       F_y is yield strength of the steel,
       L is length of the element,
       r is radius of inertia,
       t is average thickness of the weakened angle,
       $\psi = 2.62 \ [-], w = b - t$.

Corrosion on the samples was achieved by an accelerated galvanic corrosion process (see Fig. 9). In order to use this method to predict the residual load capacity more accurately, the non-uniformity and concentration of corrosion, as well as the positions of these concentrations, must be further taken into account. It would also be necessary to verify that the actual corroded specimens found on the steel structures match the specimen obtained in this experiment through the accelerated corrosion method.
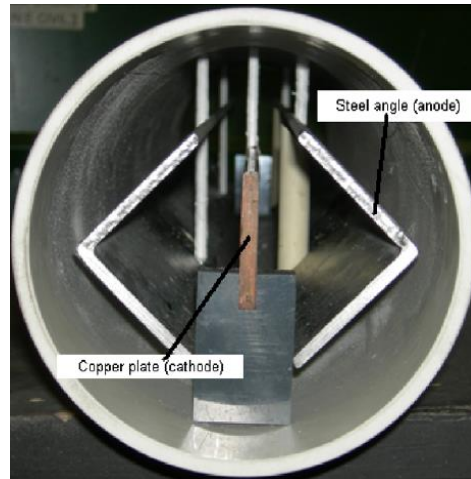

Fig. 9 Method for achieving artificial corrosion on specimens of isosceles angles - taken from [4]

A number of scientific works have been focused on the effect of corrosion on the load-bearing capacity of corroded beams, which are a widely used element in bridge or other structures (ships, etc.). Yasser Sharifi and Reza Rahgozar (2010) [19] investigated the residual bending capacity of corroded I-beams. The authors proposed 2 methods (exact and simplified) to estimate their residual bending capacity. The derived relations are not compared with experimental data, yet they can be approached as a tool for estimating the moment capacity of a corroded weakened beam. The methods provide a computational relationship between the loss of section thickness and the corresponding remaining moment capacity of the beam (expressed as a percentage of the original capacity). To determine the remaining moment capacity, only information relating to the loss in thickness of the relevant parts of the members (flange and web) and the original moment capacity of the beam is required. Information on the loss of thickness can be obtained by visual inspection or by measuring the members. These design methods can be a useful tool for engineers in practice to decide on the remaining moment capacity of corroded I-beams.

Moving on from the individual components to the whole structures, let us consider the findings from studies of steel-concrete beam bridges (from a structural point of view, these were simple beams). Jack R. Kayser and Andrzej S. Nowak (1989) [20] developed a damage model that evaluates the reliability of corroded steel beam bridges over time. The model is based on the probability of the extent and location of corrosion. The developed model was used to evaluate steel beam bridges of two typical spans (12 and 18 m). It was found that corrosion is most likely to occur on the top surface of the bottom flange, due to moisture accumulation caused by rainwater spray from traffic, and on the entire span near the abutments, due to possible leakage of the bridge closure or drainage (see Fig. 10). The loss of material at the girder has a greater effect on the web than on the flanges, causing a many percent decrease in load capacity when bending moment and shear forces are acting simultaneously. Corrosion loss has a large effect on the compressive capacity because of the possibility of buckling. The criterion that determines the load-bearing capacity or serviceability of a structure when the bridge is new may no longer be decisive if the bridge is degraded.
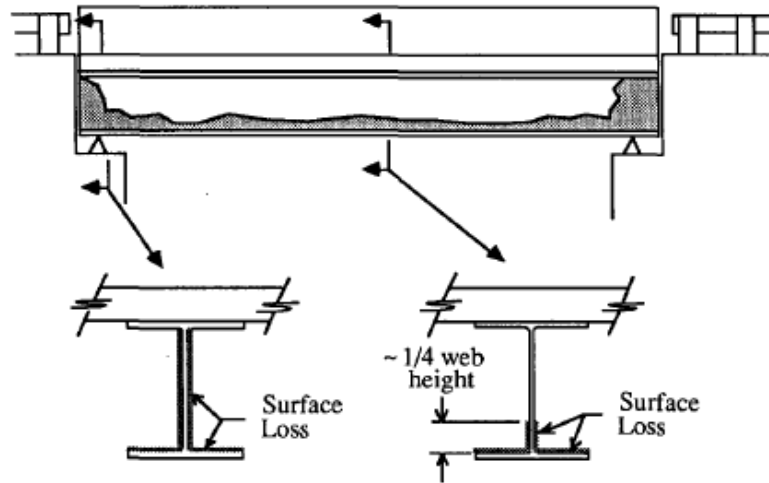
Fig. 10 The most frequent location of corrosion on beams of steel-concrete bridges [20]

In addition to steel building structures, steel is used extensively in reinforced concrete structures. The effect of corrosion on the mechanical properties of steel in reinforced concrete was discussed by Francois, Khan and Dang (2013) [21]. The evaluation of tensile tests performed on corrosion weakened and unweakened reinforcement specimens leads to the conclusion that strengthening of the material after exceeding the yield strength occurs more rapidly in the presence of corrosion than without it. It was also found that the presence of corrosion weakening on the elements results in a change in the shape of the curve showing the stress-strain relationship. The typical steady state, which marks the reaching of the yield strength of the steel, is not observed for the degraded bars and, in addition, after the maximum stress value is reached, brittle fracture occurs without the formation of a characteristic neck on the test specimen. Thus, the ultimate elongation value of the bar decreases significantly with increasing corrosion, which has a significant effect on the reliability of the structure, as the corroded steel bar no longer achieves the required ductility prescribed in standards such as Eurocode 2 [22].

A number of studies on the effects of corrosion on the change in the load capacity of structural elements have been based on statistical and probabilistic analysis. The development of time-variant reliability models for steel girder bridges was studied by Czarnecki and Nowak (2008) [23]. The approach was based on reliability analysis of elements and structural systems. The models were developed using the finite element method, and consisted of a composite reinforced concrete structure, where different number and length of beams and different sizes of beam cross-sections were considered. In the case of small-scale corrosion, the steel loss has a negligible effect on the bridge performance. On the other hand, exposure to high corrosion rates can significantly reduce the load bearing capacity of the bridge during its 100-year service life. Studies have found that the reliability of the system is much higher than that of the girder. The study also showed that bridge reliability decreases much more over time for shorter span bridges than for longer span bridges.

Darmawan et al. (2013) [24] investigated a similar issue. They focused on the reliability analysis of I-beams of steel bridges (designed according to Indonesian standards SNI T-02-2005 and SNI T-03-2005) that were subjected to corrosion. The study was concentrated, as in the case of Czarnecki and Nowak [23], on steel-concrete bridges, now with spans of 15 and 20 m and a design life of 50 years. Again, permanent and moving loads were considered. In the FEM model, the corrosion progression was taken from the research of Komp (1987) [15], according to which the relationship between corrosion time and corrosion penetration can be expressed by an exponential function. From the analysis, it can be concluded that corrosion has a more significant effect on the deflection than on the bending and shear capacity of steel I-beams. No failure due to bending moment or shear force induced by permanent or

moving loads was observed in corroded beams. As the span of the bridge increases, the probability of exceeding the allowable deflection of the corroded steel I-beams increases.

The presented results of both investigations are based on numerical modelling and more observations on real structures would be needed to verify them, in order to reveal the actual behaviour of corrosion affected bridge structures.

2.2.2. Effects of corrosion on fatigue life of steel members

Corrosion fatigue is identified as one of the main damage mechanisms for structures occurring in corrosive environments. Existing studies of corrosion pitting indicate that the crack does not necessarily occur at the bottom of the pit. Where the crack initiates in the pit depends on its shape (aspect ratio), load and corrosive environment.

Degradation due to corrosion is of course problematic for all elements of structures exposed to adverse weather conditions, but it is even more significant for welded or riveted connections of these elements. Previous research has shown that stress growth in the weld geometry and tensile residual stresses caused by the welding process are the main sources of fatigue crack initiation and propagation in welded steel structures. The problem becomes even more pronounced in the presence of a corrosive environment, as the rate of crack propagation becomes extremely high and, in the extreme case, failure of the structure can occur.

Corrosion fatigue is more damaging than either of the corrosion or fatigue phenomena themselves.

As an example of a potential risk, many of the steel truss bridges built in China in the early part of the last century are still in service. These bridges have been integrated into the local culture and their demolition would be a considerable loss. In addition, many of them are located in urbanised centres and their century-old structures still carry heavy loads from traffic. Ensuring the safety of these bridges is therefore a serious concern for local bridge management departments. However, the current methodology for evaluating degraded bridge structures, which is based largely on experience, is unreliable. Hence, the combined effects of corrosion and fatigue need to be examined in detail to be able to ensure the safety of existing structures.

A number of studies have so far concentrated on the fatigue behaviour of corroded steel plates, i.e. the basic components of steel structures, either on elements taken from actual degraded structures or on specimens with artificial corrosion weakening. Analysis of the results obtained and the findings show that the presence of corrosion pitting significantly reduces the fatigue life of corroded steel elements. The fatigue life of steel plate is significantly affected by the appearance of the surface, and as corrosion causes the surface to become rougher, the fatigue life decreases significantly. The rapid change in cross-section near the corrosion pit induces a stress concentration that causes fatigue crack initiation and propagation (see Fig. 11). It can therefore be concluded from the preceding that corrosion pits significantly affect fatigue life and the deeper the corrosion, the greater the rate of crack propagation and the more the fatigue life decreases. Fatigue fracture occurs due to the interaction of multiple corrosion pitting sites, not due to a single pitting site as described by Shan-hua Xu and Bin Qiu (2013) in their study [25].

The same issue, i.e., the evaluation of the effects of corrosion pitting on the fatigue life of steel, was investigated by Shan-hua Xu and You-de Wang (2015) [5]. In the case of both investigations, the accelerated corrosion method was used to fabricate the specimens, specifically involving the immersion of the test bodies in NaCl solution. Based on the measurements of the degraded surface, 3 typical pits were observed in terms of their proportions and appearance as shown in Fig. 12: (A) deep + narrow pit,

(C) wide + shallow pit, and (B) primary pit with secondary (secondary) pit. Deep + narrow pits, compared to wide + shallow pits, clearly show greater effects on fatigue life reduction.

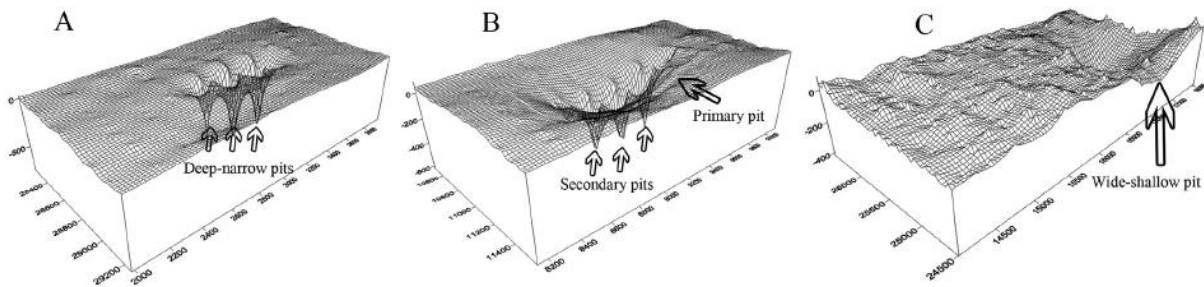*Fig. 11 Fatigue damage of the tested specimen [25]*

Fig. 12 3 typical shapes of corrosion pits [5]

As mentioned in Section 2.2, the accelerated corrosion method can be used to obtain samples with the desired corrosion loss in a short time. However, it would be necessary to verify that the actual corrosion samples found on the steel structures correspond to the corrosion sample obtained by this procedure.
The studies carried out on samples taken from actual corroded structures represent an important part of the research (note that the previous 2 studies mentioned above used the so-called accelerated corrosion). Many steel structures affected by severe corrosion are also subjected to seismic loading in some regions. For this reason, the cyclic strength and ductility of corroded steel elements were investigated by S. M. Zahrai (2003) [26]. Corroded specimens taken from the steel structure of the bridge were subjected to cyclic loading test in three-point bending. The study further focused on the rivets affected by corrosion. The evaluation of the result shows that the material properties of the sampled elements were not significantly affected by corrosion. The cyclic tests showed that the hysteretic behaviour was comparable to the uncorroded elements, but premature crack development occurred during alternate plasticisation. The irregularities of the degraded surface may therefore act as crack initiators. The rivets tested in tension and shear then showed no significant loss of strength or ductility, although they were evaluated as severely corroded on visual inspection.

Rahgozar and Sharifi (2009) [27] subjected specimens from flanges and webs of severely corroded steel beams to cyclic loading and measured the roughness of the corroded surfaces. Based on the experiments, they derived a linear relationship between the total corrosion depth and the maximum surface roughness of the steel members (see Fig. 14). They then assigned the different values of maximum roughness to the structural detail classes specified in British Standard BS 5400 (Part 10). Thus, this method indirectly

provides a relationship between pitting corrosion and the corresponding residual fatigue life of corroded steel members based on thickness loss measurements. The average corrosion weakening value d_c can be calculated according to (11) and (12) and Fig. 13 as:

$$d_c = \frac{1}{2}(t_0 - \bar{t})$$
(11)

$$\bar{t} = \frac{1}{n}\sum_{i=1}^{n} t_i$$
(12)

where: t_0 is the original thickness,

       t_i is the measured thickness of the weakened plate,

       n is the number of measurements.
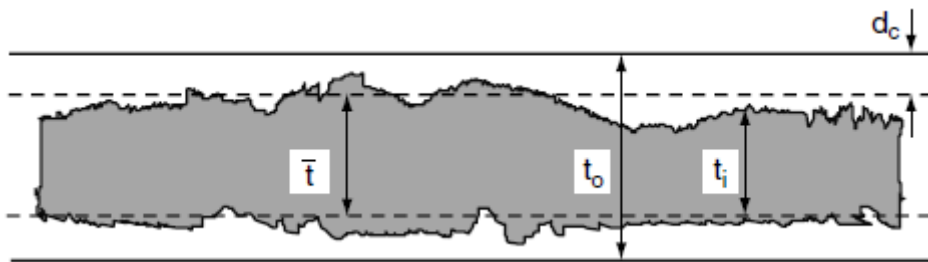
Fig. 13 Average value of corrosion weakening d_c [27]

Based on the average value of the weakening d_c, the value of the maximum surface roughness R_{max} can be found by subtracting it from the graph (see Fig. 14). In s [27]

Tab. 2, the different values of the roughness R_{max} are assigned to detail categories B to W, including the value of the slope of the detail curve m.

Fig. 14 Linear dependence of average corrosion weakening and maximum surface roughness [27]

Tab. 2 Detail categories (according to British Standard BS 5400) corresponding to different values of corroded surface roughness R_{max}

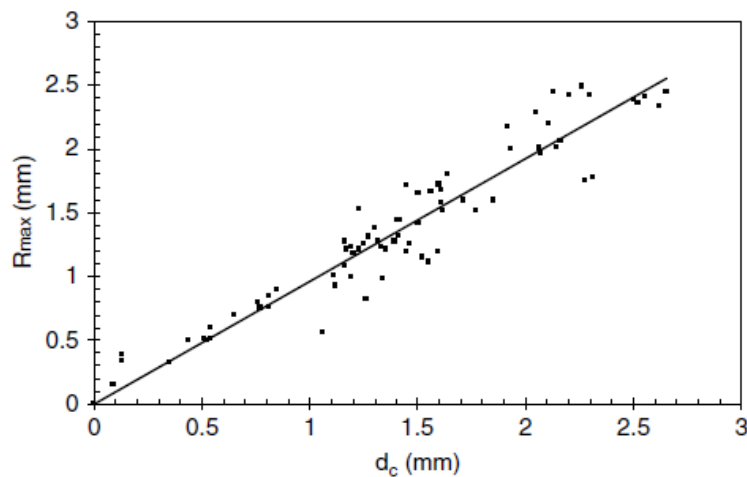| Detail category	Slope of the detail curve	Maximum surface roughness
	m	R_{max} [mm]
B	4.0	-
C	3.5	0.78
D	3.0	2.00
E	3.0	2.05
F	3.0	2.30
F2	3.0	2.40
G	3.0	2.70
W	3.0	2.85

Fatigue strength analysis was also performed on real steel specimens corroded to a small extent by Garbatov et al. (2014) [11]. A fatigue detail was subjected to cyclic loading, which was a transverse stiffener welded by fillet welds to a plate loaded by a tensile force. Based on the nominal stress approach, this detail (not weakened by corrosion) fell into category 86. The original thickness of the tensioned plate and welded stiffener was 4.5 mm, with an average corrosion weakening value of about 2.5 mm for all specimens. The initial surface roughness was analysed using a photogrammetry technique to produce a description of the idealised corroded surface. Subsequent high-cycle fatigue testing showed a significant reduction in the fatigue curve, due to severe degradation by corrosion. Statistical evaluation of the results led to the conclusion that the fatigue strength of the corroded weakened detail for 2 million cycles and a survival probability of 97.7% is 64.95 MPa.

The fatigue behaviour of degraded steel structures welded with butt welds was studied by Wahab and Sakano (2001) [28]. They observed that fatigue crack propagation in the corrosion medium is strongly influenced by the weld geometry. Weld geometry plays a significant role in the fatigue life and fatigue strength of structures welded with butt welds. Therefore, the Paris material constant needs to be determined experimentally to evaluate the corrosion fatigue life. From the experiments arranged in this test (see Fig. 15), it was found that the threshold stress intensity factor of the structures welded with butt welds reaches a much smaller value in the corrosive environment than in the air environment and its effect needs to be included in the fatigue design.
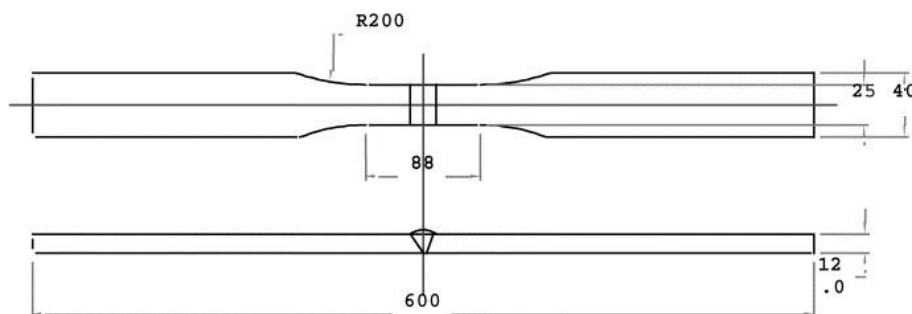

Fig. 15 Specimen for fatigue test of butt weld [28]

Several other studies have focused on the effect of corrosion pitting on crack initiation. Yan Zhang et al. (2013) [29] performed fatigue tests on specimens with smooth surfaces and specimens with corrosion

pits to investigate the effects of pits. Furthermore, they modeled different aspect ratios of the pits using the finite element method to calculate the stress concentration factor (SFC) in a bar of circular cross section loaded in tension and bending. As for the location of fatigue crack initiation, it does not necessarily occur at the bottom of the pits, but rather at the point that has the largest SCF stress concentration factor, as shown by laboratory observations. The aspect ratio of the pits greatly affects the SCF value if $a/2c$ is less than 1, but has no effect if $a/2c$ is greater than 2 (where: a = depth, $2c$ = diameter of the pit). The depth of the pit has a much greater effect on the SCF value than the width of the pit and therefore on the crack formation. Compared to artificially created pits (e.g. by milling), real corrosion pits have a smaller stress concentration factor but lead to shorter fatigue lives.

The initiation and propagation of fatigue cracks on elements corroded by seawater action was studied by Palin-Luc, Peréz-Mora et al. (2010) [30]. The authors performed high-cycle fatigue tests of up to 10^9 cycles on martensitic-bainitic hot-rolled steel specimens under 3 different conditions: (i) on newly fabricated smooth specimens (see Fig. 16), (ii) on pre-corroded specimens, and (iii) on specimens subjected to an artificial seawater current during fatigue testing. The fatigue life in the high-cyclic regime was shown to be mainly controlled by the corrosion progress during seawater flow. The fatigue strength at 10^8 cycles was significantly reduced by more than 74% compared to the newly fabricated specimens and by 71% compared to the pre-corroded specimens. Evaluation of crack growth shows that crack initiation dominates the overall fatigue life when the number of cycles is greater than 10^7 cycles.
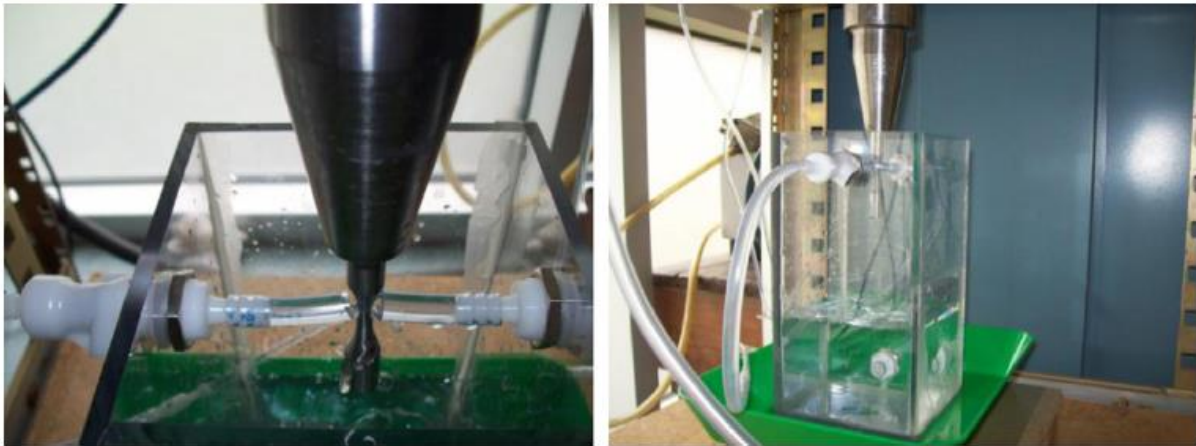

Fig. 16 Simulation of seawater current action on test samples [30]

2.2.3. Effects of corrosion on bearing capacity and fatigue behaviour of riveted connections

Assessing the condition of existing structures, especially bridges, is becoming increasingly important. Particularly for railway bridges, the operational loads and accumulation under traffic loads and the subsequent ageing of existing structures leads to the need to assess their residual fatigue life in order to decide whether only some elements need to be replaced or whether the entire bridge structure needs to be reconstructed. The condition of the individual bridge connections may be particularly important for the residual life of such a structure. The joints of structural elements are places where there is a significant concentration of stresses.

Friction in the connection of riveted structures is caused by pre-stress in the rivet, which is introduced into the rivet during the cooling of the rivet during the manufacturing of the connection. This pre-

stressing is important in that it reduces stress peaks around the holes of the individual connected components. In riveted bridges, it is usually the rivets that are attacked by corrosion first. Therefore, the question of whether and how much the prestressing of rivets will be affected by head degradation was studied by Heinemeyer and Feldmann [31]. Already the results of previous numerical studies by these authors show that a prestress of 100 MPa can be transferred by rivets that have lost 44% of their head volume by corrosion, and the investigation focused on rivets with a shank diameter of 26 mm, a head diameter of 39 mm and the material was grade 34 steel. It should be noted that the pre-stress value for these rivets embedded in the structure ranges from 20 to 220 MPa with a mean value of just 100 MPa. Subsequent experimental tests were designed to reveal at what level of degradation of the rivet head the prestressing would be reduced to 90% of its initial value. The corrosion loss on the rivet head was simulated by milling the rivet head and 2 degradation modes were considered (see Fig. 17). In the first case the milling was in the direction of the longitudinal axis of the rivet (= parallel degradation), in the second case the milling direction was deviated by 60 degrees from the longitudinal axis of the rivet. The initial prestress was set to 100 MPa. The test results indicate that at 22% head volume loss, these rivets will transfer 90% of the initial prestress (see Fig. 17). Both simulated cases led identically to this conclusion. The 22% volume loss value corresponds to a 58% reduction in head height for parallel degradation and a reduction in head diameter for degradation simulated by milling at a 60° angle. In general, therefore, a more severe reduction in prestressing can be expected with a rivet head volume loss of more than 22%. In practice, however, it is generally difficult to determine the actual loss of material on individual structural elements based on a routine visual inspection of the structure, since the layer of corroded and ineffective material on the surface needs to be removed, for example, by abrading it. However, the results of the study can be transferred to rivets of other sizes, provided that the similarity in the geometry of the rivets leads to a similarity in their stiffness.

The study also considered whether the fatigue life of the riveted joint would be affected by corrosion as a result of the reduction of the prestress in the rivet. For this purpose, experimental fatigue tests were carried out on a category 71 sheet metal connection, which is a traditional detail on a bridge structure. A prestress of 80 MPa was introduced into the rivets and the stress range during the test in the connected components was 120 MPa, i.e. 1.7 times the fatigue strength. The results showed that no damage was observed even after 2 million cycles. This means that any decrease in prestress in the rivets is not critical to the remaining life of the component.
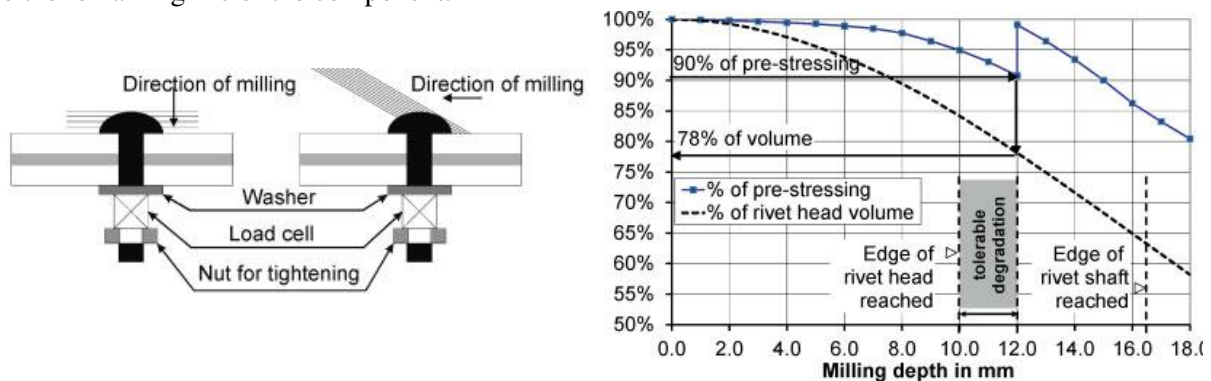

Fig. 17 Simulation of rivet damage by milling (left), reduction of prestressing force in the rivet as a function of material loss (right) [31]

Riveted joints in steel structures in most cases transfer the load by a combination of friction and shear if the rivet shank completely fills the rivet hole. From the point of view of fatigue, shear-loaded rivets correspond to non-preloaded bolts acting in shear and therefore fall into detail category 100 according to EN 1993-1-9. In order to verify the value given in Eurocode, Pipinato et al. [32] performed laboratory measurements on samples taken from a 90-year-old railway bridge structure. These were specimens of riveted connections of bracings to the main girders (see Fig. 18) and the test was designed so that

individual rivets in the connection were subjected to shear stress. Analyses carried out on the base material showed that in terms of strength it is a material that is consistent with modern steels, but is more brittle and has a different microstructural arrangement. According to tensile tests, the steel had an average yield strength of 322 MPa and a ultimate strength of 421 MPa. The notch toughness test at room temperature resulted in an average value of 11.5 J. An experiment focusing on the high-cycle fatigue behaviour of riveted connections for railway metal bridges confirmed the reported detail category of 100, despite the fact that the riveted connection samples were taken from a historic railway bridge structure. In addition, the cyclic load test did not take into account the number of cycles from traffic during operation on the bridge, therefore it can be concluded that the evaluation was on the safe side.
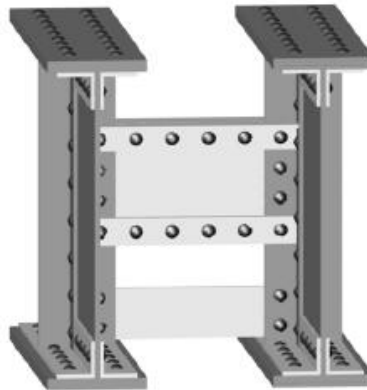

Fig. 18 Specimen taken from historic riveted bridge for fatigue test [32]

For riveted joints, it is basically necessary to distinguish between the fatigue strength of the fasteners themselves and the fatigue life of the elements that are connected by the fasteners. In the case of shear connections, experimental results show that in the absolute majority of cases fatigue damage is due to failure of the material to be connected. A study [33] carried out in 1998 compared the results of experiments on the fatigue life of riveted shear connections with the strength values given in fatigue standards and codes. These were as follows:

1. AASHTO (American Association of State Highway and Transportation Officials) - specified riveted shear connections as Detail Category D, which corresponds to a stress range of 71 MPa for 2 million cycles. The slope of the curve is 3 and the fatigue limit at constant amplitude is 48 MPa.
2. AREA (American Railway Engineering Association) - specified riveted shear connections as Detail Category D, which corresponds to a stress range of 71 MPa for 2 million cycles. The slope of the curve has a value of 3. The value of the fatigue limit is determined by the magnitude of the prestressing force in the rivets. If this force is low according to the standard, the fatigue limit at constant amplitude is set at 41 MPa for 10 million cycles. If the magnitude of the pre-stress in the rivets is normal, two categories are further distinguished according to the way the rivet holes are made (holes punched or drilled in the sheet metal).
3. AISC (American Institute of Steel Construction) - the category of detail given in this standard corresponds to the category given in AREA.
4. Eurocode 3 - This standard does not mention shear-loaded riveted connections. Assuming that a riveted shear joint corresponds to a joint made of non-prestressed high-strength bolts, then the standard prescribes Category 112 with a curve slope of 3 and a fatigue limit at constant amplitude of 83 MPa for 5 million cycles.

5. BS 5400 (British Standard) - the shear connection is specified here as Category D, which corresponds to a stress value of 91.3 MPa for 2 million cycles and a constant amplitude fatigue limit of 53 MPa for 10 million cycles.

A comparison of the experimental results of a number of authors and the relevant standards and regulations shows that the AREA Code, which classifies shear riveted connections in category 71 and considers a low pre-tensioning force, which sets the fatigue limit at constant amplitude at 41 MPa for 10 million cycles, appears to be the most appropriate.

Since the study dates back to 1998, let us add that the latest 2013 edition of Eurocode 3 [34] prescribes a detail category of 100 with a curve slope of 3 for single shear or double shear connections made from non-prestressed bolts.

Let us further mention the document IRS 77802 "Recommendations for determining the carrying capacity and fatigue risks of existing metallic railway bridges" [35]. This document recognises two groups of details sensitive to fatigue damage: (1) Fatigue Sensitive Details and (2) Fatigue Susceptible Details. In this document, 3 groups of significant fatigue sensitive details occurring in non-welded structures are distinguished. These are groups W I, W II and W III, each of which corresponds to a permissible stress range, which is furthermore different for different steel types (see Tab. 3). Group W I corresponds to the imperforated construction parts. Group W II includes imperforated construction parts but containing corrosion pits, riveted joints with cover plates on both sides, continuous riveted connections of web and flange angle of the beam, and also continuous riveted connections of flange angle and flange of the beam. The fatigue sensitive detail group W III includes riveted connections of truss members, riveted connections with cover plates only on one side, riveted connections of bracing members with tension flange of the beam and finally members with strengthening plates.

Tab. 3 Groups of fatigue-sensitive details in non-welded structures [34]

Steel	WI	WII	WIII
Wrought iron and mild steel	112 MPa	85 MPa	71 MPa
Steel St 37 / 52	163 MPa	122 MPa	100 MPa

Past experience shows that the critical detail with regard to fatigue damage is particularly the connections of the stringers to the crossbeams of riveted railway bridges (see Fig. 19). Generally, these connections have been designed with only shear forces in mind, but in reality, they are stressed by cyclic secondary bending moment due to the stiffness of the connection, which is the cause of fatigue damage. The solution of this problem in terms of numerical analysis was addressed by Imam et al. [36], [37]. Using the finite element method, they developed a model of a typical bridge deck including the mentioned connection, which was modelled in detail using solid elements. This detail is traditionally constructed by means of a pair of isosceles angles that connect the web of stringer to the web of crossbeam. Analysis under load with a model of a cargo train showed that different values of prestress in the rivets have a significant effect on the fatigue damage of the various components in the connection. The area in which the most damage occurs is around the holes of the angle leg adjacent to the web of crossbeam. On the other hand, the least damaged component in the joint in terms of fatigue is the rivets.
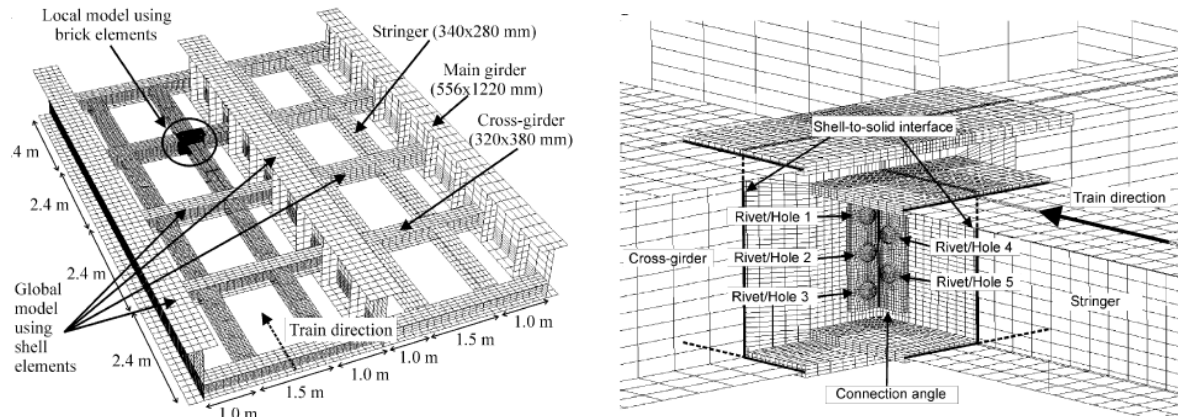
Fig. 19 Numerical model of riveted connection of stringer to crossbeam [36]

A similar issue was also the subject of research by Al-Emrani and Kliger [38]. The authors first carried out laboratory static and fatigue tests on a set of three specimens of connection of stringer to crossbeam, which were taken from an actual railway bridge structure built in 1896.

Subsequent numerical simulations showed a significant effect of the flexibility of the angles on the response of the connection to loading. In particular, the distance between the rivets and the outgoing leg of the angles was found to play a significant role. The study also shows that the magnitude of the prestressing in the rivets has only a marginal effect on the rotational stiffness of the connection and the magnitude of the stress in the angles caused by bending is also not affected by the prestressing. On the other hand, the stress range in the rivets from the applied load is dependent on the magnitude of their prestress. The higher the prestress, the more the stresses in the rivet are reduced from the normal force and bending moment. The main cause of cracks in rivets is then considered to be a combination of bending of the rivets due to the leverage force and the concentrated stress at the point between the shank and the rivet head.

The effect of corrosion weakening of individual structural elements on the global behaviour of the structure depends ultimately on the static system of the structure. As an example, an observation from the static and dynamic design of an existing riveted bridge structure can be given [39]. A detailed inspection of the state of a 90-year-old railway bridge indicated significant corrosion damage to the connections and load-bearing elements such as diagonals and the bottom chord of the truss, which was not designed with much consideration for durability, as the U-section of the chord and adjacent connections are oriented upwards, hence rainwater remains in the structure. However, despite this issue, the results from the numerical models that took into account the material loss on the elements as well as the results of the load test evaluation show that the structure is not almost sensitive to the reduction of the cross-sectional area of the elements due to corrosion. This is mainly due to the multiple static uncertainties of the truss bridge structure, which allows for the distribution of internal forces between multiple elements. Therefore, a reduction in area does not necessarily imply an increase in stresses in the element from the load. However, it should be noted that corrosion, particularly in the form of corrosion pits, can result in a change in the fatigue curve of a structural detail, namely a decrease in the fatigue curve, since surface irregularities act as notches.

2.3. Taking into consideration the effects of corrosion in current codes and standards

At present, there are still insufficient methods available for assessing steel bridge structures affected by degradation and corrosion. Assessment methods are based on the methods used for the assessment of new constructions and the degradation in design analysis is not sufficiently defined, both for static and fatigue load capacity.

To solve this problem, a small amount of backgrounds are available for structural engineers. Let us mention the approach set out in IRS 77802 "Recommendations for determining the carrying capacity and fatigue risks of existing metallic railway bridges" [35]. The method contained in the prescription is based on the application of a partial safety factor, the value of which depends on the state of the components in terms of corrosion (see Tab. 4).

Tab. 4 Partial safety factor according to the structural members conditions (IRS 77802 [35])

Material condition	Partial safety factor γ_B
As good as new or coating without damages or corrosion loss	1,0
Surface rust	1,03
Corrosion with weakening of cross-section	$1,0 + 0,05 \cdot (t/30) > 1,05$
If loss of section is determined measurement of the residual cross-section, using real dimensions for the assessment	1,0
t = time since construction or time span since last maintenance (years)	

However, this approach is insufficient in case of high level of corrosion loss and the assessment should be based on real values of corrosion loss, which can be found by measuring directly on the structure.

The consideration of degradation for assessing bridges is also stated in Standards Council of Canada code CAN/CSAS6- 06 [60]. Chapter 14 of this bridge design code, together with [60], recommends how to take into account the effects of corrosion on fatigue resistance, using a pitting factor K_p. Pitting factor is analogous to notch factor and is defined as (13):

$$K_p = 1.2 + 4.0 \cdot d_p \qquad (13)$$

where: K_p is the pitting factor,

       d_p is the depth of corrosion pith measured in inches.

Pitting factor K_p may applied to reduce calculated category A fatigue life according to Eq. (14):

$$N_p = \frac{N}{\left(K_p\right)^3} \qquad (14)$$

where: N_p is the fatigue life reduced due to pitting corrosion,

       N is the category A fatigue life calculated including section loss but neglecting the effects of pitting.

2.4. Conclusion

The degradation of steel structures is a long-term process in which the material is deteriorated, resulting in a reduction in load-bearing capacity and an increase in the deformation of the affected structure. This could result in a significant threat to its operability. In the evaluation of current state it is required to

take into consideration the corrosion of sub-elements and the associated changes in cross-sectional characteristics, reduction of fatigue strength and increased susceptibility to cracking and faster crack propagation, especially in the presence of corrosion pits. The conditions of riveted joints also plays a significant role. It should be emphasised that the load capacity and usability of a weakened structure can be decided by a criterion other than that which was primary at the beginning of the service life.

A study of available literature shows that the effects of corrosion loss on the behaviour of steel structural elements have been the subject of many research projects. The above mentioned studies were in most cases focused on the behaviour of individual steel sheets.

Many studies conducted in the past was based on the accelerated corrosion method to achieve the desired corrosion. However, the effects of real corrosion and "artificially" created corrosion may not be identical. For this reason, it is important to focus more on research in the field of real structures and to carry out experiments and measurements directly on real structures and their individual elements. This is the best way to understand the behaviour of structures and to understand their response to different loading patterns under different types of loads.

3. The goals of doctoral thesis

As confirmed by a study of the available literature, one area of research that is still not sufficiently investigated at present is the fatigue behaviour of corrosion weakened riveted connections in steel bridge structures. For this reason, this dissertation work deals with this topic. The main tool for the research of this issue is experimental tests carried out on elements of real bridge structures.

3.1. The goals of doctoral thesis

The goals of the doctoral thesis were as follows:

1. To analyse and describe the relation between corrosion and fatigue.
2. To analyse the parameters influencing corrosion and fatigue on real data.
3. Evaluate the methodology for the remaining fatigue life prediction of steel riveted bridges deteriorated by corrosion. The methodology will take into account:

   1) Various level of corrosion weakening
   2) Bridge load history
   3) Detail category
   4) Stress range
   5) Various maintenance scenarios.

3.2. Methods for the goals achievement

The stated goal of the dissertation work was achieved through the following partial steps:

   1) Detailed literature research - a summary of available knowledge on the current state of the art

In the initial phase of the solution of the given topic, an overview of the practical and theoretical knowledge of the fatigue behaviour of corroded steel structures was done. A summary of the findings of experiments, measurements, numerical analyses and analytical calculations has been made.

   2) Experimental fatigue tests

Laboratory fatigue tests were carried out on samples taken from the real bridge structure. The experiment took place in the following steps:

1. Preparation
   - Choosing and taking appropriate material
   - Numerical models of the tested elements
   - Manufacturing of test specimens
   - Preparing the experiment itself, installation the appropriate sensors.
2. Execution of the fatigue tests
3. Evaluation
   - Processing and evaluation of acquired data, detection of the influence of corrosion on the fatigue life, development of a relationship for reduction of fatigue strength due to corrosion, consideration of corrosion weakness in relation to crack propagation, support of experimental results by numerical simulations.

3) Creating an analytical software tool

Development the analytical software tool for calculation fatigue damage of structural members that are or are not deteriorated by corrosion and to estimate the remaining service life of such elements. The tool is composed of several modules that are connected together:
   - Corrosion effects
   - Stress spectrum calculation
   - Calculation of fatigue damage
   - Calculation of remaining fatigue life
   - Financial costs estimation.

4) Validation of the analytical software tool
   - Verifying and comparing the results of the software with the results of laboratory tests.

5) Case study
   - Parametric study on construction elements of the existing bridge structure.
   - Calculation the residual fatigue life of the elements when considering the different maintenance scenarios.

6) Completion of the methodology and definition of its applicability.

3.3. Intended use of doctoral thesis results

The results achieved within the doctoral thesis will serve as a basis for further research. The found relationships and dependencies including the developed methodology can serve as a basis for determining the residual service life of existing steel riveted bridge structures.

A directly usable tool in form of analytical software will be one of the outputs. This tool will make possible a residual life assessment including the management of the optimum method and maintenance procedure of the structural elements with respect to the length of the required residual life of the bridge.

4. Experimental study

The aim of the experimental study was to find how the remaining fatigue life of the steel bridge components is affected by various levels of corrosion weakening. Laboratory fatigue tests were carried out on samples taken from the real bridge structure.

4.1. Tested samples

4.1.1. Selection of tested samples

A total of four big pieces were taken from the first span of the original old railway steel bridge in Holubov (see Fig. 20, Fig. 21, Fig. 22 and Fig. 23). The Holubov Bridge was chosen because it was a typical bridge structure from the late 19th and early 20th century. The structure was designed with typical riveted joints. Moreover, due to its age, the structure was already attacked by corrosion weakening. The degree of corrosion was variable on the elements of the structure, which was very suitable for the planned experiments. The pieces were chosen to focus on details susceptible to fatigue and, at the same time, to focus on parts that will be deteriorated by corrosion. In addition, the pieces were chosen from parts where the impact of the cumulated damage is negligible or below the limit of the permanent fatigue life. Finally, the bottom flange of the truss girder was selected for the test. Smaller experimental samples were made from these parts of the riveted bridge, and were divided into two groups - uncorroded (without corrosion) and corroded.

A description of the bridge

The Holubov steel railway bridge is situated near the village of Holubov (about 20 km south-west of České Budějovice). The original structure was a steel truss riveted railway bridge with an upper deck that was built in 1892 (see Fig. 21). From the static point of view, the structure acted as a continuous beam with 2 spans (2x41.9=83.30 m). As noted above, this structure was selected because of its age and because of the significant corrosion damage, which reached variable levels. In addition, the bridge was under reconstruction (see Fig. 22 and Fig. 23).
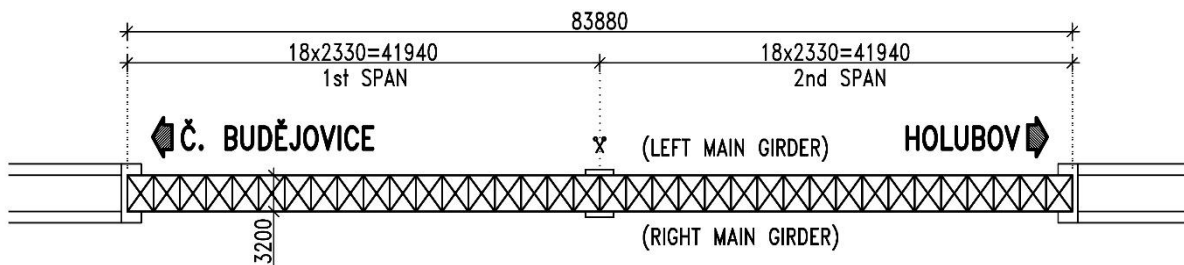

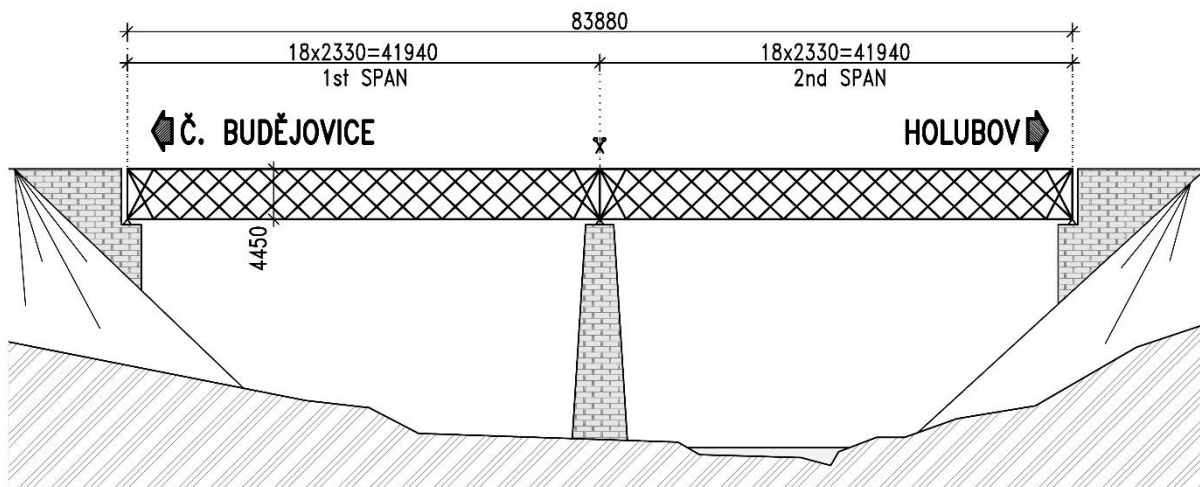*Fig. 20 Holubov Bridge – schematic view on the lower bracing*

Fig. 21 Holubov Bridge – schematic longitudinal view

*Fig. 22 Photo of Holubov Bridge during the reconstruction*

Fig. 23 Photo of Holubov Bridge during the reconstruction

Sampling of parts of the bridge structure

A total of four big pieces of the bottom flange (part 1, part 2, part3 and part 4) were taken from the first span of the old railway steel bridge in Holubov. The position of parts removed from the structure can be seen in Fig. 24, Fig. 25, Fig. 26, Fig. 27 and Fig. 28.

Part 1 and part 3 was taken from the left-hand main girder and part 2 and part 4 was taken from the right-hand girder.

SECTION 1-1: LOWER BRACING
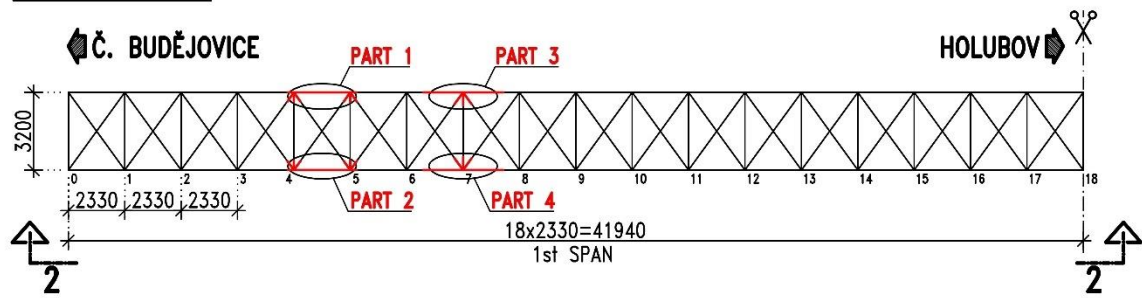
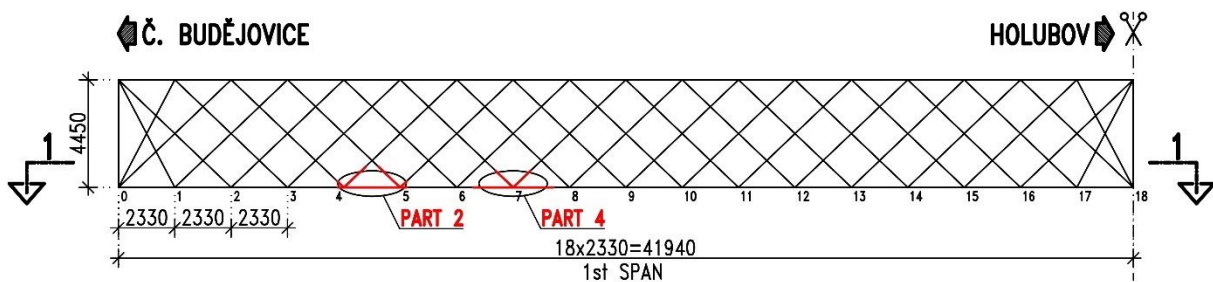## SECTION 2-2: LONGITUDINAL VIEW (RIGHT MAIN GIRDER)

Fig. 24 The position of parts removed from the bridge structure

Fig. 25 Part 1 removed from the left-hand girder of the bridge structure

Fig. 26 Part 2 removed from the right-hand girder of the bridge structure

Fig. 27 Part 3 removed from the left-hand girder of the bridge structure

Fig. 28 Part 4 removed from the left-hand girder of the bridge structure

4.1.2. Geometry of tested samples

All specimens for laboratory tests were cut from the bottom flange of the riveted truss girder (see Fig. 29 and Fig. 30). The samples were cut manually by a band saw. The final precise shape was done by milling. Due to this procedure, the temperature influence of samples was avoided. The cross-section of the bottom flange of the truss bridge was composed of:

- 3 sheets 9+9+8 mm in thickness and 400 mm in width, which formed the bottom flange (see Fig. 30),
- 1 sheet 14 mm in thickness and 500 mm in width, which formed the web,
- 2 flange angles L100x100x12, which connected the bottom flange with the web.

The most significant corrosion weakening of the samples that were taken was found on the flange angles connecting the flange to the web. For this reason, the riveted joints of the sheets forming the bottom flange with the angle mentioned above were chosen as the experimental specimens.
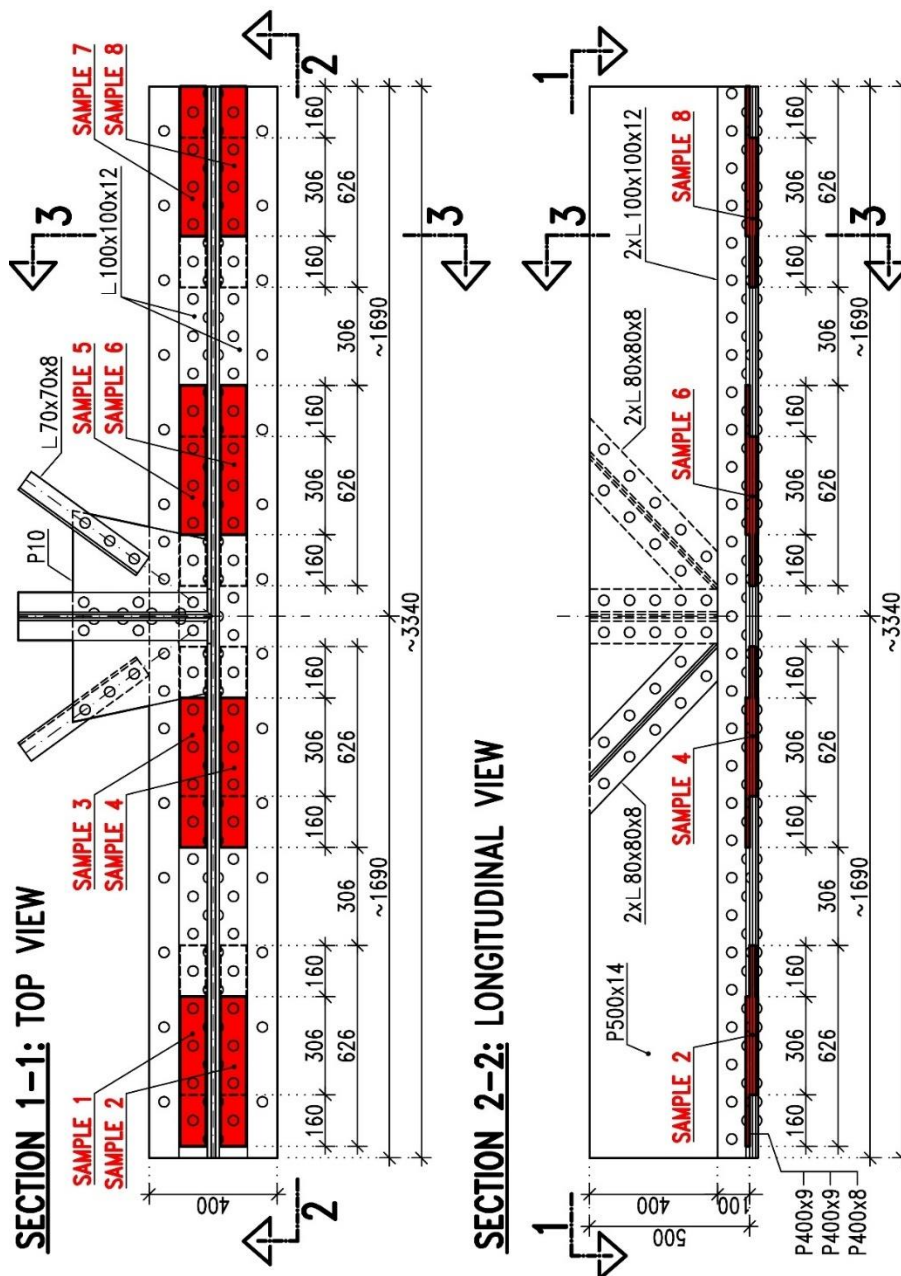

Fig. 29 Part of the bottom flange removed from the girder of the bridge structure and the position of the samples for manufacturing (top view and longitudinal view)
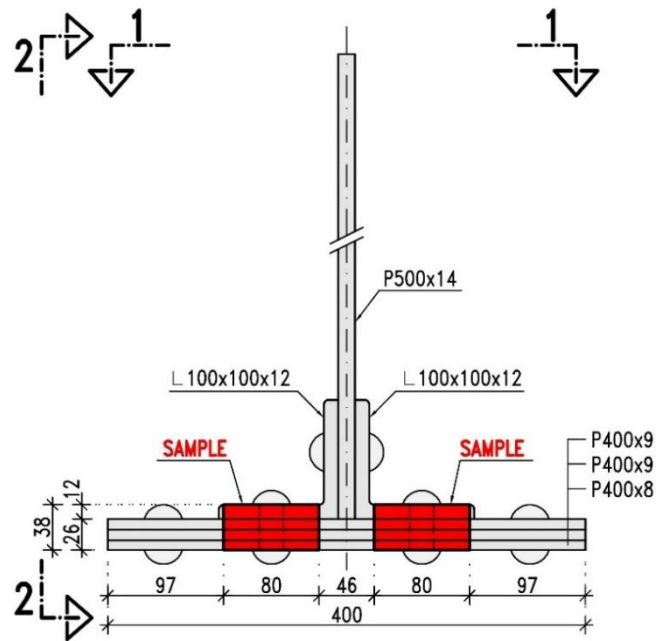
30

SECTION 3-3: CROSS-SECTION

Fig. 30 Part of the bottom flange removed from the girder of the bridge structure and the position of the samples for manufacturing (cross-section)

Geometry of tested samples

The size of the tested samples is based on the geometry of flange angle L100x100x12 and position of rivets (see Fig. 31). Each specimen consists of 4 steel sheets 12+9+9+8 mm in thickness, which are connected by 3 rivets with a shank diameter of 20 mm. The number of 3 rivets was selected with respect to adequate total length of specimen. The axial distance between rivets is 116.5 mm, and the total length of the tested specimen is 626 mm. The width of the specimens is variable, and changes from 80 mm at both ends to 60 mm in the middle of the span. The shape of the sample was used to be able to fasten the tested sample into the testing machine. The total number of specimens is 12.
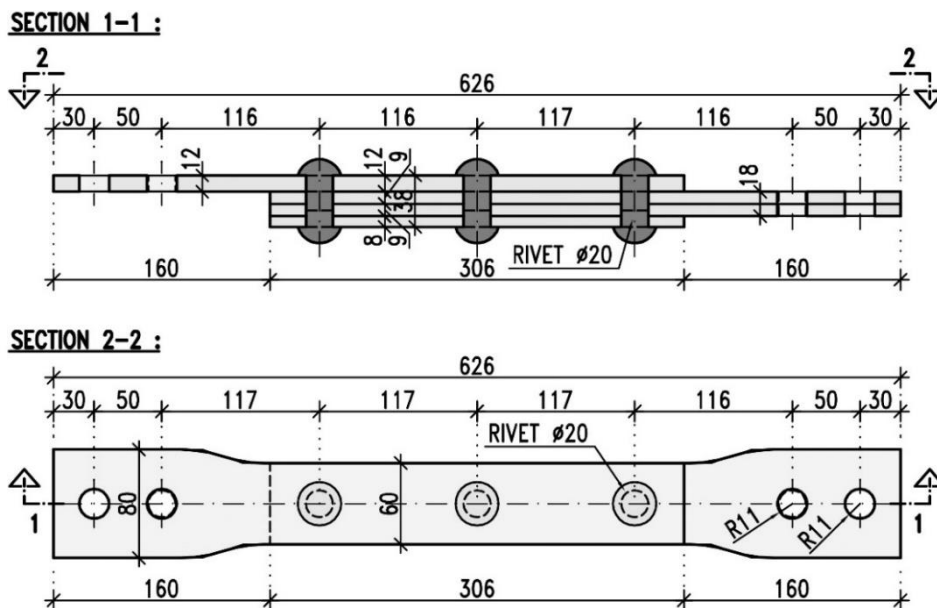

Fig. 31 The shape and geometry of tested samples (drawing)

All tested samples were divided into 3 groups on the basis of the corrosion level of the upper sheet. The corrosion level was determined as the change in cross-section area due to uniform corrosion in the place of the first rivet, and can be determined according to Eq. (15):

$$d_A = \frac{\Delta A}{A_0} = \frac{A_0 - A_1}{A_0} \quad [-]$$

(15)

where: A_0 is the cross-section area of the original uncorroded sheet in the position of the 1st rivet
A_1 is the cross-section area of the corroded sheet in the position of the 1st rivet.

The general characteristics of samples in each group is shown in Tab. 5. The division of the specimens according to coefficient d_A and the geometrical properties of each set is shown in Tab. 6. Because each sample has a more or less different level of corrosion, each set has a range of sheet thickness, cross-section area and a range of coefficient d_A.

Tab. 5 The general characteristics of samples in the group

Group of samples	Samples in the group	Characteristics of the samples in the group
1st group: Without corrosion	S1.1	• no measurable corrosion weakening, a change in surface colour only
	S1.2	
	S1.3	
	S1.4	
2nd group: Medium level of corrosion	S2.1	• a medium level of corrosion loss - especially the upper sheet and the heads of the rivets on the upper surface • medium deep (0.5 – 1.5 mm) corrosion pits on the upper sheet • a range of corrosion thickness loss of about 1-2 mm
	S2.2	
	S2.3	
3rd group: High level of corrosion	S3.1	• a high level of corrosion loss - especially the upper sheet and the heads of the rivets on the upper surface • deep corrosion pits (2 – 3 mm) on the upper sheet • a range of corrosion thickness loss from about 2-4 mm
	S3.2	
	S3.3	
4th group: Samples with missing rivet	S4.1	• no measurable corrosion weakening, a change in surface colour only • the middle rivet is missing
	S4.2	
	S4.3	

Tab. 6 Geometrical characteristics of 3 sets of tested specimens

Geometry of the specimen – nominal values								
Set of samples according to the corrosion level of the upper sheet	Sheet width	Sheet thickness		Hole diameter	Weakened cross-section area (net)		Change in cross-sectional area	
	b [mm]	t_{max} [mm]	t_{min} [mm]	d_0 [mm]	$A_{net,max}$ [mm^2]	$A_{net,min}$ [mm^2]	$d_{A,min}$ [-]	$d_{A,max}$ [-]
1 No corrosion	60.0	12.0	12.0	20.0	480.0	480.0	0.00	0.00
2 Medium level	60.0	11.0	10.0	20.0	452.0	424.0	0.06	0.12
3 High level	60.0	10.0	8.0	20.0	424.0	368.0	0.12	0.23

SECTION 1-1 :

SECTION 2-2 :
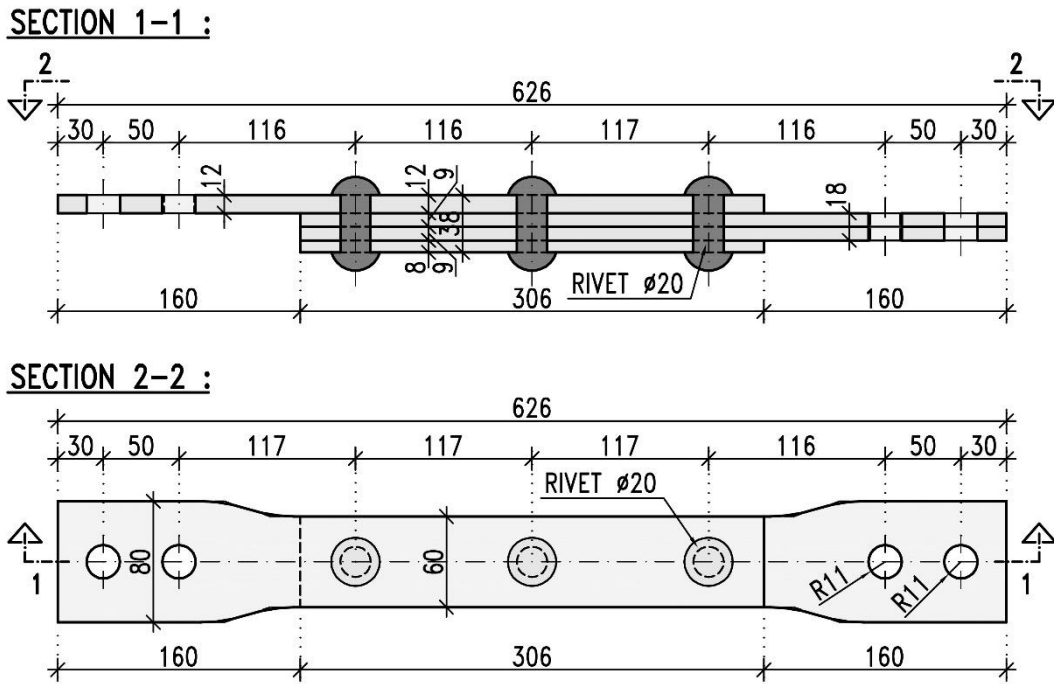
Fig. 32 Tested samples without corrosion (1ˢᵗ group of samples)

SECTION 1-1 :

CORRODED SURFACE OF THE UPPER SHEET
(CORROSION THICKNESS LOSS: 1-2 mm)

SECTION 2-2 :

CORRODED SURFACE OF THE UPPER SHEET
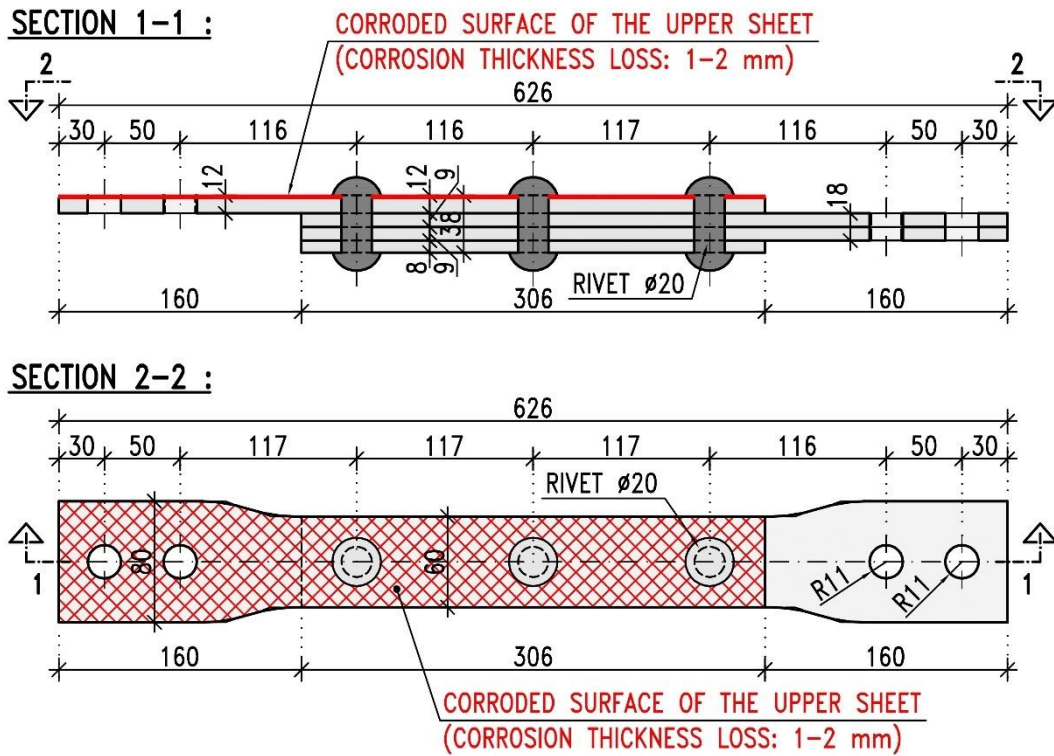(CORROSION THICKNESS LOSS: 1-2 mm)

Fig. 33 Tested samples with medium level of corrosion on the surface of the upper sheet (2ⁿᵈ group of samples)
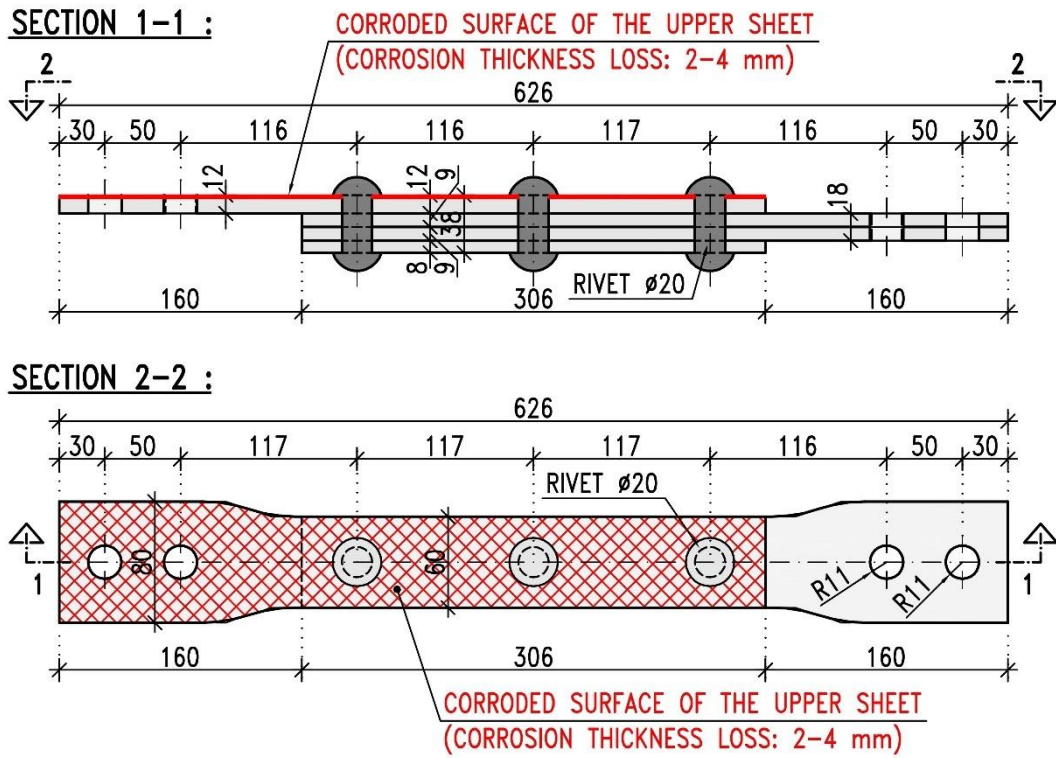
Fig. 34 Tested samples with high level of corrosion on the surface of the upper sheet (3*rd* group of samples)
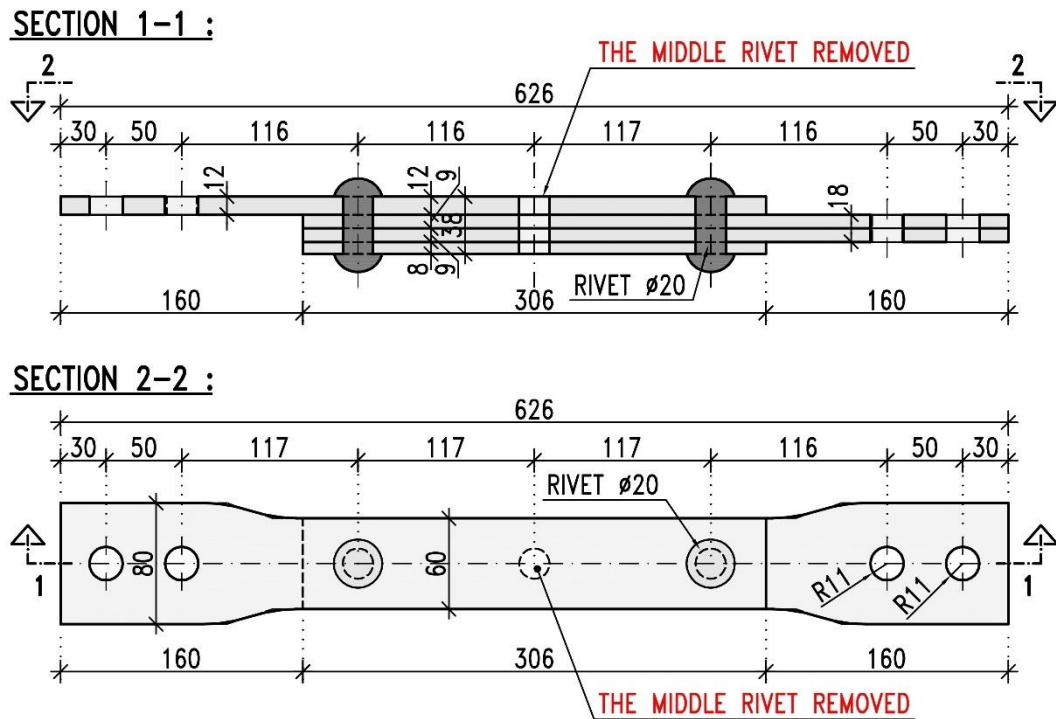

Fig. 35 Tested samples with missing rivet (4*th* group of samples)

The real geometry of manufactured samples is slightly different in comparison to the assumed geometry that is shown on Fig. 32, Fig. 33, Fig. 34 and Fig. 35.

The variation in dimensions is due to slight discontinuities in the manufacture of the samples and, of course, due to corrosion weakening of the top plate and rivets. The actual geometry of the samples was measured with a calliper. The measured values of geometry and photos of all samples, including a description of the corrosion weakening, are given in Tab. 37 (Annexe 1).

Fig. 36, Fig. 37, Fig. 38 and Fig. 39 show a photograph of a selected sample from each group. Photographs of all samples are shown in Tab. 37 (Annexe 1).
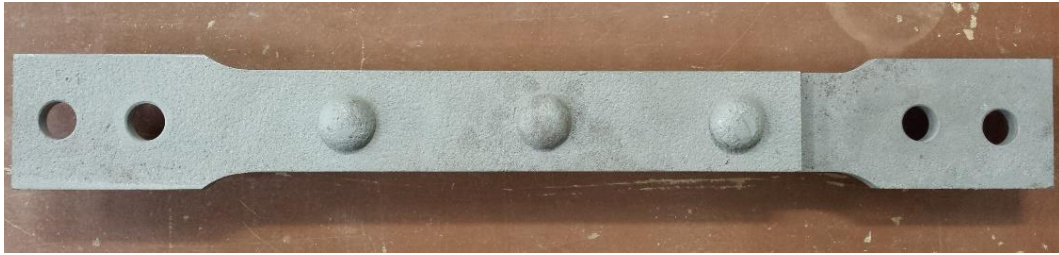

Fig. 36 Photo of tested specimen without corrosion (Example of a sample from group 1)

Fig. 37 Photo of tested specimen with a medium level of corrosion (Example of a sample from group 2)

Fig. 38 Photo of tested specimen with a high level of corrosion (Example of a sample from group 3)

Fig. 39 Photo of tested specimen with a missing rivet (Example of a sample from group 4)

All tested specimens were sandblasted to remove the corrosion layer before installing the measurement devices. The corroded surface of samples was sandblasted to the smoothness Sa2.5 by the very fine siliceous sand. In order to prevent any impact on the fatigue behaviour, the very fine siliceous sand instead of traditional steel balls was used with the small jet device. The sandblasting of surface was

necessary to do because of the installation of strain gauges and to measure the real geometry and observe the cracks on the surface. Subsequently, the photogrammetry method with sufficient accuracy ± 0.1 mm was performed to obtain a 3D model and to find the exact geometry, including corrosion pits, rivet damage and other irregularities. The depth of the corrosion pits was in the range of 0.5 – 2 mm, and for the samples with the highest level of corrosion, the depth reached a maximum value of 2.5 – 3 mm. Photogrammetry pictures of all samples are shown in Tab. 37 (Annexe 1).

The shape of the test specimens shows that the individual plates are connected to each other with eccentricity. The reason for this was the limited possibility of selecting specimens from the existing bridge structure that would be suitable both in terms of dimensions and especially in terms of corrosion weakening. Ideally, the level of corrosion weakening of the specimens should be different. For this reason, specimens were cut from the bottom flange of the lower chord of the truss girder. As the corrosion weakening was only on the upper surface of the flange, the shape of the specimens had to be adapted to this fact.

However, eccentricity of connections is common on steel riveted structures. Connections of horizontal stiffening elements are commonly made with eccentricity if the stiffening was formed by a single angle. Another eccentric connection is the connection of diagonals and verticals to the chords of the truss beam. If the diagonal or vertical section was formed by a single angle (or pair of angles) attached laterally to the web of T-cross section of the chords, then the connection was eccentric (see Fig. 40 and Fig. 41).

In general, therefore, on steel riveted bridges, if the connected members consist of only one element, the connection is unsymmetrical. For this reason, additional bending moments due to eccentricity are generated at least in the vicinity of the connection even under axial loading (the magnitude of the bending moment depends on the stiffness of the connection, the length and the slenderness of the connected member).

Fig. 40 Eccentric connection of vertical bracing members (steel riveted railway bridge in Trutnov).

Fig. 41 Eccentric connection of diagonals to the bottom chord and eccentric connection of the vertical bracing member (steel riveted railway bridge in Holubov)

In order to reduce the effects of bending moment in the laboratory tests as much as possible, the end plate of the sample was shortened so that it was not held in the test rig during the experiment. As a result, the value of the eccentricity in the connection and the effect of the bending moment were thus reduced.

4.1.3. Numerical model of tested samples

A numerical model of tested specimen has been created to see the behaviour of samples and find out the optimal values of loading force. The test specimen without corrosion weakening S1.2 was modelled in Dlubal.RFEM software (see Fig. 42 to Fig. 45). This specimen was fitted with a large number of sensors during the experiment (see Chapter 4.2.1) for subsequent comparison of the specimen response with the results from the numerical model.

Geometry

The geometry of the model of the tested sample was based on the actual geometry of the manufactured specimen. The dimensions of all specimens were measured in detail using a calliper (see Annex 1). The geometry of the fixture elements was considered according to the prescribed manufacturing documentation. All plates were modelled as 3D solid members, except fixing device. The contact friction elements were used in the gap between all plates. The properties of each contact element were:
  1. in direction perpendicular to plates: ineffectiveness in tension
  2. in direction parallel to plates: friction between steel sheets with coefficient of friction $\mu = 0.2$.

The numerical model was simplified in some details, especially in coupling elements (rivets, bolts and pins) that were not modelled as solid members, but were substituted by bar elements. Rivets were modelled by beam elements with circular shape of cross-section (Ø20 mm) that were ineffective in compression. These beams were connected with shell members along the edge of hole with only compression allowed.
The size of the finite element mesh was set to 2 mm with a thickening around the rivet holes.

Supports

The model was supported by two node supports that are located in the middle of span of pins connecting the sample to test equipment. Both supports allow rotation around the axes of pins and one of them is also free in moving along the longitudinal axe of tested sample. The second bearing do not enable moving in any direction.

Materials

A material bi-linear model of steel with material properties according to the results of material tests was used for the specimen model (see Chapter 4.1.4). For the model fixing device, a material bi-linear steel model was used with the material properties of the S355 grade steel from which the fixing elements were made. Material of pins and bolts was 8.8 steel.

Loading

In the numerical model, the specimen was loaded by axial tensile force. The load force was applied in the middle of the loading pin. The maximum magnitude of the loading force was chosen such that the nominal normal stress in the critical cross-section of the top plate weakened by the rivet hole did not exceed 180 MPa. The minimum loading value was chosen so that the nominal normal stress would be approximately 3 MPa. Thus, the load force range was chosen such that the specimen was continuously subjected to tensile force during the experiment.
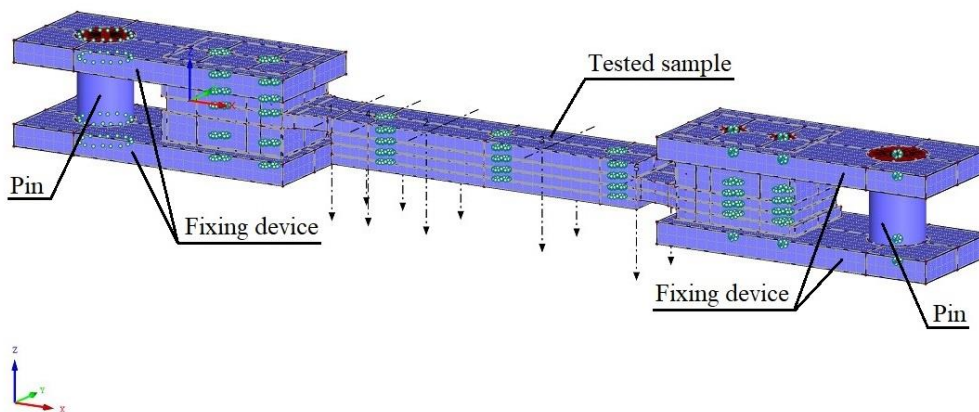

Fig. 42 Numerical model of the tested sample including fixing device (3D view)
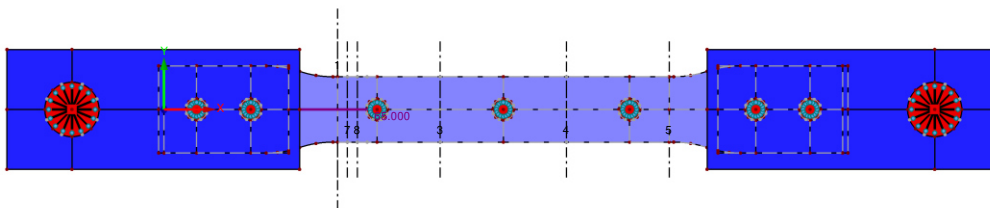

Fig. 43 Numerical model of tested sample including fixing device (view from the top)

38
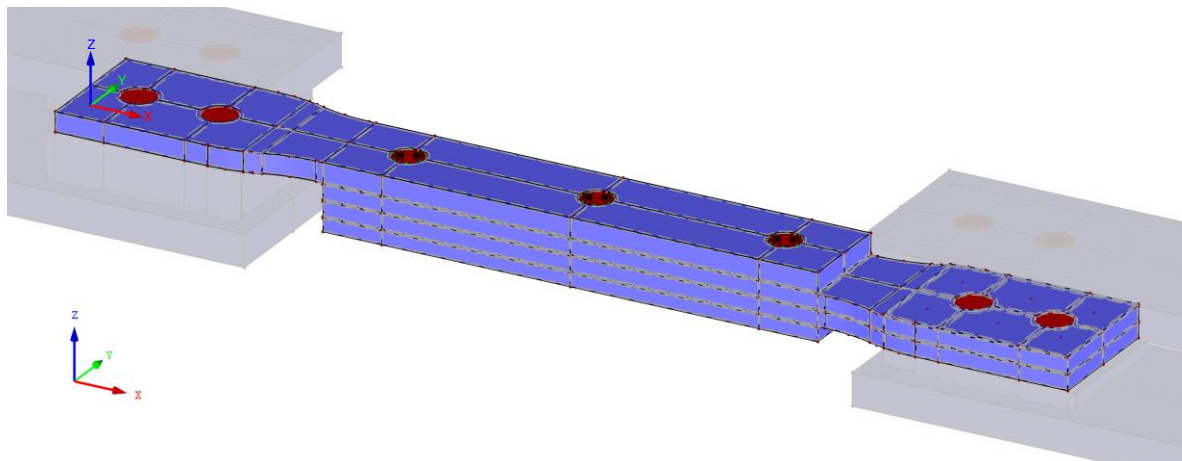
Fig. 44 Numerical model of tested sample (3D view)
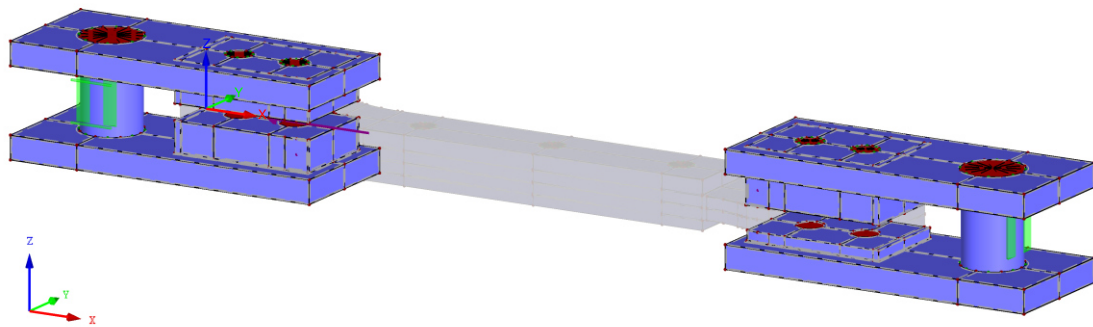
Fig. 45 Numerical model of the fixing device (3D view)

Results of numerical model

The results from the numerical model of tested sample are shown below for a load value of 91 kN, which corresponds to the maximum load value for the uncorroded specimen during the fatigue test (see Fig. 46 to Fig. 49).

Fig. 46 Results of numerical model: total displacement of tested sample

Fig. 47 Results of numerical model: normal stress σ_x in tested sample including fixing device

Fig. 48 Results of numerical model: normal stress σ_x in tested sample

Fig. 49 Results of numerical model: normal stress σ_x in tested sample

4.1.4. Material properties of the tested samples
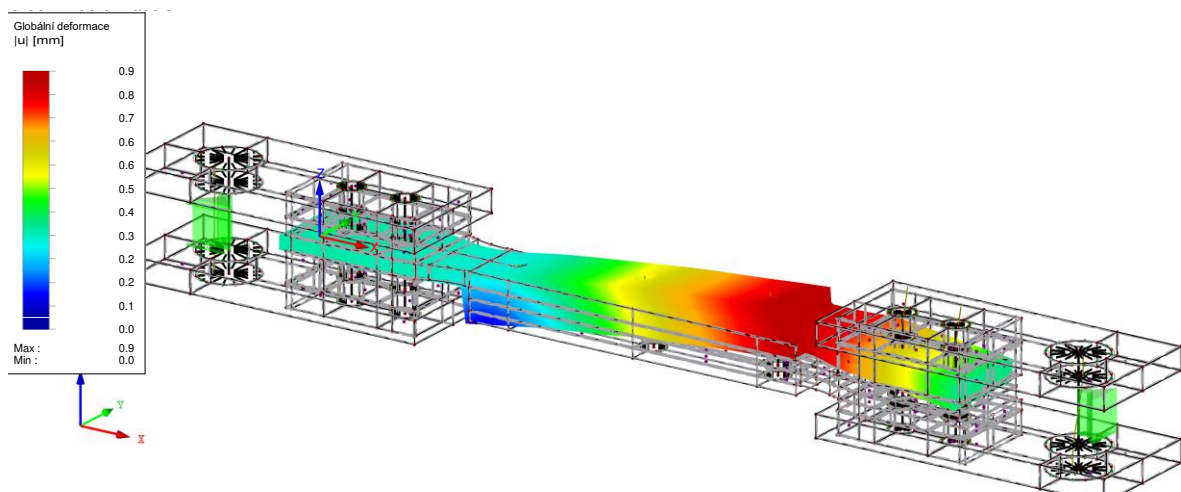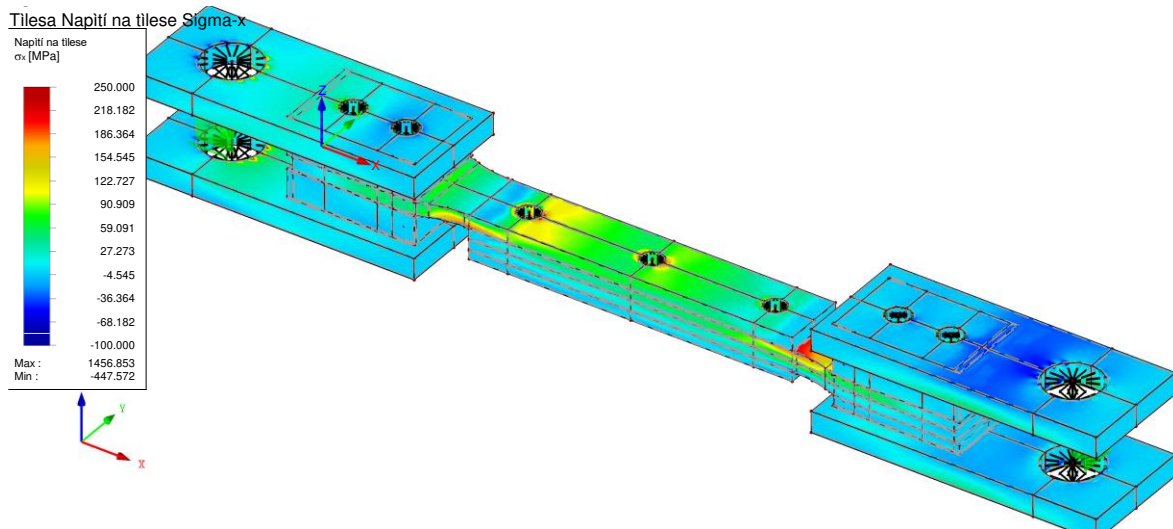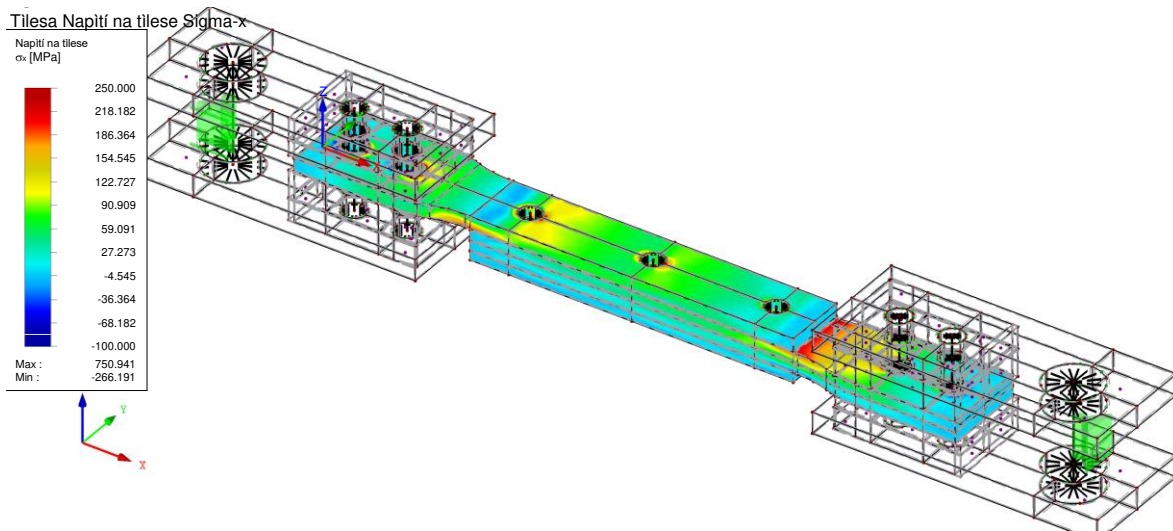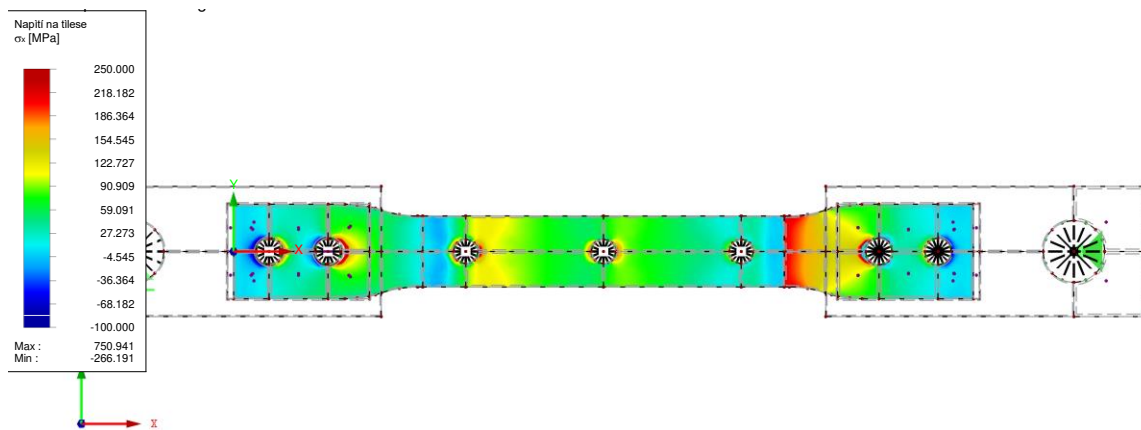
A total of 10 small samples were taken from the bottom chord of the truss girder of Holubov bridge to find the material properties of the steel. Samples for material test were taken from cervical angle, web and flange of the bottom chord. The types of material tests of steel are summarized in Tab. 7.

Tab. 7 Steel tests to determine the material properties of steel

Sample for material test				Type of test				
	Sample	Description		Test in tension	Charpy impact test		Microstructure test	Chemical composition
1	S1-1	Cervical angle	L100x100x12	x			x	X
2	S1-2	Cervical angle	L100x100x12	x				
3	S1-3	Cervical angle	L100x100x12		x	(20 °)		
4	S1-4	Cervical angle	L100x100x12		x	(-20 °C)		
5	S1-5	Web (sheet)	P14	x			x	x
6	S1-6	Flange (sheet)	P9	x				
7	S2-1	Cervical angle	L100x100x12	x				
8	S2-2	Cervical angle	L100x100x12	x				
9	S2-3	Web (sheet)	P14	x				
10	S2-4	Flange (sheet)	P9	x				

1. Mechanical properties of steel

Tests in tension on 8 samples were performed to find out the mechanical properties of steel: yield strength f_y, ultimate strength f_u, modulus of elasticity E. The measured values are stated in Tab. 8. The tensile test was carried out according to ČSN EN ISO 6892-1: 2009 [40].

Tab. 8 Results of the test in tension

Sample for material test			Test in tension - results			
	Sample	Description	Yield strength	Yield strength	Ultimate strength	Modulus of elasticity
			f_y [MPa]	$f_{y,02}$ [MPa]	f_u [MPa]	E [GPa]
1	S1-1	Cervical angle	268	240	388	205.826
2	S1-2	Cervical angle	244	229	382	206.782
5	S1-5	Web (sheet)	220	212	322	207.201
6	S1-6	Flange (sheet)	267	253	414	208.567
7	S2-1	Cervical angle	299	261	396	208.568
8	S2-2	Cervical angle	267	265	400	207.386
9	S2-3	Web (sheet)	241	216	375	207.986
10	S2-4	Flange (sheet)	299	252	388	209.809

The method according to ČSN ISO 13822 [41] was used to evaluate the yield strength of the steel. The evaluation is presented in Tab. 9. The table contains the measured yield strength values obtained from

the tensile tests for each specimen and the calculation of the characteristic yield strength value (lower 5% quantile).

Tab. 9 Evaluation of characteristic value of yield strength

Yield strength				
Sample			Measured yield strength	
Sample		Position of sampling	f_y	$(x_i\text{-}m_x)^2$
			[MPa]D	[MPa]
1	S1-1	Cervical angle	268	23.77
2	S1-2	Cervical angle	244	365.77
3	S1-5	Web (sheet)	220	1859.77
4	S1-6	Flange (sheet)	267	15.02
5	S2-1	Cervical angle	299	1287.02
6	S2-2	Cervical angle	267	15.02
7	S2-3	Web (sheet)	241	489.52
8	S2-4	Flange (sheet)	299	1287.02
			Σ	5342.88
Number of samples			$n =$ 8	samples
Arithmetic mean			$m_x =$ 263.13	[MPa]
Standard deviation			$s_x =$ 27.63	[MPa]
Coefficient of variation			$V_x = s_x/m_x =$ 0.105	[-]
Characteristic value			$X_k = m_x*(1\text{-}k_n*V_x)$	
Coefficient according NA.2			$k_n =$	1.74
Characteristic value of yield strength			$f_{yk} =$	**215.1** [MPa]

The characteristic value of yield strength (lower 5% quantile) determined from all samples is $f_{y,k}$ **= 215 MPa**. The average value of the modulus of elasticity of the steel samples is **E = 207.8 GPa**.

The bending impact test was carried out according to ČSN EN ISO 148-1 [42]. The specimens were tested at a specimen temperature of -20 °C and 20 °C, respectively, on a test rig: Charpy hammer, 300 J. The result of the test is the absorbed energy [J]. Three test specimens were made from each sample. The measured values of the absorbed energy for each test specimen are given in Tab. 10.

Tab. 10 Results of Charpy impact test

Sample for material test			Charpy impact test - results					
Sample		Description	Charpy test (+ 20 °C)			Charpy test (- 20 °C)		
			Absorbed Energy [J]			Absorbed Energy [J]		
3	S1-3	Cervical angle	73	101	37			
4	S1-4	Cervical angle				5	6	5

Completed test report of tensile tests and Charpy impact tests is included in Annexe 5: Results of material tests.

2. Microstructure of steel

The metallographic microstructure test was carried out on the samples shown in Tab. 7. The evaluation was carried out using a Neophot 32 metallographic microscope.

Sample S1-1 has a ferritic-pearlitic structure, containing tertiary cementite. The microstructure of the sample is shown in Fig. 50. Sample S1-5 has a ferritic structure, containing tertiary cementite. The microstructure of the sample is shown in Fig. 51.

According to the results, the material of the bridge components is **mild steel**. Let us recall at this point that Holubov Bridge was constructed in 1890.
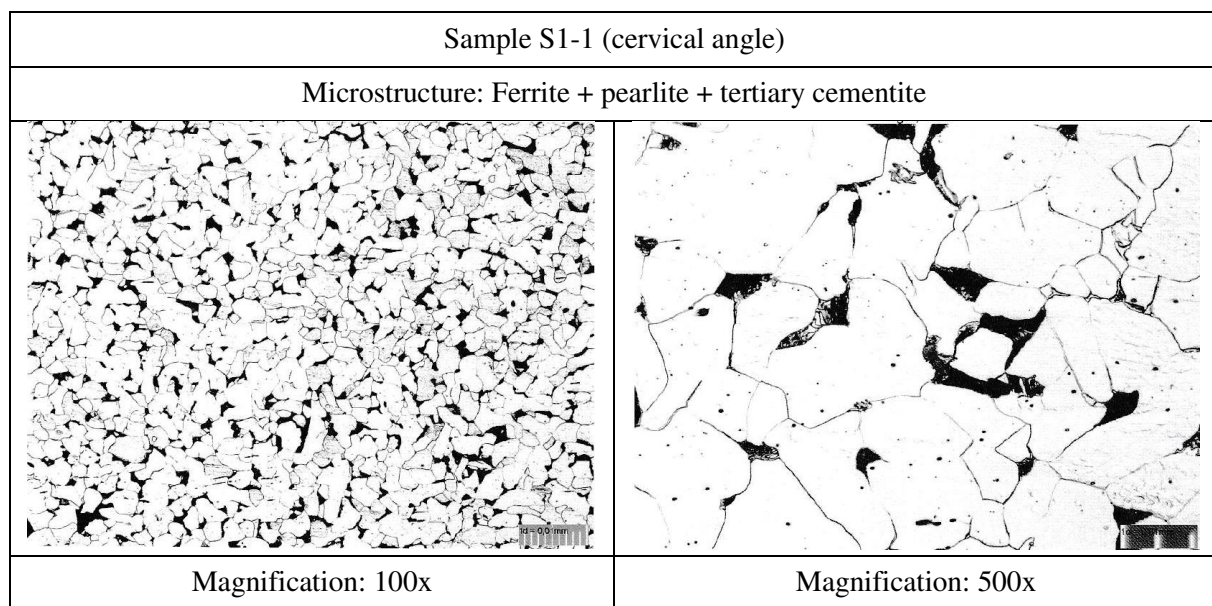
Sample S1-1 (cervical angle)	
Microstructure: Ferrite + pearlite + tertiary cementite	
Magnification: 100x	Magnification: 500x

Fig. 50 Microstructure of tested steel – sample S1-1 (cervical angle)

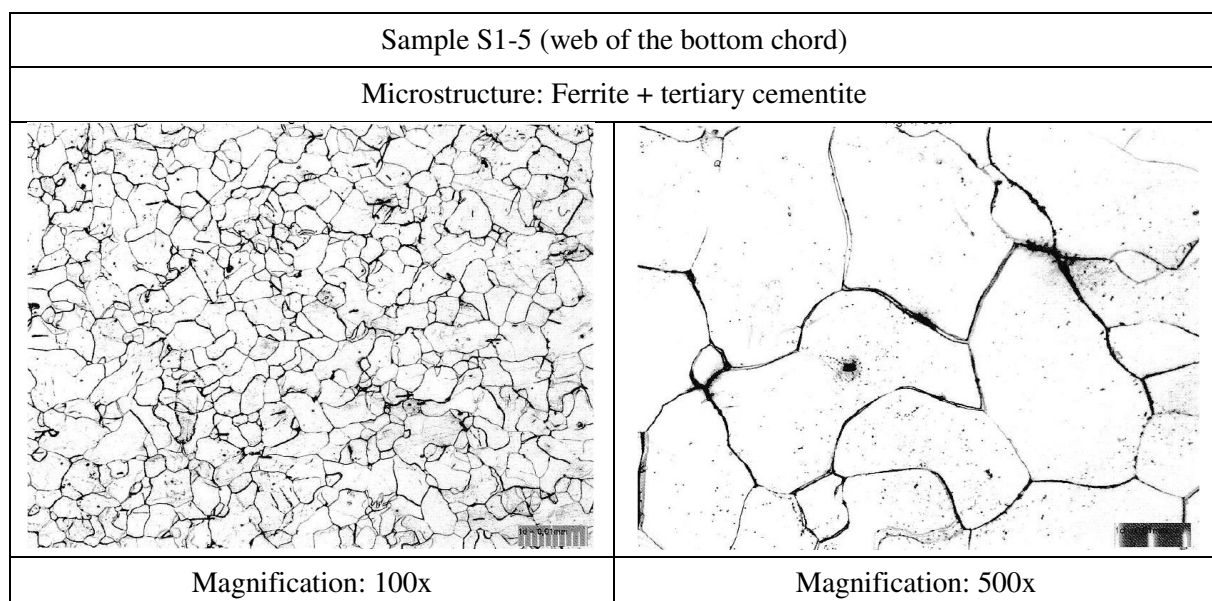| Sample S1-5 (web of the bottom chord)	
Microstructure: Ferrite + tertiary cementite	
Magnification: 100x	Magnification: 500x

Fig. 51 Microstructure of tested steel – sample S1-5 (web of the bottom chord)

3. Chemical analysis of steel

Spectral analysis of the chemical composition was performed on the samples listed in Tab. 7. The chemical composition analysis was carried out on a QUANTRON Magellan test rig. The optical emission spectrometric test method was used.

The results of the chemical composition of the steel test samples are given in Tab. 11 and Tab. 12, separately for the samples taken from the cervical angle and web of the bottom chord. The complete test report on the chemical composition of the steel is given in Annex 5.

Tab. 11 Chemical composition of tested steel - sample S1-1 (cervical angle)

Chemical composition of tested steel – sample S1-1 (cervical angle)									
Element [%]									
C	Si	Mn	P	S	Cr	Mo	Ni	Al	Co
0.17	0.00	0.30	0.032	0.030	0.01	< 0.01	0.02	0.002	0.014
Element [%]									
Cu	Nb	Ti	V	W	Pb	Sn	As	Sb	B
0.02	< 0.002	0.004	< 0.001	< 0.005	0.000	< 0.001	0.025	< 0.001	0.0015

Tab. 12 Chemical composition of tested steel - sample S1-5 (web of the bottom chord)

Chemical composition of tested steel – sample S1-5 (web of the bottom chord)									
Element [%]									
C	Si	Mn	P	S	Cr	Mo	Ni	Al	Co
0.03	0.000	0.19	0.029	0.023	0.01	< 0.01	0.02	0.001	0.015
Element [%]									
Cu	Nb	Ti	V	W	Pb	Sn	As	Sb	B
0.04	< 0.002	0.004	0.001	< 0.005	0.000	0.002	0.047	< 0.001	0.0014

4.2. Experimental fatigue tests

The test specimens presented in the previous chapter were used for laboratory fatigue tests. During the tests, the specimens were instrumented with a number of sensors to determine the behaviour of the specimens during the test and for subsequent evaluation of the tests. The instrumentation of the specimens with sensors is described in Section 4.2.1.

The procedure and arrangement of the tests is described in Section 4.2.2. The results of the tests and their evaluation are given in Section 4.3.

4.2.1. Indicators measured during the tests

The tested samples were divided into 2 groups according to the number of sensors placed on the samples. In the first group, there were 2 samples with a large number of sensors that recorded in detail the behaviour of the samples during fatigue tests. These samples were subsequently used for comparison and validation of the numerical models. The second group consisted of samples with fewer sensors. These sensors recorded the global behaviour of the samples during the tests.

1st phase samples

The first group of experimental samples contained 2 samples that were equipped with a larger number of measurement devices. One sample with a high level of corrosion weakening and one sample without corrosion were selected to represent 1st phase samples. A total of 10 (13) strain gauges were arranged on each of them to measure the relative strain during the fatigue tests. According to Fig. 52, five gauges (S1-S5 and S6-S10) were located in the middle of the gaps between rivets on the bottom and upper side of the sample (a total of 2x5=10 gauges). The remaining 3 gauges (S11-S13) were installed on the surface of the corroded sample to measure the strain in the position of the selected corrosion pit. The measured data helped to verify the numerical models of the tested samples.

Each of these tested samples was also equipped with a couple of displacement sensors, which measured the movement of individual parts: Both sensors (D1 and D2) measured the movement of the upper sheet towards the rest of the specimen, as shown in Fig. 52. These indicators were also very important for fatigue damage.

HBM strain gauges were used (1-LY11-1.5/120, 1-LY11-10/120) together with displacement inductive sensors (LVDT) Micro Epsilon of type DTA-5D-CA with nominal displacement ± 5 mm (see Tab. 13). The indication and the presence of a fatigue crack during the experiments were detected by visual inspection.
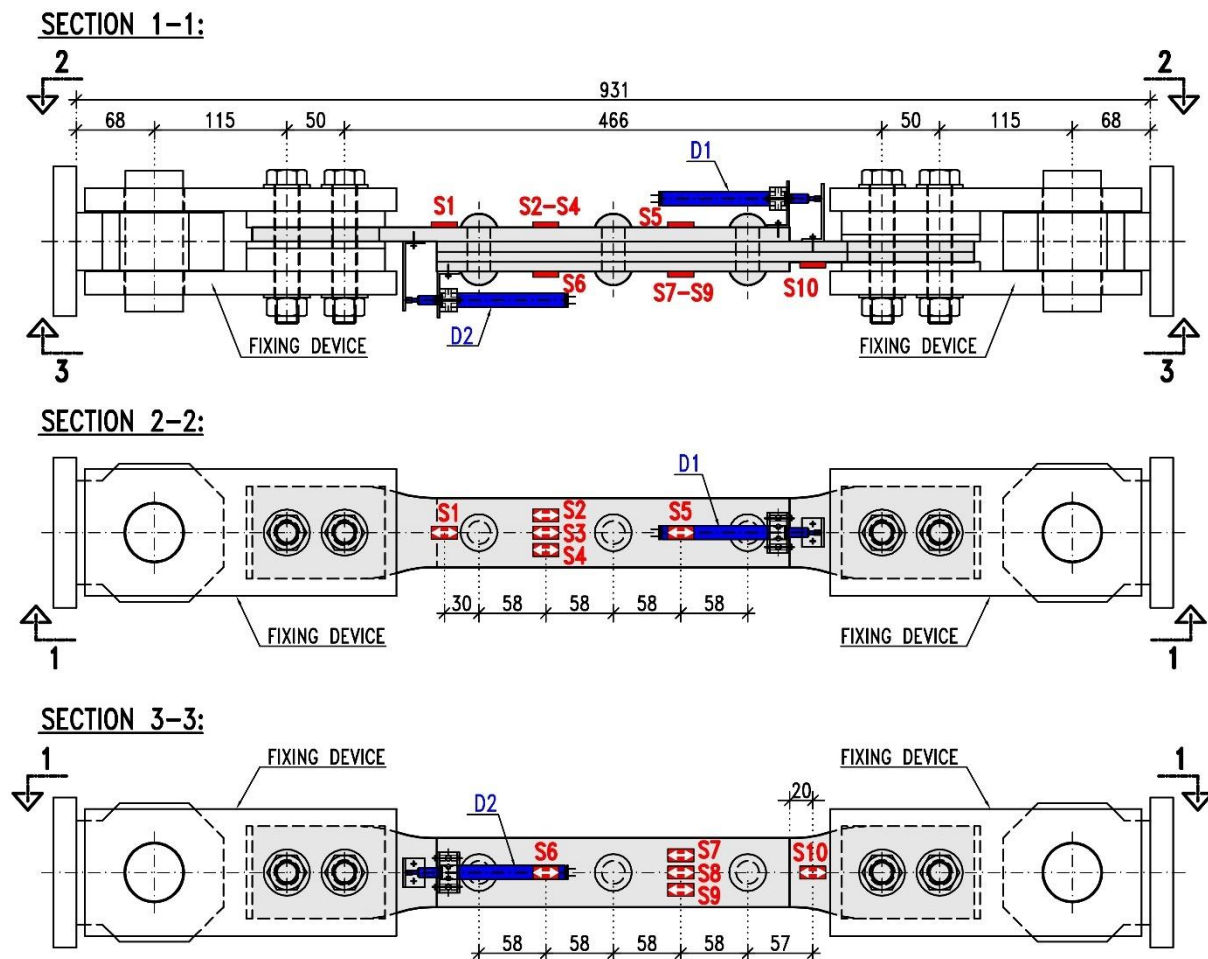

Fig. 52 1st phase samples - position of the sensors and the fixing device

Fig. 53 shows the photo of tested sample instrumented with sensors. The detail of fixing of displacement sensors is showed on Fig. 54.
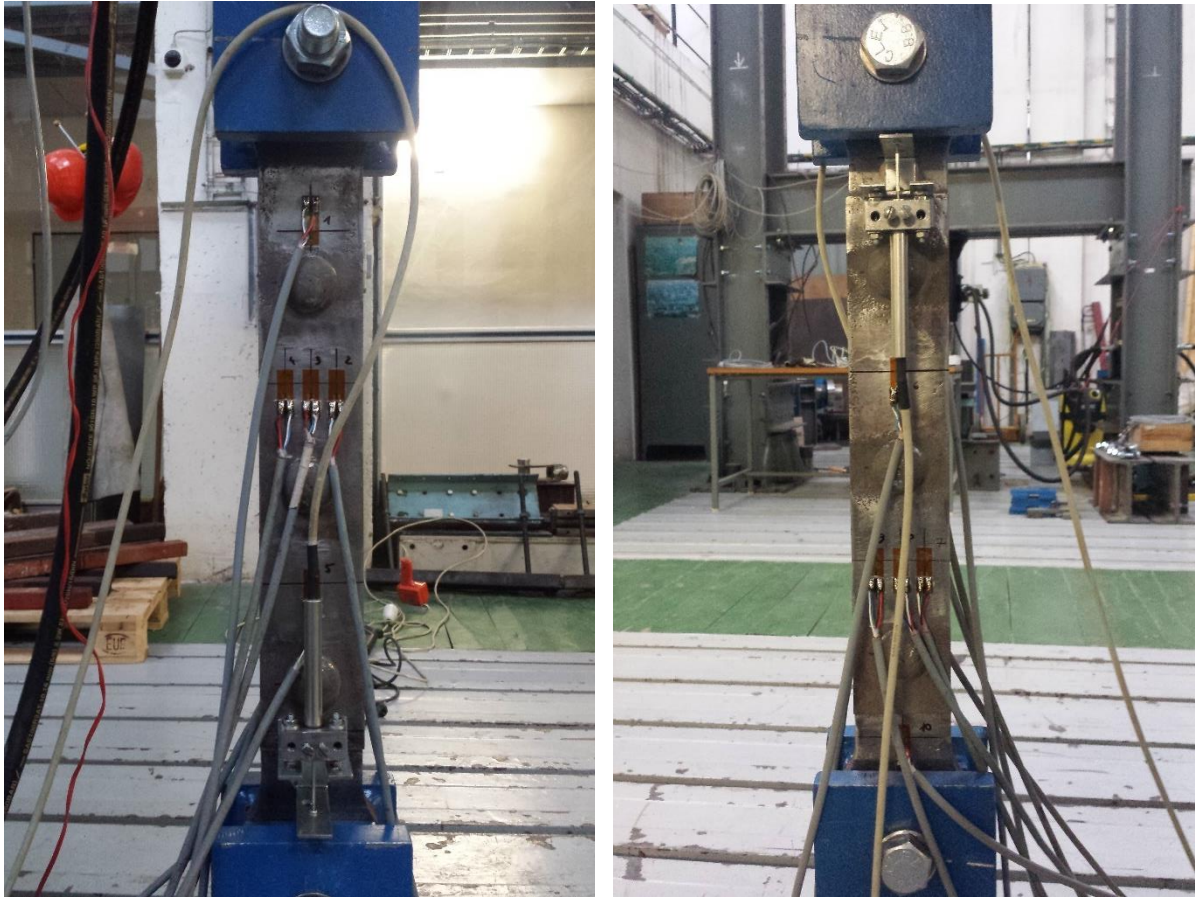
Fig. 53 Tested sample instrumented with sensors (strain gauges and displacement sensors). Tested sample is fixed by the fixing device
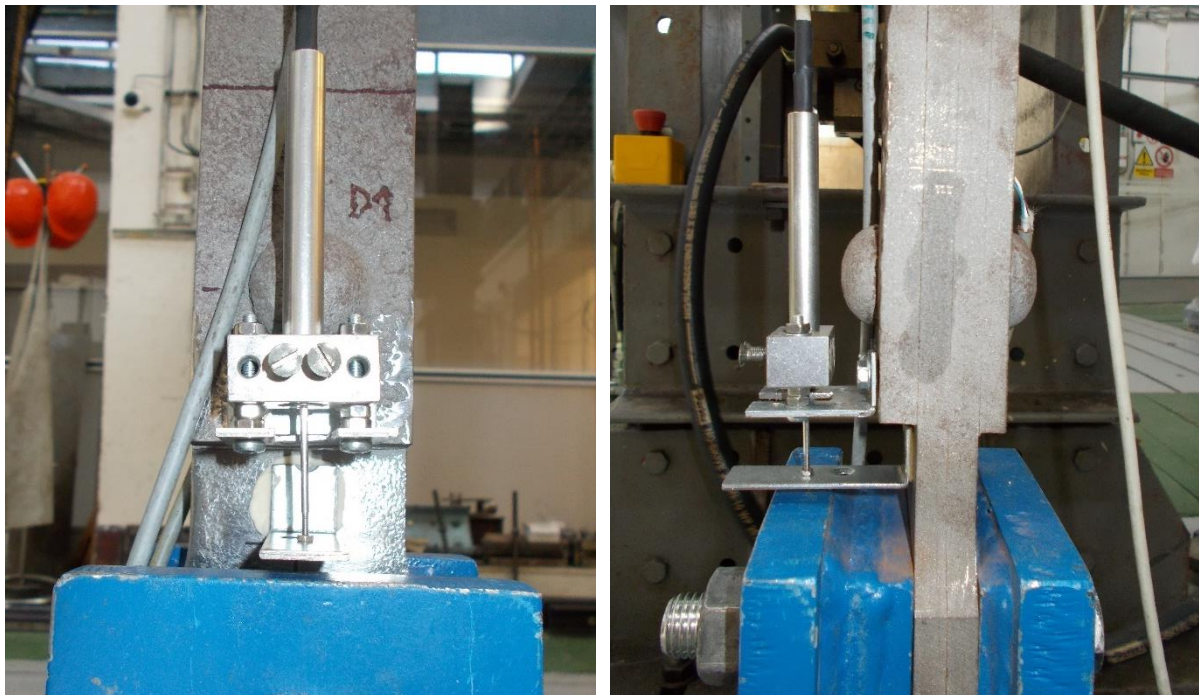

Fig. 54 Detail of fixing of displacement sensors

2nd phase samples

All the other samples (totally 9 samples) were categorized as 2nd phase samples. Unlike the previous group, in this case just 2 strain gauges were installed in the middle of the gap between rivets on the bottom and upper side of the sample (S1+S2). The number and the position of the displacement sensors correspond fully to the previous case.

HBM strain gauges were used (1-LY11-1.5/120, 1-LY11-10/120) together with displacement inductive sensors (LVDT) Micro Epsilon of type DTA-5D-CA with nominal displacement ± 5 mm (see Tab. 13). The indication and the presence of a fatigue crack during the experiments were detected by visual inspection.

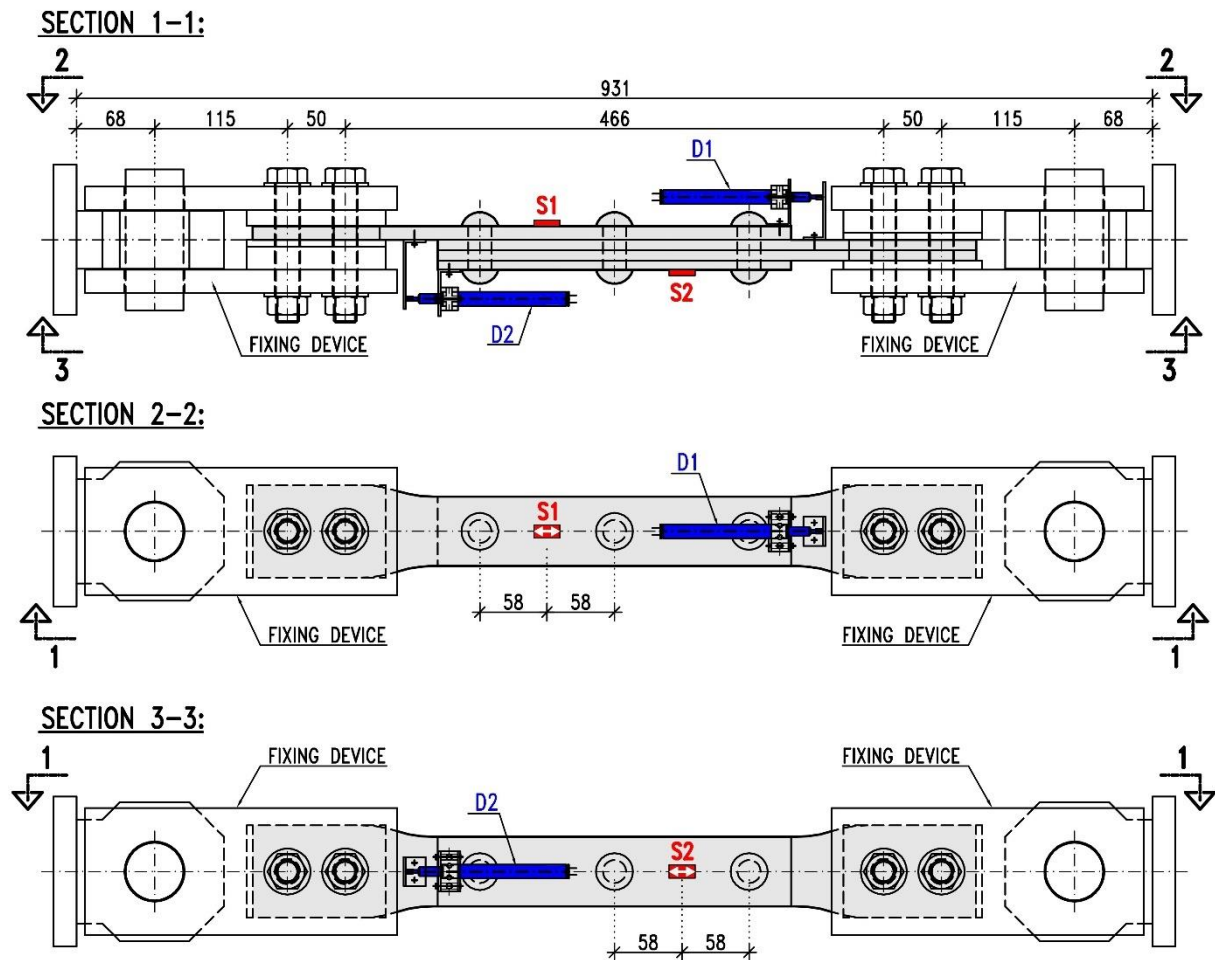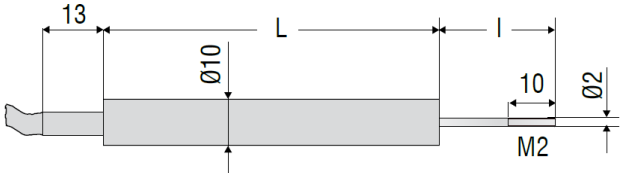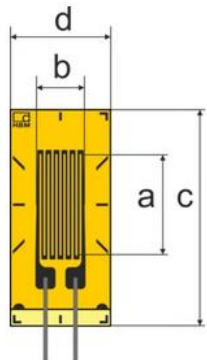The diagram in the Fig. 55 shows a tested sample equipped with the measuring sensors.

Fig. 55 2nd phase samples - position of the sensors and the fixing device

Tab. 13 Table of used sensors for experimental fatigue test

Displacement sensor	
Type of displacement sensor:	Displacement inductive sensor (LVDT) Micro Epsilon, type DTA-5D-CA
Strain gauge	
Type of strain gauge:	HBM 1-LY11-1.5/120
	HBM 1-LY11-10/120

4.2.2. Test arrangement and process of the tests

The document IRS 77802 [35] recognises two groups of details sensitive to fatigue damage: (1) Fatigue Sensitive Details and (2) Fatigue Susceptible Details. In this document, 3 groups of significant fatigue sensitive details occurring in non-welded structures are distinguished. These are groups W I, W II and W III, each of which corresponds to a permissible stress range, which is furthermore different for different steel types (see Tab. 14). Group W I corresponds to the imperforated construction parts. Group W II includes imperforated construction parts but containing corrosion pits, riveted joints with cover plates on both sides, continuous riveted connections of web and flange angle of the beam, and also continuous riveted connections of flange angle and flange of the beam. The fatigue sensitive detail group W III includes riveted connections of truss members, riveted connections with cover plates only on one side, riveted connections of bracing members with tension flange of the beam and finally members with strengthening plates.

Tab. 14 Groups of fatigue-sensitive details in non-welded structures [35]

Steel	WI	WII	WIII
Wrought iron and mild steel	112 MPa	85 MPa	71 MPa
Steel St 37 / 52	163 MPa	122 MPa	100 MPa

Fatigue susceptible details are considered to be more at risk of a rapid fatigue failure than the Fatigue Sensitive Details. Typical Fatigue Susceptible Details are areas in the vicinity of modifications to the structure, areas in the vicinity of welded repairs and attachments, flame cut holes or parts, notched parts, areas of severe corrosion or holing or areas of local damage.

The tested construction detail was considered to be a bending detail category 71, which corresponds to group WIII of fatigue sensitive details according to IRS 77802 [35]. The tested sample simulates the connection of the truss members, for example: the connection of the bracing diagonal or the connection of the diagonal and the web of the flange of the truss riveted girder. However due to the presence of corrosion weakening on the top surface of the upper plate (corrosion weakening especially in form of corrosion pits around the riveted joint), the tested detail may be considered as a fatigue susceptible detail [35].

It was assumed that during the tests a fatigue crack occurs on the upper single sheet in the cross-section containing a hole for a rivet (see Fig. 56). The original thickness of the uncorroded sheet was 12 mm; however, the geometry changed with various levels of corrosion weakening of the tested sample.
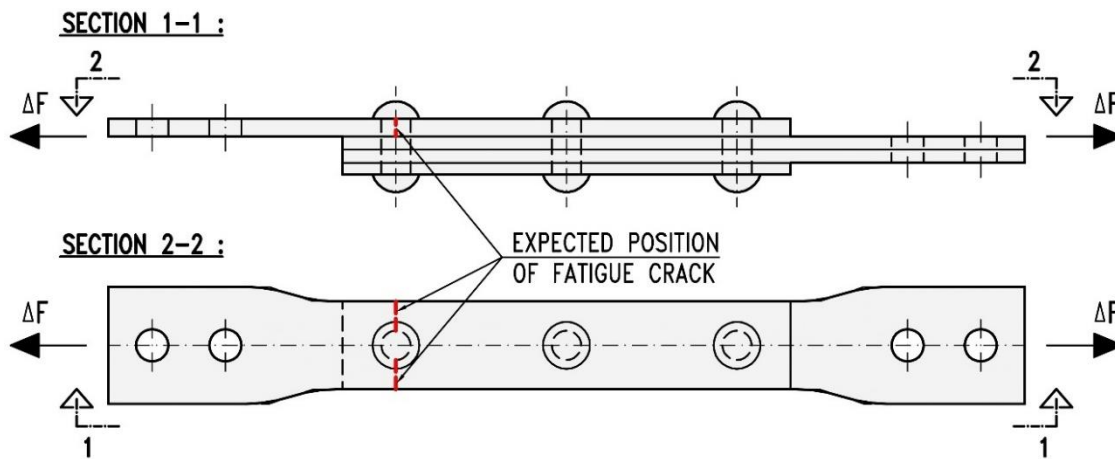

Fig. 56 Expected position of crack on tested samples

With respect to the duration of the fatigue experiments, the general characteristics of the load in tension were as follows:

Load frequency:	$f = 5.0 \, Hz$
Minimum stress:	$\sigma_{min} = 3 \, MPa$
Maximum stress:	$\sigma_{max} = 183 \, MPa$
Stress range:	$\Delta\sigma = \sigma_{max} - \sigma_{min} = 183.0 - 3.0 = 180.0 \, MPa$
Stress amplitude:	$\sigma_a = (\sigma_{max} - \sigma_{min})/2 = (183.0 - 3.0)/2 = 90 \, MPa$
Mean stress:	$\sigma_m = (\sigma_{max} + \sigma_{min})/2 = (183.0 + 3.0)/2 = 93.0 \, MPa$

If there was loss of material on the upper sheet, the value of the loading force was changed according to the level of corrosion (in cases where the cross-section area was smaller than in the case of the uncorroded specimen). With this approach, the values of the stress range were almost the same for all tested samples, and it was possible to observe the influence of irregularities of the corroded surface and the presence of corrosion pits on the number of loading cycles after which the crack occurred and the influence on the rate of crack growth.

To fulfil the stress characteristics, the following load values were prescribed for corroded and uncorroded specimens (see Tab. 15):

Tab. 15 Characteristics of the fatigue load for various sets of samples

Fatigue load characteristics						
Set of samples according to the corrosion level of the upper sheet	Minimum force	Maximum force	Force range	Force amplitude	Mean force	Frequency
	F_{min} [kN]	F_{max} [kN]	ΔF [kN]	F_a [kN]	F_{mean} [kN]	f [Hz]
1 No corrosion	4.5	91.0	86.5	43.3	47.8	5.0
2 Medium level	3.0	82.0	79.0	39.5	42.5	5.0
3 High level	3.0	74.0	71.0	35.5	38.5	5.0

Due to unsymmetrical shape of sample, there is a small effect of bending moment that causes additional normal stresses. However, the shape of testes samples was chosen to minimize this effect of bending moment. For this reason, the bottom plate was shorter so it was not held in the test equipment during the test. As a result, the value of the eccentricity in the connection and the effect of the bending moment were thus reduced Also, the fixing of samples was designed to reduce the eccentricity in connection in order to minimize the additional stresses caused by bending.

Fixing device

A special device was manufactured for fixing the samples during the experimental fatigue test (see Fig. 57, Fig. 58 and Fig. 59). Each end of the sample was fastened with 2 bolts to a couple of steel sheets 20 mm in thickness. The gap between these sheets and the sample was filled with other steel plates to get the required geometry to fix them properly to the tested machine. The materials used for fixing the device were: steel sheets: steel of grade S355J+N; bolts (M20), nuts and washers: steel 8.8.

The tested specimens fixed with this equipment were fastened to the testing machine with pins 50 mm in diameter (see Fig. 60). Loading frame ZU 200-1350 was the machine used for testing. It is a dynamic loading machine with the maximum dynamic range of loading force 0-160 kN and maximum loading frequency 5 Hz.
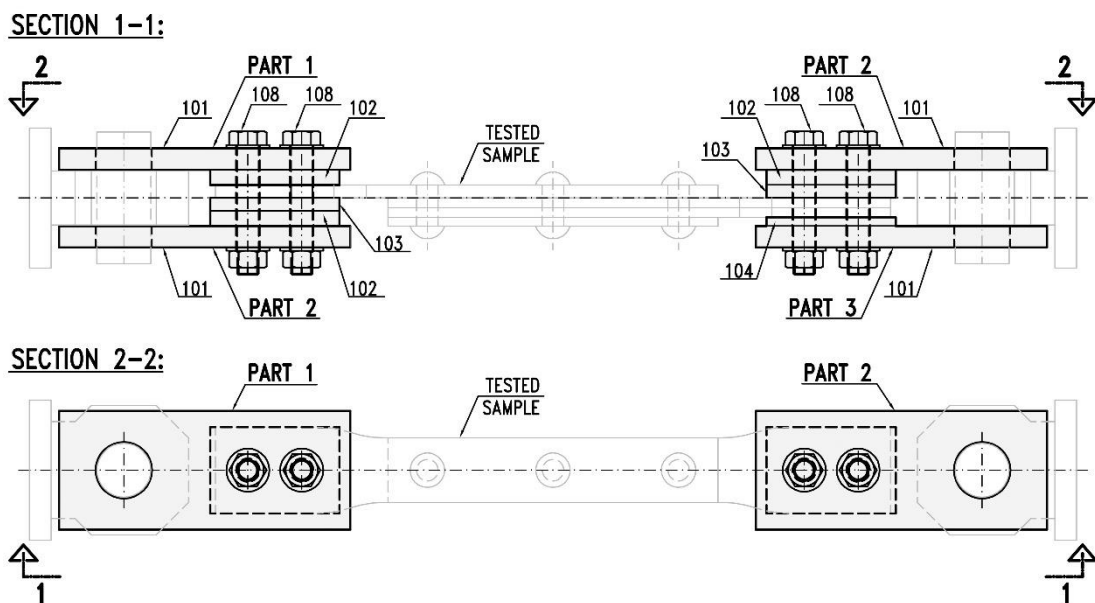

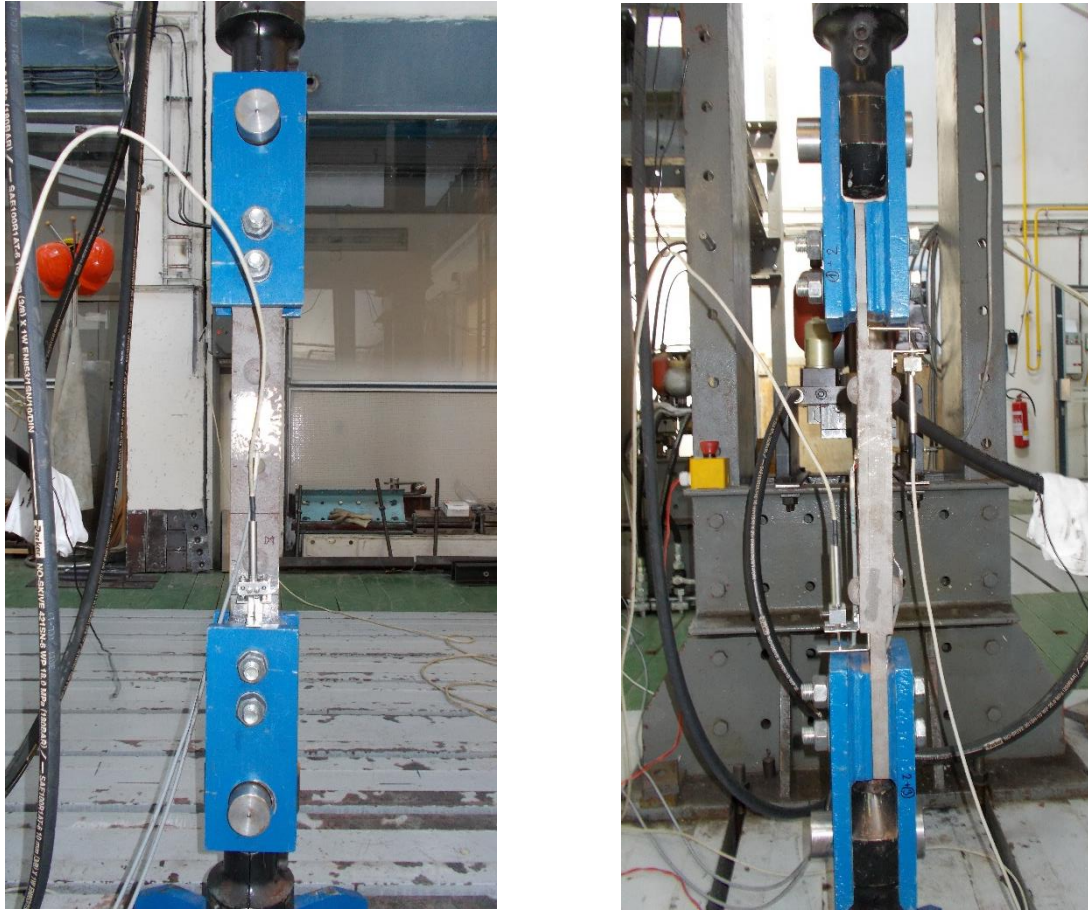*Fig. 57 Fixing device for fixing of tested samples during experimental test (drawing)*

Fig. 58 Fixing device for fixing of tested samples during experimental test (photo)

Fig. 59 Arrangement of the fatigue test; the specimen fixed by the fixing device
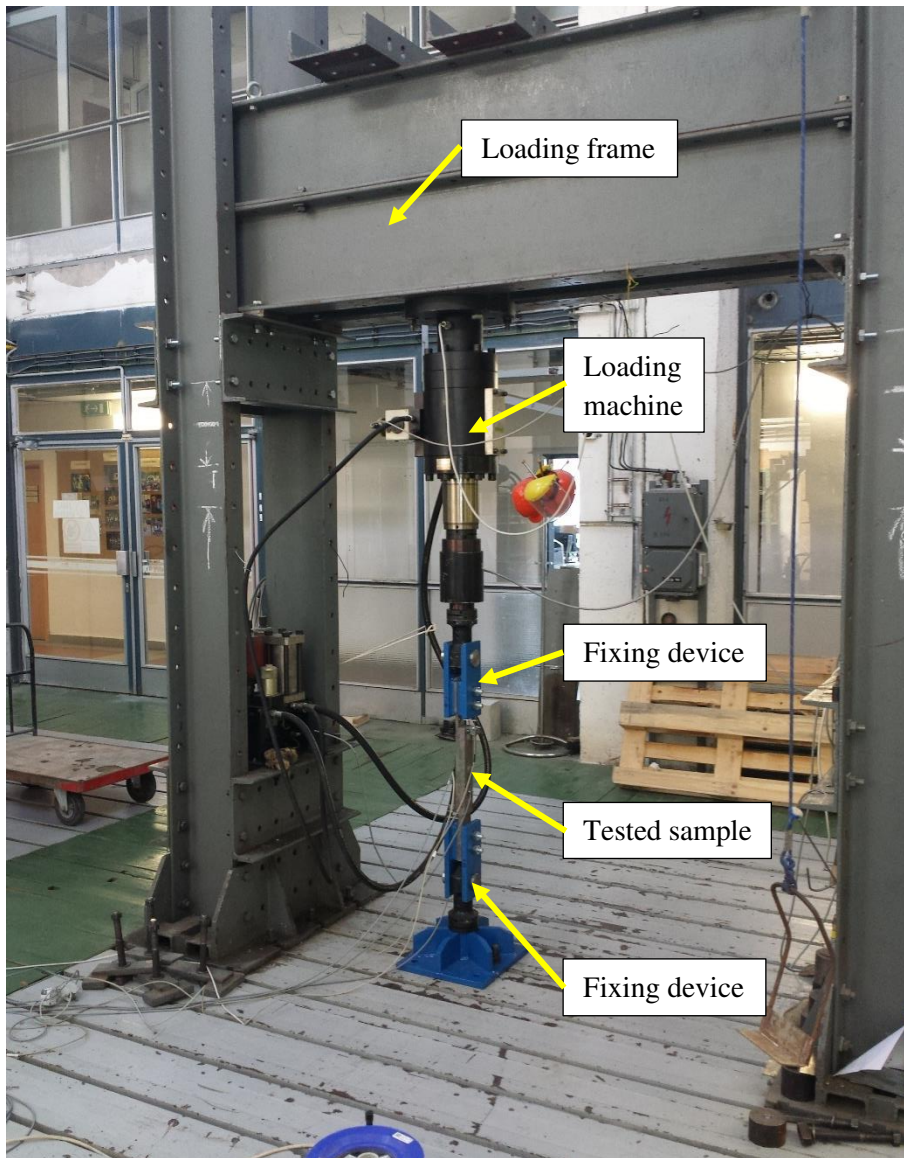
Fig. 60 Complete test set-up (tested sample, fixing device, loading frame)

End of the fatigue test

The fatigue test was considered to be ended if:

1. a fatigue crack initiated and had grown to the critical length – in our case, the critical length was considered to have been reached at the moment when the tested sample failed (we observed the number of cycles after which the crack occurred and the number of cycles after which the crack reached its critical length (= failure of the sample)), or

2. there was a large displacement, which would indicate bearing failure of connected/connecting part due to bearing from rivet holes (displacement was measured by displacement sensors), or

3. any rivet in the connection was damaged (shear failure mode of the rivet).

The values of measured data (relative strain and displacement) were observed continuously in a real time and recorded in period of each 10000 cycles in the phase before the crack initiation and then continuously until the collapse of sample occurred. The frequency of record was set to 100 Hz. Type of the measuring device was Dewetron Dewe 5000.

4.2.3. Control static load test of the tested specimen

A static load test was carried out on a non-corroded tested specimen S1.2. The test was carried out to determine the load response of the tested specimen. The specimen was loaded with a tensile force that gradually increased from 0 to 80 kN over a period of 30 seconds. The applied force of 80 kN was maintained for 30 seconds. Then, gradually, the specimen was completely unloaded to 0 kN over the next 30 seconds. This loading step was performed twice.

The loaded specimen S1.2 was equipped with a large number of sensors. A total of 10 strain gauges were arranged on the surface of sample to measure the relative strain during the load tests. According to Fig. 52, five gauges (S1-S5 and S6-S10) were located in the middle of the gaps between rivets on the bottom and upper side of the sample (a total of 2x5=10 gauges). The tested samples was also equipped with a couple of displacement sensors (D1 and D2). Both sensors measured the movement of the upper sheet towards the rest of the specimen, as shown in Fig. 52

The control static load test was performed on the same machine as the subsequent fatigue tests. The values of measured data (relative strain and displacement) were observed continuously in a real time and the data were recorded with the sampling rate 100 Hz (see Fig. 61 and Fig. 62). Type of the measuring device was Dewetron Dewe 5000. The measured data were compared with the results obtained from the numerical model of the tested sample (see Tab. 16 and Tab. 17).
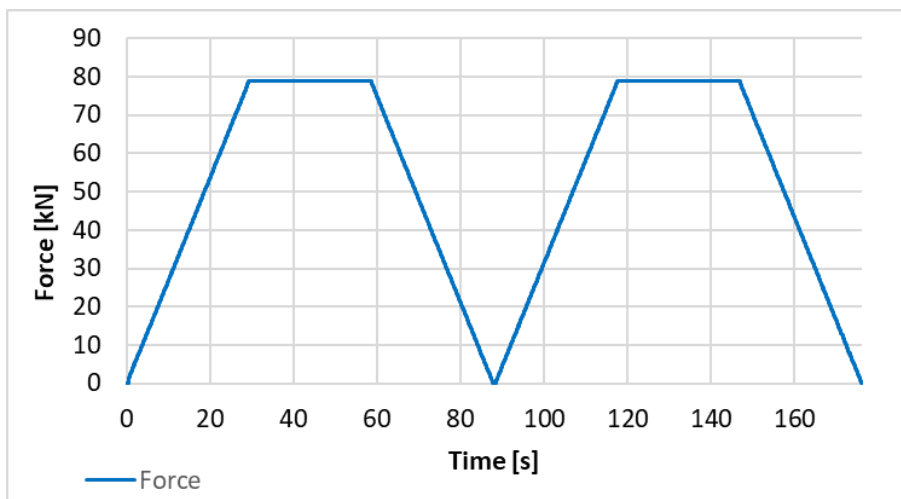

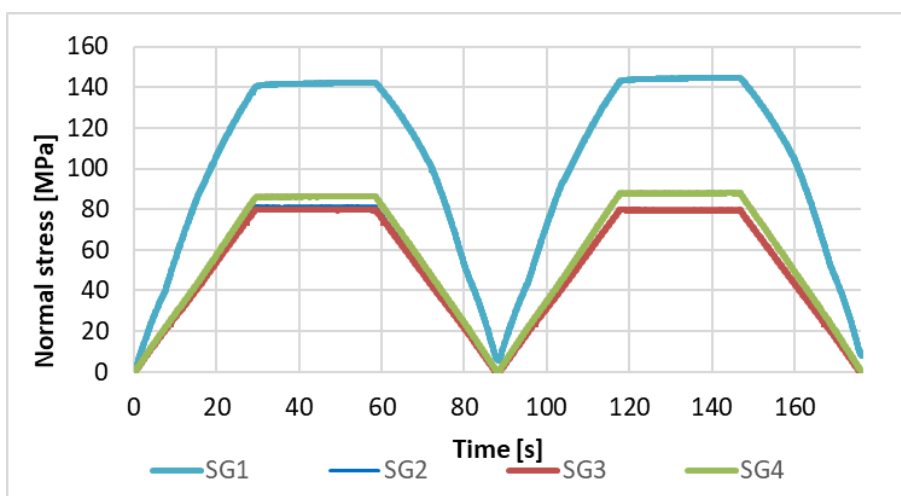Fig. 61 Loading force during control static load test of sample S1.2

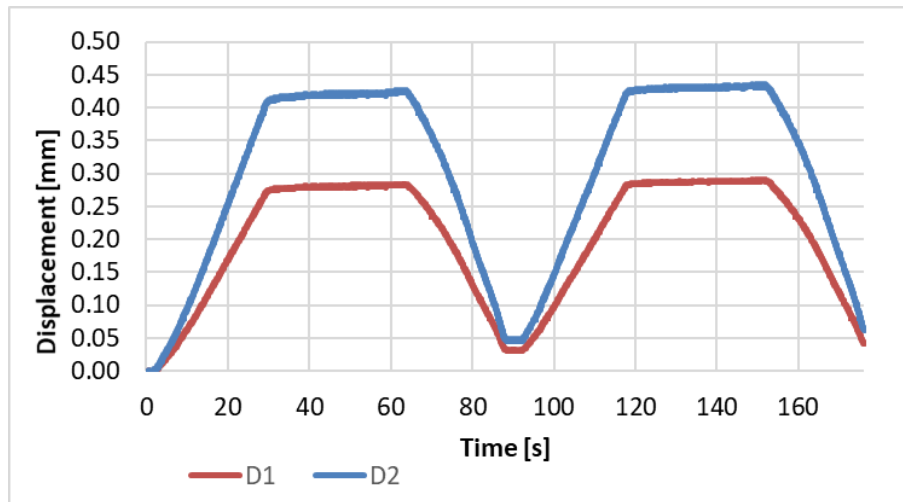Fig. 62 Normal stress during control static load test of sample S1.2

Fig. 63 Measured displacement during control static load test of sample S1.2

Tab. 16 Values of normal stresses measured during the control static load test of sample S1.2 and comparison with values obtained from numerical model

Observed place	Loading force	Normal stress		
		Experiment	Numerical model	Comparison
	F [kN]	σ_{exp} [MPa]	σ_{mod} [MPa]	$\sigma_{exp} / \sigma_{mod}$ [-]
SG1	80	145	152	0.95
SG2	80	75	83	0.90
SG3	80	81	86	0.94
SG4	80	80	88	0.91
SG5	80	88	86	1.02
SG6	80	8	18	0.44
SG7	80	15	24	0.63
SG8	80	16	26	0.62
SG9	80	18	24	0.75
SG10	80	70	79	0.89

Tab. 17 Values of displacements measured during the control static load test of sample S1.2 and comparison with values obtained from numerical model

Observed place	Loading force	Displacement		
		Experiment	Numerical model	Comparison
	F [kN]	u_{exp} [MPa]	u_{mod} [MPa]	u_{exp} / u_{mod} [-]
D1	80	0.29	0.31	0.94
D2	80	0.42	0.45	0.93

4.3. Results of measurement

The failure mode of the tested samples was as had been assumed. The first crack in all cases occurred in place of hole for the first rivet, in weakened cross-section area. The crack propagation was in direction perpendicular to main stresses. The samples became damaged after the crack reached its critical length and the weakened cross-section was not able to transfer the loading force. An example of a damaged specimen is shown in Fig. 64. Number of cycles for crack propagation are stated in Tab. 20.
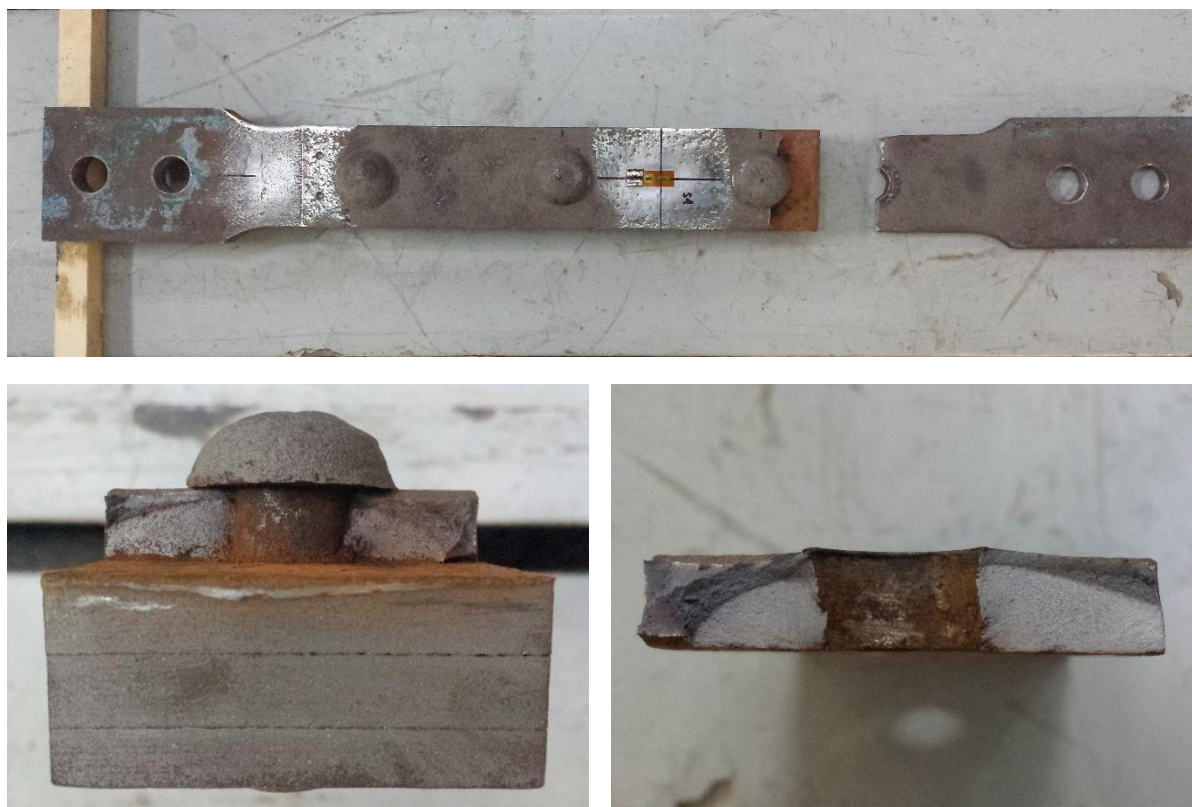

Fig. 64 A typical fatigue damage to tested sample

Tab. 18 Failure mode of tested samples

Group of samples	Sample	Failure mode	Number of cycles till failure
1st group: Without corrosion	S1.1	Fatigue crack in the cross-section weakened by hole for the 1st rivet	184452
	S1.2	Fatigue crack in the cross-section weakened by hole for the 1st rivet	251053
	S1.3	Fatigue crack in the cross-section weakened by hole for the 1st rivet	186320
	S1.4	Fatigue crack in the cross-section weakened by hole for the 1st rivet	300140
2nd group: Medium level of corrosion	S2.1	Fatigue crack in the cross-section weakened by hole for the 1st rivet	179633
	S2.2	Fatigue crack in the cross-section weakened by hole for the 1st rivet	161769
	S2.3	Fatigue crack in the cross-section weakened by hole for the 1st rivet	222551
3rd group: High level of corrosion	S3.1	Fatigue crack in the cross-section weakened by hole for the 1st rivet	139313
	S3.2	Fatigue crack in the cross-section weakened by hole for the 1st rivet	92003
	S3.3	Fatigue crack in the cross-section weakened by hole for the 1st rivet	184452

Tab. 13 (continued)

Group of samples	Sample	Failure mode	Number of cycles till failure
4th group: Samples with missing rivet	S4.1	Fatigue crack in the cross-section weakened by hole for the 1st rivet	104000
	S4.2	Fatigue crack in the cross-section weakened by hole for the 1st rivet	171843
	S4.3	Fatigue crack in the cross-section weakened by hole for the 1st rivet	313553

Fig. 66 shows the course of the normal stresses in selected places, where the strain gauges (SG2, SG3, SG7 and SG 10) were positioned during the test on the 1st phase corroded sample S3.2. It can be seen that the minimum and maximum stress values are almost constant until the initiation and propagation of a fatigue crack. In this case, the fatigue crack appeared after approximately 41,000 cycles, and it began to change in length rapidly after 50,000 cycles. Fig. 67 shows the dependence of the measured displacements and the number of cycles. In this case, too, the values started to change significantly with the growth of the crack.
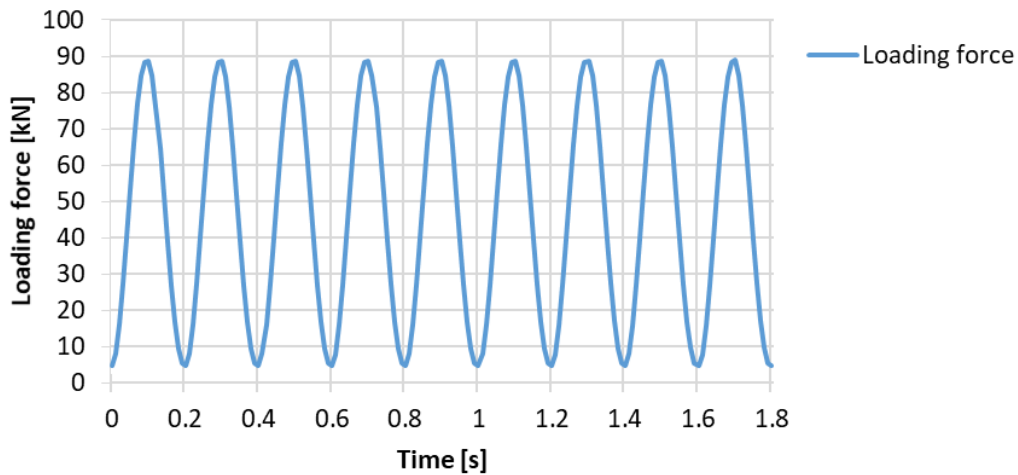

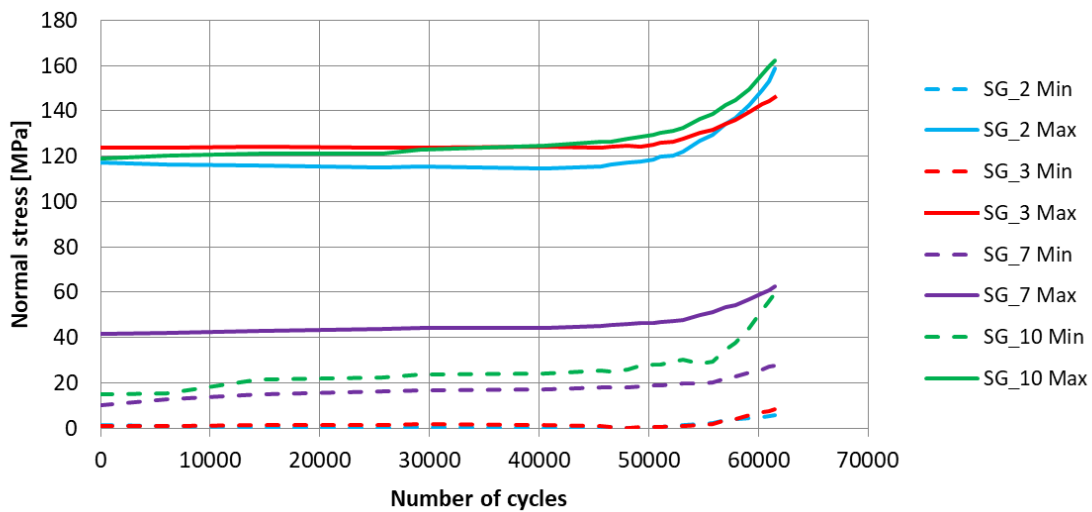*Fig. 65 An example of the loading process of specimen S1.1 during a fatigue test*

Fig. 66 Change of normal stresses in the course of the test (sample S3.2)
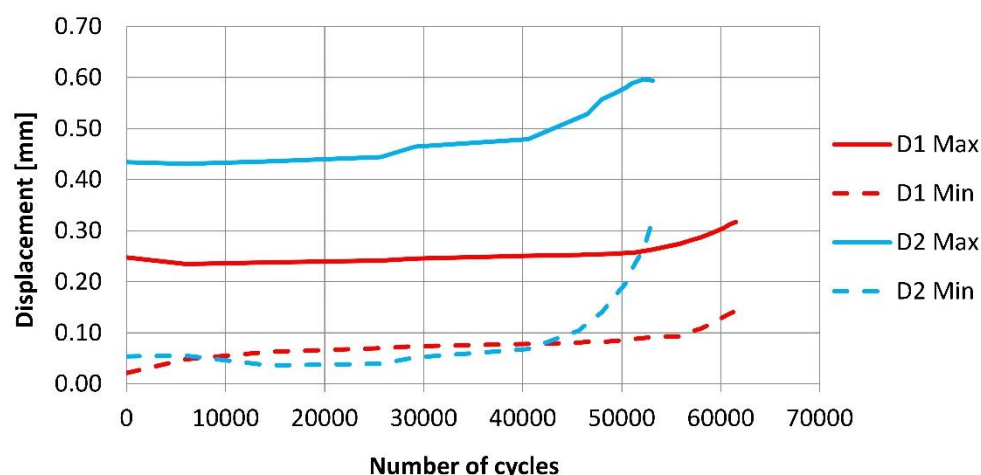
Fig. 67 Change of measured displacements in the course of the test (sample S3.2)

The real characteristics of the laboratory fatigue load and the number of cycles till total failure of the samples are shown in Tab. 19. The cross-section area A_{net} corresponds to the actual cross-section area of the scanned samples. The values of the stress range were almost the same for all samples - nearly 180 MPa. The assumption of the bending detail category for an uncorroded tested sample was 71 MPa, which corresponds to 123,000 cycles for stress range 180 MPa. The measured number of cycles was higher for uncorroded samples, and the ratio of measured-to-expected was equal to 1.5-2.4. The number of cycles for samples with a medium level of corrosion and with a high level of corrosion was also variable, but was generally lower. The ratio for medium level was: 1.3-1.8, and for high level the ratio was: 0.75-1.5.

Tab. 19 Results of the experimental fatigue test

Number	Sample	Characteristics of the real load						
		Minimum force	Maximum force	Force range	Cross-section area	Stress range	R-ratio	Number of cycles till failure
		F_{min}	F_{max}	ΔF	A_{net}	$\Delta\sigma$	R	N
		[kN]	[kN]	[kN]	[mm^2]	[MPa]	[-]	[cycles]
1	S1.1	3.84	88.84	85.00	464.9	182.8	0.043	184452
2	S1.2	3.84	94.14	90.30	501.4	180.1	0.041	251053
3	S1.3	4.14	92.44	88.60	486.9	182.0	0.045	186320
4	S1.4	3.77	89.74	85.90	483.1	177.8	0.042	300140
5	S2.1	3.62	84.34	80.50	452.0	178.1	0.043	179633
6	S2.2	3.70	80.14	76.30	427.5	178.5	0.046	161769
7	S2.3	3.68	84.34	80.50	453.5	177.5	0.044	222551
8	S3.1	2.72	71.34	67.50	380.2	177.6	0.038	139313
9	S3.2	2.75	78.94	75.10	411.3	182.6	0.035	92003
10	S3.3	2.60	83.14	79.30	448.0	177.0	0.031	182980
11	S4.1	4.25	92.94	89.10	496.2	179.6	0.046	104000
12	S4.2	4.46	95.64	91.80	509.2	179.5	0.047	171843
13	S4.3	4.92	90.54	86.70	482.9	179.6	0.054	313553

Tab. 20 and Fig. 68 summarize the number of cycles that were needed for the initiation of a crack, the number of cycles that were necessary for crack growth (propagation) and the number of cycles after which damage to the samples occurred. The ratio of the number of cycles for crack growth and for crack initiation was around 0.2 for the tested type of specimens. In comparison, the ratio of the number of cycles for crack growth and crack initiation is around 0.5 or higher for large specimens. This means that the time for crack initiation and growth is approximately the same for large samples.

According to the results stated in Tab. 20 it can be seen that there is a **downward tendency in the number of cycles for crack growth**. The **number of cycles for crack growth decreases** slightly **with the increase in corrosion weakening**. This phenomenon is very well observed on average values of number of cycles for individual sets (S1, S2 and S3). However, this effect is not so evident for individual samples, because of the fluctuation in the numbers in each set.

The faster crack initiation in samples weakened by corrosion is mainly due to the surface roughness of the tested sample. The irregularities in the form of corrosion pits cause a local increase in stress in the loaded element and at the same time the corrosion pit is the place where the fatigue crack is likely to occur first.

Tab. 20 Number of cycles needed for crack initiation and growth

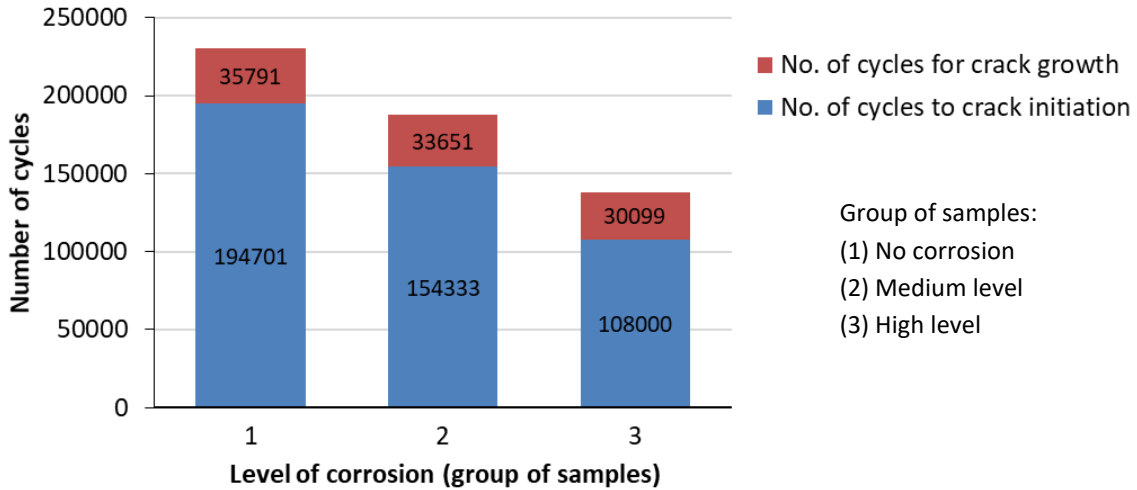| Sample	d_A	No. of cycles to crack initiation (rounded)		No. of cycles for crack growth (propagation)		No. of cycles to sample damage (failure)	
	[-]	N_i [cycles]		N_p [cycles]		N_f [cycles]	
S1.1	0.005	153000	average:	31452	average:	184452	average:
S1.2	0.001	214000		37053		251053	
S1.3	0.004	143314	194701	43006	35791	186320	230491
S1.4	0.002	268489		31651		300140	
S2.1	0.058	145000	average:	34633	average:	179633	average:
S2.2	0.127	125000		36769		161769	
S2.3	0.080	193000	154333	29551	33651	222551	187984
S3.1	0.229	107000	average:	32313	average:	139313	average:
S3.2	0.174	61000		31003		92003	
S3.3	0.095	156000	108000	26980	30099	182980	138099

Fig. 68 Number of cycles for crack initiation and growth

Tab. 21 compares the number of cycles for each set of samples. The ratio of the number of cycles for crack growth (Np) to the number of cycles required for crack initiation (Ni) is around 0.2 (0.18 for samples without corrosion weakening and 0.28 for samples with high level of corrosion weakening). Comparing the number of cycles required for crack formation between the different sets, it can be observed that for the samples with medium corrosion level, on average 79% of the number of cycles as for the samples without corrosion weakening were required, and for the samples with high corrosion weakening, on average only 55% of the number of cycles as for the samples without corrosion weakening were required.

Tab. 21 Comparison of the number of cycles for each set of samples

Set of samples according to the corrosion level of the upper sheet		Cycles to crack initiation		Cycles for crack growth		Cycles to sample damage		-
		N_i		N_p		N_f		N_p / N_i
		[cycles]		[cycles]		[cycles]		[-]
1	No corrosion	194701	-	35791	-	230491	-	0.18
2	Medium level	154333	$N_{i(2)} / N_{i(1)}$ 0.79	33651	$N_{p(2)} / N_{p(1)}$ 0.94	187984	$N_{f(2)} / N_{f(1)}$ 0.82	0.22
3	High level	108000	$N_{i(3)} / N_{i(1)}$ 0.55	30099	$N_{p(3)} / N_{p(1)}$ 0.84	138099	$N_{f(3)} / N_{f(1)}$ 0.60	0.28

5. Relationship between corrosion loss and fatigue life

The chapter deals with the description of the relationship between different levels of corrosion weakening and fatigue life of the tested samples. In the first stage, simplified relationships are presented which only take into account the change in cross-sectional area due to corrosion weakening.
The second approach is slightly more complex and takes into account both uniform and non-uniform corrosion components and their influence on the fatigue life of the elements.

Fatigue life is the expected time period until the fatigue failure occurs under the action of the design spectrum. The fatigue life is characterized by the fatigue strength curve, which is a quantitative relationship between the stress range and the number of cycles to fatigue failure.
A detail category is a numerical designation of a particular structural detail subjected to a variable stress. This designation determines the fatigue strength curve to be used for fatigue design. The detail category number $\Delta\sigma_c$ indicates the reference fatigue strength at $N_C = 2 \cdot 10^6$ cycles.

Characteristics of fatigue strength:

$\Delta\sigma_c$ detail category/reference value of the fatigue strength at $N_C = 2 \cdot 10^6$ cycles
$\Delta\sigma_D$ fatigue limit for constant amplitude stress ranges at the number of cycles N_D
$\Delta\sigma_L$ cut-off limit for stress ranges at the number of cycles N_L
m slope of the fatigue strength curve

The document IRS 77802 [35] recognises two groups of details sensitive to fatigue damage: (1) Fatigue Sensitive Details and (2) Fatigue Susceptible Details. In this document, 3 groups of significant fatigue sensitive details occurring in non-welded structures are distinguished. These are groups W I, W II and W III, each of which corresponds to a permissible stress range, which is furthermore different for different steel types (see Tab. 14). The document considers for non-welded construction details the slope of the fatigue curve with $m = 5$ (see Fig. 69).
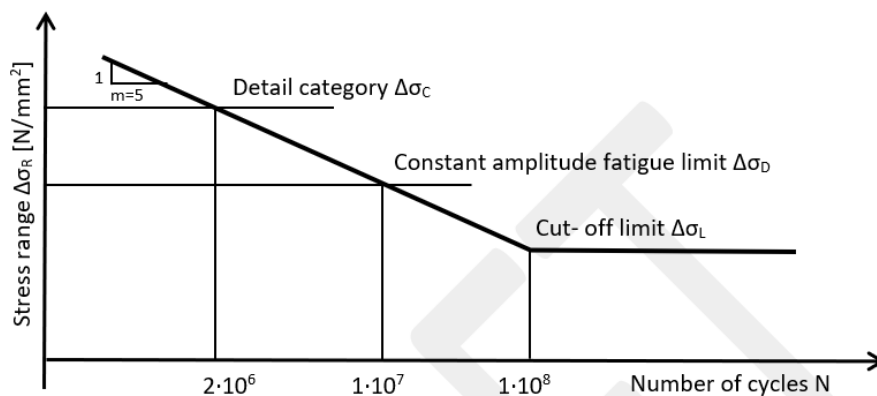

Fig. 69 Shape of fatigue strength curve for unwelded details according to IRS 77802 [35]

When considering the slope of the fatigue curve with $m = 5$ for non-welded details, the characteristics of fatigue strength are according to IRS 77802 [35] as follows:

- detail category/reference value
  of the fatigue strength $\Delta\sigma_C$ at $N_C = 2 \cdot 10^6$ cycles

- constant amplitude fatigue limit $\quad \Delta\sigma_D = \left(\dfrac{2}{10}\right)^{\frac{1}{5}} \cdot \Delta\sigma_C \qquad$ at $\quad N_D = 1 \cdot 10^7$ cycles $\qquad$ *(16)*

- cut-off limit $\quad \Delta\sigma_L = \left(\dfrac{1}{10}\right)^{\frac{1}{5}} \cdot \Delta\sigma_D \qquad$ at $\quad N_L = 1 \cdot 10^8$ cycles $\qquad$ *(17)*

Then the design life time N_R expressed as number of cycles related to a constant stress range $\Delta\sigma_R$ can be calculated as:

$$N_R = 2 \cdot 10^6 \cdot \left(\frac{\Delta\sigma_C}{\Delta\sigma_R}\right)^m \qquad \text{if} \qquad \Delta\sigma_R \geq \Delta\sigma_D \qquad\qquad (18)$$

$$N_R = 1 \cdot 10^7 \cdot \left(\frac{\Delta\sigma_D}{\Delta\sigma_R}\right)^m \qquad \text{if} \qquad \Delta\sigma_D > \Delta\sigma_R \geq \Delta\sigma_L \qquad\qquad (19)$$

$$N_R = \infty \qquad\qquad\qquad\qquad \text{if} \qquad \Delta\sigma_R < \Delta\sigma_L \qquad\qquad (20)$$

5.1. Simplified method

5.1.1. New formula development

Laboratory test was performed mainly to find out whether or not there is any change in the bending detail category when there is a corrosion weakening. In most cases, corrosion weakening consists of a uniform part and an irregular part. The irregular part means a locally increased depth of corrosion in the form of corrosion pits. As is known, surface irregularities have negative effects on the course and the distribution of the stresses in a member. The results of the test are shown in Fig. 70 in the form of the relationship between the number of cycles and the set of samples. There is a downward trend in number of cycles, accompanied by an increasing level of corrosion.
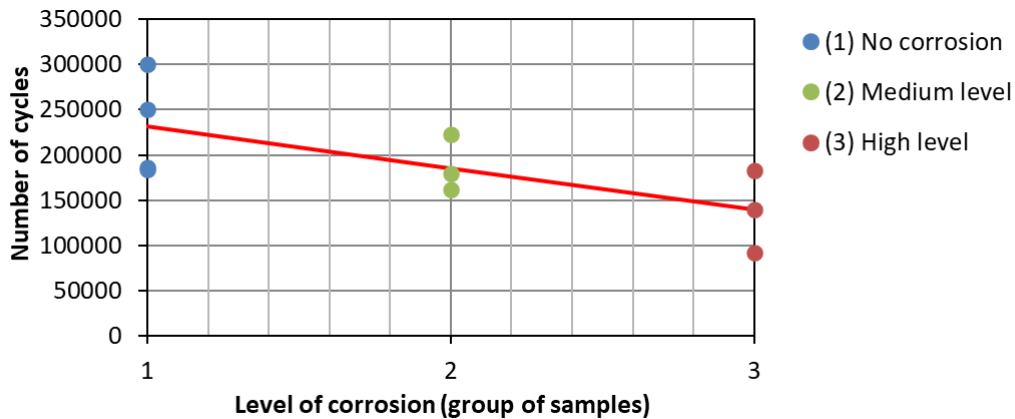

Fig. 70 Dependence of the number of cycles on the level of corrosion

The tested construction detail was considered to be a bending detail category 71, which corresponds to group WIII of fatigue sensitive details according to IRS 77802 [35]. The tested sample simulates the connection of the truss members, for example: the connection of the bracing diagonal or the connection of the diagonal and the web of the flange of the truss riveted girder.

Tab. 22 shows that the measured number of cycles was higher than the assumed number, which means that the real bending detail category must also be higher. The real parameters (geometry, load) were therefore considered for a calculation of the real bending detail category of the tested riveted joint. Detail category was based on the number of cycles that corresponded to total failure of the sample. The calculated bending detail category for uncorroded samples S1.1, S1.2, S1.3 and S1.4 reached a value of 82.5 MPa or higher, the average value was 87.4 MPa and the value of 95% quantile was 79 MPa. To fully classify the test specimens in terms of the category of detail, a series of fatigue tests would need to be performed for different levels of stress range. In terms of technological and time requirements, tests for all specimens were performed for only one stress range level (approximately 180 MPa). For specimens with corrosion loss, the average bending detail category value for a medium level of corrosion was 80.8 MPa, and for a high level of corrosion the average value was 72.7 MPa. In this case, too, a downward tendency can be observed – the higher the corrosion loss, the lower the bending detail category, in terms of average values. The evaluation was based on the fatigue curve for non-welded details taken according to IRS 77802 [35] (see introductory part of Chapter 5).

Tab. 22 Bending detail category of the tested samples

Number	Sample	Force	Stress	Cycles	Normal stress detail category		
		Δ_F [kN]	$\Delta\sigma$ [MPa]	N_i [cycles]	$\Delta\sigma_{c,R}$ [MPa]		
1	S1.1	85.0	182.8	184452	82.6	average:	95% quantile:
2	S1.2	90.3	180.1	251053	90.2		
3	S1.3	88.6	182.0	186320	82.5	**87.4**	**79.0**
4	S1.4	85.9	177.8	300140	94.5		
5	S2.1	80.5	178.1	179633	79.8	average:	95% quantile:
6	S2.2	76.3	178.5	161769	77.2	**80.8**	**75.1**
7	S2.3	80.5	177.5	222551	85.4		
8	S3.1	67.5	177.6	139313	73.1	average:	95% quantile:
9	S3.2	75.1	182.6	92003	65.4	**72.7**	**63.1**
10	S3.3	79.3	177.0	182980	79.8		
11	S4.1	89.1	179.6	104000	67.0	average:	95% quantile:
12	S4.2	91.8	179.5	171843	79.2	**81.0**	**60.9**
13	S4.3	86.7	179.6	313553	96.8		

Neglecting tested sample S3.3, the bending detail category value of which was deviated most from the other values, and using regression analysis, the dependence between the category of the detail and the change in cross-section area (see Fig. 71) can be expressed by a linear relation as (21) and (22):

$$\Delta\sigma_{c,R,50} = -108.54 \cdot d_A + 88.499 \qquad \text{[MPa]} \qquad (21)$$

$$\Delta\sigma_{c,R,95} = -185.90 \cdot d_A + 81.920 \qquad \text{[MPa]} \qquad (22)$$

After adjustment of the previous formula, the reduced bending detail category for sample with weakened cross-section can be determined by Eq. (23) and (24):

$$\Delta\sigma_{c,R,50} = \Delta\sigma_{c,50} \cdot (1 - 1.2264 \cdot d_A) \qquad [\text{MPa}] \qquad (23)$$

$$\Delta\sigma_{c,R,95} = \Delta\sigma_{c,95} \cdot (1 - 1.2264 \cdot d_A) \qquad [\text{MPa}] \qquad (24)$$

If we implement the reduction coefficient $c_{R,dA}$, then the mean value and 95% quintile value of reduced detail category for a corroded sample is computed according to Eq. (25) and Eq. (26), respectively:

$$\Delta\sigma_{c,R,50} = \Delta\sigma_{c,50} \cdot c_{R,dA} \qquad [\text{MPa}] \qquad (25)$$

$$\Delta\sigma_{c,R,95} = \Delta\sigma_{c,95} \cdot c_{R,dA} \qquad [\text{MPa}] \qquad (26)$$

The reduction coefficient $c_{R,dA}$ is calculated according to Eq. (27):

$$c_{R,dA} = (1 - 1.2264 \cdot d_A) \qquad [\text{-}] \qquad (27)$$

where: $\Delta\sigma_{c,50}$ is the mean value of original bending detail category of an uncorroded sample,

$\Delta\sigma_{c,95}$ is the 95% quintile value of original bending detail category of an uncorroded sample,

$c_{R,dA}$ is reduction coefficient,

d_A is the level of corrosion determined as the change in cross-section area for members loaded by axial force. In case of members loaded by bending moment or loaded by combination of bending moment and axial force, the level of corrosion is considered as change in cross-section area of assessed part of member.

Coefficient d_A takes into account the change in the cross-section area as a whole due to corrosion. However, it does not take into account the size and shape of individual surface irregularities. It means that the influence of irregularities of the corroded surface are not included in this calculation.
Surface irregularities may have negative effects on the course and the distribution of the stresses in a member. If the corroded surface is rough, the influence of irregularities is higher than in case of smooth surface. Then the initiation of fatigue crack might become earlier, after lower number of cycles.

Since the stated formulas are derived from the experimental tests introduced above, their applicability is limited to narrow members, i.e. to steel plates not more than 60 mm in thickness.
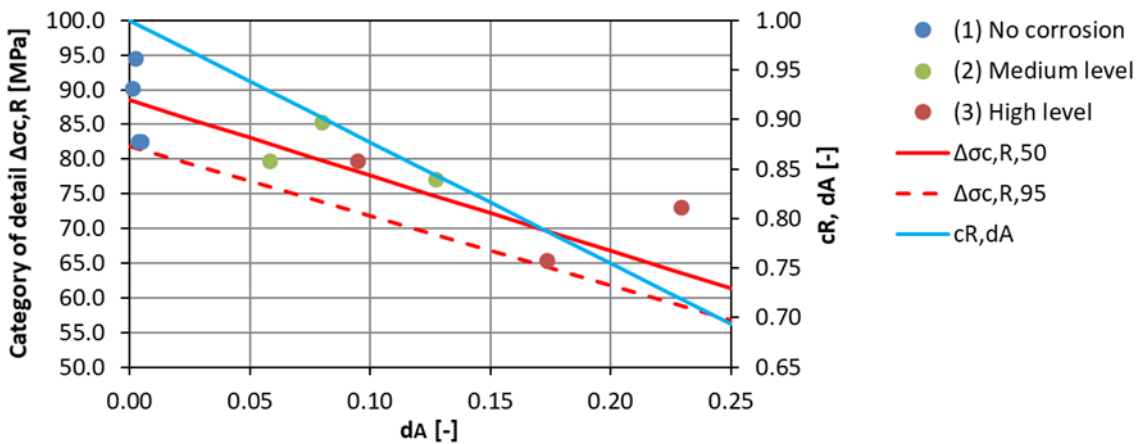

Fig. 71 Relation between bending detail category and level of corrosion weakening

The number of cycles from the time period of service life, caused by trains that came across the bridge, was disregarded, and was not taken into account. The main reason is that the railway track on which the bridge was situated falls into the lowest category in terms of the track operating load. This means that the operating load is lower than 1.825 million tons per 1 year. In fact, the traffic load on this track consists largely of passenger traffic. Passenger trains create a stress range in the lower flange of about 20 MPa, which is below the fatigue limit for the detail. The coefficient of fatigue damage was calculated using available information about the operating load, and the using the Palmgren-Miner rule. The value is D = 0.04 << 1 for the total service life of Holubov bridge, so its impact on the corrosion fatigue can be neglected here.

To find out the accuracy of the formula that has been developed, the Root Mean Square Error (RMSE) was used to calculate how much error there is between the predicted values and the observed values. For the bending detail category, the RMSE = 0.694 [-]. This error is due to the dispersion of the results from the experimental test, together with the fact that the combined effects of corrosion and fatigue phenomena are very complex. The value is therefore acceptable.

5.1.2. Discussion of results

As mentioned in section 5.1.1, the experimental fatigue tests on real steel bridge components were done and a relationship considered the change of detail category of riveted connection in time was developed. Number of cycles until the failure was calculated for all tested samples by using developed formulas and the comparison of results obtained from calculation and laboratory fatigue tests was done. Considering the values of stress ranges obtained from fatigue tests, the number of cycles until the failure was calculated (see Tab. 23 and Fig. 72). The calculated number of cycles for 95% quantil is lower in all cases in comparison with measured numbers, which means that the calculation is on a save side.

Tab. 23 Comparison the results of calculation model and laboratory fatigue tests

| Sample		Number of cycles				
		Experiment	Calculated (mean)	$N_{calc}/N_{exp,\,mean}$	Calculated (95% q.)	$N_{calc}/N_{exp,\,95\%\,q.}$
		N_{exp}	$N_{calc,\,mean}$	ΔN [-]	$N_{calc,\,95\%\,q}$	ΔN [%]
1	S1.1	184452	222915	**1.21**	176805	**0.96**
2	S1.2	251053	236210	**0.94**	187349	**0.75**
3	S1.3	186320	226975	**1.22**	180025	**0.97**
4	S1.4	300140	244360	**0.81**	193814	**0.65**
5	S2.1	179633	196409	**1.09**	155782	**0.87**
6	S2.2	161769	146552	**0.91**	116238	**0.72**
7	S2.3	222551	181998	**0.82**	144352	**0.65**
8	S3.1	139313	92117	**0.66**	73062	**0.52**
9	S3.2	92003	111091	**1.21**	88112	**0.96**
10	S3.3	182980	172647	**0.94**	136935	**0.75**
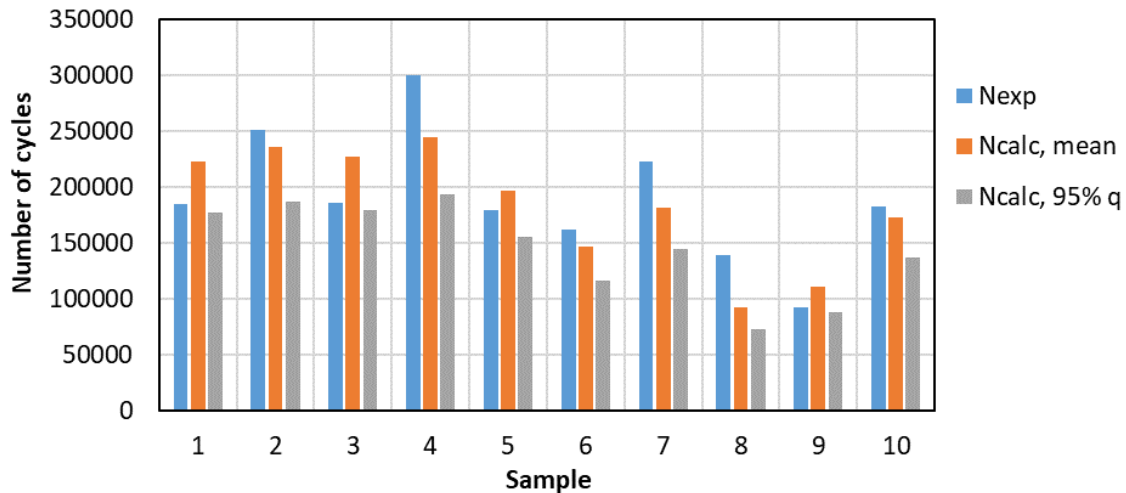
Fig. 72 Comparison the results of calculation model and laboratory fatigue tests

5.2. Complex method

The simplified method presented in Section 5.1 considered only the global change in cross-section size as an effect on the change in detail category. This approach does not distinguish what structure the surface of the corroded feature has - whether the corrosion is uniform and the surface roughness is small or whether the corrosion is non-uniform and the surface contains corrosion pits of different shapes and depths. Surface roughness plays an important role in terms of fatigue strength. As the results of study of Novovic at el. [43] show, the fatigue strength of structural elements is already influenced by the way they are manufactured. Different surface treatments, such as polishing, grinding or milling, cause different surface roughness, resulting in different fatigue strengths. In the absence of residual stresses, values of machined surface roughness exceeding 0.1 µm have a great influence on fatigue life. For surfaces with Ra < 0.1 µm, this effect is reduced because cracks are caused by persistent slip bands or at grain boundaries.

5.2.1. Effects of surface roughness

Corrosion of steel has a negative effect on the behaviour of the individual structural elements, but of course also on the response of the entire bridge structure. In the case of individual members, the consequences of corrosion are as follows:

1) Reduction of the cross-section of the corroded element, resulting in an increase in the nominal stress range (depending on the structural scheme of the structure - whether it is a lone element, a statically determined structure or a statically indeterminate structure). In addition, material loss may result in a reduction in the buckling resistance of members due to a reduction in the radius of inertia and therefore an increase in member slenderness.

2) Surface roughness in the form of corrosion pits causes a local increase in stress in these pits. These stress concentrators act as potential initiators of fatigue cracking, resulting in a reduction in fatigue strength, which can be expressed by a change in the category of detail, as found from experiments carried out by the author. The local increase in stress in the corrosion pit is expressed by stress concentration factor, which is defined as (28) [44]:

$$K_t = \frac{\sigma}{S} \hspace{4cm} [-] \hspace{4cm} (28)$$

where:　σ　　　is the axial stress in the notch

　　　　　S　　　is the nominal stress of the cross section.

We also distinguish the so-called fatigue notch factor β, which is defined as the ratio of the fatigue limit of the part without notch $\sigma_c{}^x$ to the fatigue limit of the part with notch $\sigma_c{}^*$ (29).

$$\beta = \frac{\sigma_c{}^x}{\sigma_c{}^*} \qquad\qquad [-] \qquad\qquad\qquad (29)$$

The relationship between the stress concentration factor and the fatigue notch factor can be defined [44]. The value of the notch factor is always less than the value of the stress concentration factor.
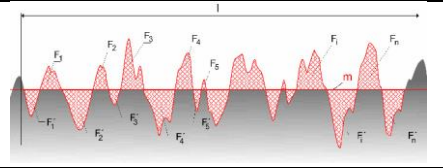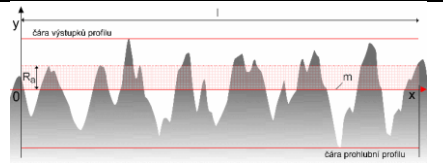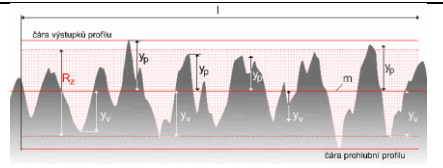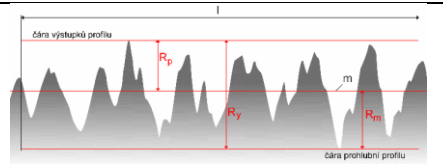
As already mentioned, the irregularities in the form of corrosion pits cause a local stress increase in the loaded member and at the same time the corrosion pit is the place where the fatigue crack is likely to appear first.

The level of surface irregularity can be expressed by the so-called surface roughness. The surface roughness depends on the following parameters:

　　1) the depth of the individual irregularities (pits) relative to an ideally flat surface = absolute depth of the irregularities, but also on the relative difference of the depths of the individual irregularities with respect to each other,

　　2) the size of the corroded area,

　　3) the shape of the individual irregularities (whether the bottom of the corrosion pit is flat, rounded or pointed) and the plan shape of the pit (circular, elliptical or sharp-edged).

The combination of these parameters affects the magnitude of stress at the site of corrosion weakening and also the rate of fatigue crack initiation.

The surface roughness can be described by the following parameters R_a, R_z and R_y [45]:

Centre line m	$\displaystyle\sum_{i=1}^{n} F_i = \sum_{i=1}^{n} F'_i$	
Mean arithmetic deviation of the profile R_a	$R_a \cong \dfrac{1}{n} \cdot \displaystyle\sum_{i=1}^{n} |y_i|$	
Height of profile roughness determined from 10 points R_z	$R_z = \dfrac{\sum_{i=1}^{n} |y_{pmax}| + \sum_{i=1}^{n} |y_{vmax}|}{5}$	
Maximum profile height R_z	$R_z = R_p + R_m$	

5.2.2. Effect of pre-stressing in the rivet on corrosion weakening of the connection

The intensity of the pre-stress in the rivet has a great influence on the course of stress in the vicinity of the hole of the riveted elements of the riveted connections. The pre-stress in the rivet is created when the rivet cools during the riveting process. The initially heated rivet is gradually cooled, which causes it to shorten and the individual elements to be joined to each other. The rivet head introduces (transverse) compressive stresses into the element (see Fig. 73) below the head, resulting in a reduction of tensile stresses in the immediate vicinity of the rivet hole. According to the available literature [31], the value of the pre-stress in the rivet reaches a magnitude of 20 to 220 MPa, with an average value of 100 MPa. However, the value depends on the length of the rivet and the number of plates connected [47]. If the ratio of the clamping length to the shank diameter is close to one, and if 2 plates are connected, then the prestressing value in the rivet is approximately 100 MPa. However, when 3 plates are connected, the value rises to approximately 60 MPa. The reason for the lower pre-stress is the misalignment of the holes in the clamped plates.
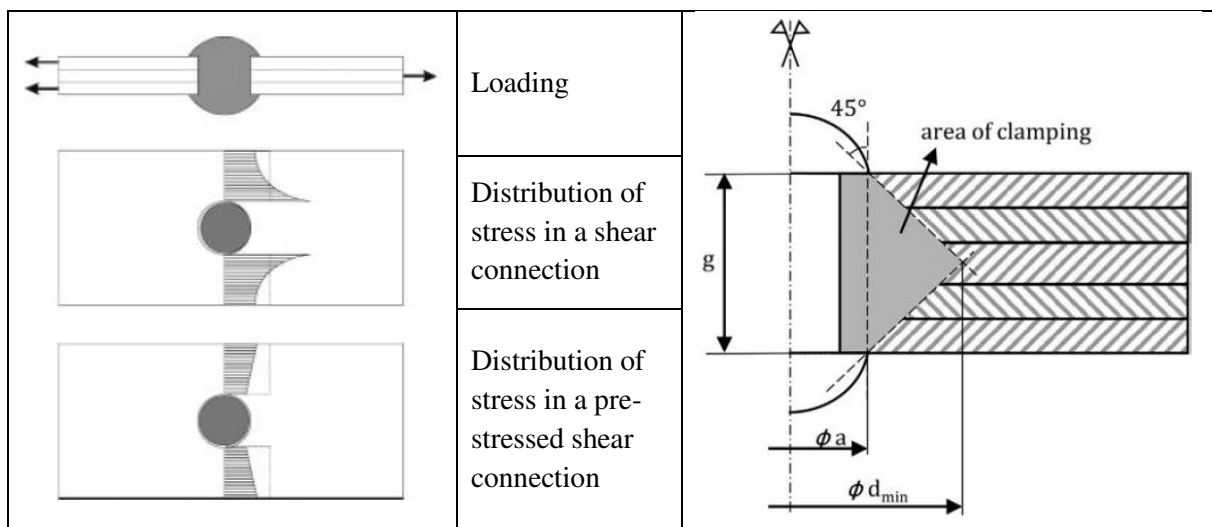

Fig. 73 Left: Stress distribution close to a rivet in riveted joint [31]. Right: definition of clamping area in riveted joint, where g… is grip length, a… is diameter of rivet head [47]

The positive effect of prestressing is also reflected in the manner and degree of corrosion weakening of the surface of the elements around the rivet head. Observation of the mode of corrosion weakening on real structures shows that if the prestressing is active in the rivet, corrosion under the rivet head does not occur or occurs only to a certain extent compared to the surface of the element in the surrounding rivet head (see Fig. 74). If the prestressing in the rivet is active, there is no corrosion of the rivet shank. This was the case for the specimens used for the experiment (see Fig. 75).

The middle rivet was removed from several test specimens. Although the top surface of the top plate of the specimen was corroded (a combination of uniform weakening and corrosion pitting), the surface of the plate below the rivet head was free of corrosion weakening. The edges and contact surfaces inside the hole of each plate were also free of corrosion weakening. The removed rivets were not available, but it can be assumed that the rivet shanks were free of corrosion weakening. Even if the rivet head is weakened, the sheet metal below the head is not corroded unless the extent of corrosion is such that a piece of the rivet head is completely missing. Otherwise, the exposed plate is also corroded (see Fig. 74).

For rivets without active prestressing, in structures exposed to unfavourable weather conditions, moisture penetrates into the area under the rivet head up to the edge of the hole, or up to the inner surfaces of the hole in the plate and up to the rivet shank (depending on how much the rivet shank fills the holes in the connected sheet metal). Corrosion then occurs in these parts of the connection as well (see Fig. 74).
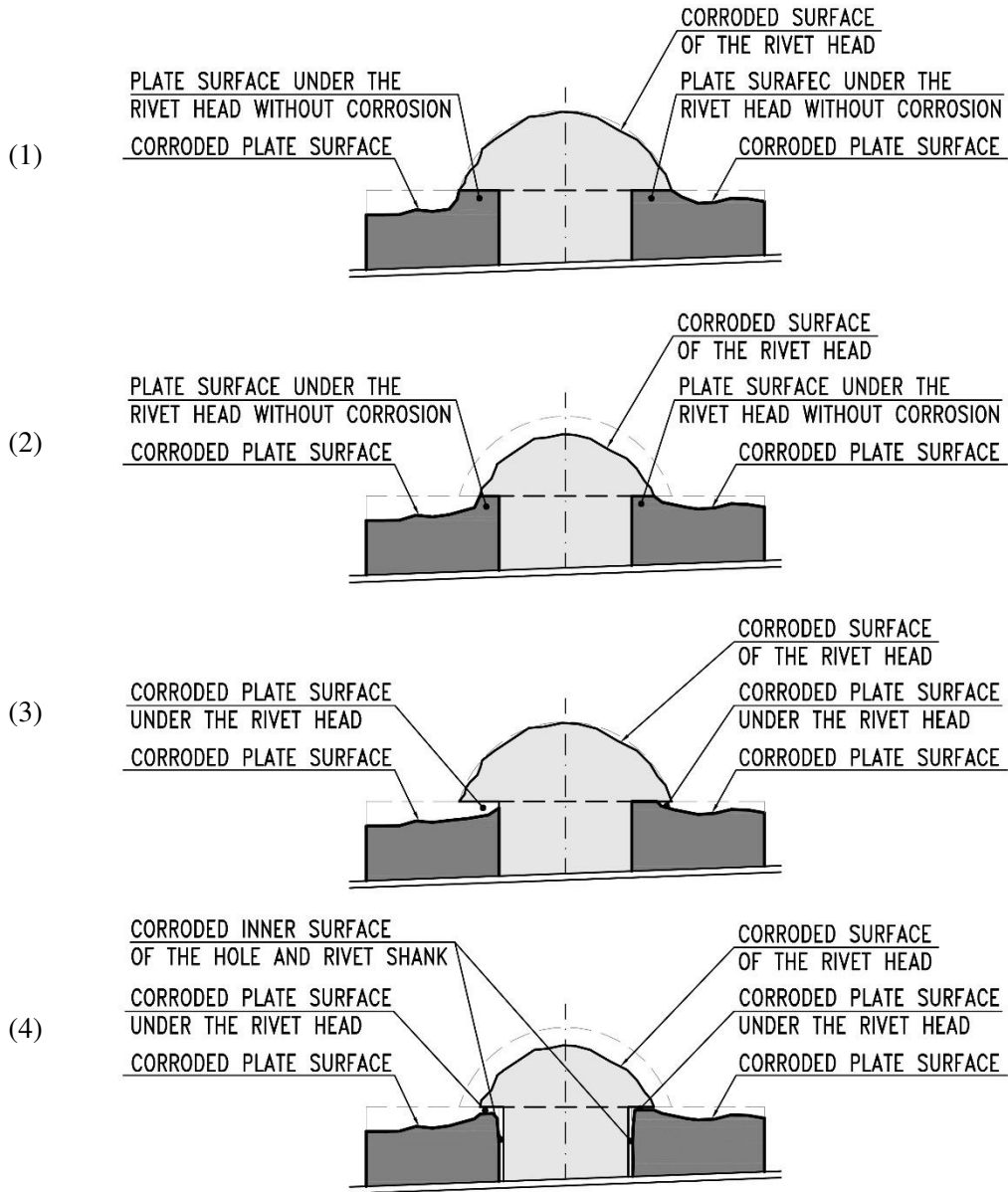

Fig. 74 Schematic illustration of corrosion loss in a joint: (1) prestressing in rivet active and mild corrosion weakening of rivet head; (2) prestressing in rivet active and heavy corrosion weakening of rivet head; (3) prestressing in rivet inactive and mild corrosion weakening; (4) prestressing in rivet inactive and heavy corrosion weakening
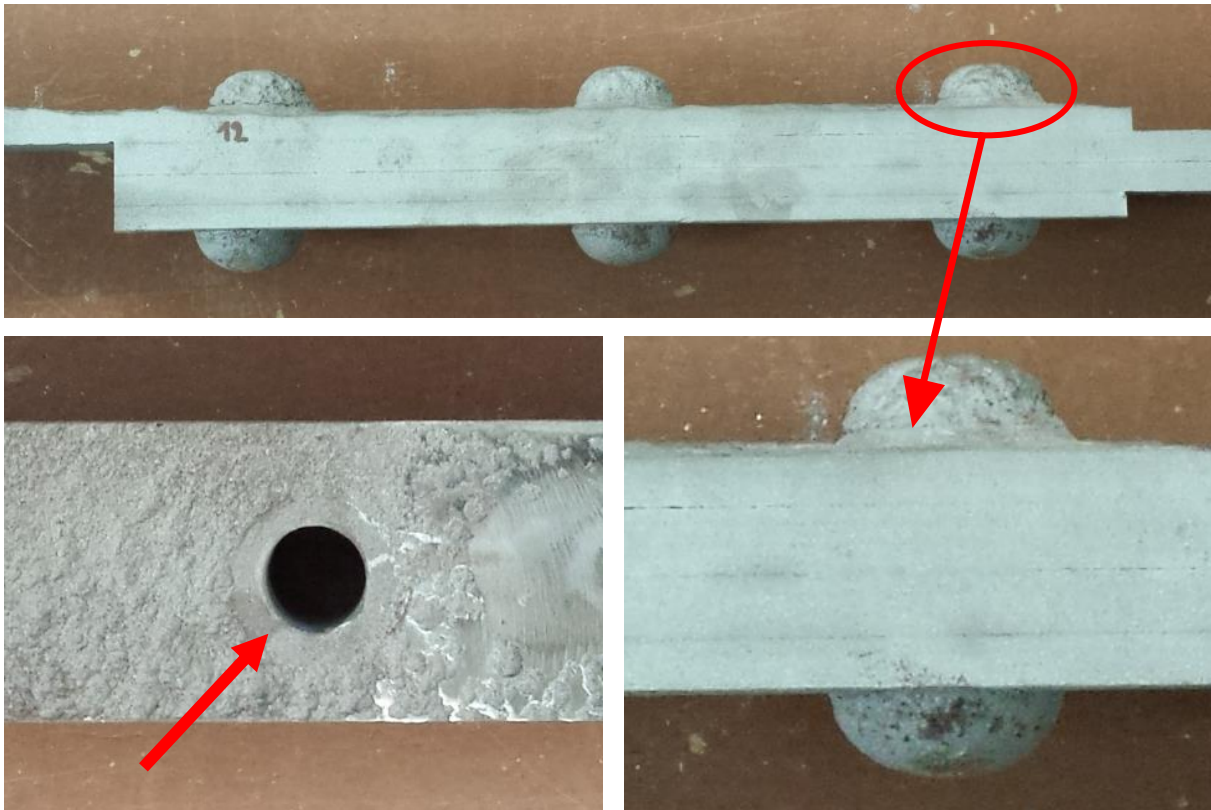
Fig. 75 The shape of the corrosion weakening of the plate surface around the rivet head. Above: side view of the tested sample. Left: view of the rivet hole after removal of the rivet (the area around the hole across the width of the rivet head is free of corrosion weakening). Right: detail of the specimen from the side (the sheet metal under the rivet head is not corrosion weakened in comparison to the rest of the sheet metal).

5.2.3. Multiparametric evaluation of experimental tests

For all test specimens, the area around the rivet where fatigue damage occurred during the experiments was examined in detail. 3D images of the specimens were used, which were created using the photogrammetric scanning method. This scanning was performed prior to the actual experiments. The accuracy of the method used was 0.1 mm. The 3D images were processed using Geomagic Wrap and Geomagic Control X computer programs from 3D Systems (free trial versions of these programs were used). These programs are also used to edit and view objects composed of point clouds, so this feature was used to process 3D images created by photogrammetry. In the Geomagic Wrap program, cross-sections were generated through the plate in the area of the rivet hole, a critical location on all specimens in terms of fatigue damage. The cross sections generated at 0.1 mm spacing were then converted to dxf format using Geomagic Control X so that they could be opened and evaluated in AutoCAD.

The following parameters, which are important in terms of fatigue strength of the tested specimens, were determined on the prepared cross-sections:

1) Ratio of the length of the curve following the corroded surface to the width of the corroded surface (Δb_c)
2) minimum thickness of plate ($t_{c,min}$)
3) thickness of the plate at a distance of 1-10 mm from the edge of the rivet hole ($t_{c,i}$)
4) cross-section area of the rivet head (A_{r1}).

The parameters were determined for the samples of set 1 (no corrosion), 2 (medium level of corrosion) and 3 (high level of corrosion). All these parameters are shown in Fig. 76.
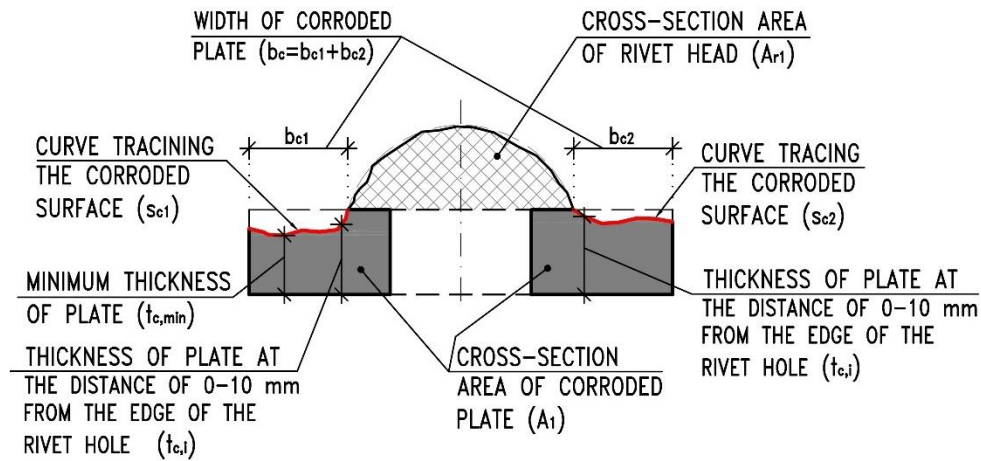
Fig. 76 Cross-section at the rivet hole and the observed parameters

Description of the observed parameters

1) Ratio of the length of the curve following the corroded surface to the width of the corroded surface (Δb_c)

The parameter Δb_c is calculated as (30):

$$\Delta b_c = \frac{s_c}{b_c} = \frac{s_{c1} + s_{c2}}{b_{c1} + b_{c2}} \qquad\qquad [-] \qquad\qquad\qquad (30)$$

- where: s_c is the length of the curve following the corroded surface determined as the sum of the lengths s_{c1} and s_{c2} according to the Fig. 76

        b_c is the width of the weakened area, which is determined as the sum of the widths b_{c1} and b_{c2} of the corroded surface according to the Fig. 76.

The parameter Δb_c takes into account any surface roughness. The parameter better describes whether the surface of the corroded element is regular or irregular compared to the parameter d_A considered in chapter 5.1. The d_A parameter only accounts for the change in cross-sectional area. The more irregular the surface, the greater the value of the Δb_c parameter. For a surface without irregularities, the value of the parameter is equal to 0.

2) Minimum thickness of plate ($t_{c,min}$)

The value of $t_{c,min}$ considers the smallest thickness of the corroded plate in the cross-section through the centre of the rivet hole. If the plate under consideration is without corrosion weakening, then the value of $t_{c,min}$ is equal to the thickness of the unweakened plate.

3) Thickness of the plate at a distance of 1-10 mm from the edge of the rivet hole ($t_{c,i}$)

The value of $t_{c,i}$ considers the thickness of the plate at a distance of 0 to 10 mm from the edge of the hole in the cross-section through the centre of the rivet hole. If the plate is free of corrosion weakening, then the $t_{c,i}$ values are equal to the thickness of the unweakened plate The greater the corrosion weakening and the closer to the edge of the hole, the greater the stress during loading at that point.
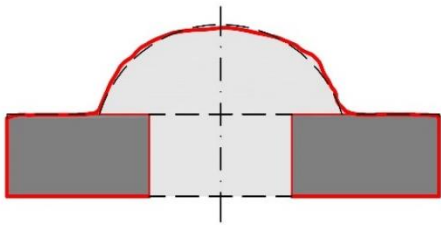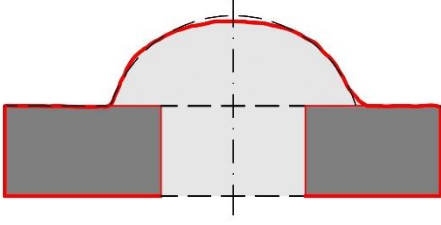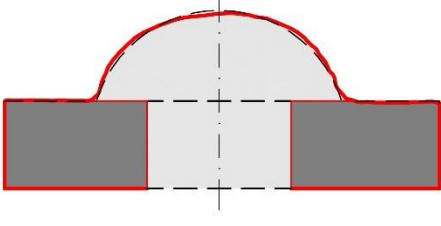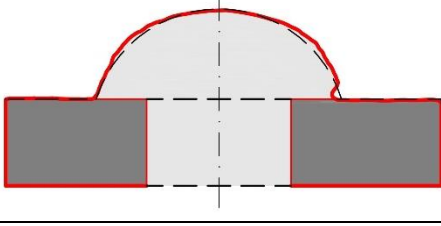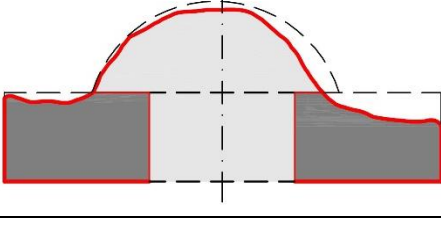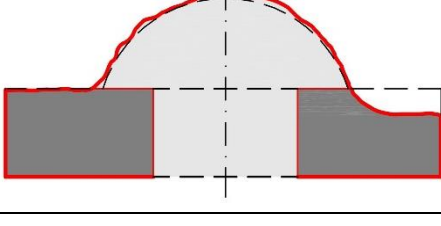
4) Cross-section area of the rivet head (A_{r1})

The cross-sectional area A_{r1} of the rivet head was measured in a cross-section through the centre of the rivet hole. Possible corrosion weakening of the rivet head may adversely affect the magnitude of the clamping force that is induced by prestressing in the rivet. A reduction in the size of the cross-sectional

area of the rivet head may result in a reduction in prestressing and therefore a reduction in clamping force.

Tab. 24 contains the measured values of parameters for each tested sample except sample S2.1 due to the absence of the photogrammetric scan. The parameter values are accompanied by an image of a cross section of the plate through the centre of the rivet hole. The red curve borderers the shape of the corroded cross-section. The dependence of the parameters on the change of the detail category was investigated.

Tab. 24 Values of parameters observed at tested samples on the cross-section at the rivet hole

	Sample: S1.1						
	Group of samples: 1 (without corrosion)						
	A_0	A_1	A_{r1}	b_c	s_c	Δb_c	$t_{c,min}$
	[mm²]	[mm²]	[mm²]	[mm]	[mm]	[-]	[mm]
	467.2	464.9	319	26.6	26.8	1.005	11.27

	Sample: S1.2						
	Group of samples: 1 (without corrosion)						
	A_0	A_1	A_{r1}	b_c	s_c	Δb_c	$t_{c,min}$
	[mm²]	[mm²]	[mm²]	[mm]	[mm]	[-]	[mm]
	502.0	501.4	305	26.4	26.5	1.004	12.32

	Sample: S1.3						
	Group of samples: 1 (without corrosion)						
	A_0	A_1	A_{r1}	b_c	s_c	Δb_c	$t_{c,min}$
	[mm²]	[mm²]	[mm²]	[mm]	[mm]	[-]	[mm]
	488.7	486.9	318	26.3	26.4	1.004	11.87

	Sample: S1.4						
	Group of samples: 1 (without corrosion)						
	A_0	A_1	A_{r1}	b_c	s_c	Δb_c	$t_{c,min}$
	[mm²]	[mm²]	[mm²]	[mm]	[mm]	[-]	[mm]
	484.3	483.1	323	27.1	27.3	1.007	11.79

	Sample: S2.2						
	Group of samples: 2 (medium level of corrosion)						
	A_0	A_1	A_{r1}	b_c	s_c	Δb_c	$t_{c,min}$
	[mm²]	[mm²]	[mm²]	[mm]	[mm]	[-]	[mm]
	489.9	427.5	258	28.5	30.4	1.068	8.19

	Sample: S2.3						
	Group of samples: 2 (medium level of corrosion)						
	A_0	A_1	A_{r1}	b_c	s_c	Δb_c	$t_{c,min}$
	[mm²]	[mm²]	[mm²]	[mm]	[mm]	[-]	[mm]
	492.9	453.5	335	26.4	27.8	1.053	8.67

Tab. 24 (continued)
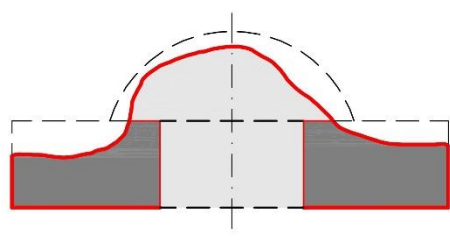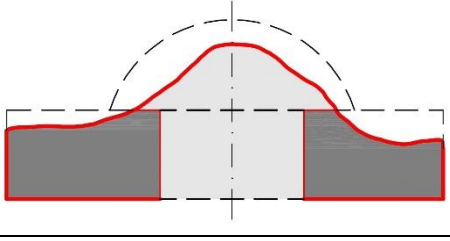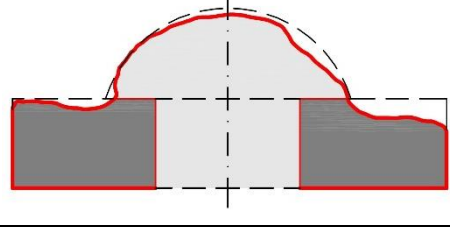
	Sample: S3.1						
	Group of samples: 3 (high level of corrosion)						
	A_0	A_1	A_{r1}	b_c	s_c	Δb_c	$t_{c,min}$
	[mm²]	[mm²]	[mm²]	[mm]	[mm]	[-]	[mm]
	493.1	380.2	204	32.4	35.5	1.096	6.97
	Sample: S3.2						
	Group of samples: 3 (high level of corrosion)						
	A_0	A_1	A_{r1}	b_c	s_c	Δb_c	$t_{c,min}$
	[mm²]	[mm²]	[mm²]	[mm]	[mm]	[-]	[mm]
	497.6	411.3	155	32.4	35.4	1.090	7.57
	Sample: S3.3						
	Group of samples: 3 (high level of corrosion)						
	A_0	A_1	A_{r1}	b_c	s_c	Δb_c	$t_{c,min}$
	[mm²]	[mm²]	[mm²]	[mm]	[mm]	[-]	[mm]
	494.8	448.0	274	27.7	31.0	1.117	8.81

Fig. 77 shows the dependence between coefficients d_A and Δb_c for each tested sample. The values of the coefficients are given in Tab. 25. The coefficient Δb_c reflects the ratio of the length of the curve following the corroded surface to the width of the corroded surface. An approximately linear relationship can be observed, with the value of Δb_c increasing with increasing d_A. From a global point of view, this means that the more the test specimen was corroded, the more irregular the surface was.

Tab. 25 Values of coefficients d_A and Δb_c for all tested samples*

Sample		Change in cross-sectional area	Ratio of the length of the curve following the corroded surface to the width of the corroded surface
		d_A [-]	Δb_c [-]
1	S1.1	0.005	1.005
2	S1.2	0.001	1.004
3	S1.3	0.004	1.004
4	S1.4	0.002	1.007
5	S2.2	0.127	1.068
6	S2.3	0.080	1.053
7	S3.1	0.229	1.096
8	S3.2	0.174	1.090
9	S3.3	0.095	1.117

* *Parameter values for sample S2.1 are not included due to the absence of the photogrammetric scan.*
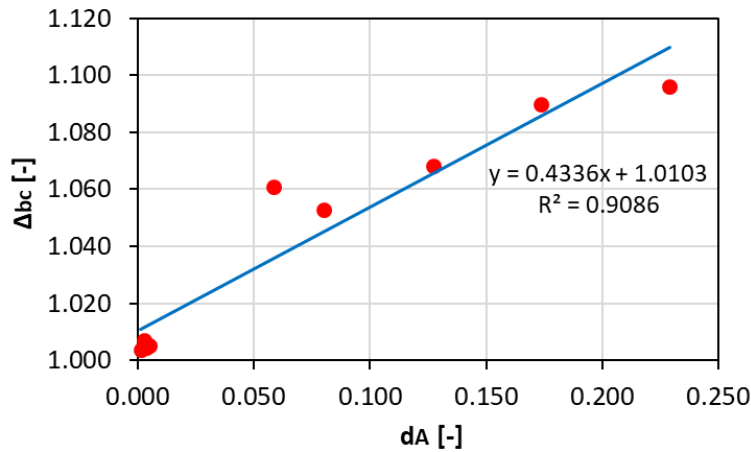
Fig. 77 Relationship between coefficients d_A and Δb_c for all tested samples

The relationship between coefficient Δb_c and detail category $\Delta_{\sigma c,R}$ is shown in Fig. 78. A downward tendency can be observed – the higher the roughness of the corroded surface, the lower the bending detail category, in terms of average values. The values of the coefficients are given in Tab. 26.

Tab. 26 Values of coefficient Δb_c depending on detail category for all tested samples*

Number	Sample	Normal stress detail category		Ratio of the length of the curve following the corroded surface to the width of the corroded surface	
		$\varDelta\sigma_{c,R}$ [MPa]		Δb_c [-]	
1	S1.1	82.6	average:	1.005	average:
2	S1.2	90.2		1.004	
3	S1.3	82.5	87.4	1.004	1.004
4	S1.4	94.5		1.007	
5	S2.2	77.2	average:	1.068	average:
6	S2.3	85.4	81.3	1.053	1.061
7	S3.1	73.1	average:	1.096	average:
8	S3.2	65.4		1.090	
9	S3.3	79.8	72.8	1.117	1.101

* Parameter values for sample S2.1 are not included due to the absence of the photogrammetric scan.
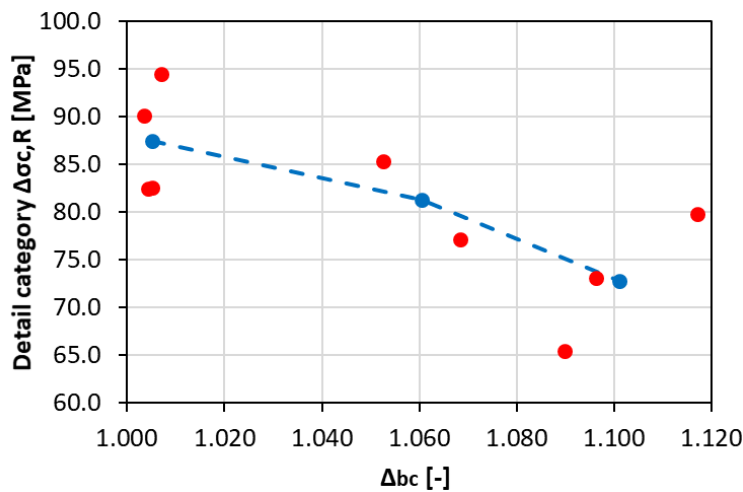

Fig. 78 Relationship between parameter Δb_c and detail category for all tested samples. The blue dots indicate the dependence of the average values for each of the three sets of samples.

As already mentioned, corrosion weakening of the rivet head may adversely affect the magnitude of the clamping force that is induced by prestressing in the rivet. The change in cross-sectional area of rivet head may be expressed as (31).

$$d_{Ar} = \frac{\Delta_{Ar}}{A_{r0}} = \frac{A_{r0} - A_{r1}}{A_{r0}} \qquad [-] \qquad d_{Ar} \geq 1,0 \qquad (31)$$

- where: A_{r0} is the theoretical cross-sectional area of unweakened riveted head. For all samples, a rivet head with a radius of 34 mm and a height of 12.5 mm is considered, therefore $A_{r0} = 312\ mm^2$

       A_{r1} is the cross-sectional area of weakened rivet head.

The values of the parameter d_{Ar} are given in Tab. 27. The dependence between the parameter d_{Ar} and detail category $\Delta_{\sigma c,R}$ of tested samples is shown in figure Fig. 79. From a global point of view, the lower the value of the parameter Δ_{Ar} (i.e. the greater the corrosion weakening of the rivet head), the lower the detail category. After applying regression analysis, an approximately linear relationship between d_{Ar} and $\Delta_{\sigma c,R}$ can be observed.

Tab. 27 Values of cross-sectional area of the unweakened and weakened rivet head and values of parameter Δ_{Ar} for all tested samples*

Number	Sample	Theoretical unweakened cross-sectional area of the rivet head	Weakened cross-sectional area of the rivet head	Change in cross-sectional area of rivet head
		A_{r0} [mm²]	A_{r1} [mm²]	d_{Ar} [-]
1	S1.1		319.5	0.000
2	S1.2		305.4	0.021
3	S1.3		318.1	0.000
4	S1.4		322.8	0.000
5	S2.2	312.0	258.3	0.048
6	S2.3		335.5	0.172
7	S3.1		204.4	0.000
8	S3.2		154.9	0.345
9	S3.3		274.4	0.503

* Parameter values for sample S2.1 are not included due to the absence of the photogrammetric scan.
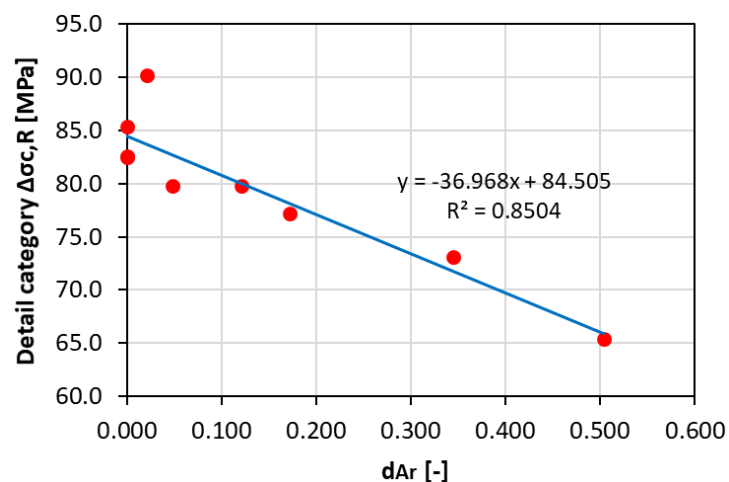

Fig. 79 Relationship between parameter d_{Ar} and detail category for all tested samples

Maximum corrosion weakening of plate in the cross-section through the centre of the rivet hole can be expressed as (32):

$$cw_{max} = t_0 - t_{c,min} \qquad \text{[mm]} \qquad\qquad (32)$$

- where: t_0 is the original thickness of the unweakened plate

$t_{c,min}$ is the minimum thickness of corroded plate.

The relationship between the maximum corrosion weakening and the detail category cannot be clearly determined. It depends very much on the distance at which the maximum corrosion weakening is located from the edge of the hole. On each specimen, the maximum weakening was located at different positions. However, in terms of average values, a decreasing trend can be observed, with the higher the maximum corrosion weakening, the lower the detail category (see Tab. 28 and Fig. 80).

Tab. 28 Values of maximum corrosion weakening of plate for all tested samples*

Sample		Normal stress detail category	Original thickness of the unweakened plate	Minimum thickness of plate	Maximum corrosion weakening of plate
		$\Delta\sigma_{c,R}$ [MPa]	t_0 [mm]	$t_{c,min}$ [mm]	cw_{mac} [mm]
1	S1.1	82.6	11.50	11.27	0.23
2	S1.2	90.2	12.43	12.32	0.11
3	S1.3	82.5	12.14	11.87	0.27
4	S1.4	94.5	12.00	11.79	0.22
5	S2.2	77.2	12.20	8.19	4.01
6	S2.3	85.4	12.20	8.67	3.54
7	S3.1	73.1	12.10	6.97	5.13
8	S3.2	65.4	12.24	7.57	4.67
9	S3.3	79.8	12.33	8.81	3.53

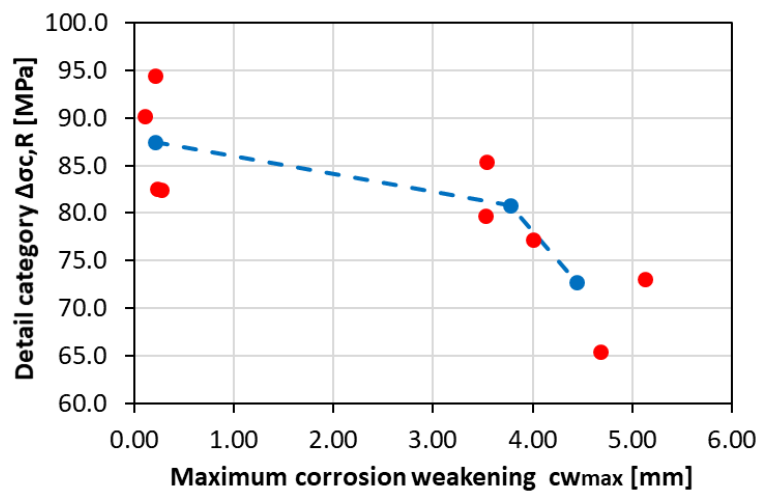** Parameter values for sample S2.1 are not included due to the absence of the photogrammetric scan.*

Fig. 80 Relationship between maximum corrosion weakening cw_{max} and detail category for all tested samples. The blue dots indicate the dependence of the average values for each of the three sets of samples.

In addition to the minimum thickness of the sheet metal, the thicknesses of the sheet metal at a distance of 0 to 10 mm from the edge of the hole in a cross section through the centre of the rivet hole were also determined. Based on the thicknesses, the corrosion weakening cw_i was calculated for each distance. The relationship between the corrosion weakening of the plate and the detail category is shown in Fig. 81. For each of the three sets of specimens, the average values of the detail category are considered, as well as the average values of the corrosion weakening of the plates at distances of 4, 5, 6, 7, 8, 9 and 10 mm from the edge of the hole (see Tab. 29). For distances closer than 4 mm to the edge of the hole, the corrosion weakening was not measurable for all samples, as the sheet metal was covered by the rivet head.

It can be seen from the graph that the closer the corrosion weakening value is to the edge of the rivet hole, the lower the detail category the sample corresponds to. For example, if a 2 mm corrosion weakening is 6 mm away from the edge of the hole, the detail category is lower than if the 2 mm weakening is 8 mm away and even lower than if it is 10 mm away from the hole edge.

Tab. 29 Average values of corrosion weakening of the plate at different distances from the edge of the rivet hole and average values of detail category for each of the three sets of samples*

Set of samples according to the corrosion level of the upper sheet		Normal stress detail category	Corrosion weakening of plate at a distance of 4 to 10 mm from the edge of the hole						
		$\Delta\sigma_{c,R}$ [MPa]	cw_4 [mm]	cw_5 [mm]	cw_6 [mm]	cw_7 [mm]	cw_8 [mm]	cw_9 [mm]	cw_{10} [mm]
1	No corrosion	87.4	0.00	0.00	0.00	0.02	0.05	0.08	0.13
2	Medium level	80.8	0.08	0.06	0.90	1.04	1.64	2.22	2.74
3	High level	72.8	0.04	0.86	1.54	2.28	2.89	3.30	3.65

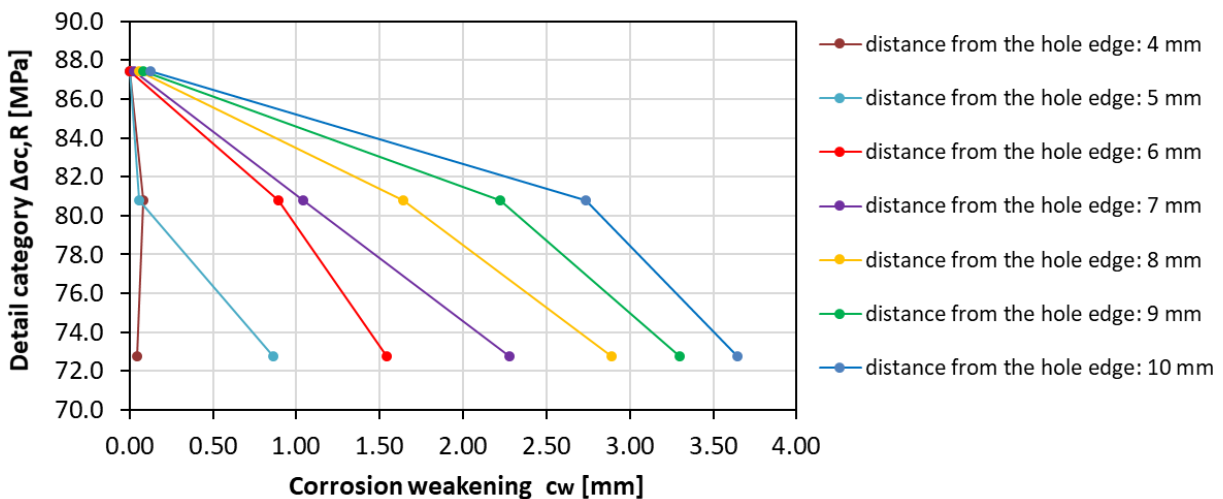* Calculated without including values for sample S2.1

Fig. 81 Relationship between the corrosion weakening of plate at a distance of 4 to 10 mm from the hole edge and the detail category

All the four observed parameters describing the corrosion weakening of the specimens (Δb_c, cw_{max}, $t_{c,i}$ and d_{Ar}) certainly have an influence on the fatigue life (see Fig. 77, Fig. 78, Fig. 79, Fig. 80 and Fig. 81). Since they act together, it cannot be clearly determined which parameter has what contribution to the fatigue life reduction. Test specimens that were corroded with either moderate or high fatigue corrosion had corrosion weakening on both the plates and the rivet heads.

The parameter d_{Ar} accounting for corrosion weakening of the rivet head affects the fatigue life indirectly. Reduction of the rivet head can lead to a reduction in the magnitude of the preload in the rivet, which can result in moisture penetration under the rivet head and into the space between the connected plates and subsequent corrosion at these locations.

The parameter cw_{max} describing the maximum corrosion weakening is an important parameter. However, the relationship between the maximum corrosion weakening and the category of detail cannot be clearly determined. It depends very much on the distance at which the maximum corrosion weakening is located from the edge of the hole. On each specimen, the maximum weakening was located at different positions.

Of all the parameters examined, the parameter Δb_c, which expresses the ratio of the length of the curve tracing the corroded surface to the width of the corroded surface, appears to be the most telling. It is the parameter that takes into account the irregularities of the corroded surface. For this reason, the change in detail category will be expressed as a function of the Δb_c parameter.

Subtracting one from the Δ_{bc} parameter gives the value of the d_{bc} coefficient (33). The relationship between the d_{bc} coefficient and the detail category $\Delta_{\sigma c,R}$ is shown in Fig. 82.

$$d_{bc} = \Delta_{bc} - 1 \qquad [-] \qquad\qquad (33)$$

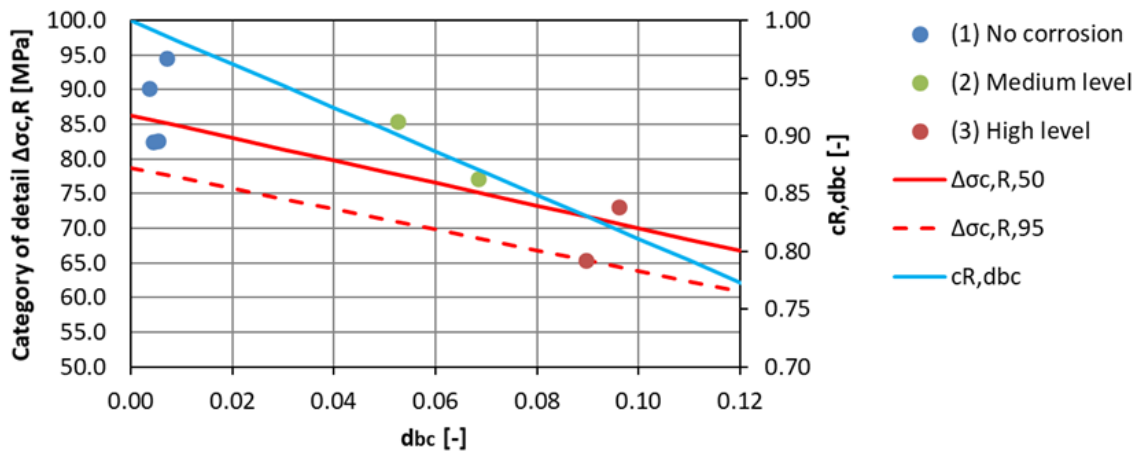- where: Δ_{bc} is calculated according to (30).

Fig. 82 Relationship between parameter d_{bc} and detail category for all tested samples

Neglecting tested sample S3.3, the bending detail category value of which was deviated most from the other values, and using regression analysis, the dependence between the category of the detail and the parameter d_{bc} (see Fig. 82) can be expressed by a linear relation as (34) and (35):

$$\Delta\sigma_{c,R,50} = -163.06 \cdot d_{bc} + 86.316 \qquad [MPa] \qquad\qquad (34)$$

$$\Delta\sigma_{c,R,95} = -288.14 \cdot d_{bc} + 78.733 \qquad \text{[MPa]} \qquad (35)$$

After adjustment of the previous formula, the reduced bending detail category for sample with weakened cross-section can be determined by Eq. (36) and (37):

$$\Delta\sigma_{c,R,50} = \Delta\sigma_{c,50} \cdot (1 - 1.8891 \cdot d_{bc}) \qquad \text{[MPa]} \qquad (36)$$

$$\Delta\sigma_{c,R,95} = \Delta\sigma_{c,95} \cdot (1 - 1.8891 \cdot d_{bc}) \qquad \text{[MPa]} \qquad (37)$$

If we implement the reduction coefficient $c_{R,dbc}$, then the mean value and 95% quintile value of reduced detail category for a corroded sample is computed according to Eq. (38) and Eq. (39), respectively:

$$\Delta\sigma_{c,R,50} = \Delta\sigma_{c,50} \cdot c_{R,dbc} \qquad \text{[MPa]} \qquad (38)$$

$$\Delta\sigma_{c,R,95} = \Delta\sigma_{c,95} \cdot c_{R,dbc} \qquad \text{[MPa]} \qquad (39)$$

The reduction coefficient $c_{R,dbc}$ is calculated according to Eq. (40):

$$c_{R,dbc} = (1 - 1.8891 \cdot d_{bc}) \qquad \text{[-]} \qquad (40)$$

where: $\Delta\sigma_{c,50}$ is the mean value of original bending detail category of an uncorroded sample,

$\Delta\sigma_{c,95}$ is the 95% quintile value of original bending detail category of an uncorroded sample,

$c_{R,dbc}$ is reduction coefficient,

d_{bc} is a parameter that takes into account the level of corrosion, which is expressed as surface roughness. The surface roughness is defined in this case as the ratio of the length of the curve tracing the corroded surface to the width of the corroded surface at the point of the cross section through the centre of the rivet hole. Parameter d_{bc} is calculated according to (33).

The parameter d_{bc} takes into account any surface roughness. The parameter better describes whether the surface of the corroded element is regular or irregular compared to the parameter d_A considered in chapter 5.1. The d_A parameter only accounts for the change in cross-sectional area. The more irregular the surface, the greater the value of the d_{bc} parameter. For a surface without irregularities, the value of the parameter is equal to 0.

The above formulas, as in the case of the formulas expressed in chapter 5.1, are derived from the experimental tests mentioned above. Their applicability is limited to narrow bars, i.e. to steel sheets with a maximum thickness of 60 mm.

5.2.4. Discussion of results

In order to determine the accuracy of the developed formulas, the number of cycles required until failure of the samples was calculated using the formulas for all tested samples. The formulas take into account the change in the category of detail depending on the level of roughness of the corroded surface. Tab. 30 summarizes the numbers of cycles to failure obtained from the experimental results and obtained by applying the derived formulas. Cycle counts for 50% and 95% confidence levels were calculated.

By comparing the results obtained by calculation and laboratory fatigue tests, a very good agreement in the number of cycles can be found (see Tab. 30 and Fig. 83). The calculated number of cycles for the lower 95% quantile is in all cases lower compared to the measured values, which means that the calculation is on the safe side.

To find out the accuracy of the formula that has been developed, the Root Mean Square Error (RMSE) was used to calculate how much error there is between the predicted values and the observed values. For the bending detail category, the RMSE = 0.736 [-]. This error is due to the dispersion of the results from the experimental test, together with the fact that the combined effects of corrosion and fatigue phenomena are very complex. The value is therefore acceptable.

Tab. 30 Comparison the results of calculation model based on parameter d_{bc} and laboratory fatigue tests

Sample		Number of cycles				
		Experiment	Calculated (mean)	$N_{calc}/N_{exp, mean}$	Calculated (95% q.)	$N_{calc}/N_{exp, 95\% q.}$
		N_{exp}	$N_{calc, mean}$	ΔN [-]	$N_{calc, 95\% q}$	ΔN [%]
1	S1.1	184452	204274	**1.11**	155022	**0.84**
2	S1.2	251053	215716	**0.86**	163705	**0.65**
3	S1.3	186320	208245	**1.12**	158035	**0.85**
4	S1.4	300140	219857	**0.73**	166847	**0.56**
5	S2.2	161769	149432	**0.92**	113403	**0.70**
6	S2.3	222551	167980	**0.75**	127479	**0.57**
7	S3.1	139313	125916	**0.90**	95557	**0.69**
8	S3.2	92003	121052	**1.32**	91866	**1.00**
9	S3.3	182980	109589	**0.60**	83167	**0.45**
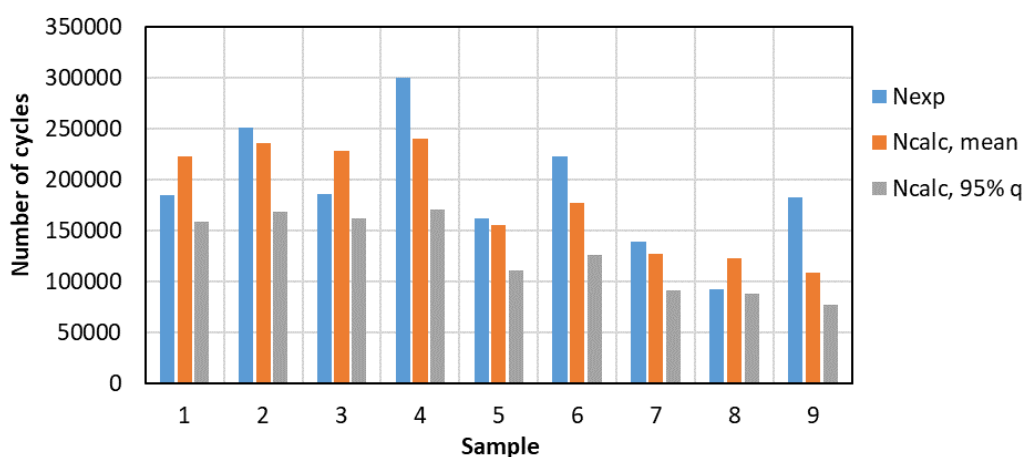
Fig. 83 Comparison the results of calculation model based on parameter d_{bc} and laboratory fatigue tests

Evaluation of results

The fatigue life of the samples used for the experimental fatigue tests was simulated using the developed formulas taking into account different corrosion weakening parameters of the elements. The simplified method, shown in Chapter 5.1.1, considers only the variation of the cross-sectional area of the corrosion

weakened elements using the parameter d_A. Chapter 5.2.3 presents a second method based on the parameter d_{bc}, which takes into account the roughness of the corroded surface. Based on the known stress range, the number of cycles to fatigue failure of the tested samples was calculated using the formulas of both approaches.

The calculations using both methods lead to very similar results (see Tab. 31). However, the parameter d_A in the simplified method does not take into account surface irregularities and in cases where the corrosion weakening is formed by a mostly uniform component, the results might not be entirely accurate. The corrosion weakening of the test specimens consisted of both a uniform and a non-uniform component, so the application of both approaches is appropriate here and leads to similar results. However, the use of formulas based on the parameter d_{bc} leads to safer results since surface irregularities cause local stress concentration and can be fatigue crack initiators.

Tab. 31 Comparison of experimental results with results of the simplified and complex methods

Sample		Number of cycles from the experiment	Calculated number of cycles	
			Simplified method	Complex method
		N_{exp}	$N_{calc,\ 95\%\ q}$	$N_{calc,\ 95\%\ q}$
		[cycles]	[cycles]	[cycles]
1	S1.1	184452	204274	155022
2	S1.2	251053	215716	163705
3	S1.3	186320	208245	158035
4	S1.4	300140	219857	166847
5	S2.2	161769	149432	113403
6	S2.3	222551	167980	127479
7	S3.1	139313	125916	95557
8	S3.2	92003	121052	91866
9	S3.3	182980	109589	83167

Due to the complexity and often limited access, we are usually not able to measure the structural elements in such detail during the inspection to obtain a curve tracing of the corroded surface. Under laboratory conditions, using an ultrasonic thickness gauge (or using a photogrammetry method where the surface of the specimen is scanned in detail) this can be achieved. In situ, a calliper or ultrasonic thickness gauge can be used to measure the element thicknesses at the measured points or the depths of the corrosion pits. In this way we are able to determine the actual cross-sectional area of the corroded element relatively accurately.

Thus, for practical use, it is advantageous to use a simplified relationship which, although slightly less accurate compared to the other approach, also gives a good result.

6. Methodology for prediction the remaining service life of steel bridge structure components deteriorated by corrosion

Decades-old steel bridges have to endure an unfavourable environment that causes the ageing and deterioration of material properties. Moreover, railway bridges in particular are exposed to a large number of stress ranges that may lead to fatigue damage. The combination of both phenomena has a significant impact on the condition of bridges and their remaining service life. In such cases, appropriate maintenance or even removal of the deteriorated structure is necessary; however, a lack of funds often makes this difficult.

At the same time, effective methods for the assessment of steel bridge structures affected by degradation and corrosion are still not available. The current load capacity assessment is based on methods used for the assessment of new structures and the consideration of degradation in the analysis of the structure is not sufficiently defined, both for static load capacity and for fatigue load capacity, where the effect of corrosion pitting on local stresses and subsequent fatigue life is not satisfactorily addressed.

Considering the above-mentioned reasons, the main focus of the doctoral thesis was to analyse and describe the relation between corrosion and fatigue. The research was based on experimental fatigue tests performed on corrosion-weakened. The relationships between various parameters characterizing the corroded surface of the specimens and the fatigue life were investigated. Based on the experimental research, a methodology was developed to assess the remaining service life of existing steel bridge components with respect to fatigue and corrosion effects. The methodology is mainly focused on railway riveted bridges.

The methodology is designed to calculate fatigue damage of structural members that are or are not deteriorated by corrosion and to estimate the remaining service life of such elements. The methodology takes into account the following aspects that affect the fatigue life of structural details and that determine their residual service life:

1) Various level of corrosion weakening
2) Bridge load history
3) Detail category
4) Stress range
5) Various maintenance scenarios.

Using the proposed methodology, it is possible to determine and calculate the following characteristics and parameters, which tell whether or not the theoretical fatigue life of the element under consideration has already been exhausted and which maintenance scenario is the most appropriate to choose with respect to the required residual service life and the financial cost to be spent on the maintenance:

a) Corrosion effects
b) Stress spectrum calculation
c) Calculation of fatigue damage
d) Calculation of remaining fatigue life
e) Financial costs estimation.

6.1. Structure of the methodology

This chapter provides the tools and describes the procedures for determining and calculating the characteristics and parameters (a) to (e) listed in the introduction to Chapter 6, which indicate the current condition and residual lifetime of the elements under assessment.

6.1.1. Corrosion effects and corrosion models

Corrosion process of steel is affected by many factors, such as kind of steel and surface protection; environment impact; presence of pollutants, cracks and stresses. The loss of material may result in a reduction of cross-sectional area and thereby increase the stress level for a given load or increase the stress range for cycling loads. In addition, it can lead to a reduction in buckling resistance of elements or initiation of fractures. Generally, loss of cross-section results in a decrease in geometric parameters such as moment of inertia and radius of inertia.

For the assessment of existing steel members, the loss of material may be taken into account by using corrosion models. Corrosion models depict the dependence of corrosion loss on time. There are many types of models that have been developed [48]. The differences between individual types of corrosion models are given by: various mathematical functions that describe the development of corrosion loss in time, various corrosion environments that are considered (rural, urban, etc.) or various type of steel material.

The rate of corrosion loss is taken into account by corrosion models. Several corrosion models are included into the methodology:

1) Power model [15]
2) Corrosion model by Guedes Soares and Garbatov [49]
3) Corrosion model by Klinesmith et al. [50].

1) Power model

The dependence of corrosion loss in time can be calculated by using Power model [15] as:

$$C_{(t)} = A \cdot (t - T_c)^B \qquad\qquad (41)$$

where: $C_{(t)}$ … corrosion depth [µm],

t …   exposure time [years],

T_c …   coating life [years],

A …   corrosion rate in the first year of exposure,

B …   corrosion rate long-term decrease.

Depending on the type of steel and the type of environment, the following values of parameters A and B are recommended:

Type of steel		Carbon steel		Weathering steel	
Coefficient		A	B	A	B
Environment	Rural	34.0	0.65	33.3	0.50
	Urban	80.2	0.59	50.7	0.57
	Marine	70.6	0.79	40.2	0.56

The development of corrosion loss in time according to Power model is shown in Fig. 84. The upper graph reflects the corrosion rate without the effects of coating. We can expect that usually the coating was applied on structure, minimally in time of construction or later during a reconstruction. If there was/is a presence of coating on steel structure, which is exposed to unfavourable environment, we can suppose that there is no corrosion loss for time of coat durability (the bottom graph reflects the corrosion

rate with the effects of coating). But usually there are no information and details in documentation regarding coating application in history of bridge structure. It can be estimated that the lifetime of the coating applied at the time of construction was approximately 20 years.
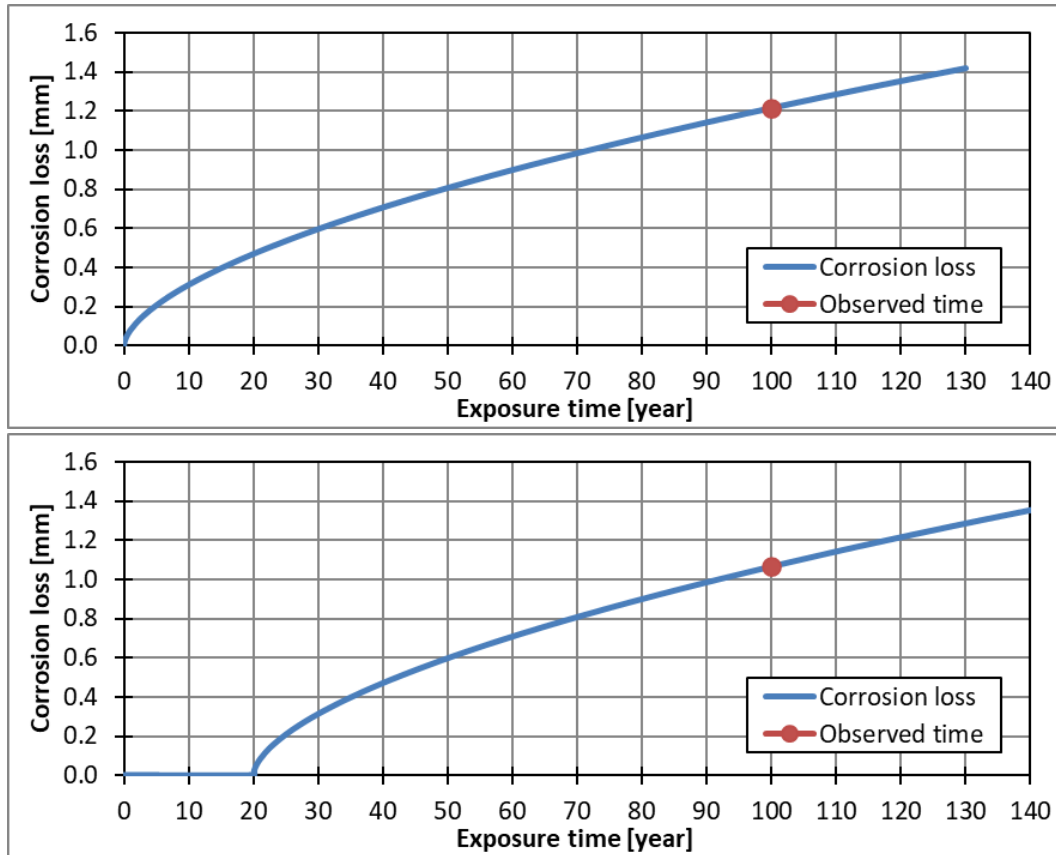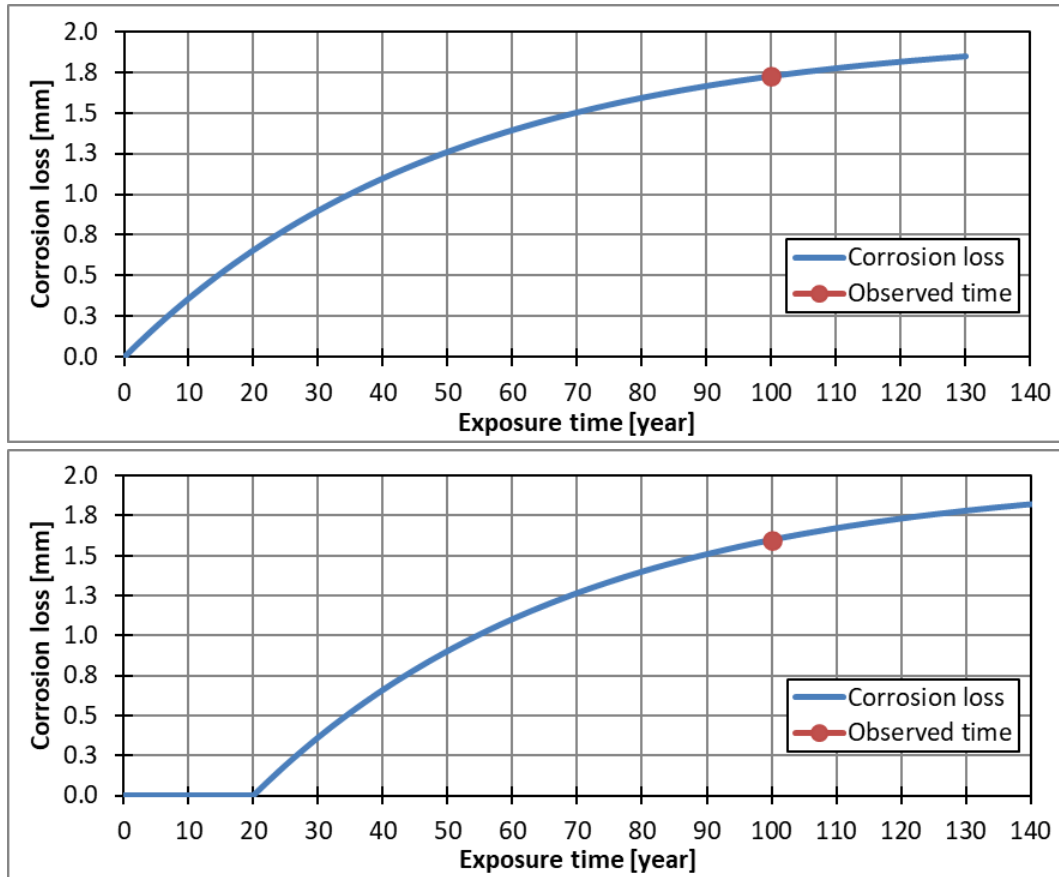

Fig. 84 Increase of corrosion loss in time according to Power model (without and with effects of coating)

2) Corrosion model by Guedes Soares and Garbatov

The dependence of corrosion loss in time can be calculated by using corrosion model developed by Guedes Soares and Garbatov [49] as:

$$C_{(t)} = d_\infty \cdot \left(1 - e^{-(t-T_c)/T_t}\right) \tag{42}$$

where: $C_{(t)}$ ... corrosion depth [μm],

d_∞ ... parameter describing corrosion process [mm]

t ... exposure time [years]

T_c ... coating life [years],

T_t ... transition time.

The evolution of corrosion loss in time according to corrosion model developed by Guedes Soares and Garbatov with and without effects of coating is shown in Fig. 85.

Fig. 85 Increase of corrosion loss in time according to corrosion model by Soares and Garbatov (without and with effects of coating)

3) Corrosion model by Klinesmith et al.

The dependence of corrosion loss in time can be calculated by using corrosion model developed by Klinesmith et al [50] as:

$$y_{(t)} = A \cdot (t - T_c)^B \cdot \left(\frac{TOW}{C}\right)^D \cdot \left(1 + \frac{[SO_2]}{E}\right)^F \cdot \left(1 + \frac{[Cl]}{G}\right)^H \cdot e^{J \cdot (T + T_0)} \qquad (43)$$

where: $y_{(t)}$ …   corrosion depth [μm],

t …   exposure time [years],

TOW … time of wetness [h/years],

SO_2 …   sulphur dioxide concentration [μg/m3],

Cl …   chloride deposition rate [mg/m2/day]

T …   air temperature [°C]

$A, B, C, D, E, F, G, H, J, T_0$ … empirical coefficients, values can be found in [50].

The evolution of corrosion loss is linear in this model, but the progression depends on several parameters that support the initiation and rate of corrosion progression. The values of the coefficients can be obtained from meteorological data.

The evolution of corrosion loss in time according to corrosion model developed by Klinesmith et al with and without effects of coating is shown in Fig. 86.
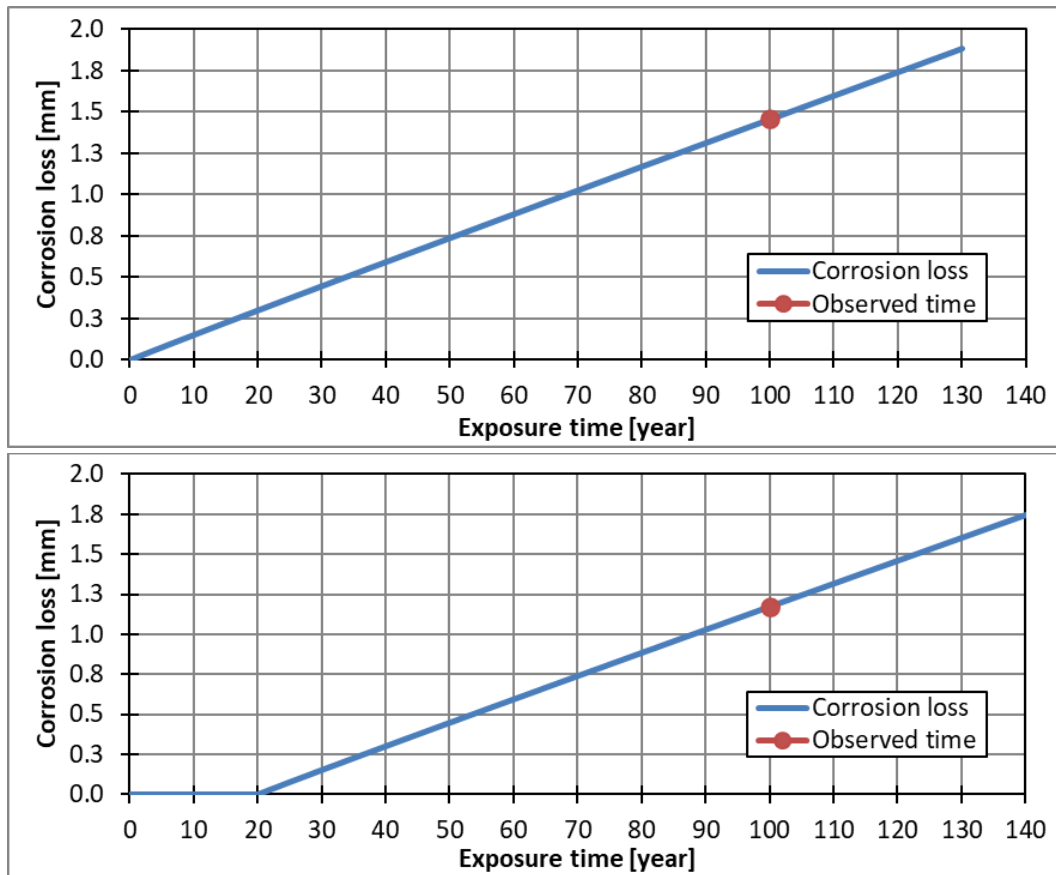
Fig. 86 Increase of corrosion loss in time according to corrosion model by Klinesmith et al. (without and with effects of coating)

These 3 corrosion models are considered in the methodology. Taking into account the climatic conditions of the Czech Republic, all 3 corrosion models can be considered for an approximate estimation of the corrosion loss in time. However, for a more accurate determination, the local conditions and characteristics of the structure need to be taken into account. In particular, the location where the structure under consideration is located and local influences that may affect the rate and mode of corrosion, such as the orientation of the structure with respect to the cardinal direction, the distance from industrial areas, the specific position of the details on the structure (whether or not it is exposed to unsteady rain, salt, etc.). Last but not least, the method and regularity of maintenance of the structure is important. All of these have an influence on the rate and extent of corrosion and these influences need to be taken into account. To determine the actual condition, it is most effective to carry out a detailed corrosion survey of the structure.

6.1.2. Fatigue damage calculation

Lots of damage accumulation models have been developed until this time [51]. The models may be classified into two categories: (1) linear damage cumulative theories and (2) nonlinear damage cumulative theories.

The linear damage accumulation theory, also known as Palmgren–Miner's rule [52], is the most commonly used approach for the cumulative fatigue damage analysis. Relative simplicity is the advantage of this method. Coefficient of fatigue damage according to Palmgren-Miner rule can be calculated as:

$$D = \sum_{i=1}^{n} \frac{n_{Ei}}{N_{Ri}} \qquad (44)$$

where: n_{Ei} ...   number of cycles associated with the stress range $\gamma_{Ff}\Delta\sigma_i$ for band i in the factored
spectrum

N_{Ri} ...   endurance (in cycles) obtained from the factored curve for a stress range of $\gamma_{Ff}\Delta\sigma_i$

The end of fatigue life is given by reaching: $D \geq 1$.

However, there are some disadvantages of Palmgren-Miner method with comparison to nonlinear damage cumulative theories: Palmgren-Miner rule does not consider load history, load interaction effects are not considered and cumulative damage has no relationship with load sequence effects. For this reason, models of nonlinear damage cumulation were developed. These models take into account load interaction effects:

A) Corten-Dolan model [53]
The criterion of failure for Corten-Dolan model is:

$$1 = \sum_{i=1}^{n} \frac{n_i}{N_1 \cdot \left(\frac{\sigma_{max}}{\sigma_i}\right)^d} \qquad (45)$$

where: d ...   Corten-Dolan exponent

The value of the coefficient d ranges from (6.2-6.7), with an average value of $d = 6.57$. The value for a particular material is determined experimentally.

B) Morrow's plastic work interaction rule [54]
Coefficient of fatigue damage under variable amplitude loading spectrum can be expressed as:

$$D = \sum_{i}^{n} \frac{n_i}{N_i} \cdot \left(\frac{\sigma_i}{\sigma_{max}}\right)^f \qquad (46)$$

where: f ...   is an exponent taking into account the sensitivity of the material to the history of varying stress amplitude. The value is determined experimentally. If the value is not known, value -0.5 may be considered [55].

C) V. Dattoma's model [56]
Coefficient of fatigue damage can be calculated as:

$$D = 1 - \left[1 - \left(\frac{n_i}{N_f}\right)^{1/(1-\alpha)}\right]^{1/(1-\beta)} \qquad (47)$$

where: α ...   is a function in the damage model and depends on the loading [56],
β ...   is a coefficient of the damage model dependent on material [56].

The above-mentioned damage accumulation models are included in the methodology and any of them can be used to calculate the fatigue damage coefficient. The calculation using non-linear models is more complex and challenging to find the input coefficients, which are usually found experimentally, but provides slightly more accurate results compared to the linear model, which is more conservative.

Besides the mentioned models, there are many other models that belong to nonlinear damage cumulative theories [51]: Freudenthal-Heller model, Carpinteri's model, etc.

6.1.3. Stress spectrum calculation

In case that the effects of traffic loads are known it is possible to make a more accurate calculation of remaining fatigue life by determining the equivalent stress range using some of cycle counting method and the approach of cumulation fatigue damage. Then, the stress spectrum, which is stress range and the associated number of cycles in descending order, is necessary to know. The inputs data for calculation stress spectrum may be obtained by several ways:

1) Real data obtained from measurement on existing structure:
   Permanent or temporary monitoring of bridge structures is very important method used during the bridge diagnostic. In this case, measured devices and sensors like strain gauges are installed on selected places of the structure. Relative strain dependent on time is the most common form of data obtained by this method. Bridge monitoring is applied during load tests or for getting the information about effects of common transport. According to the length of monitoring time, the obtained data may contain effects of one or more trains that crossed over the bridge. For evaluation of the data some of sorting method can be used. The result of this method is the stress spectrum obtained in place, where the strain gauge was located on the structure.

2) Data obtained from numerical model of the evaluated bridge:
   The use of suitable software that enables time history analysis, is the second way how to get the data for the stress spectrum calculation. Numerical model of the bridge is loaded by load model LM71 or models of real trains and effects on bridge structure behaviour are observed. The result of this method is stress range (or stress amplitude) on individual components obtained from one crossing of load model.

Stress Spectrum Generator

Computer programme called "Stress Spectrum Generator" was created by author in MATLAB® software. It is a tool for stress spectrum calculation. Computation algorithm is based on rainflow counting method.

The inputs data have a form of stress (or strain) over time. If the input data have a form of relative strain, the values are multiplied by modulus of elasticity and converted into stress values. The outputs from the program are stress ranges divided into selected number of intervals and number of cycles of stress ranges falling into individual intervals. The mean value of each interval is the representative value of stress range. These data are automatically saved into Excel file.

In case that the input data were obtained from static load test, the values of stress range may be multiplied by dynamic factor that is computed according to selected method.

An example of the Stress Spectrum Generator interface can be seen in Fig. 87 and Fig. 88. Detail description of the program including instruction manual is stated in Annexe 2.

Fig. 87 Sample of the Stress Spectrum Generator interface

Fig. 88 Sample of the Stress Spectrum Generator interface

6.1.4. Prediction the remaining service life with respect to various maintenance scenarios

The calculation of remaining service life in the methodology is based on the computational relationships of linear and nonlinear theories mentioned in Chapter 6.1.2. In addition, various scenarios considering the different ways of maintenance are taken into account. Scenarios for the maintenance of structural members or the whole structure are stated in Tab. 32.

Tab. 32 Scenarios considered for remaining service life calculation

Scenario	Scenario title	Scenario description
1	No maintenance	There is no maintenance of structure and structure elements from the corrosion point of view. The coating is not applied → the corrosion process continues → the detail category is getting worse → the remaining life of structure element is the shortest.
2	Coating application	The coating is applied on the whole structure or on the critical members → the corrosion process does not continue during the coating lifetime. The detail category is not getting worse if: 1) the coating lifetime is longer or is equal to required remaining life of structure; 2) the coating is re-applied before the end of its lifetime. In case the effectiveness of coating is loss and there is no re-application, the corrosion process continues and the detail category is getting worse with time. In the final consequence, the remaining life of structure element is longer than in the first case.
3	Strengthening of the critical members	The strengthening of the critical members is applied - for example: the steel sheet is welded to the bottom flange of crossbeam → the strain of the members is increasing → the stress range is increasing. At the same time, it is prevented from increasing the corrosion loss due to coating application and the impacts are the same like in scenario 2. The remaining life of structure element is longer than in two first scenarios.
4	Replacement of the critical members	The critical structure member is replaced by new element → the detail category is equal (or higher) to the detail category of original uncorroded member. The remaining life of structure element is longer than in scenario 1, 2 and 3.

For each scenario the following values are calculated: coefficient of fatigue damage in the future, remaining service life and total service life of assessed element.

6.1.5. Financial costs calculation

The amount of financial costs necessary to maintain the structure during the required remaining service life is estimated on the base of various scenarios. The scenarios stated in Tab. 32 are considered for calculation. Activities and sub-activities related to these scenarios are introduced in Tab. 33. Of course, not all items are included in the costs, but the most important ones for each maintenance scenario are considered. The total financial costs associated with the maintenance are subsequently calculated for each scenario as the sum of costs for individual activities.

Approach taking into account the net present value (NPV) is used to compare past and future cash flows with the current ones. Costs are discounted to a common time to be time equivalent. The discount rate of money reflects the cost of the investor's missed opportunities over time. The net present value for costs, taking into account inflation, is determined according to the following equation (48):

$$NPV = \sum_{t=t_M}^{n} \frac{IM \cdot (1+i)^t}{(1+d)^t}$$

(48)

where: IM is financial costs for the maintenance [CZK/EUR]

      i is inflation rate [%]

      d is discount rate [%]

t_M is year of maintenance

n is required remaining service life of a bridge [years]

Tab. 33 Activities related to financial costs in terms of maintenance

No.	Scenario title	Activities and financial costs related to maintenance		
		Activity	Costs [CZK or EURO]	
1	No maintenance	None	-	-
2	Coating application	1) Sandblasting of corroded surface	Costs Area	[CZK/m^2] [m^2]
		2) Grease removing	Costs Area	[CZK /m^2] [m^2]
		3) Coating application	Costs Area Number of coating layers	[CZK /m^2/1 layer] [m^2] [layers]
		4) Additional costs		[CZK]
3	Strengthening of the critical members + coating application	1) Sandblasting of corroded surface	Costs Area	[CZK /m^2] [m^2]
		2) Grease removing	Costs Area	[CZK /kg] [m^2]
		3) Strengthening application	Costs Weight	[CZK /kg] [kg]
		4) Coating application	Costs Area Number of coating layers	[CZK /m^2/1 layer] [m^2] [layers]
		5) Traffic closure	Costs Time	[CZK /1 hour] [hour]
		6) Additional costs		[CZK]
4	Replacement of the critical members	1) Removing the original member	Costs Weight	[CZK /kg] [kg]
		2) New steel members including coating application	Costs Weight	[CZK /kg] [kg]
		3) Traffic closure	Costs Time	[CZK /1 hour] [hour]
		4) Coating application in the future	Costs Area Number of coating layers	[CZK /m^2/1 layer] [m^2] [layers]
		6) Additional costs		[CZK]

6.1.6. The process of assessment and prediction of residual life using the methodology

The individual steps of fatigue damage assessment and residual life prediction using the developed methodology are as follows with respect to Chapters 6.1.1 to 6.1.5:

1.1 measurement of the actual geometry of the elements under assessment, measurement of the corrosion weakening of the elements;

1.2 selection of a corrosion model and calculation of the evolution of corrosion weakening over time in history (depending on the lifetime of the original corrosion protection);

1.3. calculation of the change of the detail category over time in history (depending on the lifetime of the original corrosion protection);

1.4 according to monitoring data or numerical model of the bridge and known traffic intensity, calculation of stress spectra in history;

1.5 choice of approach for fatigue damage calculation and calculation of fatigue damage coefficient for traffic loading effects in history;

2.1 selecting maintenance scenarios and completing the financial cost items associated with them;

2.2 calculating the evolution of corrosion weakening over time in the future (depending on the maintenance scenarios and the intensity of corrosion protection renewal and its lifetime);

2.3. calculation of the change in the category of detail over time in the future (depending on maintenance scenarios and the intensity and lifetime of corrosion protection renewal);

2.4 calculation of stress spectra in the future according to monitoring data or numerical model of the bridge and prediction of traffic intensity;

2.5 choice of approach for fatigue damage calculation and calculation of fatigue damage coefficient in the future;

2.6 prescribing the required residual service life of the structure;

2.7 calculation of residual fatigue life and comparison with the required life;

2.8 calculation of the financial cost over time for the selected maintenance scenarios until the end of the required service life of the structure.

6.2. FALCom programme

Using MATLAB® software, a program for the prediction of the remaining fatigue life of bridge elements has been developed by author. It is the analytical software tool called FALCom, which is the abbreviation of „Fatigue Assessment on Level of Component ". The whole methodology stated in Chapter 6.1 is included in this programme. For an example of the FALCom interface see Fig. 89 and Fig. 90.

For the calculation of fatigue damage and residual fatigue life, linear and non-linear damage accumulation models are included in the program.

The program takes into account possible corrosion weakening of the elements under consideration when calculating fatigue damage and residual life. Corrosion weakening is taken into account by changing the fatigue curve over time. The relationship for the reduction of the detail category was taken from the results of laboratory tests on the fatigue behaviour of degraded elements (see Chapters 5.1.1 and 5.2.3). These laboratory tests were carried out and evaluated in the initial phase of the author's research. A graph of the dependence of the detail category and corrosion weakening is shown in Fig. 71 and Fig. 82.

The algorithm from the "Stress spectrum generator" program, which is used to calculate the stress spectra of the traffic load, was also integrated into the FALCom program.

In addition, different scenarios are considered according to the maintenance of the structural elements or the whole structure (see Tab. 32). For each of these scenarios, the fatigue damage coefficients from

traffic loading expected in the future, the remaining service life and the overall service life of the element under consideration are calculated by the program. The estimation of the residual life is based on the computational relationships of the linear and non-linear theories presented above.

Based on the maintenance scenarios, the amount of financial costs needed to provide the maintenance for the required residual lifetime of the structure is also estimated.
For the cost calculation, the same scenarios as in the previous case for the calculation of the residual lifetime are considered. The total financial cost of maintenance is then given for each scenario by the sum of the costs for each activity.

The outputs from the FALCom program are as follows:

1. Stress spectrum calculated for all train units crossing over the bridge: number of cycles per crossing and per one year.
2. Coefficient of fatigue damage in history: includes the time period from bridge construction (or from the start of operation on the bridge) to the assessment.
3. Coefficient of fatigue damage in the future: includes the time period from the assessment (or since the completion of bridge reconstruction) to the expiration of required remaining life (for example, the bridge is required to remain in service for another 30 years).
4. Remaining service life (years).
5. Total service life (years).
6. Financial costs for the owner necessary to maintain the structure during the required remaining service life.

Points 3–6 are calculated for various scenarios, which depend on the maintenance method or on the type of reconstruction.

Detail description of the FALCom program including instruction manual is stated in Annexe 3.

Potential application and use of the FALCom programme
FALCom programme is a usable tool in form of analytical software. This tool will make possible a residual life assessment including the management of the optimum method and maintenance procedure of the structural elements with respect to the length of the required residual life of the bridge.
With the knowledge of the effects of traffic loads, which can be obtained from measurements directly on the structure or from a computational numerical model, the residual service life of the structural elements can be calculated in a simple way using the program.
After filling in and entering all the necessary input data and setting up the required calculations and outputs, the user obtains from the program the parameters characterising the fatigue life of the element under consideration.
The developed methodology including FALCom software may be a suitable tool for more accurate evaluation of the current state of historical steel riveted bridges. Finally, the methodology can lead to cost savings, as historic bridges can be in operation for a long time without the need for extensive reconstruction.

The application of the methodology and the use of the FALCom program is shown in the case study in Chapter 6.4.
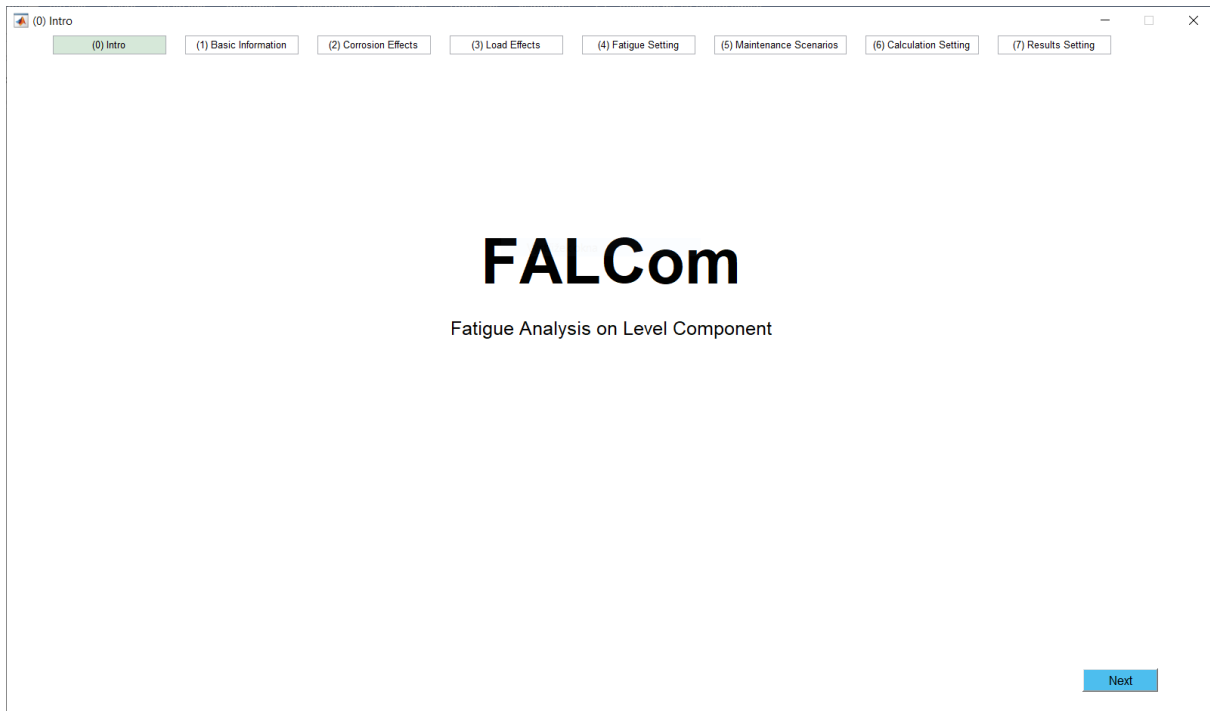
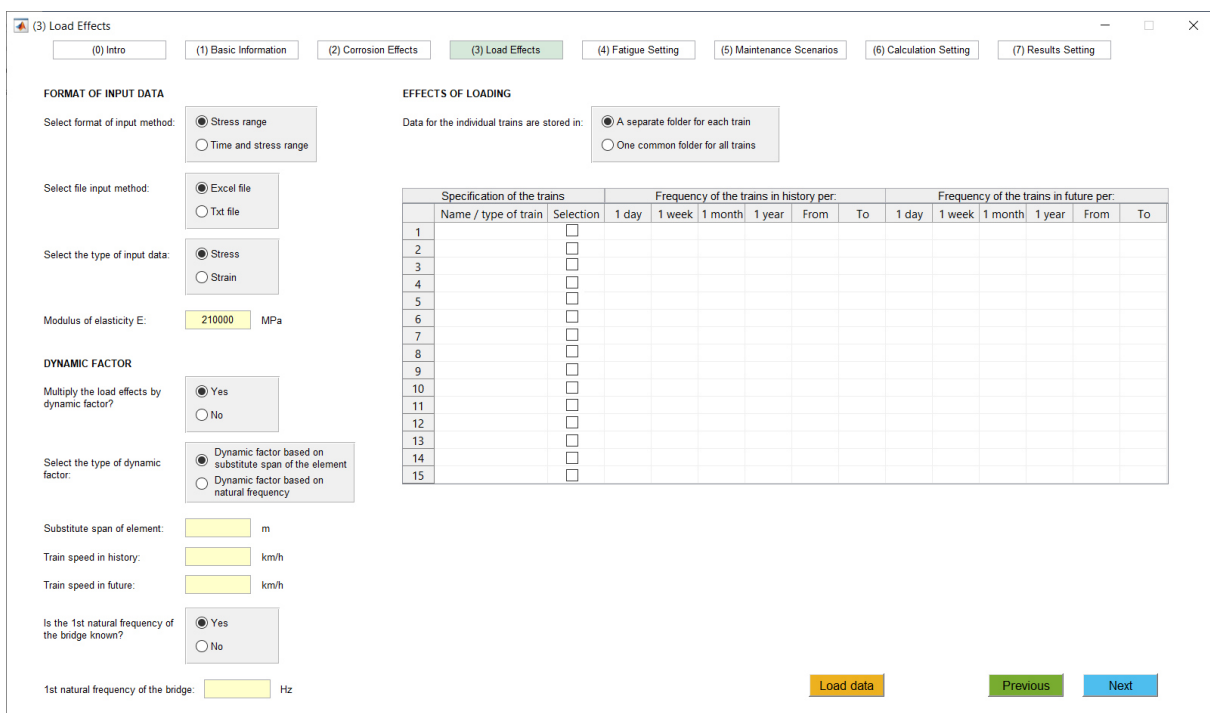*Fig. 89 Sample of the FALCom interface (program introduction screen)*

Fig. 90 Sample of the FALCom interface (window for entering traffic load effects)

6.3. Assessment procedure of fatigue life of existing steel railway bridges

The fatigue assessment procedure for steel structures is quite complex and demanding, especially with regard to the input data. In particular, information on traffic loading (traffic composition and intensity) during the history of the structure. The complexity of the design increases further, especially if it is determined by calculation that the fatigue life has been exhausted or is close to exhaustion.

This chapter is devoted to the process and possibilities of fatigue assessment of structural elements. Diagrams have been produced showing the steps of the different assessment approaches. The diagrams are given in Annex 4. The diagrams describe what inputs and activities are needed to carry out the assessment and the outputs that can be obtained from each approach. Basic measures are also stated for the case where it is determined by calculation that the fatigue life has already been exhausted or that the residual life would be shorter than the required residual life.

Three different assessment approaches were considered:
1. Approach of equivalent stresses
2. Approach of damage accumulation
3. Fracture mechanics approach.

Approach of equivalent stresses
Approach of equivalent stresses je the basic approach for the design of structural elements for fatigue. The principle is to compare the design category of the assessed detail with the design value of nominal stress range related to 2 million cycles.
The base formulas for the approach of equivalent stresses are [34], [57]:

$$\frac{\gamma_{Ff} \cdot \Delta\sigma_{E,2}}{\Delta\sigma_C / \gamma_{Mf}} \leq 1 \qquad\qquad (49)$$

$$\frac{\gamma_{Ff} \cdot \Delta\tau_{E,2}}{\Delta\tau_C / \gamma_{Mf}} \leq 1 \qquad\qquad (50)$$

where: $\Delta\sigma_C, \Delta\tau_C$ is the reference value of the fatigue strength at 2 million cycles,
$\Delta\sigma_{E,2}, \Delta\tau_{E,2}$ is the equivalent constant amplitude stress range related to 2 million cycles
γ_{Ff} is the partial factor for equivalent constant amplitude stress ranges $\Delta\sigma_E, \Delta\tau_E$
γ_{Mf} is the partial factor for fatigue strength $\Delta\sigma_C, \Delta\tau_C$.

This approach is very useful for the design of new structures. However, for the assessment of existing structures, it is preferable to use the damage accumulation approach, which can be used to determine the residual fatigue life.
The basic input parameters for this approach are:

- stress range caused by the fatigue loads,
- detail category of the assessed element,
- dynamic factor.

The calculation can be used to determine:

- fatigue damage of structural member related to 2 million cycles.

Approach of damage accumulation
Approach of damage accumulation is based on the theory of linear or nonlinear damage accumulation. The basic relationships for this approach were presented in Chapter 6.1.2.
The advantage of the damage accumulation approach is that the fatigue damage coefficient and the remaining fatigue life can be determined (with knowledge of the stress spectra), which tells us more about the state of the structure than the equivalent stress approach. However, as mentioned, a

disadvantage of this design approach is the requirement of knowing the stress spectra throughout the bridge history, from which the subsequent accuracy of the calculation is derived.

The basic input parameters for this approach are:
- load history during the bridge operation,
- expected traffic composition in the next years of bridge operation,
- stress spectrum caused by the fatigue loads,
- detail category of the assessed element,
- required remaining service life of the bridge,
- corrosion properties.

The calculation can be used to determine:
- fatigue damage of structural member at observed time,
- fatigue damage of structural member at the end of required time,
- remaining fatigue life.

Fracture mechanics approach
In case there is a crack presence on some component, the linear or nonlinear theory of fracture mechanics is used instead of approach of damage accumulation. Using this method, it is possible to determine the number of cycles that are needed for crack growth from initial length to the critical length.
The formulae for this approach and a more detailed description of the approach will not be given here as it is not the central focus of this dissertation work.
The basic input parameters for this approach are:
- expected traffic composition in the next years of bridge operation,
- stress spectrum caused by the fatigue loads,
- geometry of assessed element,
- type of crack,
- initial crack length,
- critical crack length,
- material properties like: material constant in the Paris equation (D), strain hardening coefficient in Paris equation (m), threshold stress intensity factor (K_{th}), fracture toughness (K_c).

The calculation can be used to determine:
- time to crack growth to the critical length
- remaining service life.

For each approach, a flowchart has been created to show the general steps of the procedure (see Annex 4). The assessment process is divided into 3 phases in the flowcharts:
1) Phase 1: Preliminary activities necessary to be done before the assessment
2) Phase 2: Assessment of remaining fatigue life of structure elements and the whole bridge structure
3) Phase 3: Measures (limitations, recommendations, ...)

1) Phase 1: Preliminary activities necessary to be done before the assessment
In the first phase, preparatory work is carried out to make a fatigue assessment of the elements or the whole structure. If the original documentation is available, a study of this documentation is carried out. Subsequently, the bridge is inspected for defects and failures, corrosion survey is carried out, the actual geometry of the structure is verified and compared with the drawings. If the materials used are not known, sampling shall be carried out to determine the material characteristics [58]. If the composition

of the traffic on the bridge is not known, long-term monitoring shall be carried out to determine the stress spectra. To validate the numerical model and to determine the actual behaviour of the structure, static and dynamic load tests shall be carried out.

2) Phase 2: Assessment of remaining fatigue life of structure elements and the whole bridge structure

For the assessment, one of the above approaches shall be carried out. In the case of fatigue life assessment, the equivalent stress or damage accumulation approach shall be used. In case a crack is already present on the element under assessment, fracture mechanics procedures shall be used. If fatigue life exhaustion is determined by the calculations, the necessary measures shall be designed and implemented (see Phase 3). If the theoretical fatigue life has not been exhausted, the residual fatigue life can be calculated and compared with the required fatigue life. If fracture mechanics is used, the time when the crack reaches the critical length is calculated. If this calculated time is shorter than the required residual life, again the necessary measures need to be taken (see phase 3).

3) Phase 3: Measures (limitations, recommendations, ...)

If in phase 2 it is determined by calculation that the fatigue life of a structural element has already been exhausted, safety measures must be taken. If the load-bearing capacity and reliability of the structure as a whole is endangered, it is necessary to stop operation and carry out reconstruction of the bridge. If the load-bearing capacity and reliability of the structure as a whole is not at risk, it is recommended to implement measures based on monitoring of the bridge condition (regular inspections of the critical details and members or long-term monitoring of the critical details and members with an early warning system). Alternatively, measures providing the extension of the service life (strengthening of critical members or reconstruction of the critical members) can be implemented. If the theoretical fatigue life has not yet been exhausted, but the theoretical residual life is shorter than the required residual life, appropriate measures must be proposed: if the load-bearing capacity and reliability of the structure as a whole is endangered, safe operation must be ensured by one of the following measures:

- Measures providing the extension of the service life:
    - Strengthening of critical members
    - Reconstruction of the critical members

- Other measures:
    - Limitation of the traffic (max. train velocity, max. axle load)

- Alternatively:
    - Fracture mechanics approach if a fatigue crack has appeared and calculation the time of crack growth (see approach 3).

If the load-bearing capacity and reliability of the structure as a whole is not at risk, the next operation of the bridge is possible, but the measure in form of the bridge condition monitoring is necessary:

- Regular inspections of the critical details and members
- Long-term monitoring of the critical details and members with an early warning system.

6.4. Case study

The application of above-mentioned methodology for the assessment of remaining fatigue life of components is shown on a practical example. The most critical components with respect to fatigue of an old railway steel bridge were assessed and the possibilities of extension the service life of the bridge were analysed.

Bridge description

The existing steel railway bridge is used to shown the methodology in practice (see Fig. 91). The bridge is situated in Prague in Hlubočepské valley and takes the railway single-track over Dalejský brook. The angle of crossing is 70 degrees. The track on the bridge is located in right-hand arc with diameter of 334.0 m and the cant is 97 mm. The span is 10.0 m, the width is 5.65 m and the total length of the bridge is 26.70 m. From the static point of view, the bridge acts as a simply supported beam. Design velocity of track is 70 km/h. The bridge was built in 1872.

(a)   *(b)*

Fig. 91 Railway bride: a) longitudinal view; b) view on the superstructure

The load bearing structure consists of two main riveted steel girders of length 10.60 m and the axial distance between them is 2.16 m. The height of girders is not constant, but it changes along the length, which is caused by various thickness of the upper and the bottom flange: the outside parts: 890 mm, intervening parts: 900 mm and the middle part: 918 mm. The upper flange is composed of 2-4 steel sheets of thickness 8-12 mm that are connected with rivets. The bottom flange is composed of 1-2 steel sheets with thickness of 10-30 mm. The number of sheets changes along the span of girders. The width of both flanges is the same – 350 mm. The web consists of steel sheets with dimensions 830x8x1441-2630 mm. The interaction between flanges and webs is ensure by isosceles angles L78x78x11 that are joined with webs and flanges by rivets.

Transverse bracing of the bridge is composed of total 7 steel riveted crossbeams. Each of them consists of 4 isosceles angles L80x80x10 and diagonals L70x70x8. The axial distance of bracing is from 1.99 to 2.15 m. The length of crossbeams is 2.16 m, which is the same value as axial distance of the main girders.

Longitudinal bracing of the bridge is composed of bars with cross-section of angles L70x70x8. These bars with the length of 3.0 m create a truss structure and each couple of crossing members is joined with one rivet. This bracing is connected to the upper bars of lateral bracing and to the upper flanges of the main girders.

The current state of the bridge

The detailed inspection of the bridge has been done and the following damages has been discovered: The upper flanges of main girders are weakened by corrosion pits and the measured difference between

original and current thickness is 5-6 mm in some parts. The average value of corrosion loss is about 3 mm. Some of rivets are affected by corrosion too and the material loss of rivet heads is 30-40 % in some cases. The corrosion weakening of bottom flanges is caused by presence of soil, dust and vegetation. Flange angle is the member, which is affected the most by corrosion. The average corrosion loss on flange angle is about 4 mm, especially on the upper surface of horizontal flange. This fact may have a big influence on load bearing capacity and fatigue behaviour of damaged elements and also the whole structure.

The members of transverse and longitudinal bracing are not affected by corrosion or mechanical damage.

Material of steel structure is mild steel with material properties according to [58]:
- Modulus of elasticity: E = 200 000 MPa
- Yield strength: fy = 210 MPa
- Ultimate strength: fu = 340 MPa

Fatigue load and corrosion exposure

For the fatigue assessment, only the effects of traffic load that belongs to group of variable loads, were considered. Other effects of variable loads like wind load, snow load and temperature effects were neglected.

The load development in time on the track, where the bridge is situated, was taken according to [57] and [59]. Fig. 92 shows how a passenger and heavy transport was changed during the service life of the bridge. It can be seen that there was a big load fluctuation in history. At the beginning of the bridge operation, in 1872, the value of total load was 0.1 million tons per year. Afterwards, the gradual increase in passenger and heavy traffic was followed. The most significant changes occurred in time period after the Second World War and the maximum value of load track (2 million tons per year) was reached in 1988. Since then, the value of heavy transport started to decrease rapidly (until 2004), even though the increase in passenger transport continued.

Year 2018 is considered as the year of the assessment and the value of total track load is 0.98 million of tons per 1 year. In contrast to history, at present the passenger transport represents greater portion of the total load than the heavy transport.

For the future a slight increase of traffic load may be expected. For this reason, the development of traffic load on the bridge in the future is predicted as follow: load caused by passenger and heavy transport will increase by 0.5 % per 1 year (see Fig. 92). These data are used for remaining service life calculation.
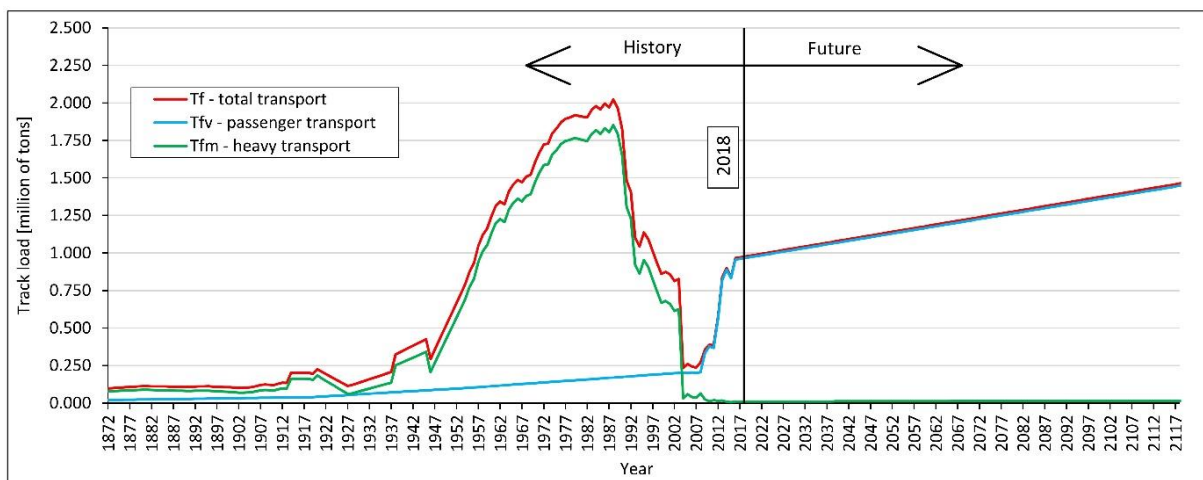
Fig. 92 Bridge load in history and future prediction

The number of trains crossing over the bridge during one day in 2018 was find out according to the train timetable:
- slow passenger train: 13
- passenger train: 58
- cargo train: 2.

Total five train units were chosen to represent the movable load on the bridge. Two of them belong to "slow passenger trains", where any axle force is not higher than 120 kN. Another two train units with axle forces higher than 120 kN for each driving vehicle fall into "passenger train". The last one of the train units is a cargo train, which consists of 1 locomotive and 17 railway cars with a total weight of 5060 tons. An overview of train units crossing over the bridge at present time is stated in Tab. 34.

Tab. 34 Train units crossing over the bridge at present

Train unit	No.	Driving vehicle	Axle forces
Slow passenger train	1	Multiple unit train 814 (62.3 t)	3x (2x 118.3 kN)
	2	Motor-coach train 810 (20 t)	2x (2x 110 kN)
Passenger train	1	Locomotive 754 (74.4 t)	4x 187.5 kN + 3x (4x 120 kN)
	2	Motor-coach train 854 (50.3 t)	4x 140 kN + 2x (4x 112.5 kN)
Cargo train	1	Locomotive 742 (64 t)	4x 160 kN + 17x (4x 65 kN)

As had been described, the main beams are affected by corrosion especially due to negative impact of weather. The average value of corrosion loss on the upper and the bottom flanges is 3 and 4 mm respectively. This fact is taken into account for the assessment of remaining fatigue life of bridge components. Corrosion models are used for calculation of corrosion rate in history and for prediction of corrosion rate in the future. The assumption is that the coating was applied just during the bridge

construction and not re-applied later up to the present. The effectiveness of the coating was estimated at 20 years.

Numerical model

The 3D numerical model of the bridge was created in CSI Bridge software for determination of stress ranges that were used for fatigue assessment. All bridge components were modelled as bar elements (1D) with the real cross-section characteristics (see Fig. 93 and Fig. 94). Corrosion loss was taken into account by thickness reduction of plates and flange angles of the bottom and upper flange of the main girders.

Three different cross-sections of main girders due to various thickness of flanges were taken into account in model. Transverse bracing was composed of 2 isosceles angles L80x80x10 in the upper plane and 2 isosceles angles L80x80x10 in the bottom plane. 4 crossed diagonals with the cross-section L70x70x8 filled in the space between the mentioned upper and bottom angles. Connections of 2L80x80x10 to main girders were modelled by articulated joints in horizontal and vertical direction as well as the connection of bars L70x70x8 with 2L80x80x10. Connection of crossed diagonals were modelled by articulated crossing to ensure interaction between them.

Horizontal bracing was modelled using bar elements with cross-section of angles L70x70x8. Bars were connected to main girders by solid bonds, however joints, which allow rotation in both vertical and horizontal directions, were placed on both ends of bracing. Fixed bearings of the bridge, which are located closer to Prague - Smíchov station, were modelled as flexible in longitudinal and transversal direction of the bridge. One direction movable bearings that are situated closer to the Rudná station, were modelled as flexible in the transversal direction of the bridge.
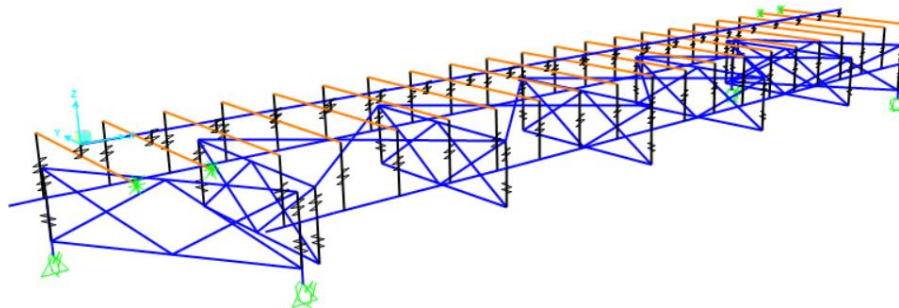
Fig. 93 Numerical model of the bridge - spatial bar model
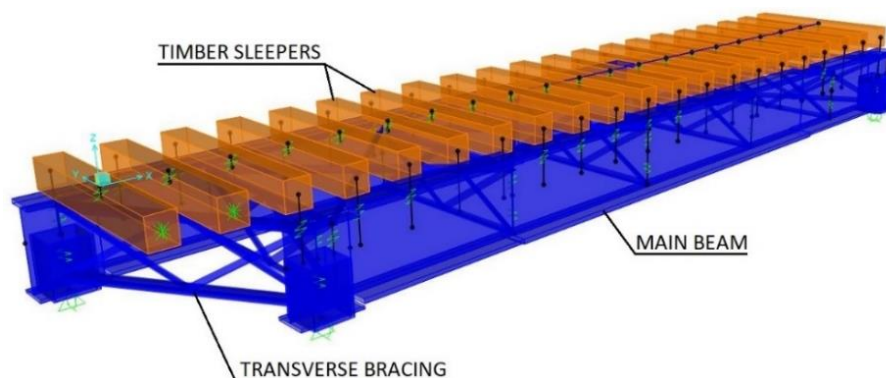
Fig. 94 Numerical model of the bridge - spatial model with real cross-sections

Train units that are currently crossing over the bridge were modelled as a movable load. Axle forces and distances between them fully corresponded to diagrams stated in Tab. 34. Crossing time of each train

unit was set up on base of the total train length and the speed of 70 km/h, which is the maximum allowed train speed on the bridge. The value of modal damping was set up to 0.01.

Movable load was located on a track whose position was the same as position of railway track axis. The track was modelled as a curved bar with radius R=334 m and was situated 47 mm above sleepers. The track was joined with the sleepers using solid bonds. Cross-sectional characteristics of the bar were the same as characteristics of 2 rails S49.

Time history analysis was applied to calculate the dependence of stress on time in evaluated elements and cross-sections. After that, the stress spectrum caused by one crossing of train unit was calculated by using Stress Spectrum Generator. The same procedure was applied to all models of train units. In the next step, the stress spectra for years in history were calculated on base of ratio of track load in 2018 to individual years in history.

Members under the assessment

The main beams of the bridge were selected for fatigue assessment and evaluation of remaining fatigue life, because of several reasons: (1) low detail category of connections according to [35], (2) high value of stress range caused by effects of real trains and (3) high level of corrosion weakening, especially on the upper and the bottom flange (see Fig. 95).

Detail categories occurred on the main beam:

- detail category 71: in place, where the number of sheets, which create the bottom flange, changes. In our case: the bottom flange in part P3 consists of 2 sheets (thickness: 30+10 mm) and the part P2 consists of 1 sheet (thickness: 30 mm); the cross-section including last row of rivets in part P2 before the change in number of sheets was assessed.
- detail category 85: continuous connection of flange angle and flange; the detail was assessed in place of maximum bending moment caused by models of real trains.

Value of partial factor for fatigue strength is taken as: $\gamma_{Mf} = 1.15$ [58].

Detail category		Scheme
71	At the end of strengthening plates (e.g. at flange curtailment)	
85	Continuous connection of flange angle and flange. (Rivets subject to shear due to bending moments)	

(a)   *(b)*
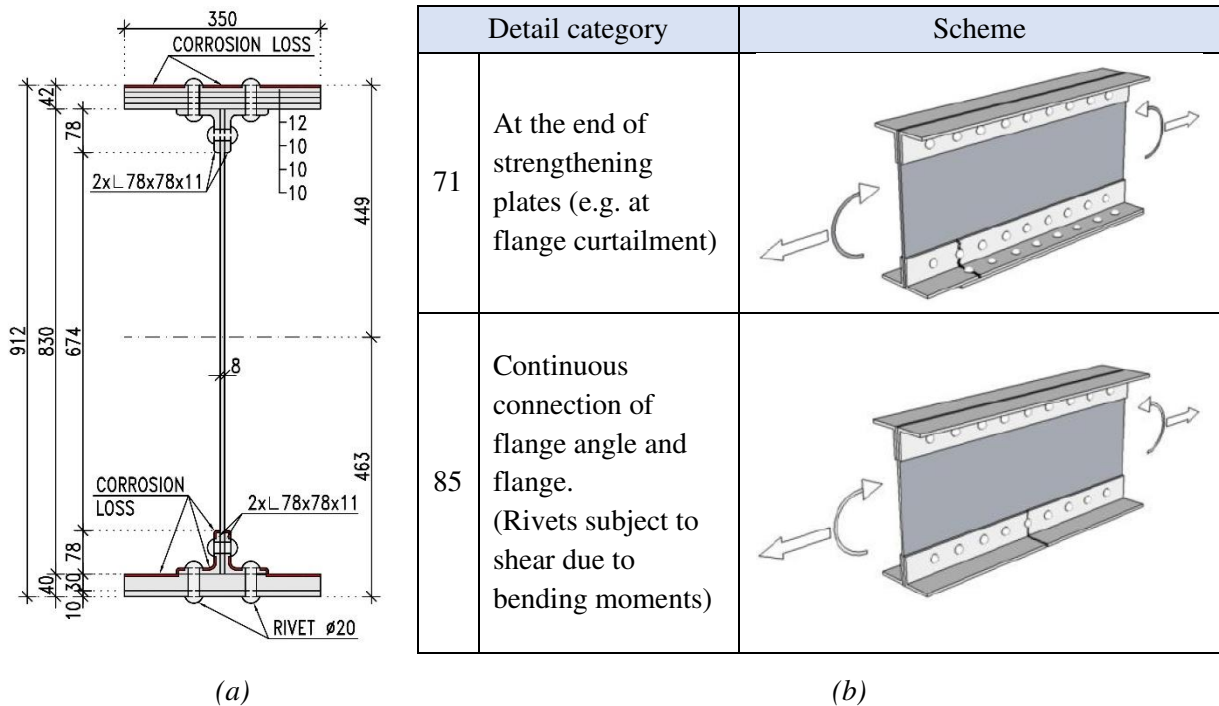
Fig. 95 a) Beam cross-section; b) Evaluated detail category [35]

Maintenance scenarios

For the future service life assessment, the following four scenarios (see Fig. 96) related to maintenance were considered according to the methodology stated in Chapter 6.1.4:

- 1st scenario "No maintenance": there is no maintenance of the beams → corrosion process continues and category detail is getting worse in time. There are no costs for the owner.
- 2nd scenario "Coating application": the coating of the beams is renovated several times in a row (scenario 2a) or one time (scenario 2b) according to the required remaining service life of the bridge. Corrosion process does not continue and category detail is not getting worse.
- 3rd scenario "Strengthening of the critical members and coating application": the additional steel plates are put on the bottom flange of riveted beam for the purpose of increasing the cross-section area. The coating is applied several times in a row (scenario 3a) or one time (scenario 3b). Corrosion process does not continue, category detail is not getting worse and the values of stress ranges are lower because of the strengthening.
- 4th scenario "Replacement of the critical members": the original corroded beams are replaced by new elements. A coating of new beams is applied several times in a row (scenario 4a) or one time (scenario 4b).

It is assumed that all of these scenarios are applied in the same year as the bridge assessment is being done. It means in 2018.

Tab. 35 contains the inputs for calculation the financial costs for each scenario. Corresponding activities and costs are filled in the table according to the type of a maintenance. There are zero costs for the bridge owner in terms of maintenance in case of the 1st scenario that simulates no maintenance during the future service life of the bridge. The 2nd and 3rd scenario includes activities related to coating application and strengthening of the critical members. Financial costs are dependent on surface area of both main beams, number of coatings and weight of additional steel plates in case of the 3rd scenario. Among the other things, the costs of 4th scenario, which is focused on replacement of the critical members, take into account the costs related to traffic closure that is necessary during the time of reconstruction.
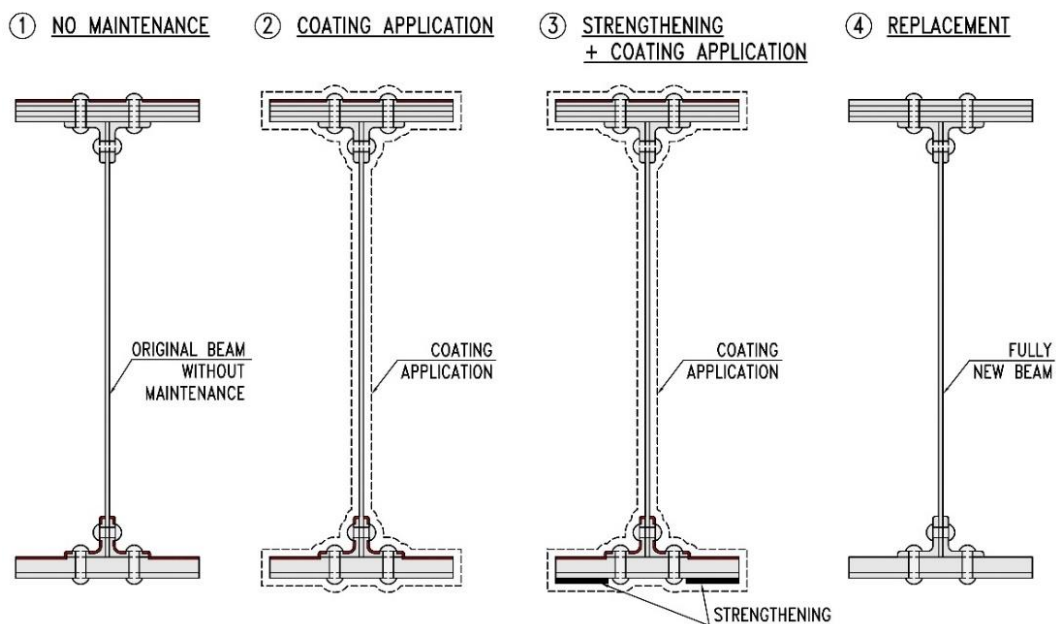
Fig. 96 Maintenance scenarios considered for the assessment of remaining service life

Tab. 35 Financial costs related to maintenance scenarios

Sc.	Scenario title	Activities and financial costs related to maintenance			
		Activity	Costs		Unit
1	No maintenance	None	-	0	[€]
2	Coating application	1) Sandblasting of corroded surface	Costs	4	[€/m²]
			Area	65	[m²]
		2) Grease removing	Costs	1	[€/m²]
			Area	65	[m²]
		3) Coating application	Costs	40	[€/m²/1 layer]
			Area	65	[m²]
			Number of coatings	3	[coatings]
		4) Additional costs		0	[€]
3	Strengthening of the critical members + coating application	1) Sandblasting of corroded surface	Costs	4	[€/m²]
			Area	65	[m²]
		2) Grease removing	Costs	2	[€/m²]
			Area	65	[m²]
		3) Strengthening application	Costs	8	[€/kg]
			Weight	165	[kg]
		4) Coating application	Costs	40	[€/m²/1 layer]
			Area	65	[m²]
			Number of coatings	3	[coatings]
		5) Additional costs		0	[€]
4	Replacement of the critical members	1) Removing the original member	Costs	0.5	[€/kg]
			Weight	8970	[kg]
		2) New steel members including coating application	Costs	6	[€/kg]
			Weight	8970	[kg]
		3) Traffic closure	Costs	200	[€/hour]
			Time	72	[hour]
		4) Coating application	Costs	40	[€/m²/1 layer]
			Area	65	[m²]
			Number of coatings	3	[coatings]
		5) Additional costs		0	[€]

Results and evaluation of the assessment

Applying the developed methodology and FALCom software, the assessment of remaining fatigue life of steel riveted bridge was done. The most critical components with respect to fatigue and corrosion loss were assessed and the possibilities of extension the service life of the bridge were analysed. On the base of made calculations, the detail category 71 was the decisive detail from the length of remaining fatigue life point of view. For this reason, the results are shown for the assessment of this detail.

Corrosion loss is one of the parameters that affect the length of fatigue life. Corrosion models were used to calculate corrosion rate on the bridge in history and in the future. Fig. 97 shows the dependence of corrosion loss of the bottom flange on bridge age. The dependence was determined by Klinesmith's linear corrosion model [50]. The effectiveness of the original protective coating was estimated at 20

years. After the effectiveness of coating was lost, the corrosion weakening began to initiate. At the time of bridge assessment, the average corrosion loss value was equal to 4 mm, which corresponds to the measured value. Regarding the corrosion loss in the future, the 1st scenario leads to the highest value. Each of scenarios 2, 3 and 4 is divided into two cases: the full lines correspond to the situation, when the coating is applied repeatedly, which means that the corrosion loss is not increasing anymore. On the other hand, the dashed lines symbolise the only one application of coating with the effectiveness of 20 years. The red and green lines of 2nd and 3rd scenario overlap because of the similar maintenance procedure. The bridge age at the time of evaluation was 147 years.
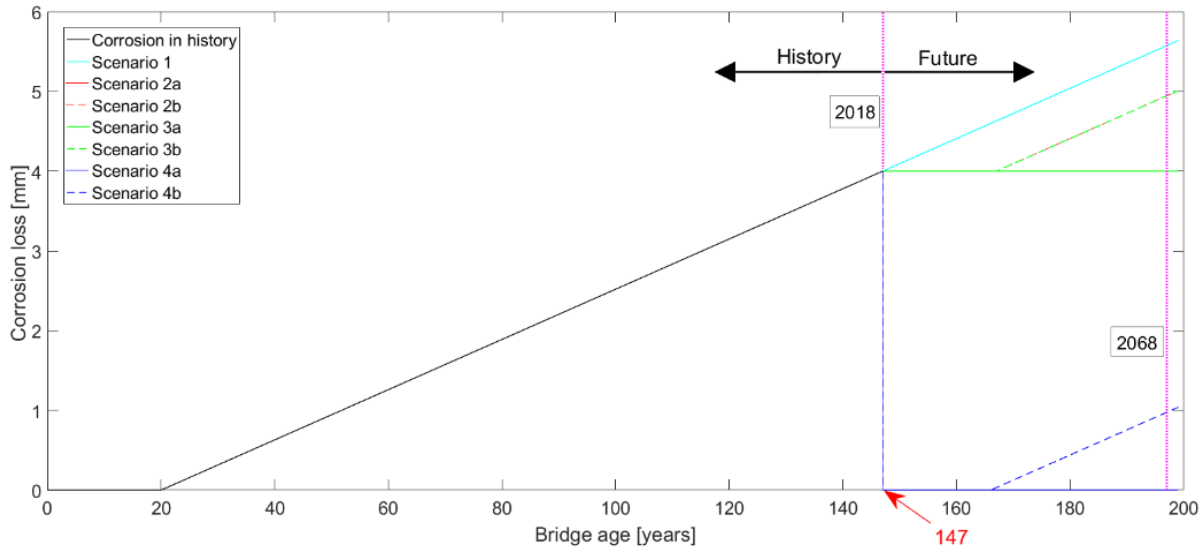
Fig. 97 Change of corrosion loss in time on the bottom flange

The presence of corrosion loss has a negative impact on fatigue behaviour of corroded elements. The main reason is the changing of detail category with various corrosion level. The change of detail category in time is shown in Fig. 98. The original detail category of evaluated member was assumed to be 71. In case of the 1st scenario, which corresponds to no bridge maintenance, the detail category is getting worse during the whole service life of the bridge in the future, because the process of corrosion loss is not stopped or interrupted. Scenarios 2 and 3 have the similar effect - the detail category is not getting worse during the time of coating effectiveness. Finally, the assumption of the 4th scenario is that the detail category of new construction member is higher than the original one, in our case 85 instead of 71.
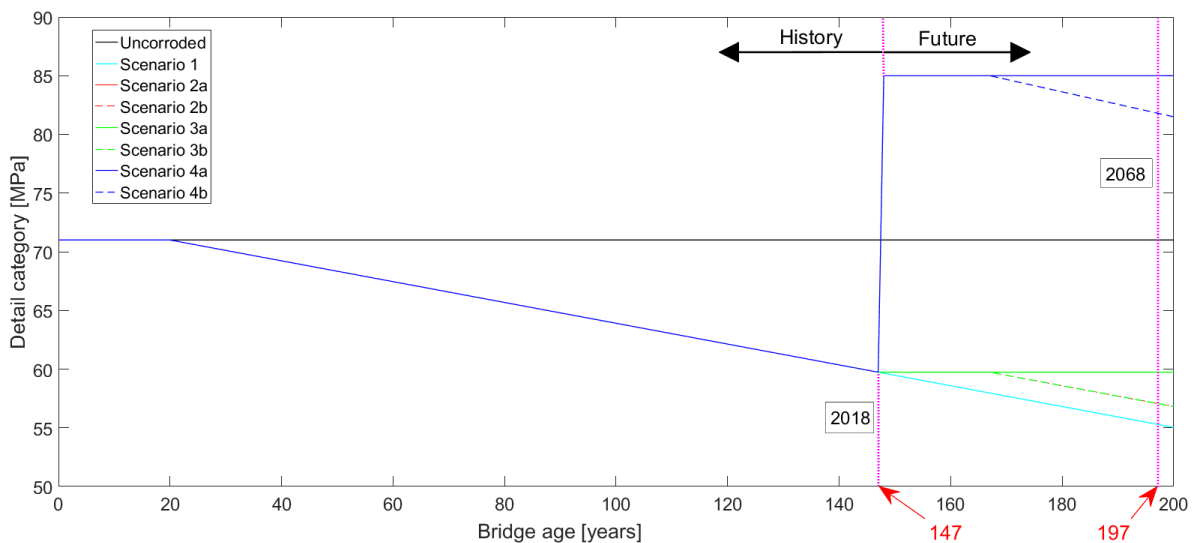
Fig. 98 Change of detail category in time due to corrosion weakening
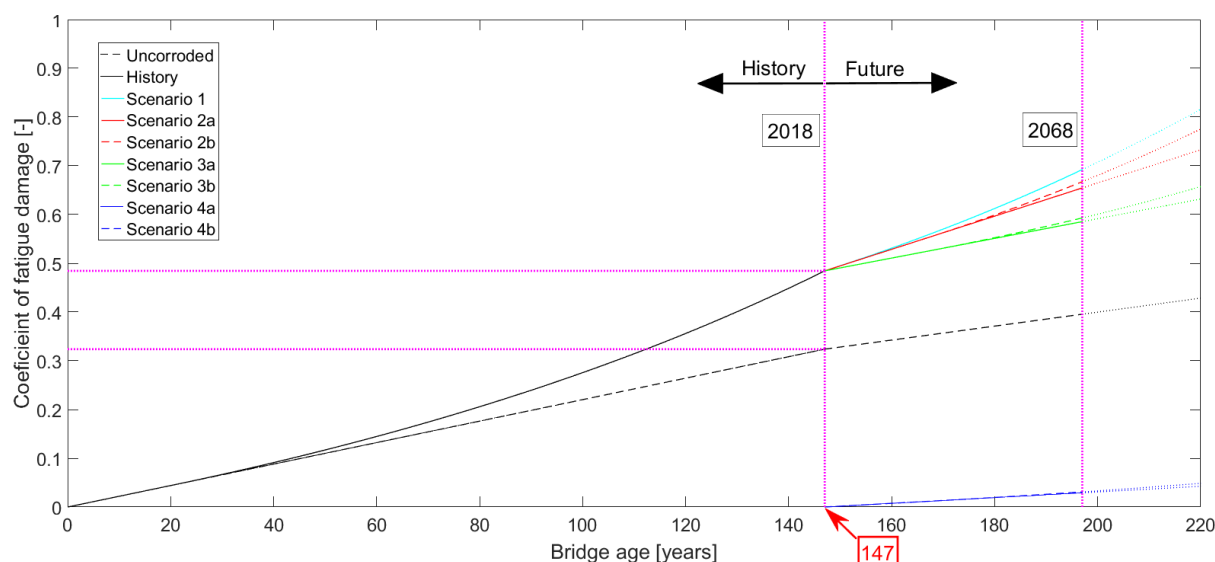
Fig. 99 The dependence of fatigue damage coefficients on time (Palmgren¬-Miner linear theory)

Tab. 36 summarizes the results of the assessment. The calculations are divided for each scenario according to the approaches of fatigue assessment (linear and non-linear theories). In the first step, coefficient of fatigue damage values were calculated in time of bridge assessment (2018) and at the end of the required service life (2068). The required remaining service life was set up to 50 years. Afterward, the remaining service life of the detail was calculated for all scenarios. The total service life is given as a sum of current structure age and calculated remaining service life. The dependence of coefficients of fatigue damage on time for all scenarios and approach of linear theory is shown in Fig. 99.

Calculated remaining service life for all scenarios is longer than the required (coefficients of fatigue damage is lower than 1). However, comparing the results, the 1st scenario leads to the shortest service life of the bridge. Remaining service life for the 1st scenario is 102 years according to the calculations. Comparing scenarios 2 and 3, we find that scenario 3 leads to a longer lifetime. This is due to the fact that scenario 3 is based on the renewal of the corrosion coating and the strengthening of the structural element. The strengthening of the bottom flange of the main beams leads to a reduction of the stress range, which ultimately results in a lower value of the fatigue damage coefficient and therefore an increase in the residual life of the element (compared to scenario 2 where only the anti-corrosion coating was renewed). The 4th scenario provides the longest service life of the bridge. Calculated remaining service life is longer than 300 years.

According to the results stated in Tab. 36, on-linear approaches of calculation provide favourable results in comparison to linear approach. The main reason is that non-linear approaches take into account the load interaction effects.

From the bridge owner point of view, financial costs play an important role in his decision-making. The final costs related to all considered scenarios were calculated and the results are stated in Fig. 100. The developed methodology takes into account the net present value to compare past and future cash flows with the current ones. The value of discount rate was set up to 0.5 %. The inflation rate was taken into account by value 2.0 %. On the base of Tab. 35, there are zero costs in case of 1st scenario due to absence of maintenance works. On the other hand, the 4th scenario leads to the longest service life, however the costs are the highest for the owner. Fig. 100 shows maintenance costs over time.

105

Tab. 36 Results of the assessment using approach of linear and non-linear damage cumulative theories

Palmgren-Miner			Scenario							No corrosion	Year
			1	2a	2b	3a	3b	4a	4b		
CFD	In time of bridge construction	[-]	0.0	0.0	0.0	0.0	0.0	0.0	0.0	0.0	1872
	In time of assessment	[-]	0.49	0.49	0.49	0.49	0.49	0.49	0.49	0.32	2018
	At the end of required service life	[-]	0.69	0.66	0.68	0.58	0.60	0.03	0.03	0.39	2068
Service life	Required remaining service life	[years]	50								-
	Calculated remaining service life	[years]	102	151	112	182	135	>300	>300	>300	-
	Total service life	[years]	249	298	259	329	282	>500	>500	>500	-
Corten-Dolan			Scenario							No corrosion	Year
			1	2a	2b	3a	3b	4a	4b		
CFD	In time of bridge construction	[-]	0.0	0.0	0.0	0.0	0.0	0.0	0.0	0.0	1872
	In time of assessment	[-]	0.44	0.44	0.44	0.44	0.44	0.44	0.44	0.29	2018
	At the end of required service life	[-]	0.64	0.61	0.62	0.53	0.55	0.02	0.02	0.36	2068
Service life	Required remaining service life	[years]	50								-
	Calculated remaining service life	[years]	109	162	120	197	146	>300	>300	>300	-
	Total service life	[years]	256	309	267	344	293	>500	>500	>500	-
Morrow			Scenario							No corrosion	Year
			1	2a	2b	3a	3b	4a	4b		
CFD	In time of bridge construction	[-]	0.0	0.0	0.0	0.0	0.0	0.0	0.0	0.0	1872
	In time of assessment	[-]	0.43	0.43	0.43	0.43	0.43	0.43	0.43	0.29	2018
	At the end of required service life	[-]	0.64	0.60	0.61	0.53	0.55	0.01	0.02	0.36	2068
Service life	Required remaining service life	[years]	50								-
	Calculated remaining service life	[years]	110	163	121	199	147	>300	>300	>300	-
	Total service life	[years]	257	310	268	346	294	>500	>500	>500	-
V. Dattoma			Scenario							No corrosion	Year
			1	2a	2b	3a	3b	4a	4b		
CFD	In time of bridge construction	[-]	0.0	0.0	0.0	0.0	0.0	0.0	0.0	0.0	1872
	In time of assessment	[-]	0.42	0.42	0.42	0.42	0.42	0.42	0.42	0.28	2018
	At the end of required service life	[-]	0.62	0.59	0.60	0.51	0.53	0.01	0.01	0.35	2068
Service life	Required remaining service life	[years]	50								-
	Calculated remaining service life	[years]	112	167	124	204	151	>300	>300	>300	-
	Total service life	[years]	259	314	271	351	298	>500	>500	>500	-

Note: CDF… coefficient of fatigue damage

Scenario	Costs [EURO]
Scenario 1	0
Scenario 2a	68,000
Scenario 2b	22,000
Scenario 3a	77,000
Scenario 3b	30,000
Scenario 4a	165,000
Scenario 4b	119,000

(a)   *(b)*
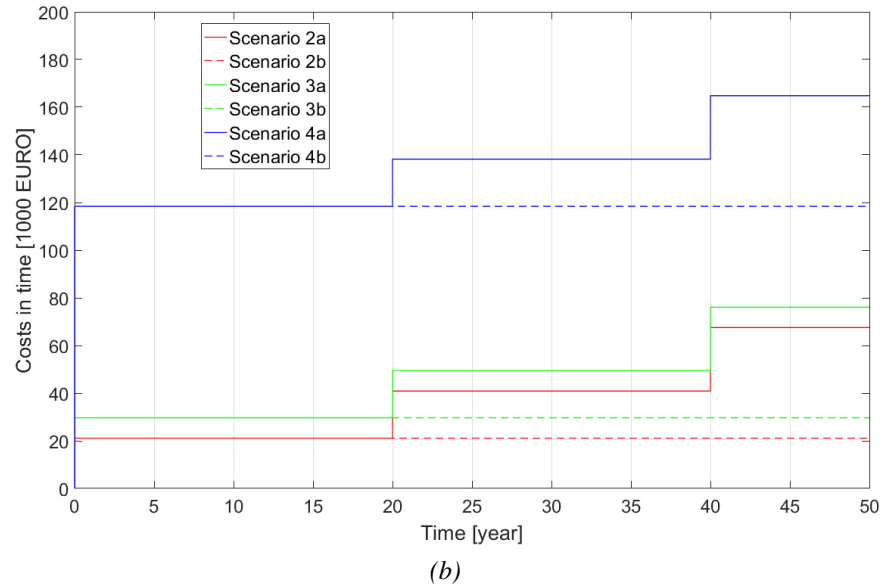
Fig. 100 Financial costs in the future: (a) Total financial costs; (b) Financial costs over time

Conclusion of the case study

The application of the developed methodology for the assessment of remaining fatigue life of components was shown on a practical example. The most critical components with respect to fatigue of an old railway steel bridge were assessed and the possibilities of extension the service life of the bridge were analysed by using the developed FALCom software.

The following conclusions may be observed from the case study:

- Calculated remaining fatigue life of the assessed detail for all scenarios is longer than the required one. The longest remaining service life is ensured by the 4th scenario, which is based on the replacement of the critical components. In this case, the both main beams were replaced.

- On the base of calculations, the bridge may be in service for another 100 years without any maintenance. However, there are several uncertainties, such as the development of traffic intensity or composition of traffic in the future.

- In case the required service life would be longer than the current 50 years, the 2nd and 3rd scenarios would be suitable solutions to ensure efficient fatigue capacity of the bridge. Scenarios 2a and 3b provides the similar remaining service life for approximately the same financial costs.

- Approach of non-linear cumulation of fatigue damage provides favourable results from the length of service life point of view. The values of coefficients of fatigue damage are lower in case of nonlinear approaches.

- The developed methodology including FALCom software may be a suitable tool for more accurate evaluation of the current state of historical steel riveted bridges. In the final consequence, the methodology can lead to cost savings, while historic bridges can be in operation for a long time without the need for extensive reconstruction. Of course, regular inspections of the bridge are essential to ensure that the current condition of the structure is known and to detect any failures that may occur during the operation life of the structure.

7. Conclusion of doctoral thesis

7.1. Summary of the scientific achievements of doctoral thesis

The subject of the doctoral thesis was to analyse and describe the relation between corrosion and fatigue. The research was based on experimental fatigue tests performed on corrosion-weakened specimens taken from a bridge structure more than 120 years old. The relationships between various parameters characterizing the corroded surface of the specimens and the fatigue life were investigated.

Subsequently, a methodology was developed to predict the remaining service life of existing steel riveted bridges considering the effects of fatigue and corrosion. The developed methodology was subsequently implemented in a computer program created by the author. The developed program allows the assessment of the residual service life, including the management of the optimal method and procedure for the maintenance of structural elements with respect to the length of the required remaining service life of the bridge.

1) Experimental fatigue tests results and the relationship between corrosion loss and fatigue life

To investigate the relationship between corrosion weakening and fatigue life, experimental fatigue tests were performed on specimens taken from a nearly 120-year-old railway steel bridge structure. The tested construction detail was considered to be a bending detail category 71, which corresponds to group WIII of fatigue sensitive details according to IRS 77802 [35]. The tested samples simulated the connection of the truss members, for example the connection of the bracing diagonal or the connection of the diagonal and the web of the flange of the truss riveted girder. The individual tested specimens were weakened by corrosion to different degrees, and were divided into 3 groups: (1) Samples with no corrosion, (2) Samples with medium level of corrosion, (3) Samples with high level of corrosion.

The specimens were tested to complete failure, with a characteristic failure mode such that a fatigue crack developed in the plate weakened by the hole at the first rivet, followed by crack propagation in direction perpendicular to main stresses and then complete failure of the specimen. The strain gauges placed on the samples showed almost constant values of the minimum and maximum stress are until the initiation and propagation of a fatigue crack. After the crack initiation, the length began to change rapidly and the measured values of stress range started to increase significantly with the growth of the crack.

The number of cycles to crack initiation and to complete failure of the specimens was measured during the tests. The assumption of the bending detail category for an uncorroded tested sample was 71 MPa, which corresponds to 123,000 cycles for stress range 180 MPa. The measured number of cycles was higher for uncorroded samples, and the ratio of measured-to-expected was equal to 1.5-2.4. The number of cycles for samples with a medium level of corrosion and with a high level of corrosion was also variable, but was generally lower. The ratio for medium level was: 1.3-1.8, and for high level the ratio was: 0.75-1.5.

The ratio of the number of cycles for crack growth and for crack initiation was around 0.2 for the tested type of specimens. This means that for the tested specimens, the number of cycles for crack initiation exceeded the number of cycles for crack propagation. In comparison, the ratio of the number of cycles for crack growth and crack initiation is usually around 0.5 or higher for large specimens. This means that the time for crack initiation and growth is approximately the same for large samples.

Measured cycle counts show that there is a **downward tendency in the number of cycles for crack growth**. The **number of cycles for crack growth decreases slightly with the increase in corrosion weakening**. This phenomenon is very well observed on average values of number of cycles for individual sets (no corrosion, medium level of corrosion, high level of corrosion). However, this effect is not so evident for individual samples, because of the fluctuation in the numbers in each set. The faster crack initiation in samples weakened by corrosion is mainly due to the surface roughness of the tested

sample. The irregularities in the form of corrosion pits cause a local increase in stress in the loaded element and at the same time the corrosion pit is the place where the fatigue crack is likely to occur first. As already mentioned, the ratio of the number of cycles for crack growth (Np) to the number of cycles required for crack initiation (Ni) is around 0.2 (0.18 for samples without corrosion weakening and 0.28 for samples with high level of corrosion weakening). Comparing the number of cycles required for crack initiation between the different sets, it can be observed that for the samples with medium corrosion level, on average 79% of the number of cycles as for the samples without corrosion weakening were required, and for the samples with high corrosion weakening, on average only 55% of the number of cycles as for the samples without corrosion weakening were required.

Laboratory tests were performed mainly to find out whether or not there is any change in the bending detail category when there is a corrosion weakening. By comparing the relationship between the number of cycles to failure of the specimens and the corrosion level, a **decreasing trend in the number of cycles with increasing corrosion level** was found.

The real parameters (geometry, load) were considered for a calculation of the real bending detail category of the tested riveted joints. Detail category was based on the number of cycles that corresponded to total failure of the sample. The evaluation was based on the fatigue curve for non-welded details taken according to IRS 77802 [35].

The calculated bending detail category for uncorroded samples S1.1, S1.2, S1.3 and S1.4 reached a value of 82.6 MPa or higher, the average value was 87.4 MPa and the value of 95% quantile was 79 MPa. To fully classify the test specimens in terms of the category of detail, a series of fatigue tests would need to be performed for different levels of stress range. In terms of technological and time requirements, tests for all specimens were performed for only one stress range level (approximately 180 MPa). For specimens with corrosion loss, the 95% quantile value of bending detail category for a medium level of corrosion was 75.1 MPa, and for a high level of corrosion the 95% quantile value was 63.1 MPa. In this case, too, a **downward tendency can be observed – the higher the corrosion loss, the lower the bending detail category**, in terms of average and 95% quantile values.

The change in the length of the fatigue life can be described by the change in the fatigue curve in dependence on the corrosion level. **The relation between the bending detail category and the corrosion loss may be expressed by a linear function** (Eq. (25) and (26)), and the new detail category for narrow members can be calculated using reduction coefficient $c_{R,\mathrm{dA}}$. Reduction coefficient $c_{R,\mathrm{dA}}$ depends on coefficient of corrosion level d_A which is determined as the change in cross-section area for members loaded by axial force. In case of members loaded by bending moment or loaded by combination of bending moment and axial force, the level of corrosion is considered as change in cross-section area of assessed part of member. Coefficient d_A takes into account the change in the cross-section area as a whole due to corrosion. However, it does not take into account the size and shape of individual surface irregularities. It means that the influence of irregularities of the corroded surface are not included in this calculation.

In the next phase, a **multiparametric evaluation of the experimental tests** was performed. The following parameters, which are important in terms of fatigue strength of the tested specimens, were determined on the cross-section at the 1st rivet hole of testes samples:

   1) Ratio of the length of the curve following the corroded surface to the width of the corroded surface (Δb_c)

   2) minimum thickness of plate ($t_{c,min}$)

   3) thickness of the plate at a distance of 1-10 mm from the edge of the rivet hole ($t_{c,i}$)

   4) cross-section area of the rivet head (A_{r1}).

The parameter Δb_c takes into account any surface roughness. The parameter better describes whether the surface of the corroded element is regular or irregular compared to the parameter d_A. The d_A parameter only accounts for the change in cross-sectional area. The more irregular the surface, the greater the value of the Δb_c parameter. For a surface without irregularities, the value of the parameter is equal to 0.

The dependence between coefficients d_A and Δb_c for each tested sample provides an approximately linear relationship, with the value of Δb_c increasing with increasing d_A. From a global point of view, this means that **the more the test specimen was corroded, the more irregular the surface was**.

The relationship between coefficient Δb_c and detail category $\Delta_{\sigma c,R}$ provides a downward tendency – **the higher the roughness of the corroded surface, the lower the bending detail category**, in terms of average values.

The cross-sectional area A_{r1} of the rivet head was measured in a cross-section through the centre of the 1st rivet hole. Possible corrosion weakening of the rivet head may adversely affect the magnitude of the clamping force that is induced by prestressing in the rivet. A reduction in the size of the cross-sectional area of the rivet head may result in a reduction in prestressing and therefore a reduction in clamping force.

The dependence between the parameter Δ_{Ar} and detail category $\Delta_{\sigma c,R}$ of tested samples shows from a global point of view, **the lower the value of the parameter Δ_{Ar} (i.e. the greater the corrosion weakening of the rivet head), the lower the detail category**. After applying regression analysis, an approximately linear relationship between Δ_{Ar} and $\Delta_{\sigma c,R}$ can be observed.

The value of minimum thickness of plate $t_{c,min}$ considers the smallest thickness of the corroded plate in the cross-section through the centre of the 1st rivet hole. If the plate under assessment is without corrosion weakening, then the value of $t_{c,min}$ is equal to the thickness of the unweakened plate. The maximum corrosion weakening cw_{max} is then given as the difference between the values of the original thickness and the minimum thickness of the plate.

The relationship between the maximum corrosion weakening and the detail category cannot be clearly determined. It depends very much on the distance at which the maximum corrosion weakening is located from the edge of the hole. On each specimen, the maximum weakening was located at different positions. However, in terms of average values, **a decreasing trend can be observed, with the higher the maximum corrosion weakening, the lower the detail category**.

In addition to the minimum thickness of the sheet metal, the thicknesses $t_{c,i}$ of the sheet metal at a distance of 0 to 10 mm from the edge of the hole in a cross section through the centre of the 1st rivet hole were also determined. Based on the thicknesses $t_{c,i}$, the corrosion weakening cw_i was calculated for each distance (0 - 10 mm). For each of the three sets of specimens, the average values of the detail category were considered, as well as the average values of the corrosion weakening cw_i of the plates at distances of 4, 5, 6, 7, 8, 9 and 10 mm from the edge of the hole.

From the relationship between the corrosion weakening of the plate cw_i and the detail category (in terms of the average values) it can be indicated that **the closer the corrosion weakening value is to the edge of the rivet hole, the lower the detail category** the sample corresponds to.

Of all the parameters observed, **the parameter Δ_{bc} which takes into account the irregularities of the corroded surface, seems to be the most reflective**. By introducing the coefficient d_{bc}, **the relationship between the parameter Δ_{bc} and the bending detail category may be expressed as an approximately linear function** (Eq. (38) and (39)).

The parameter Δ_{bc} (respectively d_{bc}) takes into account any surface roughness. The parameter better describes whether the surface of the corroded element is regular or irregular compared to the parameter d_A (Eq. (25) and (26)). The d_A parameter only accounts for the change in cross-sectional area. The more irregular the surface, the greater the value of the d_{bc} parameter. For a surface without irregularities, the value of the parameter is equal to 0.

For practical applications where corrosion weakening is measured on the structure in situ, it is preferable to use a simplified relationship (based on d_A parameter) which, although slightly less accurate than the second approach, still gives good results.

The developed formulas are derived from the experimental tests mentioned above. Their applicability is limited to narrow bars, i.e. to steel sheets with a maximum thickness of 60 mm.

2) Methodology for prediction the remaining service life of steel bridge structure components deteriorated by corrosion

The methodology designed to calculate fatigue damage of structural members that are or are not deteriorated by corrosion and to estimate the remaining service life of such elements was developed. The methodology takes into account the following aspects that affect the fatigue life of structural details and that determine their residual service life:

1) Various level of corrosion weakening
2) Bridge load history
3) Detail category
4) Stress range
5) Various maintenance scenarios.

Using the proposed methodology, it is possible to determine and calculate the following characteristics and parameters, which tell whether or not the theoretical fatigue life of the element under assessment has already been exhausted and which maintenance scenario is the most appropriate to choose with respect to the required residual service life and the financial cost to be spent on the maintenance:

a) Corrosion effects
b) Stress spectrum calculation
c) Calculation of fatigue damage
d) Calculation of remaining fatigue life
e) Financial costs estimation.

Corrosion effects are taken into account by using corrosion models. Corrosion models depict the dependence of corrosion loss on time. Several corrosion models are included into the methodology:

1) Power model [15]
2) Corrosion model by Guedes Soares and Garbatov [49]
3) Corrosion model by Klinesmith et al. [50].

Rainflow counting method is used to calculate stress spectrum. Real data obtained from measurement on existing structure or data obtained from numerical model of the evaluated structure can be used as the inputs for stress spectrum calculation.

Several models of linear and nonlinear damage cumulative theories are used in the methodology for calculation of coefficient of fatigue damage and remaining service life. In addition, various scenarios considering the different ways of maintenance are taken into account:

1. No maintenance - there is no maintenance of structure and structure elements from the corrosion point of view

2. Coating application - the coating is applied on the whole structure or on the critical members
3. Strengthening of the critical members - the strengthening of the critical members is applied
4. Replacement of the critical members - the critical structural member is replaced by new element.

For each scenario the following values are calculated: coefficient of fatigue damage in the future, remaining service life and total service life of assessed element.

The amount of financial costs necessary to maintain the structure during the required remaining service life is estimated on the base of various scenarios. The above-mentioned scenarios are considered for calculation. Approach taking into account the net present value (NPV) is used to compare past and future cash flows with the current ones.

Within the developed methodology, several flowcharts were also developed to include procedures and possibilities for fatigue assessment of structural elements. Flowcharts have been developed showing the general steps of the different assessment approaches. The flowcharts describe what inputs and activities are needed to carry out the assessment and the outputs that can be obtained from each approach. Basic measures are also stated for the case where it is determined by calculation that the fatigue life has already been exhausted or that the residual life would be shorter than the required residual life.
Three different assessment approaches were considered in the diagrams:
1. Approach of equivalent stresses
2. Approach of damage accumulation
3. Fracture mechanics approach.

For each approach, a flowchart has been created to show the steps of the procedure (see Annex 4). The assessment process is divided into 3 phases in the flowcharts:
1) Phase 1: Preliminary activities necessary to be done before the assessment
2) Phase 2: Assessment of remaining fatigue life of structure elements and the whole bridge structure
3) Phase 3: Measures (limitations and recommendations).

3) FALCom programme
Using MATLAB® software, a program for the prediction of the remaining fatigue life of bridge elements has been developed by author. It is the analytical software tool called FALCom, which is the abbreviation of „Fatigue Assessment on Level of Component ". The developed methodology is included in this programme.
The outputs from the FALCom program are as follows:

1. Stress spectrum calculated for all train units crossing over the bridge
2. Coefficient of fatigue damage in history: includes the time period from bridge construction (or from the start of operation on the bridge) to the assessment.
3. Coefficient of fatigue damage in the future: includes the time period from the assessment (or since the completion of bridge reconstruction) to the expiration of required remaining life (for example, the bridge is required to remain in service for another 30 years).
4. Remaining service life (years).
5. Total service life (years).
6. Financial costs for the owner necessary to maintain the structure during the required remaining service life.

FALCom programme is a usable tool in form of analytical software. This tool will make possible a residual life assessment including the management of the optimum method and maintenance procedure of the structural elements with respect to the length of the required residual life of the bridge.

With the knowledge of the effects of traffic loads, which can be obtained from measurements directly on the structure or from a computational numerical model, the residual service life of the structural elements can be calculated in a simple way using the program.

After filling in and entering all the necessary input data and setting up the required calculations and outputs, the user obtains from the program the parameters characterising the fatigue life of the element under assessment.

The developed methodology including FALCom software may be a suitable tool for more accurate evaluation of the current state of historical steel riveted bridges. Finally, the methodology can lead to cost savings, as historic bridges can be in operation for a long time without the need for extensive reconstruction.

7.2. Suggestions for subsequent research

The topic of the effect of corrosion weakening on the fatigue behaviour of steel riveted bridges is a vast topic. It is difficult to cover all the content of this issue within one stage of research. The research carried out in this doctoral thesis was focused on the fatigue behaviour of classic riveted connections of historic structures. The tested construction detail was considered to be a bending detail category 71, which corresponds to group WIII of fatigue sensitive details according to IRS 77802 [35]. The tested sample simulated the connection of the truss members, for example the connection of the bracing diagonal or the connection of the diagonal and the web of the flange of the truss riveted girder. The individual tested specimens were weakened by corrosion to different degrees.

There are several other activities that would be useful to build on the research carried out in the framework of this doctoral thesis and that would help to extend the knowledge in the field of the influence of corrosion on the fatigue life of steel structures.

1) Effects of corrosion on the fatigue life of riveted details of different types and dimensions

In the context of further research, it would be beneficial to carry out another series of fatigue tests focused on other types of fatigue details. Typical details of riveted bridges are connections of truss members, continuous connection of web and flange angle, continuous connection of flange angle and flange or connections of bracing members. Again, it would be beneficial if the test specimens were taken from the real structure and were weakened by varying levels of corrosion. Natural corrosion weakening better represents the actual condition of the elements compared to corrosion created by an artificially accelerated process.

In the next stage, it is important to look at whether corrosion weakening has the same effect on lower and higher categories of detail. Whether it can be expected that the effect of corrosion increases with a lower detail category and decreases with a higher detail category at the same level of corrosion weakening. A further question is whether the influence of corrosion effects on fatigue life varies with the value of the stress range.

Focusing on these questions will help to better understand the fatigue behaviour of corrosion weakened elements.

2) Experimental fatigue test on riveted connections with inactive rivets

Prestressing in the rivet of riveted connections has an influence on the mode and degree of corrosion weakening of the surface of the elements around the rivet head. Observation of the mode of corrosion weakening on real structures shows that if the prestressing in the rivet is active, corrosion under the rivet head does not occur or occurs only to a certain extent, compared to the surface of the element around the rivet head. If the prestressing in the rivet is active, corrosion of the rivet shank does not occur. This was the case for the specimens used for the experiment in this dissertation.

For rivets without active prestressing in structures subjected to adverse weather conditions, moisture penetrates into the space below the rivet head to the edge of the hole or to the inner surfaces of the hole in the sheet metal and the rivet shank (depending on the extent to which the rivet shank fills the holes in the sheet metal to be joined). Corrosion then occurs in these parts of the connection as well.

For this reason, it is also important to focus on experiments on specimens with inactive rivets to observe how corrosion affects their fatigue behaviour.

3) Mapping the effects of corrosion on steel bridges with respect to their type, age and location

The next area for research on this issue is the specification of the effects of corrosion on bridge structures with respect to various indicators. In order to more accurately determine the evolution of corrosion weakening, it is important to map the extent and mode of corrosion weakening on existing bridge structures.

On existing structures, the most common location and extent of corrosion weakening needs to be specified, taking into account the geographical location of the bridge, the orientation of the structure with respect to cardinal points, the location with respect to cities and industrial areas, the type and age of the structure and the frequency of maintenance work. Knowing this information, the development of corrosion weakening on existing and new structures can be better and more accurately predicted. Following the knowledge of the evolution of the rate and extent of corrosion weakening, it would be possible to more accurately predict changes in the load-bearing and fatigue behaviour of structures.

4) Optimising maintenance scenarios with respect to achieving the longest possible residual lifetime at the lowest possible financial cost

The next phase of this research can be focused on optimizing maintenance scenarios. The method and frequency of maintenance has a major impact on the condition of the structure. If the maintenance is sufficient there is no growth of corrosion weakening and deterioration. However, regular and efficient maintenance is conditioned by sufficient financial costs, which, moreover, increase over time due to the rising prices of the required materials and the influence of inflation.

Determining an effective maintenance procedure for the bridge with regard to the required service life and financial costs is therefore appropriate. By optimising the maintenance scenarios, it would be possible to achieve the required service life of the bridge at the lowest possible financial cost.

However, as mentioned in the doctoral thesis above, this requires a very good understanding of how corrosion weakening affects the load capacity and fatigue life of structures and the ability to predict the evolution of load capacity and fatigue life over time.

7.3. Contribution to the solved issue

According to the author, the submitted doctoral thesis is beneficial in the following points:

- Experimental fatigue tests were performed on corrosion weakened riveted joint specimens. The tests showed the effect of corrosion on the reduction of fatigue life.
- The relationships between various parameters characterizing the corroded surface of the specimens and the fatigue life were investigated. The reduction in fatigue life can be described as a change (reduction) in the category of the detail due to corrosion.
- Relationships for the reduction of the detail category due to corrosion weakening were derived.
- A methodology for predicting the residual fatigue life of riveted structural members was developed.
- The developed methodology was implemented in an analytical software tool created by the author. The program allows the assessment of the residual service life, including the management of the optimal method and procedure for the maintenance of structural elements with respect to the length of the required remaining service life of the bridge.

8. List of figures

9. List of tables

10.List of references

[1] MARS G. FONTANA. *Corrosion engineering*. 3rd ed. New Delhi: Tata McGraw-Hill, 2005.

[2] BENEŠOVÁ, J. *Konzervování a restaurování kovů: ochrana předmětů kulturního dědictví z kovů a jejich slitin*. Brno: Technické muzeum v Brně - Metodické centrum konzervace. 2011.

[3] HAI, Dinh Tuan. Current status of existing railway bridges in Vietnam: An overview of steel deficiencies. *Journal of Constructional Steel Research* [online]. 2006, 62(10), 987-994.

[4] BEAULIEU, L.-V., F. LEGERON and S. LANGLOIS. Compression strength of corroded steel angle members. *Journal of Constructional Steel Research* [online]. 2010, 66(11), 1366-1373.

[5] XU, Shan-hua and You-de WANG. Estimating the effects of corrosion pits on the fatigue life of steel plate based on the 3D profile. *International Journal of Fatigue* [online]. 2015, 72, 27-41.

[6] ASTM G85-11, Standard Practice for Modified Salt Spray (Fog) Testing, ASTM International, West Conshohocken, PA, 2011.

[7] ČSN EN ISO 9227. Korozní zkoušky v umělých atmosférách - Zkoušky solnou mlhou. 2007.

[8] CAPRILI, S. and W. SALVATORE. Cyclic behaviour of uncorroded and corroded steel reinforcing bars. *Construction and Building Materials* [online]. 2015, 76, 168-186.

[9] KAITA, T., J.M.R.S. APPUHAMY, K. ITOGAWA, M. OHGA and K. FUJII. Experimental Study on Remaining Strength Estimation of Corroded Wide Steel Plates under Tensile Force. *Procedia Engineering* [online]. 2011, 14, 2707-2713.

[10] SAAD-ELDEEN, S., Y. GARBATOV and C. GUEDES SOARES. Experimental assessment of corroded steel box-girders subjected to uniform bending. *Ships and Offshore Structures* [online]. 2013, 8(6), 653-662.

[11] GARBATOV, Y., C. G. SOARES and J. PARUNOV. Fatigue strength experiments of corroded small scale steel specimens. *International Journal of Fatigue* [online]. 2014, 59, 137-144.

[12] SHARIFI, Y. and R. RAHGOZAR. Fatigue Notch Factor in Steel Bridges Due to Corrosion. *Archives of Civil and Mechanical Engineering* [online]. 2009, 9(4), 75-83.

[13] ALBRECHT, P. and A. NAEEMI. *Performance of weathering steel in bridges*. Washington, D.C.: Transportation Research Board, National Research Council, 1984, 164 p. Report (National Cooperative Highway Research Program, 272.

[14] TOWNSEND, H. E. and J. C. ZOCCOLA. Eight-year atmospheric corrosion performance of weathering steel in industrial, rural, and marine environments. *Atmospheric Corrosion of Metals*, ASTM STP, 1982, 767, 45-59.

[15] KOMP, M. Atmospheric corrosion rating of weathering steels. *Calculations and significance. Mater Performance*. 1987, 26(7).

[16] RAHBAR-RANJI, Ahmad. Ultimate strength of corroded steel plates with irregular surfaces under in-plane compression. *Ocean Engineering* [online]. 2012, 54, 261-269.

[17] NAKAI, T., MATSUSHITA, H. and N. YAMAMOTO. Effect of pitting corrosion on the ultimate strength of steel plates subjected to in-plane compression and bending. *Journal of Marine Science and Technology* [online]. 2006, 11(1), 52-64.

[18] CHEN, Y., LI, X., Y. CHAI and J. ZHOU. Assessment of the flexural capacity of corroded steel pipes. *International Journal of Pressure Vessels and Piping* [online]. 2010, 87(2-3), 100-110.

[19] SHARIFI, Y. and R. RAHGOZAR. Remaining moment capacity of corroded steel beams. *International Journal of Steel Structures* [online]. 2010, 10(2), 165-176.

[20] KAYSER, J. R. and A. S. NOWAK. Reliability of corroded steel girder bridges. *Structural Safety* [online]. 1989, 6(1), 53-63.

[21] FRANÇOIS, R., KHAN, I. and V. H. DANG. Impact of corrosion on mechanical properties of steel embedded in 27-year-old corroded reinforced concrete beams. *Materials and Structures* [online]. 2013, 46(6), 899-910.

[22]   ČSN EN 1992-1-1 Eurokód 2: Navrhování betonových konstrukcí - Část 1-1: Obecná pravidla a pravidla pro pozemní stavby. 2004.

[23]   CZARNECKI, A. A. and A. S. NOWAK. Time-variant reliability profiles for steel girder bridges. *Structural Safety* [online]. 2008, 30(1), 49-64.

[24]   DARMAWAN, M. Sigit, A.N. REFANI, M. IRMAWAN, R. BAYUAJI and R.B. ANUGRAHA. Time Dependent Reliability Analysis of Steel I Bridge Girder Designed Based on SNI T-02-2005 and SNI T-3-2005 Subjected to Corrosion. *Procedia Engineering* [online]. 2013, 54, 270-285.

[25]   XU, Shan-hua and Bin QIU. Experimental study on fatigue behaviour of corroded steel. *Materials Science and Engineering: A* [online]. 2013, 584, 163-169.

[26]   ZAHRAI, S.M. Cyclic strength and ductility of rusted steel members. *Asian journal of civil engineering (building and housing)* [online]. 2003, 4(2-4), 135-148.

[27]   RAHGOZAR, R. and Y. SHARIFI. Remaining Fatigue Life of Corroded Steel Structural Members. *Advances in Structural Engineering* [online]. 2011, 14(5), 881-890.

[28]   WAHAB, M.A. and M. SAKANO. Experimental study of corrosion fatigue behaviour of welded steel structures. *Journal of Materials Processing Technology* [online]. 2001, 118(1-3), 116-121.

[29]   ZHANG X.-Y., LI S.-X., LIANG R. and R. AKID. Effect of corrosion pits on fatigue life and crack initiation. *13th International Conference on Fracture*. Peking, Čína. 2013.

[30]   PALIN-LUC, T., PÉREZ-MORA, R., BATHIAS, C., DOMÍNGUEZ, G., PARIS, P.C. and J. L. ARANA. Fatigue crack initiation and growth on a steel in the very high cycle regime with sea water corrosion. *Engineering Fracture Mechanics* [online]. 2010, 77(11), 1953-1962.

[31]   HEINEMEYER, Ch. and M. FELDMANN. The influence of rivet corrosion on the durability of riveted connections. *Steel Construction* [online]. 2011, 4(3), 188-192.

[32]   PIPINATO, A., C. PELLEGRINO, O.S. BURSI and C. MODENA. High-cycle fatigue behavior of riveted connections for railway metal bridges. *Journal of Constructional Steel Research* [online]. 2009, 65(12), 2167-2175.

[33]   DIBATTISTA, J. D., ADAMSON, D. E. J. and G. L. KULAK. Fatigue Strength of Riveted Connections. *Journal of Structural Engineering* [online]. 1998, 124(7), 792-797.

[34]   ČSN EN 1993-1-9 Eurokód 3: Navrhování ocelových konstrukcí - Část 1-9: Únava. 2013.

[35]   IRS 77802 "Recommendations for determining the carrying capacity and fatigue risks of existing metallic railway bridges. 2018.

[36]   IMAM, B. M., RIGHINIOTIS, T. D. and M. K. CHRYSSANTHOPOULOS. Numerical modelling of riveted railway bridge connections for fatigue evaluation. *Engineering Structures* [online]. 2007, 29(11), 3071-3081.

[37]   RIGHINIOTIS, Timothy D., Boulent M. IMAM and Marios K. CHRYSSANTHOPOULOS. Fatigue analysis of riveted railway bridge connections using the theory of critical distances. *Engineering Structures* [online]. 2008, 30(10), 2707-2715.

[38]   AL-EMRANI, M. and R. KLIGER. FE analysis of stringer-to-floor-beam connections in riveted railway bridges. *Journal of Constructional Steel Research* [online]. 2003, 59(7), 803-818.

[39]   BRENCICH, A. and L. GAMBAROTTA. Assessment procedure and rehabilitation of riveted railway girders: The Campasso Bridge. *Engineering Structures* [online]. 2009, 31(1), 224-239.

[40]   ČSN EN ISO 6892-1. Kovové materiály – Zkoušení tahem – Část 1: Zkušební metoda za pokojové teploty. 2009.

[41]   ČSN ISO 13822. Zásady navrhování konstrukcí – Hodnocení existujících konstrukcí. 2005.

[42]   ČSN EN ISO 148-1. Kovové materiály – Zkouška rázem v ohybu metodou Charpy – Část 1: Zkušební metoda. 2017.

[43]   NOVOVIC, D., DEWES, R. C., ASPINWALL, D. K., VOICE, W. and BOWEN, P., 2004. The effect of machined topography and integrity on fatigue life. *International Journal of Machine Tools and Manufacture*. 2004. Vol. 44, no. 2–3, pp. 125–134.

[44]   ÅS, S., SKALLERUD, B. and TVEITEN, B. Surface roughness characterization for fatigue life predictions using finite element analysis. *International Journal of Fatigue*. 2008. Vol. 30, no. 12, pp. 2200–2209.

[45]   LUKÁŠ, P. and M. KLESNIL. Fatigue limit of notched bodies. *Materials Science and Engineering*. 1978. Vol. 34, no. 1, pp. 61–66.

[46]   GADELMAWLA, E. S., KOURA, M. M., MAKSOUD, T. M.A., ELEWA, I. M. and H. H. SOLIMAN. Roughness parameters. *Journal of Materials Processing Technology*. 2002. Vol. 123, no. 1, pp. 133–145.

[47]   LEONETTI, D., MALJAARS, J., PASQUARELLI, G. and G. BRANDO. Rivet clamping force of as-built hot-riveted connections in steel bridges. *Journal of Constructional Steel Research*. 2020. Vol. 167.

[48]   LANDOLFO, R., CASCINI, L. and F. PORTIOLI. Modeling of metal structure corrosion damage: A state of the art report. *Sustainability*. 2010. Vol. 2, no. 7, pp. 2163–2175.

[49]   SOARES, G. and Y. GARBATOV, Y. Reliability of maintained, corrosion protected plates subjected to non-linear corrosion and compressive loads. *Marine Structures*. 1999. Vol. 12, no. 6, pp. 425–445.

[50]   KLINESMITH, Dawn E., MCCUEN, Richard H. and ALBRECHT, Pedro, 2007. Effect of Environmental Conditions on Corrosion Rates. *Journal of Materials in Civil Engineering*. Online. 2007. Vol. 19, no. 2, pp. 121–129.

[51]   LV, Z., HUANG, H., ZHU, S., GAO, H. and ZUO, F. 2014. A modified nonlinear fatigue damage accumulation model. Online. 2014. Vol. 24, no. 2, 168–181.

[52]   MILTON MINER, B.Y. and MONICA, S. Cumulative Damage in Fatigue. *Journal of Applied Mechanics*. Online. 1 September 1945. Vol. 12, no. 3, pp. A159–A164.

[53]   CORTEN, H.T. and DOLAN, T.J. Cumulative fatigue damage. *Proceedings of the International Conference on Fatigue of Metals, Institute of Mechanical Engineering, London*, 1956: 235–246.

[54]   MORROW, D.J. The effect of selected subcycle sequences in fatigue loading histories. *Random Fatigue Life Predictions*. ASME. 1986; 72: 43–60.

[55]   CHEN, X., JIN, D. and KIM, K. S., 2006. A weight function-critical plane approach for low-cycle fatigue under variable amplitude multiaxial loading. *Fatigue and Fracture of Engineering Materials and Structures*. 2006. Vol. 29, no. 4, pp. 331–339.

[56]   DATTOMA, V., GIANCANE, S., NOBILE, R. and PANELLA, F. W., 2006. Fatigue life prediction under variable loading based on a new non-linear continuum damage mechanics model. *International Journal of Fatigue*. 2006. Vol. 28, no. 2, pp. 89–95.

[57]   ŽEMLIČKOVÁ, L. and ROTTER, T. Equivalent constant amplitude stress range of railway bridges. Dissertation work, ČVUT Praha, 2004.

[58]   SŽ S5/1 Diagnostika, zatížitelnost a přechodnost železničních mostních objektů. 2021.

[59]   FRÝBA, L. Dynamics of Railway Bridges. Academia: Praha, 1992.

[60]   CAN/CSA-S6-06. *Canadian Highway Bridge Design Code*. Canadian Standards Association: Toronto, 2012.

[61]   KULICKI, J.M., PRUCS, Z., SORGENFREI, D.F., MERTZ, D.R. *Guidelines for Evaluating Corrosion Effects in Existing Steel Bridges*. National Cooperative Highway Research Program, Report No. 333, 1990.

[62]   HAGHANI, R., AL-EMRANI, M., HESHMATI, M. Fatigue-prone details in steel bridges. *Buildings*. 2012. Vol. 2, no. 4, pp. 456-476.

[63]   SŽDC a.s, státní organizace, Technická ústředna dopravní cesty. *Poruchy železničních mostů*. Praha, 2009.

11. Annexes

11.1. Annexe 1: Geometry of tested samples

Annexe 1 consists of summary tables (see Tab. 37) containing the real geometry of tested samples, including photo and description of the corrosion weakening.

The real geometry of the samples was measured using a calliper with an accuracy of 0,01 mm. The following dimensions were measures for all tested samples (see Fig. 101):

L	total length,
L1	length of the upper steel sheet,
L2	length of the bottom steel sheet,
L3	distance from the beginning of the specimen to the centre of the first rivet,
L4	distance from the centre of the third rivet to the end of the upper steel sheet,
W1	width of the extended part of the top steel sheet,
W2, W3, W4	width of the specimen at the centre of the first, second and the third rivet,
W5	width of the extended part of the bottom steel sheet,
T1	thickness of the extended part of the top steel sheet,
T2	thickness of the second steel sheet,
T3	thickness of the third steel sheet,
T4	thickness of the bottom steel sheet,
T5, T6	thickness of the beginning of the narrowed part of the top plate,
T7, T8, T9	total thickness of the specimen at the position of the first, second and the third rivet,
T10	total thickness of the narrow part of the second and the third steel sheet.

The description of the corrosion weakening was based on a detailed visual inspection and measurement of the fabricated samples.

The photogrammetry method with sufficient accuracy ± 0.1 mm was performed to obtain a 3D model of tested samples and to find the exact geometry, including corrosion pits, rivet damage and other irregularities. The photogrammetry pictures are stated in the summary tables.
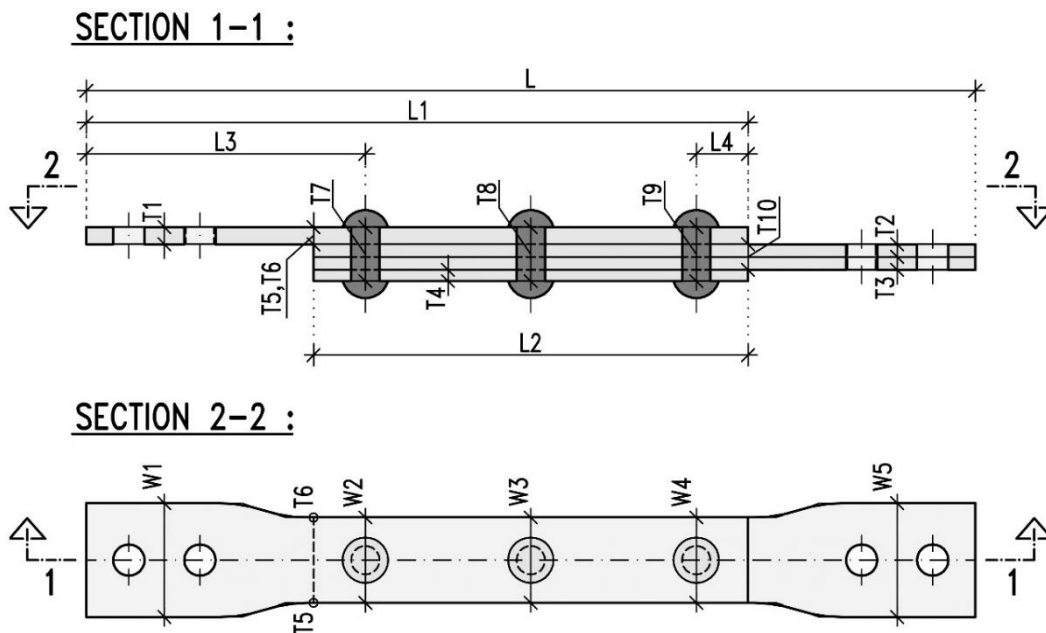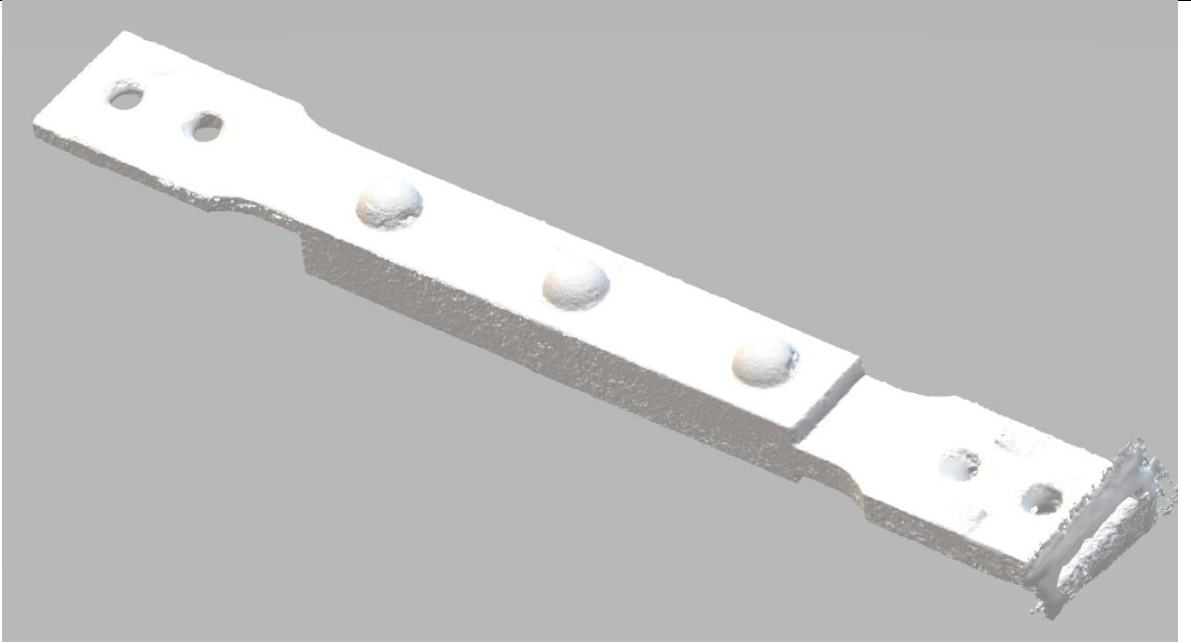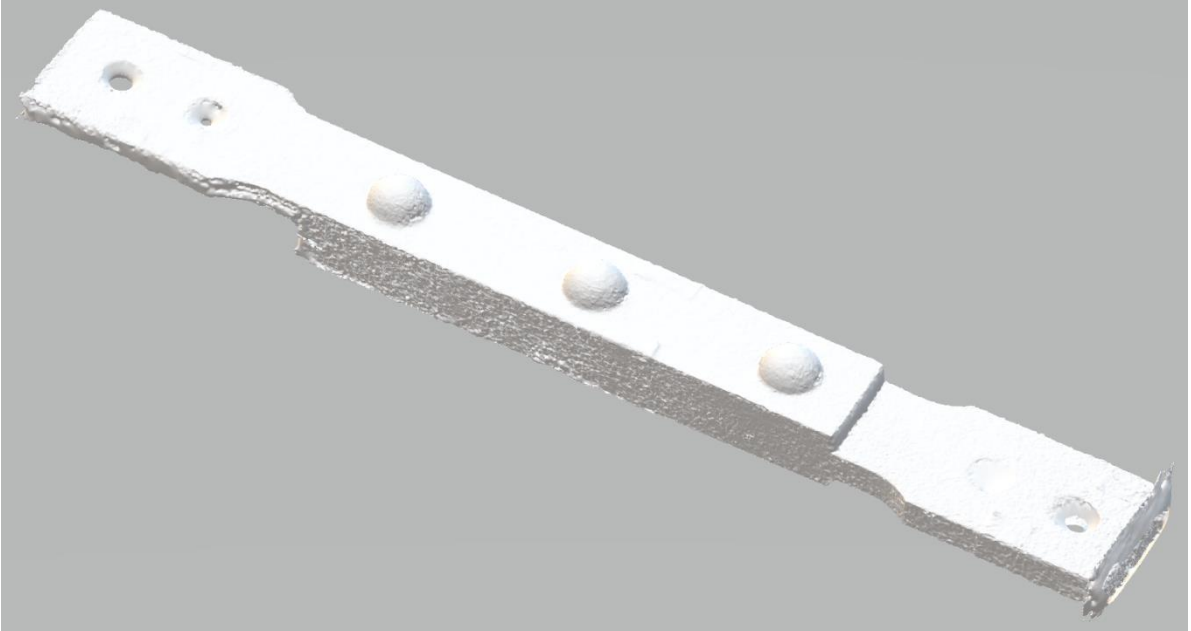
Fig. 101 The position of the measured dimensions on the samples
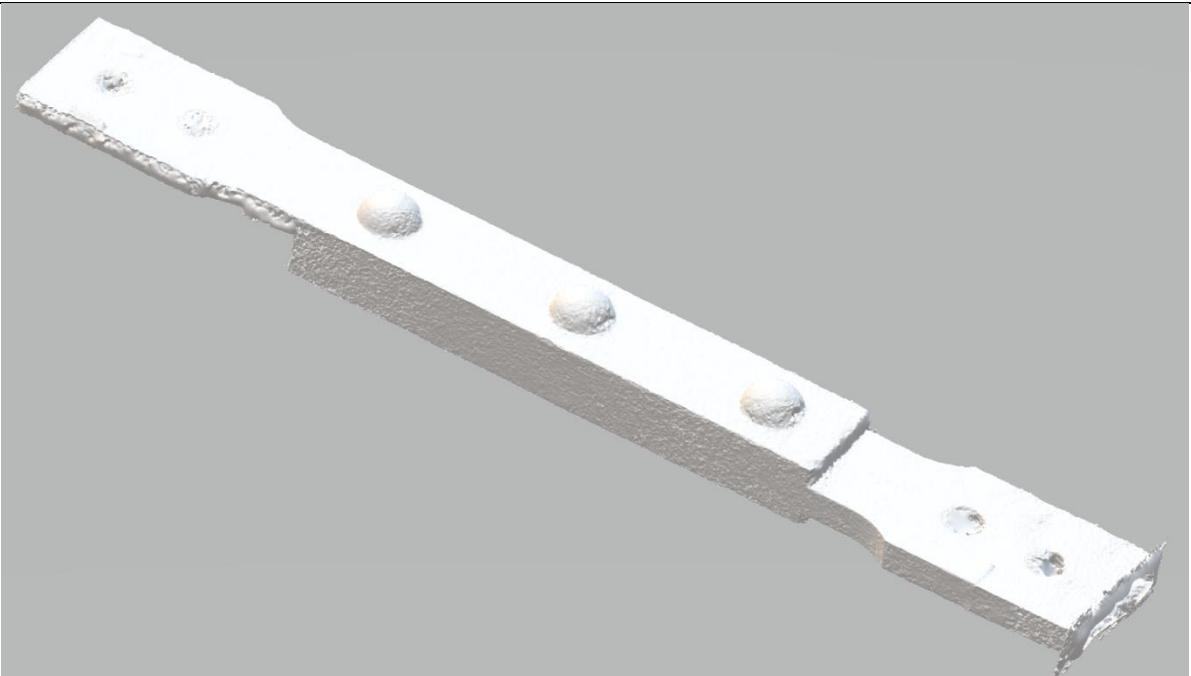
Tab. 37 The real geometry of tested samples, including photo and description of the corrosion weakening

Sample: S1.1					Group of samples: 1 (without corrosion)				
Photo:									
Photogrammetry picture:									
Geometry of sample:									
L [mm]	L1 [mm]	L2 [mm]	L3 [mm]	L4 [mm]	W1 [mm]	W2 [mm]	W3 [mm]	W4 [mm]	W5 [mm]
626,50	467,00	305,00	197,00	34,00	80,62	60,62	60,56	60,51	80,85
T1 [mm]	T2 [mm]	T3 [mm]	T4 [mm]	T5 [mm]	T6 [mm]	T7 [mm]	T8 [mm]	T9 [mm]	T10 [mm]
11,82	9,40	8,99	7,27	11,80	11,64	37,93	38,08	38,02	18,84
Description of corrosion weakening:									
Sheets	• no measurable corrosion weakening • a change in surface colour only								
Rivets	• no measurable corrosion weakening • a change in surface colour only								
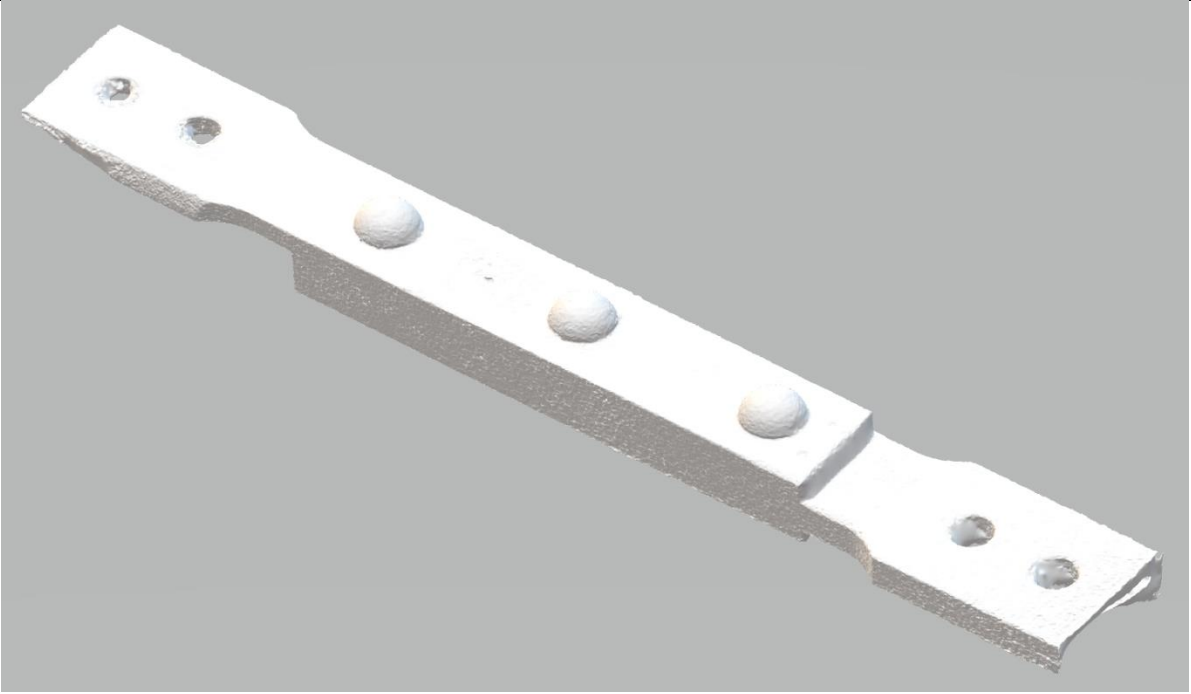
Tab. 37 (continued)

Sample: S1.2	Group of samples: 1 (without corrosion)

Photo:

Photogrammetry picture:

Geometry of sample:

L [mm]	L1 [mm]	L2 [mm]	L3 [mm]	L4 [mm]	W1 [mm]	W2 [mm]	W3 [mm]	W4 [mm]	W5 [mm]
630,00	471,50	313,50	200,50	38,00	79,20	60,78	60,71	60,78	79,51
T1 [mm]	T2 [mm]	T3 [mm]	T4 [mm]	T5 [mm]	T6 [mm]	T7 [mm]	T8 [mm]	T9 [mm]	T10 [mm]
12,20	9,03	9,07	8,03	12,07	12,16	38,56	38,51	38,30	18,24

Description of corrosion weakening:

Sheets	• no measurable corrosion weakening • a change in surface colour only
Rivets	• no measurable corrosion weakening • a change in surface colour only

Tab. 37 (continued)

Sample: S1.3	Group of samples: 1 (without corrosion)

Photo:

Photogrammetry picture:

Geometry of sample:

L [mm]	L1 [mm]	L2 [mm]	L3 [mm]	L4 [mm]	W1 [mm]	W2 [mm]	W3 [mm]	W4 [mm]	W5 [mm]
638,00	473,50	309,50	194,50	38,00	80,61	60,42	60,34	60,32	80,86
T1 [mm]	T2 [mm]	T3 [mm]	T4 [mm]	T5 [mm]	T6 [mm]	T7 [mm]	T8 [mm]	T9 [mm]	T10 [mm]
12,04	9,04	9,08	8,24	11,97	12,14	38,30	38,50	38,62	18,40

Description of corrosion weakening:	
Sheets	• no measurable corrosion weakening • a change in surface colour only
Rivets	• no measurable corrosion weakening • a change in surface colour only

125

Tab. 37 (continued)

Sample: S1.4					Group of samples: 1 (without corrosion)				
Photo:									
Photogrammetry picture:									
Geometry of sample:									
L [mm]	L1 [mm]	L2 [mm]	L3 [mm]	L4 [mm]	W1 [mm]	W2 [mm]	W3 [mm]	W4 [mm]	W5 [mm]
626,00	465,50	306,00	196,00	40,00	80,42	60,87	60,78	60,79	80,31
T1 [mm]	T2 [mm]	T3 [mm]	T4 [mm]	T5 [mm]	T6 [mm]	T7 [mm]	T8 [mm]	T9 [mm]	T10 [mm]
12,24	9,46	9,02	7,40	12,08	12,19	38,51	38,34	38,40	18,66
Description of corrosion weakening:									
Sheets	• no measurable corrosion weakening • a change in surface colour only								
Rivets	• no measurable corrosion weakening • a change in surface colour only								

126

Tab. 37 (continued)

Sample: S2.1		Group of samples: 2 (medium level of corrosion)	
Photo:			
Photogrammetry picture:			
Photogrammetry of the sample was not available			
Geometry of sample:			

L [mm]	L1 [mm]	L2 [mm]	L3 [mm]	L4 [mm]	W1 [mm]	W2 [mm]	W3 [mm]	W4 [mm]	W5 [mm]
626,50	466,50	305,00	197,00	37,00	80,15	60,48	60,67	60,56	80,22
T1 [mm]	T2 [mm]	T3 [mm]	T4 [mm]	T5 [mm]	T6 [mm]	T7 [mm]	T8 [mm]	T9 [mm]	T10 [mm]
12,12	9,05	9,10	8,01	11,54	11,21	37,56	36,96	37,13	18,54

Description of corrosion weakening:	
Sheets	• corrosion loss on the top surface of the upper sheet, corrosion loss consists of uniform corrosion and corrosion pits • deep of corrosion pits on the top surface of the upper sheet: 0,5 – 1,5 mm • range of corrosion thickness loss of the upper sheet: 1 - 2 mm
Rivets	• corrosion loss on the top surface of the rivets head, corrosion loss consists of uniform corrosion and corrosion pits • deep of corrosion pits on the top surface of rivets head: 0,5 – 1 mm • range of corrosion thickness loss of the rivets head: 0 - 1 mm

Tab. 37 (continued)

Sample: S2.2		Group of samples: 2 (medium level of corrosion)	
Photo:			
Photogrammetry picture:			
Geometry of sample:			

L [mm]	L1 [mm]	L2 [mm]	L3 [mm]	L4 [mm]	W1 [mm]	W2 [mm]	W3 [mm]	W4 [mm]	W5 [mm]
626,50	464,50	306,00	201,50	39,00	80,27	60,54	60,22	60,23	80,46
T1 [mm]	T2 [mm]	T3 [mm]	T4 [mm]	T5 [mm]	T6 [mm]	T7 [mm]	T8 [mm]	T9 [mm]	T10 [mm]
12,24	9,11	9,14	7,96	10,98	11,05	37,84	37,05	37,26	18,63

Description of corrosion weakening:

Sheets	- corrosion loss on the top surface of the upper sheet, corrosion loss consists of uniform corrosion and corrosion pits - deep of corrosion pits on the top surface of the upper sheet: 0,5 – 1,5 mm - range of corrosion thickness loss of the upper sheet: 1 – 2,5 mm
Rivets	- corrosion loss on the top surface of the rivets head, corrosion loss consists of uniform corrosion and corrosion pits - deep of corrosion pits on the top surface of rivets head: 0,5 – 1 mm - range of corrosion thickness loss of the rivets head: 0 - 1 mm

Tab. 37 (continued)

Sample: S2.3	Group of samples: 2 (medium level of corrosion)

Photo:	

Photogrammetry picture:

Geometry of sample:									
L [mm]	L1 [mm]	L2 [mm]	L3 [mm]	L4 [mm]	W1 [mm]	W2 [mm]	W3 [mm]	W4 [mm]	W5 [mm]
627,00	465,50	303,50	198,00	39,50	79,49	60,41	60,37	60,38	80,17
T1 [mm]	T2 [mm]	T3 [mm]	T4 [mm]	T5 [mm]	T6 [mm]	T7 [mm]	T8 [mm]	T9 [mm]	T10 [mm]
12,15	9,21	8,96	7,68	11,23	10,97	37,66	36,79	36,89	18,29

Description of corrosion weakening:	
Sheets	- corrosion loss on the top surface of the upper sheet, corrosion loss consists of uniform corrosion and corrosion pits - deep of corrosion pits on the top surface of the upper sheet: 0,5 -1,5 mm - range of corrosion thickness loss of the upper sheet: 0 - 2 mm
Rivets	- mild corrosion loss on the top surface of the rivets head, corrosion loss consists of uniform corrosion and corrosion pits - deep of corrosion pits on the top surface of rivets head: max. 0,5 mm - range of corrosion thickness loss of the rivets head: 0 - 1 mm

Tab. 37 (continued)

Sample: S3.1	Group of samples: 3 (high level of corrosion)

Photo:

Photogrammetry picture:

Geometry of sample:

L [mm]	L1 [mm]	L2 [mm]	L3 [mm]	L4 [mm]	W1 [mm]	W2 [mm]	W3 [mm]	W4 [mm]	W5 [mm]
626,50	466,50	305,50	198,00	37,00	81,88	61,18	60,98	60,83	81,70
T1 [mm]	T2 [mm]	T3 [mm]	T4 [mm]	T5 [mm]	T6 [mm]	T7 [mm]	T8 [mm]	T9 [mm]	T10 [mm]
7,00	9,50	8,85	7,56	8,08	10,11	34,58	35,00	35,45	18,70

Description of corrosion weakening:	
Sheets	• corrosion loss on the top surface of the upper sheet, corrosion loss consists of uniform corrosion and corrosion pits • deep of corrosion pits on the top surface of the upper sheet: 2 - 3 mm • range of corrosion thickness loss of the upper sheet: 2 - 5 mm • no corrosion loss on the sheets under the rivet heads
Rivets	• corrosion loss on the top surface of the rivets head, corrosion loss consists of uniform corrosion and corrosion pits • deep of corrosion pits on the top surface of rivets head: 1 - 3 mm • range of corrosion thickness loss of the rivets head: 2 - 5 mm

Tab. 37 (continued)

Sample: S3.2	Group of samples: 3 (high level of corrosion)

<table>
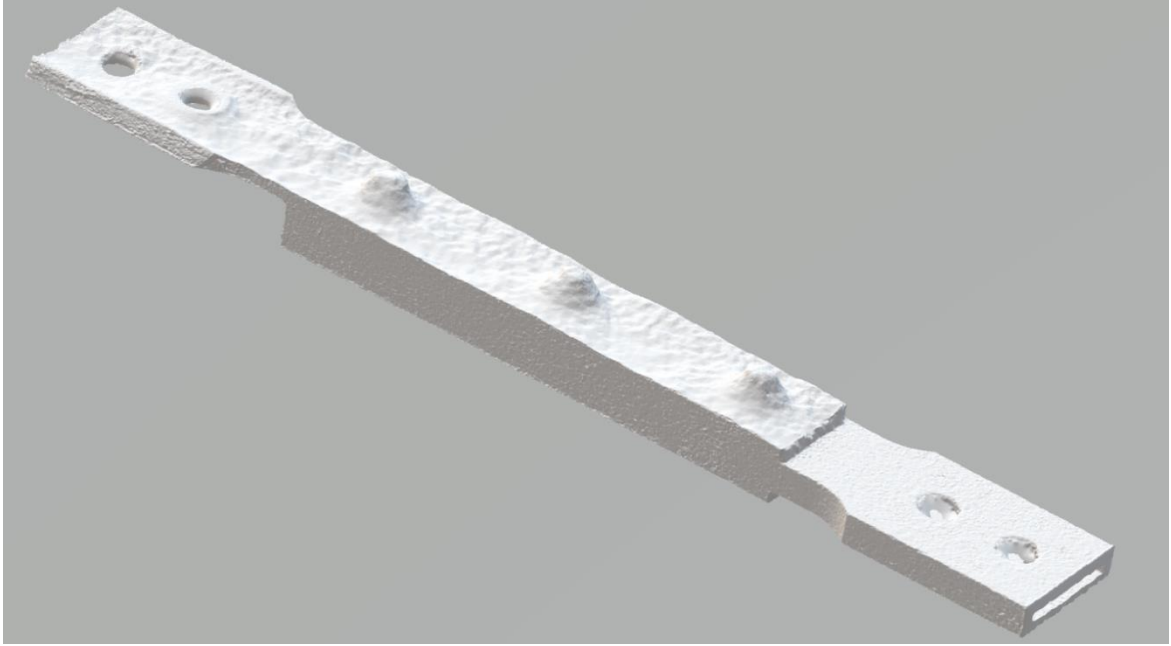<tr><td colspan="2" align="center">Photo:</td></tr>
</table>

<table>
<tr><td colspan="2" align="center">Photogrammetry picture:</td></tr>
</table>

<table>
<tr><td colspan="10" align="center">Geometry of sample:</td></tr>
<tr>
<td>L [mm]</td><td>L1 [mm]</td><td>L2 [mm]</td><td>L3 [mm]</td><td>L4 [mm]</td><td>W1 [mm]</td><td>W2 [mm]</td><td>W3 [mm]</td><td>W4 [mm]</td><td>W5 [mm]</td>
</tr>
<tr>
<td>626,00</td><td>465,00</td><td>305,00</td><td>201,00</td><td>38,50</td><td>80,00</td><td>60,80</td><td>60,65</td><td>60,59</td><td>80,45</td>
</tr>
<tr>
<td>T1 [mm]</td><td>T2 [mm]</td><td>T3 [mm]</td><td>T4 [mm]</td><td>T5 [mm]</td><td>T6 [mm]</td><td>T7 [mm]</td><td>T8 [mm]</td><td>T9 [mm]</td><td>T10 [mm]</td>
</tr>
<tr>
<td>12,24</td><td>9,18</td><td>8,87</td><td>7,50</td><td>10,27</td><td>9,34</td><td>35,63</td><td>34,45</td><td>35,48</td><td>18,50</td>
</tr>
</table>

<table>
<tr><td colspan="2" align="center">Description of corrosion weakening:</td></tr>
<tr>
<td>Sheets</td>
<td>

corrosion loss on the top surface of the upper sheet, corrosion loss consists of uniform corrosion and corrosion pits
deep of corrosion pits on the top surface of the upper sheet: 1 - 2 mm
range of corrosion thickness loss of the upper sheet: 2 - 4 mm
no corrosion loss on the sheets under the rivet heads

</td>
</tr>
<tr>
<td>Rivets</td>
<td>

corrosion loss on the top surface of the rivets head, corrosion loss consists of uniform corrosion and corrosion pits
deep of corrosion pits on the top surface of rivets head: 1 - 3 mm
range of corrosion thickness loss of the rivets head: 2 - 4 mm

</td>
</tr>
</table>

Tab. 37 (continued)

Sample: S3.3	Group of samples: 3 (high level of corrosion)

Photo:	

Photogrammetry picture:

Geometry of sample:									
L [mm]	L1 [mm]	L2 [mm]	L3 [mm]	L4 [mm]	W1 [mm]	W2 [mm]	W3 [mm]	W4 [mm]	W5 [mm]
627,50	467,00	305,00	199,50	40,50	79,61	60,26	60,20	60,20	80,04
T1 [mm]	T2 [mm]	T3 [mm]	T4 [mm]	T5 [mm]	T6 [mm]	T7 [mm]	T8 [mm]	T9 [mm]	T10 [mm]
12,33	9,77	9,15	7,72	9,00	11,20	37,00	35,70	34,83	18,62

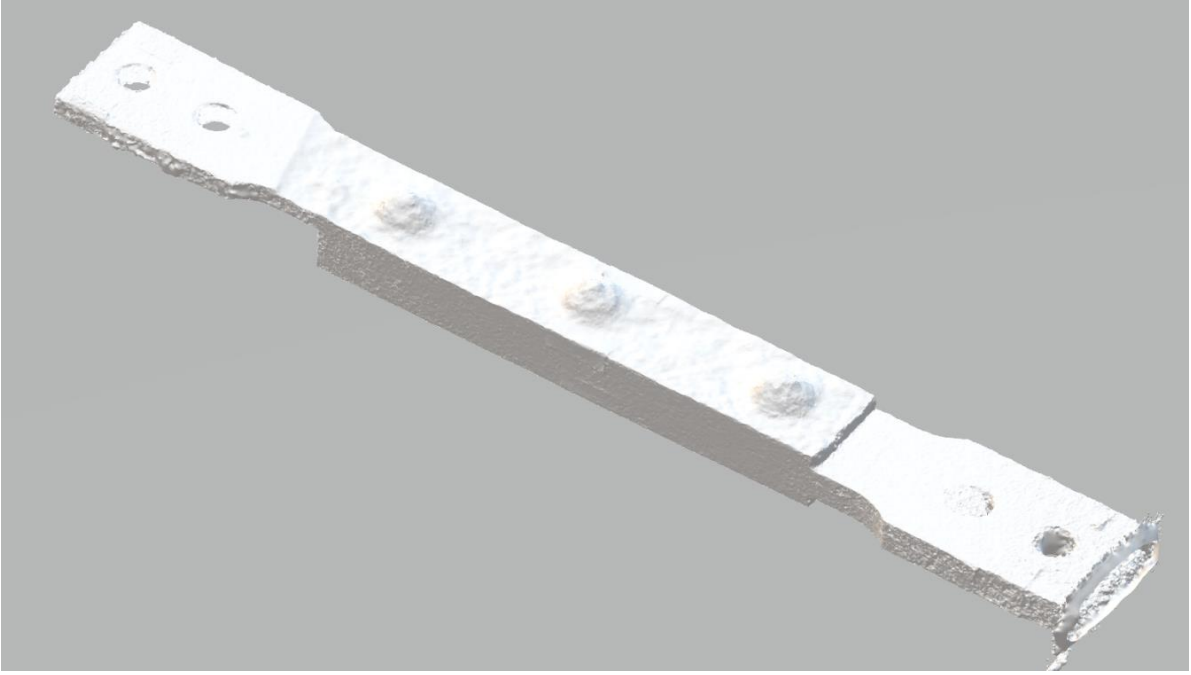| Description of corrosion weakening:	
Sheets	• corrosion loss on the top surface of the upper sheet, corrosion loss consists of uniform corrosion and corrosion pits • deep of corrosion pits on the top surface of the upper sheet: 1 - 2 mm • range of corrosion thickness loss of the upper sheet: 1 - 4 mm • no corrosion loss on the sheets under the rivet heads
Rivets	• corrosion loss on the top surface of the rivets head, corrosion loss consists of uniform corrosion and corrosion pits • deep of corrosion pits on the top surface of rivets head: 1 - 2 mm • range of corrosion thickness loss of the rivets head: 1 - 3 mm
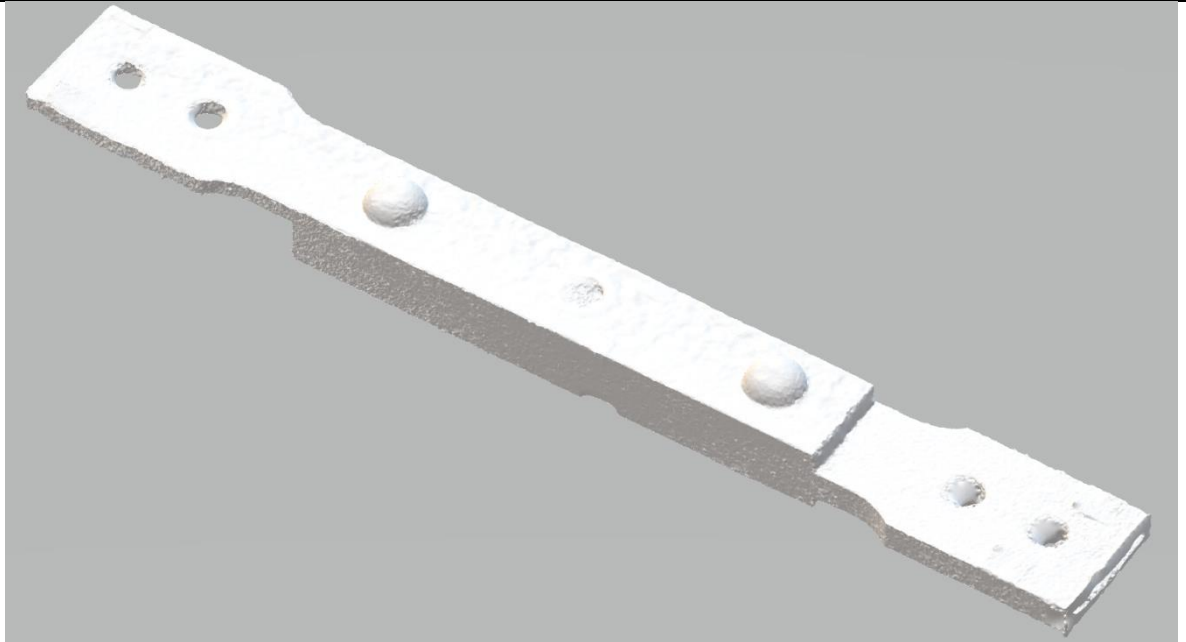
Tab. 37 (continued)

Sample: S4.1	Group of samples: 3 (samples with missing rivet)

Photo:	

Photogrammetry picture:

Geometry of sample:									
L [mm]	L1 [mm]	L2 [mm]	L3 [mm]	L4 [mm]	W1 [mm]	W2 [mm]	W3 [mm]	W4 [mm]	W5 [mm]
631,00	469,00	307,00	203,50	33,50	80,34	60,62	60,17	60,20	80,11
T1 [mm]	T2 [mm]	T3 [mm]	T4 [mm]	T5 [mm]	T6 [mm]	T7 [mm]	T8 [mm]	T9 [mm]	T10 [mm]
12,30	9,08	9,10	7,92	12,34	12,09	38,83	39,10	38,66	18,30

Description of corrosion weakening:	
Sheets	• no measurable corrosion weakening • a change in surface colour only
Rivets	• no measurable corrosion weakening, a change in surface colour only • the middle rivet is missing

Tab. 37 (continued)

Sample: S4.2	Group of samples: 3 (samples with missing rivet)

Photo:

Photogrammetry picture:

Geometry of sample:

L [mm]	L1 [mm]	L2 [mm]	L3 [mm]	L4 [mm]	W1 [mm]	W2 [mm]	W3 [mm]	W4 [mm]	W5 [mm]
629,00	466,50	305,50	197,50	36,50	80,85	60,59	60,75	60,76	80,54
T1 [mm]	T2 [mm]	T3 [mm]	T4 [mm]	T5 [mm]	T6 [mm]	T7 [mm]	T8 [mm]	T9 [mm]	T10 [mm]
12,62	9,02	8,90	7,95	12,75	12,34	39,30	39,31	39,40	18,20

Description of corrosion weakening:	
Sheets	• no measurable corrosion weakening • a change in surface colour only
Rivets	• no measurable corrosion weakening, a change in surface colour only • the middle rivet is missing

Tab. 37 (continued)

Sample: S4.3	Group of samples: 3 (samples with missing rivet)

Photo:	

Photogrammetry picture:

Geometry of sample:

L [mm]	L1 [mm]	L2 [mm]	L3 [mm]	L4 [mm]	W1 [mm]	W2 [mm]	W3 [mm]	W4 [mm]	W5 [mm]
638,00	477,50	320,00	203,50	42,00	81,05	60,73	60,81	61,00	80,68
T1 [mm]	T2 [mm]	T3 [mm]	T4 [mm]	T5 [mm]	T6 [mm]	T7 [mm]	T8 [mm]	T9 [mm]	T10 [mm]
12,15	9,14	8,90	7,90	12,26	11,45	38,69	38,94	39,15	18,44

Description of corrosion weakening:

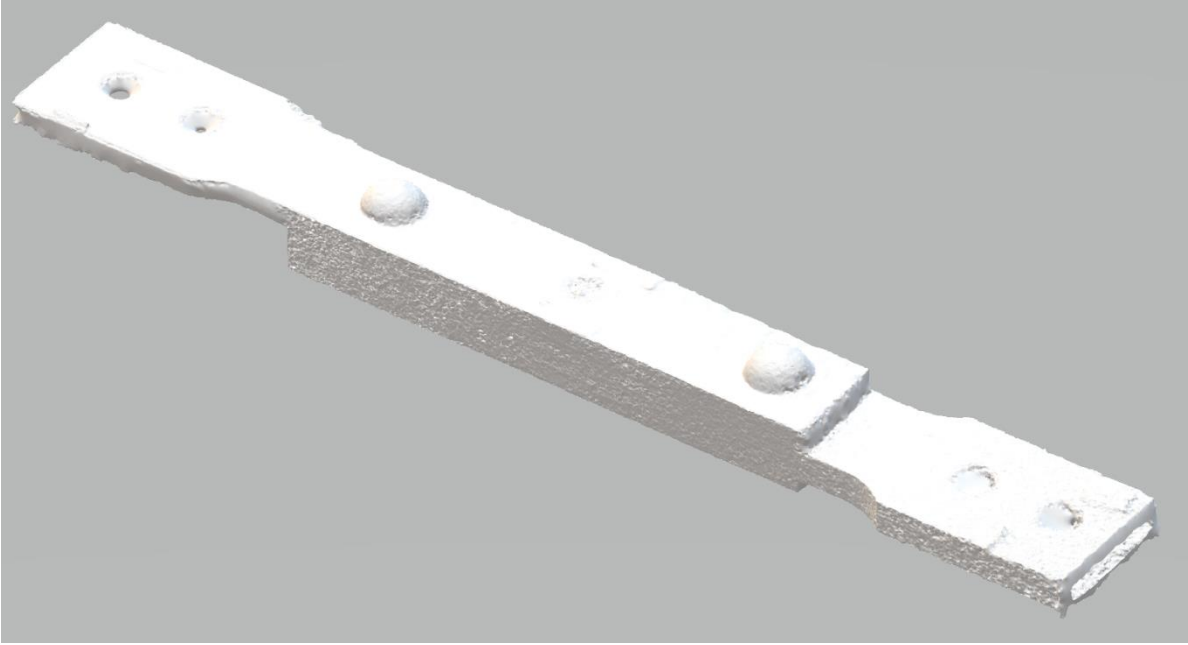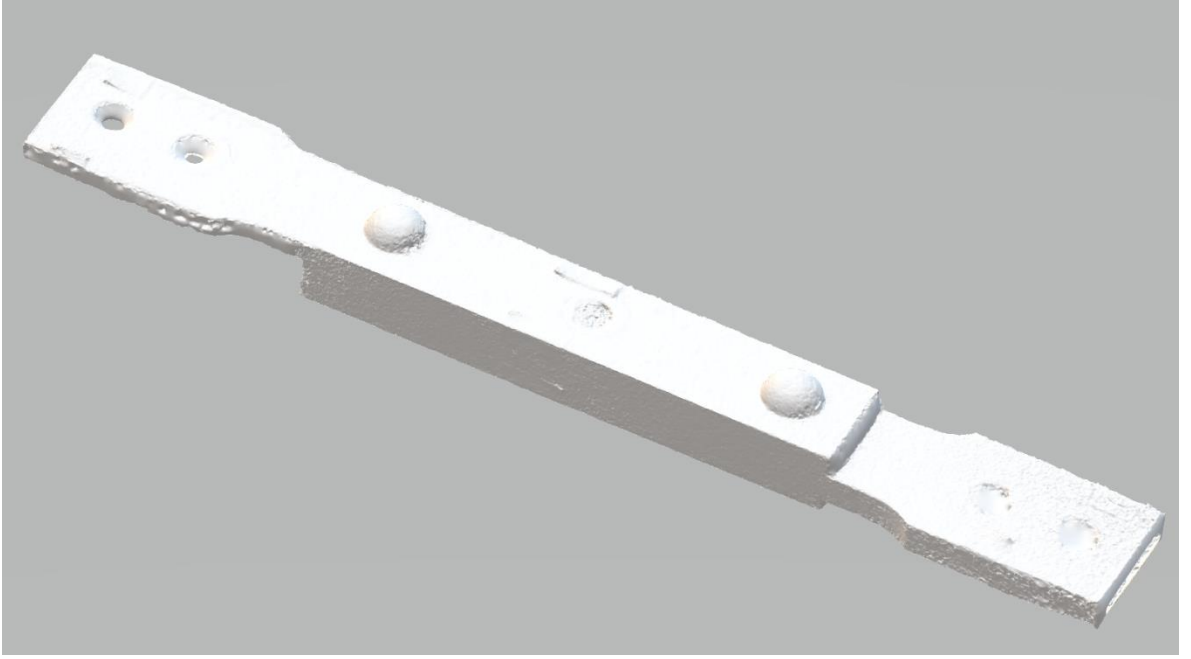| Sheets	• mild corrosion loss on the top surface of the upper sheet, corrosion loss consists of uniform corrosion and corrosion pits • deep of corrosion pits on the top surface of the upper sheet: 0,5 - 1 mm • range of corrosion thickness loss of the upper sheet: 0 - 1,5 mm
Rivets	• mild corrosion loss on the top surface of the rivets head, corrosion loss consists of uniform corrosion and corrosion pits • deep of corrosion pits on the top surface of rivets head: max. 0,5 mm • range of corrosion thickness loss of the rivets head: 0 - 1 mm • the middle rivet is missing

11.2. Annexe 2: Stress Spectrum Generator
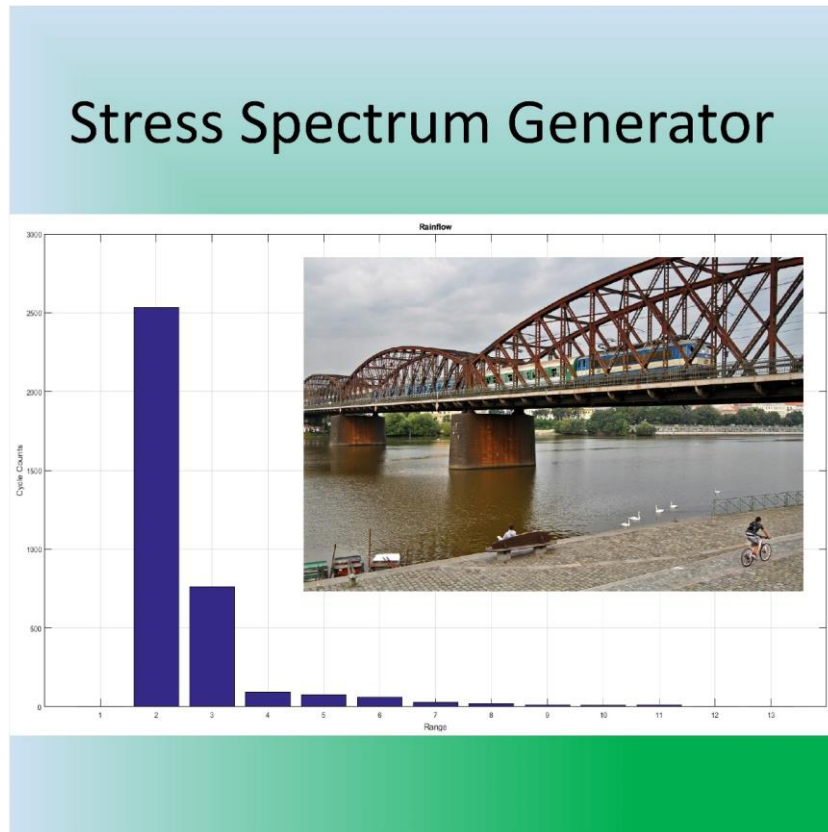
11.2.1. Instructions for installing the software

Download the package called Stress Spectrum Generator.rar from the website and then extract it.

The following files are included in the package:

1) *Stress Spectrum Generator* - the program itself (exe application)
2) *Results_one.xlsx* - template for the results (excel file)
3) *Results_one.xlsx* - template for results (excel file)
4) *Input_data_example.xlsx* - sample input data (stress waveform from one train crossing)
5) *Stress Spectrum Generator_manual* - software manual (PDF document)

For successful installation of the software, you must have MATLAB Runtime installed on your computer, which can be downloaded from:
http://www.mathworks.com/products/compiler/mcr/index.html.

To start the installation of the software, double click on the icon called Stress Spectrum Generator. Then follow the on-screen instructions. An internet connection is required to install the software.

11.2.2. Software description

The "Stress Spectrum Generator" software was created in the "Guide" interface of the MATLAB® software. The program allows the calculation of the stress spectrum from input data that have the stress-time format or strain-time format. The calculation itself is based on the Rainflow method, which is integrated into the program by means of code. For a successful installation of the program, it is necessary

to have MATLAB Runtime installed on the computer. The MATLAB® software itself does not need to be installed.

11.2.2.1 Input data

Input data can be uploaded to the software in two possible formats: (1) data stored in an Excel file; (2) data stored in a text file. It is also possible for the imported data to contain a stress (or strain) that is either (a) time-dependent, meaning that the input file takes the form of, for example, an excel file that contains 2 columns of data, with the first containing the stress values and the second containing the time, or (b) time-independent, where the excel file contains only the column containing the stress (or strain) values.

11.2.2.2 Calculation algorithm

First, we briefly describe the Rainflow sorting method.

Rainflow method (= "trickle drop" method)

The name of the method is derived from the analogy of a raindrop flowing down a "roof" if we rotate the time record by 90 degrees (see Fig. 102).

The condition for this method to work properly is to filter out the points between the local extremes (maxima and minima) of the record. The initial and final extremes of a half cycle need not be consecutive - there may be other cycles in between. Those extremes that form a hysteresis loop are related to each other. The following rules apply for evaluation:

1. Inside each extreme, a half-cycle (dripping drop) begins.
2. A half-cycle ends if:
   a) its initial level is reached (points 1-4, 2-3, 4-5 in Fig. 102),
   b) the drop hits a drop flowing from a higher roof (points 3-2, 7-6 in Fig. 102).
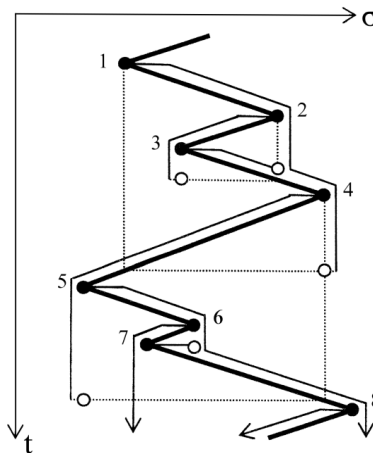
Fig. 102 Rainflow method ("trickle drop" method)

The algorithm itself for calculating the stress spectrum from the effects of a particular load vehicle consists of several sub-steps:

1. Reading the input data.
2. Conversion of relative strain values to stresses.
3. Filtering out possible effects of temperature change
4. Data sorting = finding local extremes and filtering out points lying between these extremes (maxima and minima) of the record (see Fig. 103 and Fig. 104) + removing points with identical

stress values. The result is a stress record consisting exclusively of local extremes, i.e. maxima ('peaks') and minima ('valleys').

5. The calculation of stress variations and cycle numbers is based on the Rainflow method

     5.1   Based on the rules mentioned in the introduction of this chapter, half-cycles are evaluated, each starting at each minimum ("valley"). The magnitude of the stress range for each half-cycle is equal to the difference in stress between its start and end.

     5.2.   Based on the rules mentioned in the introduction to this chapter, half-cycles are evaluated, each starting at each maximum ('peak'). The magnitude of the stress range for each half-cycle is equal to the difference in stress between its start and end.

     5.3.   All the values of the stress ranges (for each of which the number of cycles is equal to 0.5 cycle) shall be ranked from largest to smallest.

6. The ranges are then sorted into a multistage spectrum = into a selected number of intervals (see Fig. 105) and for each interval the number of cycles of stress ranges is calculated (by summation of half-cycles). The number of cycles is calculated both for 1 load vehicle crossing over the bridge and for crossings during the whole year, if the data on the number of crossings are known and filled into the program.

7. In case the input data are obtained from a static load test or if they do not include the influence of dynamic effects, the values of the stress ranges are multiplied by the dynamic coefficient, which is calculated according to the chosen method. The multiplication is carried out if this option is checked in the program before the calculation.

8. Save the resulting stress spectra from each load vehicle in an excel file (see Fig. 105 for an example).
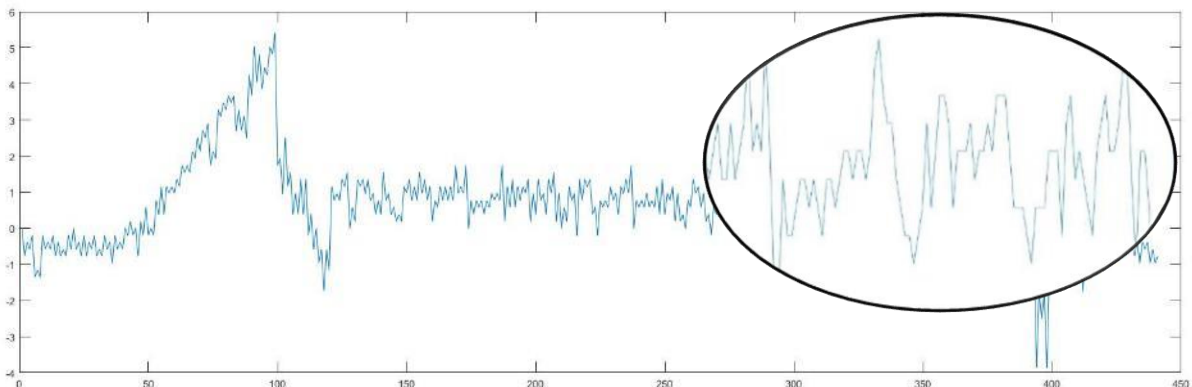
Fig. 103 Stress profile record before data sorting
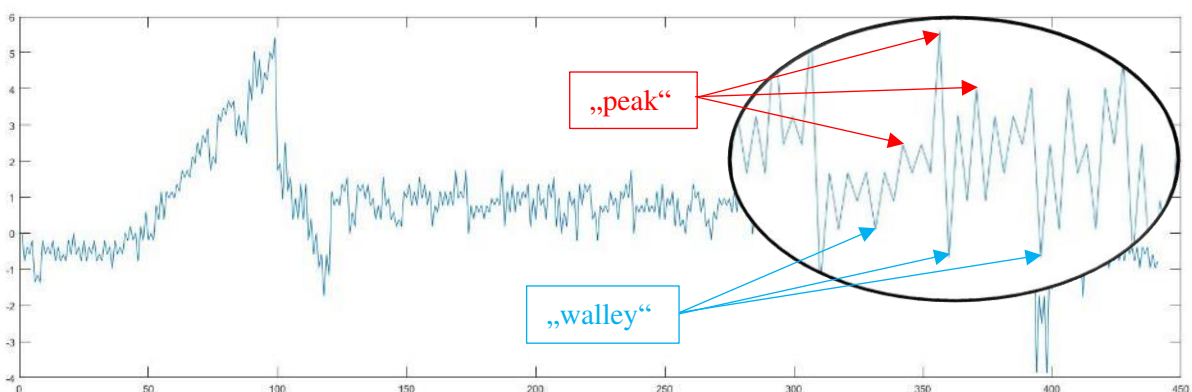
Fig. 104 Stress profile record after data sorting (the record consists of local extremes only)

11.2.2.3 Outputs from the software

The output of the "Stress Spectrum Generator" software is the stress ranges divided into a selected number of intervals + the number of cycles of the given stress ranges falling into each interval (all from individual load vehicles). The mean value of each interval is then the representative value of the stress range. This data is automatically saved to an excel file, which can be freely named before saving and the location where it will be saved can also be selected. The data can be saved in a completely new file, or a predefined template, which is also included with the software, can be used and its contents overwritten. There are 2 templates with the names (1) *Results_one.xlsx* and (2) *Results_all.xlsx*. The first template, Results_one.xlsx, can be used when the time record of the stress from the effect of each train is stored in a separate excel file. Conversely, the *Results_all.xlsx* template will be used when the time record of the stresses from the effects of each train is stored in a single excel file (for example: 1 file containing 10 columns of data - each column records the stress profile caused by the crossing of one of the 10 trains). If you do not use a predefined template but save the results in a new file, you need to add the *.xlsx* extension to the file name.

An example of the output of the program can be seen in Fig. 105.

Dynamic factor:			STRESS SPECTRUM CAUSED BY INDIVIDUAL TRAINS			
1.307						
		Train:	1		2	
		Type:	Passenger_1		Passenger_2	
			stress range	N	stress range	N
Interval	Lower range	Upper range	[MPa]	[cycles]	[MPa]	[cycles]
1	52.14	54.89	53.51	0.5	53.51	0
2	49.40	52.14	50.77	0.5	50.77	0.5
3	46.65	49.40	48.03	0	48.03	0
4	43.91	46.65	45.28	0	45.28	0.5
5	41.17	43.91	42.54	0	42.54	0
6	38.42	41.17	39.79	0	39.79	0
7	35.68	38.42	37.05	0	37.05	0
8	32.93	35.68	34.30	0	34.30	0
9	30.19	32.93	31.56	0	31.56	0
10	27.44	30.19	28.82	0	28.82	0
11	24.70	27.44	26.07	0	26.07	0
12	21.95	24.70	23.33	2	23.33	0
13	19.21	21.95	20.58	8	20.58	9
14	16.47	19.21	17.84	0	17.84	1
15	13.72	16.47	15.09	0	15.09	0
16	10.98	13.72	12.35	1	12.35	0
17	8.23	10.98	9.61	0	9.61	1
18	5.49	8.23	6.86	10	6.86	6
19	2.74	5.49	4.12	0	4.12	4
20	0.00	2.74	1.37	44	1.37	44

Distribution of stress ranges into intervals. Each interval is characterized by a lower and an upper limit.

Effects from individual load vehicles (trains).

Fig. 105 Example of output from "Stress spectrum generator" (effects of 2 trains, effects always from 1 crossing, values of stress ranges multiplied by dynamic coefficient).

11.2.2.4 Description of the software interface
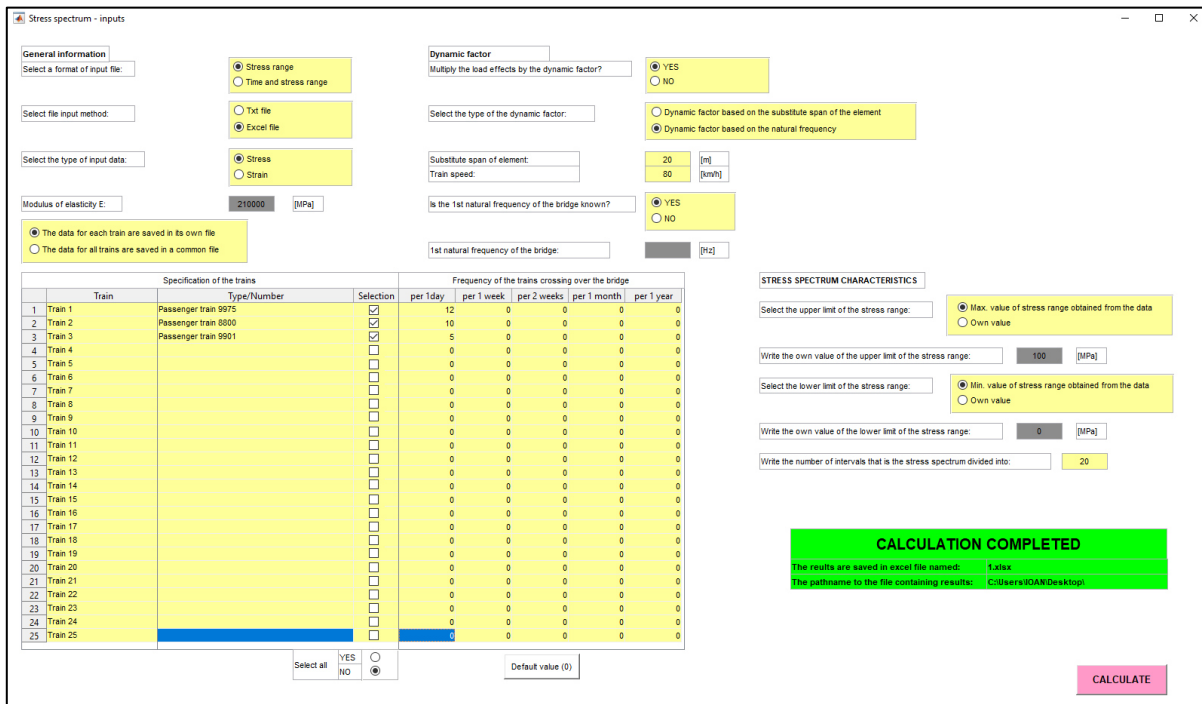
Fig. 106 Main window of Stress spectrum generator

The description of the main software window (see Fig. 106) is divided into several parts for better clarity (see Fig. 107 to Fig. 111):
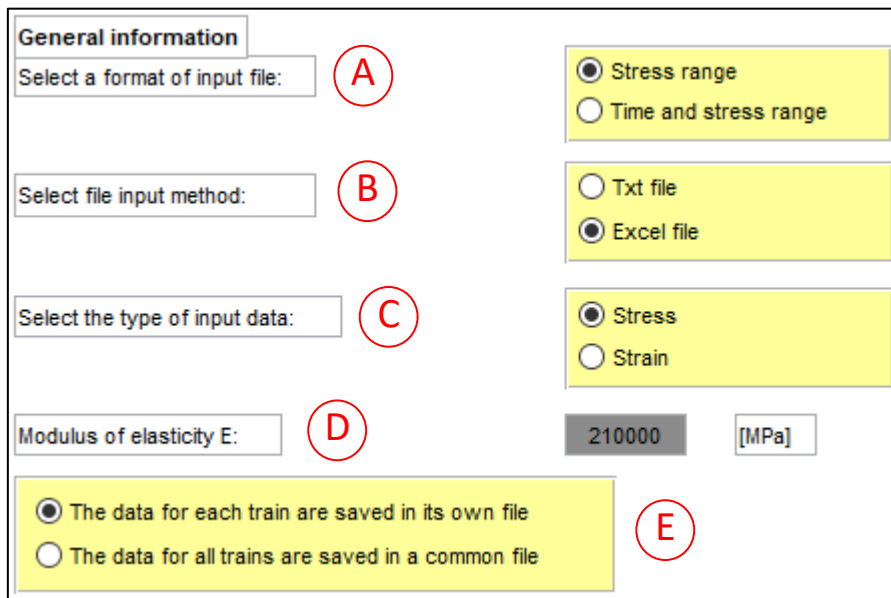
Fig. 107 Main window of Stress spectrum generator – part 1

(A) Selection of the input data type: (1) stress is either not time dependent (selection: "*Stress range*") - the input file is for example an excel file containing only 1 column of stress values, or (2) stress is time dependent (selection: "Time and stress range") - in this case the file contains 2 columns of data, the first one containing stress values and the second one containing time.

(B) Selection of input data format: (1) text file (selection: "*Txt file*") or (2) excel file (selection: "*Excel file*").

(C) Selection of input data type: (1) stress (selection: "*Stress*") or (2) strain (selection "*Strain*").

(D) Value of modulus of elasticity of steel - the box is active and is filled in if the input data type is selected "*Strain*".

(E) Selection of (1) whether the time record of the stress from the action of each train is saved in a separate excel file (selection: "*The data for each train are saved in its own file*") or (2) whether the time record of the stress from the action of each train is saved in one single excel file (selection: "*The data for all trains are saved in one common file*").

Fig. 108 Main window of Stress spectrum generator – part 2

(F) Section of the main window of the program dedicated to input information for the calculation of the dynamic coefficient - the cells for this section (H to L) are active (i.e. in yellow) only if the option to multiply stress ranges by the dynamic coefficient is selected (see row (G)).

(G) Selection of whether to multiply load effects by the dynamic factor: (1) YES (selection: "*YES*"), (2) NO (selection: "*NO*").

(H) Selection of the method for calculating the dynamic factor: (1) dyn. factor dependent on the substitute length of the element and the train speed (calculation according to EN 1991-2, Annex D) (selection: "*Dynamic factor based on the substitute span of the element*"); (2) dyn. factor dependent on the substitute span of the element, train speed and 1. natural frequency of the bridge (calculation according to EN 1991-2, Annex C) (selection: "*Dynamic factor based on the natural frequency*").

(I) Substitute element length [m].

(J) Speed of the load vehicle (train) when crossing the bridge [km/h].

(K) Selection whether or not the 1st natural frequency of the bridge is known. Cells are only active if the dynamic coefficient (2) is selected.

(L) Value of the 1st natural frequency [Hz]. The cell is active if the value is known. If it is not known, the program calculates it based on the filled substitute element length.

	Train	Type/Number	Selection	per 1 day	per 1 week	per 2 weeks	per 1 month	per 1 year
1	Train 1	Passenger train 9975	☑	12	0	0	0	0
2	Train 2	Passenger train 8800	☑	10	0	0	0	0
3	Train 3	Passenger train 9901	☑	5	0	0	0	0
4	Train 4		☐	0	0	0	0	0
5	Train 5		☐	0	0	0	0	0
6	Train 6		☐	0	0	0	0	0
7	Train 7		☐	0	0	0	0	0
8	Train 8		☐	0	0	0	0	0
9	Train 9		☐	0	0	0	0	0
10	Train 10		☐	0	0	0	0	0
11	Train 11		☐	0	0	0	0	0
12	Train 12		☐	0	0	0	0	0
13	Train 13		☐	0	0	0	0	0
14	Train 14		☐	0	0	0	0	0
15	Train 15		☐	0	0	0	0	0
16	Train 16		☐	0	0	0	0	0
17	Train 17		☐	0	0	0	0	0
18	Train 18		☐	0	0	0	0	0
19	Train 19		☐	0	0	0	0	0
20	Train 20		☐	0	0	0	0	0
21	Train 21		☐	0	0	0	0	0
22	Train 22		☐	0	0	0	0	0
23	Train 23		☐	0	0	0	0	0
24	Train 24		☐	0	0	0	0	0
25	Train 25		☐	0	0	0	0	0

(M) Specification of the trains (N) Selection (P) Frequency of the trains crossing over the bridge

(O) Select all — YES ○ / NO ◉   Default value (0)

Fig. 109 Main window of Stress spectrum generator – part 3

(M) Identification (type/number) of the load vehicle.

(N) Selection of trains whose effects are considered in the calculation of the stress spectrum (tick the box if the train effects are to be taken into account); (O) Option to quickly select/deselect all trains.

(P) Table for entering the intensities of vehicle (train) crossings over the bridge for a certain time period, if known. For each vehicle, it is possible to enter the intensity of crossings per day/ 1 week/ 2 weeks/ 1 month/ 1 year (only the intensity for one time period must be filled in - for example only per day, not per day and week). This information is used to determine the number of cycles from crossings over a period of 1 year. The number of cycles from a single crossing is always calculated and the results are always stored in the first sheet of the excel file. For trains where the box is ticked, the level crossing intensity must be filled in.

(Q) STRESS SPECTRUM CHARACTERISTICS

(R) Select the upper limit of the stress range: ◉ Max. value of stress range obtained from the data / ○ Own value

(S) Write the own value of the upper limit of the stress range: 100 [MPa]

(T) Select the lower limit of the stress range: ◉ Min. value of stress range obtained from the data / ○ Own value

(U) Write the own value of the lower limit of the stress range: 0 [MPa]

(V) Write the number of intervals that is the stress spectrum divided into: 20

Fig. 110 Main window of Stress spectrum generator – part 4

(Q) Section of the main program window specifying the stress spectrum parameters. To better compare the effects of individual vehicles crossing the bridge structure, the program automatically divides the stress spectra from each vehicle into an equal number of intervals (for example, 25), with each interval covering the same stress range. The upper and lower limits of the stress range between which the calculated stress spectra will lie can be directly determined by a specific numerical value (see row "S" and "U") or determined by the program as follows: the maximum value of the stress range is equal to the highest ever value of the stress range caused by any of the vehicles considered and the minimum value of the stress range is equal to the lowest ever value of the stress range caused by any of the vehicles considered (in most cases 0 MPa). The difference between this highest and lowest stress range value is then divided into a prescribed number of intervals (see row 'V' and Fig. 110). The larger the number of intervals, the more accurate the spectra obtained (for example, 20 or 25 intervals). The representative stress range value for each interval is given by the mean stress range value in the interval. The calculated stress ranges are then divided into these intervals according to their magnitude and the total number of cycles for each interval is given by: the number of stress ranges falling within the interval "times" 0.5 cycles. This procedure is applied to the stress ranges from all vehicles.

(R) Choice of whether the maximum limiting value of the stress range shall be taken as the highest value of the stress range caused by any vehicle considered or whether the value shall be directly prescribed numerically.

(S) Prescription of the maximum limiting value of the stress range. The cell is active if the prescription option is selected (see line "R").

(T) Selection of whether the minimum limit value of the stress range will be taken as the lowest stress range value caused by any vehicle under consideration or whether the value will be directly prescribed numerically.

(U) Prescription of the minimum limit value of the stress range. The cell is active if the prescription option is selected (see line "T").

(V) Prescription of the number of intervals into which the stress ranges will be divided.

(W) Successful completion information containing the name of the results file and the path to the file (displayed when the calculation is complete).

(X) "Button" to start the calculation of stress spectra.
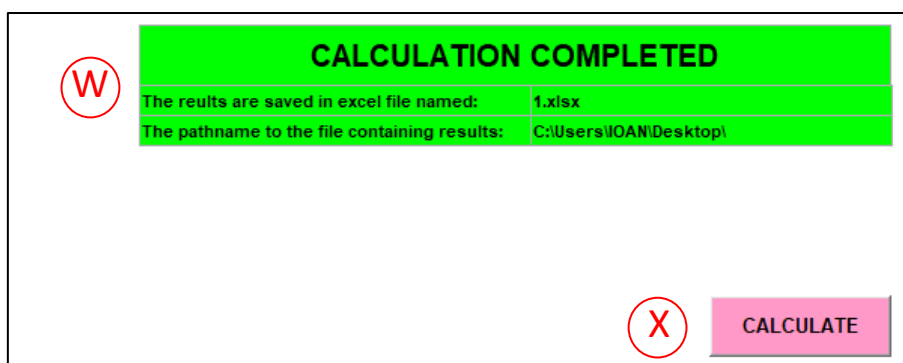
Fig. 111 Main window of Stress spectrum generator – part 5

After starting the calculation, a window will automatically open to select the files containing the input data. If the effects of multiple trains are calculated (or if more than one box is ticked in the "N" table), the data files for each train will be selected sequentially, i.e. the file selection window will open as many

times as the number of ticked boxes. After all input files have been loaded, a window will open to select the name and storage location of the results file. You can create a completely new excel sheet and name it freely, or you can overwrite the existing *Results_one.xlsx* and *Results_all.xlsx* templates mentioned in the introduction of chapter 11.2.2.3.

11.2.3.   Examples

11.2.3.1 Example 1

We consider the effects from 3 trains that regularly cross the bridge. We have a time record of the stresses from 1 crossing for each train stored in a separate excel file (3 files in total, each containing one column of data). We know the intensity of each train crossing: train 1: 15 times per day, train 2: 8 times per day, train 3: 5 times per week. The load effects will be multiplied by the dynamic coefficient according to EN 1991-2, Annex D; where the substitute length of the element under assessment is 10 m and the speed of the crossing trains is 60 km/h. The stress spectra are divided into 20 intervals.

Program input data
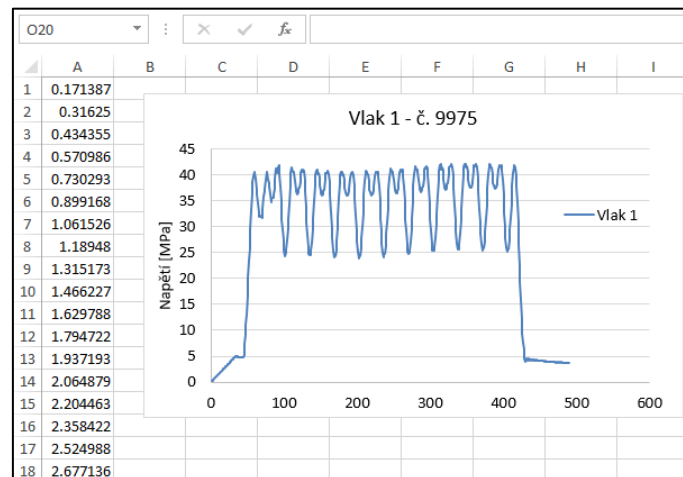
Fig. 112 Program input data - stress waveform from the effect of train 1

Fig. 113 Program input data - stress waveform from the effect of train 2

Fig. 114 Program input data - stress waveform from the effect of train 3

Entering input data into the program

Fig. 115 Input data entry - part 1

Fig. 116 Input data entry - part 2

	Specification of the trains			Frequency of the trains crossing over the bridge				
	Train	Type/Number	Selection	per 1day	per 1 week	per 2 weeks	per 1 month	per 1 year
1	Train 1	Passenger_9975	☑	15	0	0	0	0
2	Train 2	Passenger_8800	☑	8	0	0	0	0
3	Train 3	Passenger_9901	☑	0	5	0	0	0
4	Train 4		☐	0	0	0	0	0
5	Train 5		☐	0	0	0	0	0
6	Train 6		☐	0	0	0	0	0
7	Train 7		☐	0	0	0	0	0
8	Train 8		☐	0	0	0	0	0
9	Train 9		☐	0	0	0	0	0
10	Train 10		☐	0	0	0	0	0
11	Train 11		☐	0	0	0	0	0
12	Train 12		☐	0	0	0	0	0
13	Train 13		☐	0	0	0	0	0
14	Train 14		☐	0	0	0	0	0
15	Train 15		☐	0	0	0	0	0
16	Train 16		☐	0	0	0	0	0
17	Train 17		☐	0	0	0	0	0
18	Train 18		☐	0	0	0	0	0
19	Train 19		☐	0	0	0	0	0
20	Train 20		☐	0	0	0	0	0
21	Train 21		☐	0	0	0	0	0
22	Train 22		☐	0	0	0	0	0
23	Train 23		☐	0	0	0	0	0
24	Train 24		☐	0	0	0	0	0
25	Train 25		☐	0	0	0	0	0

Select all   YES ○   NO ◉   Default value (0)

Fig. 117 Input data entry - part 3

STRESS SPECTRUM CHARACTERISTICS

Select the upper limit of the stress range:	◉ Max. value of stress range obtained from the data ○ Own value

Write the own value of the upper limit of the stress range: 100   [MPa]

Select the lower limit of the stress range:	◉ Min. value of stress range obtained from the data ○ Own value

Write the own value of the lower limit of the stress range: 0   [MPa]

Write the number of intervals that is the stress spectrum divided into: 20

Fig. 118 Input data entry - part 4

CALCULATION COMPLETED

The reults are saved in excel file named:	Results_one.xlsx
The pathname to the file containing results:	C:\Users\IOAN\Desktop\

Fig. 119 Information about the successful completion of the calculation containing the name of the results file and the path to the file

Output from the programme

Dynamic factor:			STRESS SPECTRUM CAUSED BY INDIVIDUAL TRAINS CROSSING OVER THE B					
1								
		Train:	1		2		3	
		Type:	Passenger_9975		Passenger_8800		Passenger_9901	
			stress range	N	stress range	N	stress range	N
Interval	Lower range	Upper range	[MPa]	[cycles]	[MPa]	[cycles]	[MPa]	[cycles]
1	39.90	42.00	40.95	0.5	40.95	0	40.95	0
2	37.80	39.90	38.85	0.5	38.85	0.5	38.85	0
3	35.70	37.80	36.75	0	36.75	0	36.75	0
4	33.60	35.70	34.65	0	34.65	0.5	34.65	0
5	31.50	33.60	32.55	0	32.55	0	32.55	0
6	29.40	31.50	30.45	0	30.45	0	30.45	0
7	27.30	29.40	28.35	0	28.35	0	28.35	0
8	25.20	27.30	26.25	0	26.25	0	26.25	0
9	23.10	25.20	24.15	0	24.15	0	24.15	0
10	21.00	23.10	22.05	0	22.05	0	22.05	0
11	18.90	21.00	19.95	0	19.95	0	19.95	0
12	16.80	18.90	17.85	2	17.85	0	17.85	0
13	14.70	16.80	15.75	8	15.75	9	15.75	0
14	12.60	14.70	13.65	0	13.65	1	13.65	0
15	10.50	12.60	11.55	0	11.55	0	11.55	1
16	8.40	10.50	9.45	1	9.45	0	9.45	0
17	6.30	8.40	7.35	0	7.35	1	7.35	0
18	4.20	6.30	5.25	10	5.25	6	5.25	0
19	2.10	4.20	3.15	0	3.15	4	3.15	2
20	0.00	2.10	1.05	44	1.05	44	1.05	27

*Fig. 120 Calculated stress spectrum - effects of 3 trains, number of cycles from 1 train crossing, values of stress ranges **are not** multiplied by dynamic coefficient*

Dynamic factor:			STRESS SPECTRUM CAUSED BY INDIVIDUAL TRAINS CROSSING OVER THE B					
1								
		Train:	1		2		3	
		Type:	Passenger_9975		Passenger_8800		Passenger_9901	
			stress range	N	stress range	N	stress range	N
Interval	Lower range	Upper range	[MPa]	[cycles]	[MPa]	[cycles]	[MPa]	[cycles]
1	39.90	42.00	40.95	2737.5	40.95	0	40.95	0
2	37.80	39.90	38.85	2737.5	38.85	1460	38.85	0
3	35.70	37.80	36.75	0	36.75	0	36.75	0
4	33.60	35.70	34.65	0	34.65	1460	34.65	0
5	31.50	33.60	32.55	0	32.55	0	32.55	0
6	29.40	31.50	30.45	0	30.45	0	30.45	0
7	27.30	29.40	28.35	0	28.35	0	28.35	0
8	25.20	27.30	26.25	0	26.25	0	26.25	0
9	23.10	25.20	24.15	0	24.15	0	24.15	0
10	21.00	23.10	22.05	0	22.05	0	22.05	0
11	18.90	21.00	19.95	0	19.95	0	19.95	0
12	16.80	18.90	17.85	10950	17.85	0	17.85	0
13	14.70	16.80	15.75	43800	15.75	26280	15.75	0
14	12.60	14.70	13.65	0	13.65	2920	13.65	0
15	10.50	12.60	11.55	0	11.55	0	11.55	260
16	8.40	10.50	9.45	5475	9.45	0	9.45	0
17	6.30	8.40	7.35	0	7.35	2920	7.35	0
18	4.20	6.30	5.25	54750	5.25	17520	5.25	0
19	2.10	4.20	3.15	0	3.15	11680	3.15	520
20	0.00	2.10	1.05	240900	1.05	128480	1.05	7020

*Fig. 121 Calculated stress spectrum - effects of 3 trains, number of cycles from 1 train crossing per 1 year, values of stress ranges **are not** multiplied by dynamic coefficient*

Dynamic factor: 1.11			STRESS SPECTRUM CAUSED BY INDIVIDUAL TRAINS CROSSING OVER THE E						
		Train:	1		2		3	
		Type:	Passenger_9975		Passenger_8800		Passenger_9901	
			stress range	N	stress range	N	stress range	N
Interval	Lower range	Upper range	[MPa]	[cycles]	[MPa]	[cycles]	[MPa]	[cycles]
1	44.27	46.60	45.44	0.5	45.44	0	45.44	0
2	41.94	44.27	43.11	0.5	43.11	0.5	43.11	0
3	39.61	41.94	40.78	0	40.78	0	40.78	0
4	37.28	39.61	38.45	0	38.45	0.5	38.45	0
5	34.95	37.28	36.12	0	36.12	0	36.12	0
6	32.62	34.95	33.79	0	33.79	0	33.79	0
7	30.29	32.62	31.46	0	31.46	0	31.46	0
8	27.96	30.29	29.13	0	29.13	0	29.13	0
9	25.63	27.96	26.80	0	26.80	0	26.80	0
10	23.30	25.63	24.47	0	24.47	0	24.47	0
11	20.97	23.30	22.14	0	22.14	0	22.14	0
12	18.64	20.97	19.81	2	19.81	0	19.81	0
13	16.31	18.64	17.48	8	17.48	9	17.48	0
14	13.98	16.31	15.15	0	15.15	1	15.15	0
15	11.65	13.98	12.82	0	12.82	0	12.82	1
16	9.32	11.65	10.49	1	10.49	0	10.49	0
17	6.99	9.32	8.16	0	8.16	1	8.16	0
18	4.66	6.99	5.83	10	5.83	6	5.83	0
19	2.33	4.66	3.50	0	3.50	4	3.50	2
20	0.00	2.33	1.17	44	1.17	44	1.17	27

*Fig. 122 Calculated stress spectrum - effects of 3 trains, number of cycles from 1 train crossing, values of stress ranges **are** multiplied by dynamic coefficient*

Dynamic factor: 1.11			STRESS SPECTRUM CAUSED BY INDIVIDUAL TRAINS CROSSING OVER THE B						
		Train:	1		2		3	
		Type:	Passenger_9975		Passenger_8800		Passenger_9901	
			stress range	N	stress range	N	stress range	N
Interval	Lower range	Upper range	[MPa]	[cycles]	[MPa]	[cycles]	[MPa]	[cycles]
1	44.27	46.60	45.44	2737.5	45.44	0	45.44	0
2	41.94	44.27	43.11	2737.5	43.11	1460	43.11	0
3	39.61	41.94	40.78	0	40.78	0	40.78	0
4	37.28	39.61	38.45	0	38.45	1460	38.45	0
5	34.95	37.28	36.12	0	36.12	0	36.12	0
6	32.62	34.95	33.79	0	33.79	0	33.79	0
7	30.29	32.62	31.46	0	31.46	0	31.46	0
8	27.96	30.29	29.13	0	29.13	0	29.13	0
9	25.63	27.96	26.80	0	26.80	0	26.80	0
10	23.30	25.63	24.47	0	24.47	0	24.47	0
11	20.97	23.30	22.14	0	22.14	0	22.14	0
12	18.64	20.97	19.81	10950	19.81	0	19.81	0
13	16.31	18.64	17.48	43800	17.48	26280	17.48	0
14	13.98	16.31	15.15	0	15.15	2920	15.15	0
15	11.65	13.98	12.82	0	12.82	0	12.82	260
16	9.32	11.65	10.49	5475	10.49	0	10.49	0
17	6.99	9.32	8.16	0	8.16	2920	8.16	0
18	4.66	6.99	5.83	54750	5.83	17520	5.83	0
19	2.33	4.66	3.50	0	3.50	11680	3.50	520
20	0.00	2.33	1.17	240900	1.17	128480	1.17	7020

*Fig. 123 Calculated stress spectrum - effects of 3 trains, number of cycles from 1 train crossing per 1 year, values of stress ranges **are** multiplied by dynamic coefficient*

11.2.3.2 Example 2

We consider the effects from all trains that regularly cross the bridge during 1 day (174 trains in total). We have the time record of the stresses from 1 crossing of each train stored in one single excel file (i.e. 1 file containing 174 columns of data - each column records the stresses caused by one train crossing). The load effects will be multiplied by the dynamic coefficient according to EN 1991-2, Annex C; where the substitute length of the element under assessment is 20 m and the speed of the crossing trains is 50 km/h and the 1st natural frequency of the bridge is 1.8 Hz. The stress spectra are divided into 25 intervals.

Program input data

Fig. 124 Input data to the program - stress waveform from the effects of all trains (each column contains the effects from 1 train => 174 columns in total)

Entering input data into the program

Fig. 125 Input data entry - part 1

Dynamic factor

Multiply the load effects by the dynamic factor?	⦿ YES ○ NO

Select the type of the dynamic factor:	○ Dynamic factor based on the substitute span of the element ⦿ Dynamic factor based on the natural frequency

Substitute span of element:	20	[m]
Train speed:	50	[km/h]

Is the 1st natural frequency of the bridge known?	⦿ YES ○ NO

1st natural frequency of the bridge:	1,8	[Hz]

Fig. 126 Input data entry - part 2

	Specification of the trains			Frequency of the trains crossing over the bridge				
	Train	Type/Number	Selection	per 1day	per 1 week	per 2 weeks	per 1 month	per 1 year
1	Train 1		☐	0	0	0	0	0
2	Train 2		☐	0	0	0	0	0
3	Train 3		☐	0	0	0	0	0
4	Train 4		☐	0	0	0	0	0
5	Train 5		☐	0	0	0	0	0
6	Train 6		☐	0	0	0	0	0
7	Train 7		☐	0	0	0	0	0
8	Train 8		☐	0	0	0	0	0
9	Train 9		☐	0	0	0	0	0
10	Train 10		☐	0	0	0	0	0
11	Train 11		☐	0	0	0	0	0
12	Train 12		☐	0	0	0	0	0
13	Train 13		☐	0	0	0	0	0
14	Train 14		☐	0	0	0	0	0
15	Train 15		☐	0	0	0	0	0
16	Train 16		☐	0	0	0	0	0
17	Train 17		☐	0	0	0	0	0
18	Train 18		☐	0	0	0	0	0
19	Train 19		☐	0	0	0	0	0
20	Train 20		☐	0	0	0	0	0
21	Train 21		☐	0	0	0	0	0
22	Train 22		☐	0	0	0	0	0
23	Train 23		☐	0	0	0	0	0
24	Train 24		☐	0	0	0	0	0
25	Train 25		☐	0	0	0	0	0

Select all	YES ○ NO ⦿		Default value (0)

Fig. 127 Input data entry - part 3 (the table is not active in this case - the train crossing intensities are not filled in the result of the calculation are the stress spectra from one train crossing)

Fig. 128 Input data entry - part 4

Fig. 129 Information about the successful completion of the calculation containing the name of the results file and the path to the file

Output from the programme

Dynamic factor:			STRESS SPECTRUM CAUSED BY INDIVIDUAL TRAINS CROSSING OVER THE BRIDGE (1 crossing over the bridge), STRESS								
1.000											
		Train:	1		2		3		4		5	
			stress range	N	stress range	N	stress range	N	stress range	N	stress range	N
Interval	Lower range	Upper range	[MPa]	[cycles]	[MPa]	[cycles]	[MPa]	[cycles]	[MPa]	[cycles]	[MPa]	[cycles]
1	15.34	15.98	15.66	0	15.66	0	15.66	0	15.66	0	15.66	0
2	14.71	15.34	15.03	0	15.03	0	15.03	0	15.03	0	15.03	0
3	14.07	14.71	14.39	0	14.39	0	14.39	0	14.39	0	14.39	0
4	13.43	14.07	13.75	0	13.75	0	13.75	0	13.75	0	13.75	0
5	12.79	13.43	13.11	0	13.11	0	13.11	0	13.11	0	13.11	0
6	12.15	12.79	12.47	0	12.47	0	12.47	0	12.47	0.5	12.47	0
7	11.51	12.15	11.83	0	11.83	0	11.83	0	11.83	0	11.83	0
8	10.87	11.51	11.19	0	11.19	0	11.19	0	11.19	0.5	11.19	0
9	10.23	10.87	10.55	0	10.55	0	10.55	0	10.55	0	10.55	0
10	9.59	10.23	9.91	0	9.91	0.5	9.91	0	9.91	1	9.91	1
11	8.95	9.59	9.27	0	9.27	1	9.27	0	9.27	0	9.27	0.5
12	8.31	8.95	8.63	0	8.63	0.5	8.63	0	8.63	0	8.63	0.5
13	7.67	8.31	7.99	0	7.99	1	7.99	0	7.99	0	7.99	0.5
14	7.03	7.67	7.35	0	7.35	1	7.35	0.5	7.35	0.5	7.35	1.5
15	6.39	7.03	6.71	1.5	6.71	0	6.71	1	6.71	0.5	6.71	0
16	5.75	6.39	6.07	0.5	6.07	0	6.07	0.5	6.07	0	6.07	0
17	5.11	5.75	5.43	0.5	5.43	0	5.43	1	5.43	0	5.43	0
18	4.48	5.11	4.8	1.5	4.8	0	4.8	1	4.8	1	4.8	0
19	3.84	4.48	4.16	0	4.16	1	4.16	0	4.16	0	4.16	0
20	3.20	3.84	3.52	0	3.52	0	3.52	0	3.52	0	3.52	2
21	2.56	3.20	2.88	0	2.88	1	2.88	0	2.88	0	2.88	0
22	1.92	2.56	2.24	2	2.24	0	2.24	1	2.24	0.5	2.24	0
23	1.28	1.92	1.6	0.5	1.6	0.5	1.6	1.5	1.6	0	1.6	0.5
24	0.64	1.28	0.96	0	0.96	0	0.96	0	0.96	1	0.96	0
25	0.00	0.64	0.32	60.5	0.32	74.5	0.32	47.5	0.32	67	0.32	45.5

*Fig. 130 Calculated stress spectrum - effects of individual trains, number of cycles from 1 train crossing, stress range values **are not** multiplied by dynamic coefficient*

EFFECTS OF ALL TRAINS				
Interval	Lower range	Upper range	[MPa]	[cycles]
1	15.34	15.98	15.66	0.5
2	14.71	15.34	15.03	0.5
3	14.07	14.71	14.39	0
4	13.43	14.07	13.75	3
5	12.79	13.43	13.11	0.5
6	12.15	12.79	12.47	3
7	11.51	12.15	11.83	8.5
8	10.87	11.51	11.19	10
9	10.23	10.87	10.55	11
10	9.59	10.23	9.91	34.5
11	8.95	9.59	9.27	32
12	8.31	8.95	8.63	40
13	7.67	8.31	7.99	90
14	7.03	7.67	7.35	151
15	6.39	7.03	6.71	102
16	5.75	6.39	6.07	102
17	5.11	5.75	5.43	190
18	4.48	5.11	4.80	137
19	3.84	4.48	4.16	109.5
20	3.20	3.84	3.52	170
21	2.56	3.20	2.88	125
22	1.92	2.56	2.24	311.5
23	1.28	1.92	1.60	112.5
24	0.64	1.28	0.96	103
25	0.00	0.64	0.32	15198

*Fig. 131 Calculated stress spectrum - the effects of **all trains together**, number of cycles from 1 train crossing, values of stress range **are not** multiplied by the dynamic coefficient*

Dynamic factor:			STRESS SPECTRUM CAUSED BY INDIVIDUAL TRAINS CROSSING OVER THE BRIDGE (1 crossing over the bridge), STRESS RA									
1.433												
		Train:	1		2		3		4		5	
			stress range N		stress range N		stress range N		stress range N		stress range N	
Interval	Lower range	Upper range	[MPa]	[cycles]	[MPa]	[cycles]	[MPa]	[cycles]	[MPa]	[cycles]	[MPa]	[cycles]
1	21.98	22.90	22.44	0	22.44	0	22.44	0	22.44	0	22.44	0
2	21.07	21.98	21.52	0	21.52	0	21.52	0	21.52	0	21.52	0
3	20.15	21.07	20.61	0	20.61	0	20.61	0	20.61	0	20.61	0
4	19.23	20.15	19.69	0	19.69	0	19.69	0	19.69	0	19.69	0
5	18.32	19.23	18.78	0	18.78	0	18.78	0	18.78	0	18.78	0
6	17.40	18.32	17.86	0	17.86	0	17.86	0	17.86	0.5	17.86	0
7	16.49	17.40	16.94	0	16.94	0	16.94	0	16.94	0	16.94	0
8	15.57	16.49	16.03	0	16.03	0	16.03	0	16.03	0.5	16.03	0
9	14.65	15.57	15.11	0	15.11	0	15.11	0	15.11	0	15.11	0
10	13.74	14.65	14.20	0	14.20	0.5	14.20	0	14.20	1	14.20	1
11	12.82	13.74	13.28	0	13.28	1	13.28	0	13.28	0	13.28	0.5
12	11.91	12.82	12.37	0	12.37	0.5	12.37	0	12.37	0	12.37	0.5
13	10.99	11.91	11.45	0	11.45	1	11.45	0	11.45	0	11.45	0.5
14	10.08	10.99	10.53	0	10.53	1	10.53	0.5	10.53	0.5	10.53	1.5
15	9.16	10.08	9.62	1.5	9.62	0	9.62	1	9.62	0.5	9.62	0
16	8.24	9.16	8.70	0.5	8.70	0	8.70	0.5	8.70	0	8.70	0
17	7.33	8.24	7.79	0.5	7.79	0	7.79	1	7.79	0	7.79	0
18	6.41	7.33	6.87	1.5	6.87	0	6.87	1	6.87	1	6.87	0
19	5.50	6.41	5.95	0	5.95	1	5.95	0	5.95	0	5.95	0
20	4.58	5.50	5.04	0	5.04	0	5.04	0	5.04	0	5.04	2
21	3.66	4.58	4.12	0	4.12	1	4.12	0	4.12	0	4.12	0
22	2.75	3.66	3.21	2	3.21	0	3.21	1	3.21	0.5	3.21	0
23	1.83	2.75	2.29	0.5	2.29	0.5	2.29	1.5	2.29	0	2.29	0.5
24	0.92	1.83	1.37	0	1.37	0	1.37	0	1.37	1	1.37	0
25	0.00	0.92	0.46	60.5	0.46	74.5	0.46	47.5	0.46	67	0.46	45.5

*Fig. 132 Calculated stress spectrum - effects of individual trains, number of cycles from 1 train crossing, stress range values **are** multiplied by dynamic coefficient*

EFFECTS OF ALL TRAINS				
Interval	Lower range	Upper range	[MPa]	[cycles]
1	21.98	22.90	22.44	0.5
2	21.07	21.98	21.52	0.5
3	20.15	21.07	20.61	0
4	19.23	20.15	19.69	3
5	18.32	19.23	18.78	0.5
6	17.40	18.32	17.86	3
7	16.49	17.40	16.94	8.5
8	15.57	16.49	16.03	10
9	14.65	15.57	15.11	11
10	13.74	14.65	14.20	34.5
11	12.82	13.74	13.28	32
12	11.91	12.82	12.37	40
13	10.99	11.91	11.45	90
14	10.08	10.99	10.53	151
15	9.16	10.08	9.62	102
16	8.24	9.16	8.70	102
17	7.33	8.24	7.79	190
18	6.41	7.33	6.87	137
19	5.50	6.41	5.95	109.5
20	4.58	5.50	5.04	170
21	3.66	4.58	4.12	125
22	2.75	3.66	3.21	311.5
23	1.83	2.75	2.29	112.5
24	0.92	1.83	1.37	103
25	0.00	0.92	0.46	15198

*Fig. 133 Calculated stress spectrum - the effects of **all trains together**, number of cycles from 1 train crossing, values of stress range **are** multiplied by the dynamic coefficient*

11.3. Annexe 3: FALCom software
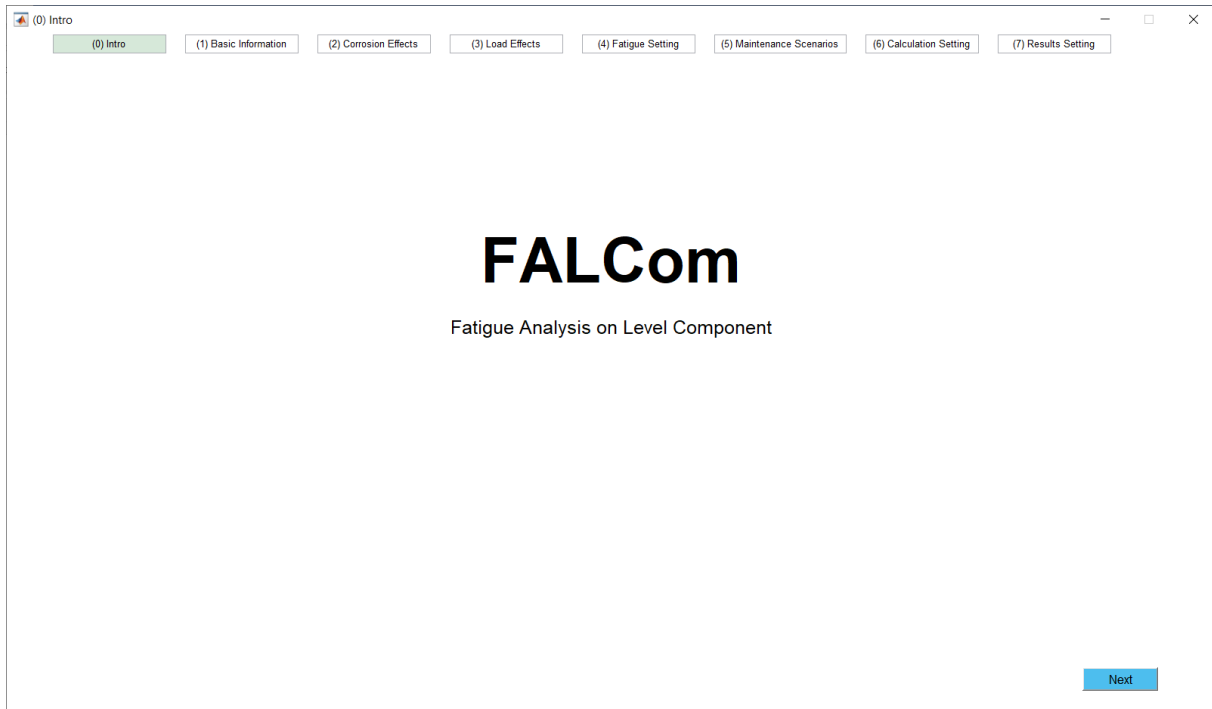
11.3.1. Instructions for installing the software

Download the package called FALCom.rar from the website and then extract it.

The following files are included in the package:

1) *FALCom* - the software itself (exe application)
2) *Results.xlsx* - template for the results (excel file)
3) *FALCom_manual* - software manual (PDF document)

For successful installation of the software, you must have MATLAB Runtime installed on your computer, which can be downloaded from:
http://www.mathworks.com/products/compiler/mcr/index.html.

To start the installation of the software, double click on the icon called FALCom. Then follow the on-screen instructions. An internet connection is required to install the software.

11.3.2. Software description

The "FALCom" software was created in the "Guide" interface of the MATLAB® software. It is the analytical software tool called FALCom, which is the abbreviation of „Fatigue Assessment on Level of Component ". The whole methodology stated in Chapter 6.1 is included in this programme.
FALCom programme is a usable tool in form of analytical software. This tool makes possible a residual life assessment including the management of the optimum method and maintenance procedure of the structural elements with respect to the length of the required residual life of the bridge.
With the knowledge of the effects of traffic loads, which can be obtained from measurements directly on the structure or from a computational numerical model, the residual service life of the structural elements can be calculated in a simple way using the program.

After filling in and entering all the necessary input data and setting up the required calculations and outputs, the user obtains from the program the parameters characterising the fatigue life of the element under assessment.
For the calculation of fatigue damage and residual fatigue life, linear and non-linear damage accumulation models are included in the program.

The program takes into account possible corrosion weakening of the elements under consideration when calculating fatigue damage and residual life. Corrosion weakening is taken into account by changing the fatigue curve over time. The relationship for the reduction of the detail category was taken from the results of laboratory tests on the fatigue behaviour of degraded elements.

The algorithm from the "Stress spectrum generator" software, which is used to calculate the stress spectra of the traffic load, was also integrated into the FALCom software.
In addition, different scenarios are considered according to the maintenance of the structural elements or the whole structure. For each of these scenarios, the fatigue damage coefficients from traffic loading expected in the future, the remaining service life and the overall service life of the element under consideration are calculated by the software. The estimation of the residual life is based on the computational relationships of the linear and non-linear theories presented above.

Based on the maintenance scenarios, the amount of financial costs needed to provide the maintenance for the required residual lifetime of the structure is also estimated.
For the cost calculation, the same scenarios as in the previous case for the calculation of the residual lifetime are considered. The total financial cost of maintenance is then given for each scenario by the sum of the costs for each activity.

For a successful installation of the program, it is necessary to have MATLAB Runtime installed on the computer. The MATLAB® software itself does not need to be installed.

11.3.2.1 Input data
The input data is filled in directly in the program. Check boxes are used to select from multiple options. Input data related to traffic effects can be uploaded to the software in two possible formats: (1) data stored in an Excel file; (2) data stored in a text file. It is also possible for the imported data to contain a stress (or strain) that is either (a) time-dependent, meaning that the input file takes the form of, for example, an excel file that contains 2 columns of data, with the first containing the stress values and the second containing the time, or (b) time-independent, where the excel file contains only the column containing the stress (or strain) values.

11.3.2.2 Outputs from the software
The outputs from the FALCom sotware are as follows:

1. Stress spectrum calculated for all train units crossing over the bridge: number of cycles per one crossing and per one year.
2. Coefficient of fatigue damage in history: includes the time period from bridge construction (or from the start of operation on the bridge) to the assessment.
3. Coefficient of fatigue damage in the future: includes the time period from the assessment (or since the completion of bridge reconstruction) to the expiration of required remaining life (for example, the bridge is required to remain in service for another 30 years).
4. Remaining service life (years).

5. Total service life (years).
6. Financial costs for the owner necessary to maintain the structure during the required remaining service life.

Points 3–6 are calculated for various scenarios, which depend on the maintenance method or on the type of reconstruction.

All the calculated results are automatically saved to an excel file, which can be freely named before saving and the location where it will be saved can also be selected. The data can be saved in a completely new file, or a predefined template, which is also included with the software, can be used and its contents overwritten. There is one template with the names *Results.xlsx.* If you do not use a predefined template but save the results in a new file, you need to add the *.xlsx* extension to the file name.

11.3.2.3 Description of the software interface

The FALCom interface consists of a total of seven input windows (see Fig. 134 to Fig. 140):

1) Basic information
2) Corrosion effects
3) Load effects
4) Fatigue setting
5) Maintenance scenarios
6) Calculation setting
7) Results setting

1) Basic information
In this input window, basic information about the bridge and the element to be assessed is entered:

- the year the bridge was built (or the year the bridge was put into service)
- the year in which the bridge assessment is carried out
- geometry of the assessed element.

2) Corrosion effects
In this input window, information about corrosion effects is entered. The effects of uniform and non-uniform corrosion are distinguished.
In the case of uniform corrosion, one of three corrosion models can be selected:

- Power model
- Corrosion model by Guedes Soares and Garbatov
- Corrosion model by Klinesmith et al.

In the case of non-uniform corrosion, the surface roughness parameter Δb_c is entered. More information about parameter Δb_c are stated in Chapter 5.2.3.
In addition, the expected effectiveness (in years) of the corrosion coating applied to the bridge during construction or reconstruction is entered.

3) Load effects
In this input window, information on vehicle load effects is entered. The format and type of input data are selected. In addition, the necessary information for the calculation of the dynamic coefficient is entered if the dynamic coefficient is to be taken into account in the calculation.

The table shall specify the loading vehicles and enter the crossing intensities of each vehicle in the historical period (from the time the bridge was built to the time of the assessment) and in the future period (from the time of the assessment or from the end of the reconstruction).

4) Fatigue setting

This input window specifies how the fatigue damage is calculated. Any of the following damage accumulation models can be selected:

1. Palmgren-Miner rule
2. Corten-Dolan model
3. Morrow's plastic work interaction rule
4. V. Dattoma's model

The required residual life of the bridge is also filled in.

5) Maintenance scenarios

Any of the following different ways maintenance scenarios can be considered when calculating the residual service life:

1. No maintenance - there is no maintenance of structure and structure elements from the corrosion point of view
2. Coating application - the coating is applied on the whole structure or on the critical members
3. Strengthening of the critical members - the strengthening of the critical members is applied
4. Replacement of the critical members - the critical structural member is replaced by new element.

For each scenario the following values are calculated: coefficient of fatigue damage in the future, remaining service life and total service life of assessed element.

6) Calculation setting

This input window specifies the characteristics of the stress spectra:

- the minimum and maximum limit value of the stress range
- the number of intervals into which the stress ranges will be divided.

7) Results setting

In this input window, you can select which graphs will or will not be plotted after the calculation.

The application of FALCom software for the assessment of remaining fatigue life of components is shown on a practical example in frame of case study in Chapter 6.4.

157

(1) Basic Information

× □ |

(0) Intro   (1) Basic Information   (2) Corrosion Effects   (3) Load Effects   (4) Fatigue Setting   (5) Maintenance Scenarios   (6) Calculation Setting   (7) Results Setting

BRIDGE INFORMATION

Year of bridge construction:

Year of bridge assessment:

GEOMETRY OF THE ASSESSED ELEMENT

Initial sheet thickness: mm

Initial sheet width: mm

Diameter of rivet shank: mm

Diameter of rivet head: mm

Load data   Previous   Next

Fig. 134 Input window (1): Basic information

Fig. 135 Input window (2): Corrosion effects

Fig. 136 Input window (3): Load effects

Fig. 137 Input window (4): Fatigue setting

(5) Maintenance Scenarious

| (0) Intro | (1) Basic Information | (2) Corrosion Effects | (3) Load Effects | (4) Fatigue Setting | (5) Maintenance Scenarios | (6) Calculation Setting | (7) Results Setting |

MAINTENANCE SCENARIOS

☑ SCENARIO 1: NO MAINTENANCE

☑ SCENARIO 2: COATING APPLICATION

Year of application of the scenario: [ ] year   (Min. the following year after the year of the assessment)

Coating lifetime: [ ] year

Coating re-aplication before the lifetime expiration?
- ◉ Yes
- ○ No
- ○ Both variants

☑ SCENARIO 3: STRENGTHENING OF CRITICAL MEMBERS + COATING APPLICATION

Year of application of the scenario: [ ] year   (Min. the following year after the year of the assessment)

Coating lifetime: [ ] year

Coating re-aplication before the lifetime expiration?
- ◉ Yes
- ○ No
- ○ Both variants

☑ SCENARIO 4: REPLACEMENT OF CRITICAL MEMBERS

Detail category of new member: [ ] MPa

Year of application of the scenario: [ ] year   (Min. the following year after the year of the assessment)

Coating lifetime: [ ] year

Coating re-aplication before the lifetime expiration?
- ◉ Yes
- ○ No
- ○ Both variants

Load data   Previous   Next

Fig. 138 Input window (5): Maintenance scenarios

(6) Calculation Setting

(0) Intro | (1) Basic Information | (2) Corrosion Effects | (3) Load Effects | (4) Fatigue Setting | (5) Maintenance Scenarios | (6) Calculation Setting | (7) Results Setting

STRESS SPECTRUM CHARACTERISTICS

Select the upper limit of the stress range:
- ◉ Max. value of stress range obtained from the data
- ○ Own value

Write the own value of the upper limit of the stress range: [ ] MPa

Select the lower limit of the stress range:
- ◉ Min. value of stress range obtained from the data
- ○ Own value

Write the own value of the upper limit of the stress range: [ ] MPa

Write the number of intervals into that the stress spectrum is divided: [ ]

Load data | Previous | Next

Fig. 139 Input window (6): Calculation setting

Fig. 140 Input window (7): Results setting

11.4. Annexe 4: Flowchart - Assessment procedure of fatigue life of existing steel railway bridges

FLOWCHART FOR THE ASSESSMENT OF FATIGUE LIFE OF EXISTING STEEL RAILWAY BRIDGES (List 2 of 5)

PHASE 2: ASSESSMENT OF REMAINING FATIGUE LIFE OF STRUCTURE ELEMENTS AND THE WHOLE BRIDGE STRUCTURE

1) Method of Equivalent stresses

Inputs:
- Stress range
- Category detail
- Dynamic factor
- Corrosion properties

Load tests
Bridge monitoring
Numerical model

Eurocode
Documents (e.x. IRS 77802)

Corrosion inspection

Outputs:
Fatigue damage of structural member(s) related to $2 \cdot 10^6$ cycles
(Coefficient od fatigue damage D_E)

Corrosion process:
1) Continues
2) Do not contionue (caoting application)
3) Strengthening of corroded members

Has been the fatigue life of structural member(s) exhaused? ($D_E >= 1$)

YES

Is the load capacity or serviceability of the bridge structure endangered?

Criteria for collapse of a steel railway bridge structure:
Ultimate limit state (ULS):
• Stress
Serviceability limit state (SLS):
• Maximum vertical displacement
• Maximum vertical acceleration
• Maximum oscillation

PHASE 3: MEASURES (LIMITATIONS, RECOMMENDATIONS, ...)

YES

NO

NO

Measures:
• A reconstruction of the bridge has to be done

Measures:
Measures based on a monitoring of the condition of the bridge:
• Regular inspections of the critical details and members
• Long-term monitoring of the critical details and members with an early warning system
Measures providing the extension of the service life:
• Strengthening of critical members
• Reconstruction of the critical members

The traffic is possible wihout limitations

It is not possible to calculate the remaining fatigue life of structural member(s) by using this method.
If possible, better to use the 2nd method bases on damage accumulation, which is more accurate.

FLOWCHART FOR THE ASSESSMENT OF FATIGUE LIFE OF EXISTING STEEL RAILWAY BRIDGES (List 3 of 5)

PHASE 2: ASSESSMENT OF REMAINING FATIGUE LIFE OF STRUCTURE ELEMENTS AND THE WHOLE BRIDGE STRUCTURE

Data from:
- Load tests
- Bridge monitoring
- Numerical model

2) Method of damge accumulation

Stress spectrum generator

Eurocode Documents (e.x. IRS 77802)

Long-term bridge monitoring

Corrosion inspection

Inputs:
- Stress spectrum
- Category detail
- Load history
- Corrosion properties

Outputs:
- Fatigue damage of structure member(s) at observed time (Coefficient od fatigue damage D)

Corrosion process:
1) Continues
2) Does not contionue (caoting application)
3) Strengthening of corroded members

Has been the fatigue life of structural member(s) exhaused? (D>=1)

YES

NO

Is the load capacity or serviceability of the bridge structure endangered?

Criteria for collapse of a steel railway bridge structure:
Ultimate limit state (ULS):
- Stress
Serviceability limit state (SLS):
- Maximum vertical displacement
- Maximum vertical acceleration
- Maximum oscillation

(List 4 of 5)

PHASE 3: MEASURES (LIMITATIONS, RECOMMENDATIONS, ...)

YES

NO

The next operation of the bridge is not possible

The next operation of the bridge is possible just in case of taking the meausures that ensure the safe traffic

Measures:
- A reconstruction of the bridge has to be done

Measures:
Measures based on a monitoring of the condition of the bridge:
- Regular inspections of the critical details and members
- Long-term monitoring of the critical details and members with an early warning system
Measures providing the extension of the service life:
- Strengthening of critical members
- Reconstruction of the critical members

167

FLOWCHART FOR THE ASSESSMENT OF FATIGUE LIFE OF EXISTING STEEL RAILWAY BRIDGES   (List 4 of 5)

PHASE 2: ASSESSMENT OF REMAINING FATIGUE LIFE OF STRUCTURE ELEMENTS AND THE WHOLE BRIDGE STRUCTURE

2) Method of damge accumulation... continue

Has been the fatigue life of structural member(s) exhaused? (D>=1)

NO

YES

(List 3 of 5)

Calculation:
- Fatigue damage at the end of required time
- Real remaining fatigue life
- Real fatigue life

Is the calculated remaining fatigue life of struture member(s) longer then the reqired remaining life of the bridge?

NO

Can be expected that the load capacity or serviceability of the bridge structure will be endangered in the future?

Criteria for collapse of a steel railway bridge structure:
Ultimate limit state (ULS):
- Stress
Serviceability limit state (SLS):
- Maximum vertical displacement
- Maximum vertical acceleration
- Maximum oscillation

PHASE 3: MEASURES (LIMITATIONS, RECOMMENDATIONS, ...)

YES

YES

NO

The next operation of the bridge is possible without limitations

The next operation of the bridge is possible just in case of taking the meausures that ensure the safe traffic

The next operation of the bridge is possible, but the measure in form of the bridge condition monitoring is necessary

Measures:
- Regular inspections of the critical details and members
- Long-term monitoring of the critical details and members with an early warning system

Is the condition of the critical elements getting worse?
For examle: the fatigue crack has appeared

YES

NO

Measures:
Measures providing the extension of the service life:
- Strengthening of critical members
- Reconstruction of the critical members
Other measures
- Limitation of the trafic (max. train velocity, max. axle load)
Alternatively:
- Fracture mechanics approach if a fatigue crack has appeared and calculation the time of crack growth (see Method 3)

FLOWCHART FOR THE ASSESSMENT OF FATIGUE LIFE OF EXISTING STEEL RAILWAY BRIDGES   (List 5 of 5)

PHASE 2: ASSESSMENT OF REMAINING FATIGUE LIFE OF STRUCTURE ELEMENTS AND THE WHOLE BRIDGE STRUCTURE

3) Fracture mechanics approach

Data from:
• Load tests
• Bridge monitoring
• Numerical model

Inputs:

Stress spectrum generator → Expected stress spectrum in the future

Documentation → Goemetry of element

Bridge inspection → Type of a crack

Material tests → Initial crack length

Corrosion inspection → Critical crack length

Material properties (Kth, Kc, D, m)

Corrosion properties

Corrosion process:
1) Continues
2) Do not contionue (caoting application)
3) Strengthening of corroded members

Outputs:

Time of crack growth to the critical length of the structural member(s)

Is the calculated time of crack growth of the structural member(s) longer than the required remaining service life?

NO

Criteria for collapse of a steel railway bridge structure:
Ultimate limit state (ULS):
• Stress
Serviceability limit state (SLS):
• Maximum vertical displacement
• Maximum vertical acceleration
• Maximum oscillation

Can be expected that the load capacity or serviceability of the bridge structure will be endangered in the future?

PHASE 3: MEASURES (LIMITATIONS, RECOMMENDATIONS, …)

YES

The traffic is possible wihout limitations, but regular inspections of critical details and members has to prescribed

YES

The next operation of the bridge is possible just in case of taking the meausures that ensure the safe traffic

NO

The next operation of the bridge is possible, but the measure in form of the bridge condition monitoring is necessary

Measures:
• Regular inspections of the critical details and members containing a crack
• Long-term monitoring of the critical details and members containing a crack with an early warning system

Is the condition of the critical elements getting worse? For exemple: the fatigue crack is growing faster than was expected

YES

NO

Measures:
Measures providing the extension of the service life:
• Strengthening of critical members
• Reconstruction of the critical members
Other measures
• Limitation of the trafic (max. train velocity, max. axle load)

11.5. Annexe 5: Results of material tests

11.5.1. Tensile test and Charpy impact test

CZ FERMET s.r.o.
LABORATORY CZ FERMET
Testing laboratory No. 1409 accredited by CAI according to ČSN EN ISO/IEC 17025

Buštěhradská 283, Kladno 272 03

L 1409

page 1/11

Test Certificate
No. 325/2016/LAZ-m

Customer :   České vysoké učení technické v Praze
Fakulta stavební

Address :   Thákurova 7
166 29 Praha 6

Order No. :   1113460040

TENSILE TEST according to PP – M – 01 (ČSN EN ISO 6892-1)
CHARPY PENDULUM IMPACT TEST according to PP-M-02 (ČSN ISO 148-1)

Specimen No. :   S1-1, S1-2, S1-3, S1-4, S1-5, S1-6
S2-1, S2-2, S2-3, S2-4

Pages :   11
Supplements : 8

Results are related only to the samples under the test.
This protocol is not allowed to be reproduced incomplete without Laboratory CZ FERMET agreement.

Kladno, 6.6.2016

170

Customer	Received	Specimen No.	Order No.	Tested
ČVUT v Praze Fakulta stavební	6.6.2016	S1-1, S1-2, S1-3, S1-4, S1-5, S1-6	1113460040	6.6.2016

Note	S1-1, S1-2, S1-3, S1-4	Carvical square	L100x100-12
	S1-5	Wall (sheet)	P14
	S1-6	Flange (sheet)	P9
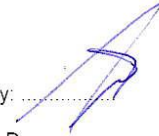
Results:

Standard For Testing	ČSN EN ISO 6892-1:2009; A113							
Testing Method	Tensile Test							
Apparatus	INSTRON 1196, serial number H2068							
Specimen No.	Specimen Orientation	Dimension Ø [mm]	Gage Length L_0 [mm]	Yield Strength Reh [MPa]	Yield Strength $R_{p0,2}$ [MPa]	Tensile Strength R_m [MPa]	Elongation A 5 [%]	Reduction in Area Z [%]	E (GPa)
S1-1	L	8,01	40	268	240	388	40,8	69,4	205,826
S1-2	L	8,00	40	244	229	382	38,3	68,8	206,782
S1-5	L	8,00	40	220	212	322	44,0	79,6	207,201
S1-6	L	6,01	30	267	253	414	40,0	67,6	208,567

Standard For Testing	ČSN ISO 148-1				
Testing Method	Charpy Pendulum Impact Test				
Apparatus	Charpy Impact Machine AMSLER RKP 300, serial number 93				
Specimen No.	Testing Bar	Specimen Orientation	Initial Potential Energy [J]	Testing Temperature [°C]	Absorbed Energy [J]
S1-3	KV_2 300	L	300	20	73
	KV_2 300	L	300	20	101
	KV_2 300	L	300	20	37
S1-4	KV_2 300	L	300	-20	5
	KV_2 300	L	300	-20	6
	KV_2 300	L	300	-20	5

Written by: ....

K LAZ-m Martin Bambas

Checked and approved by: ....

VL Ing. L. Procházka, Ph.D.

171

Customer	Received	Specimen No.	Order No.	Tested
ČVUT v Praze Fakulta stavební	6.6.2016	S2-1, S2-2, S2-3, S2-4	1113460040	6.6.2016

		S2-1, S2-2	Carvical square	L100x100-12
Note		S2-3	Wall (sheet)	P14
		S2-4	Flange (sheet)	P9

Results:

Standard For Testing	ČSN EN ISO 6892-1:2009; A113
Testing Method	Tensile Test
Apparatus	INSTRON 1196, serial number H2068

Specimen No.	Specimen Orientation	Dimension Ø [mm]	Gage Length L_o [mm]	Yield Strength Reh [MPa]	Yield Strength $R_{p0.2}$ [MPa]	Tensile Strength R_m [MPa]	Elongation A 5 [%]	Reduction in Area Z [%]	E (GPa)
S2-1	L	8,00	40	299	261	396	32,0	65,6	208,568
S2-2	L	8,01	40	267	265	400	31,8	63,8	207,386
S2-3	L	8,00	40	241	216	375	40,8	69,5	207,986
S2-4	L	6,01	30	299	252	388	41,7	73,0	209,809

Written by: ....

K LAZ-m Martin Bambas

Checked and approved by: ....
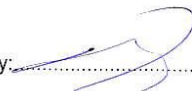
VL Ing. L. Procházka, Ph.D.

Supplement No.1
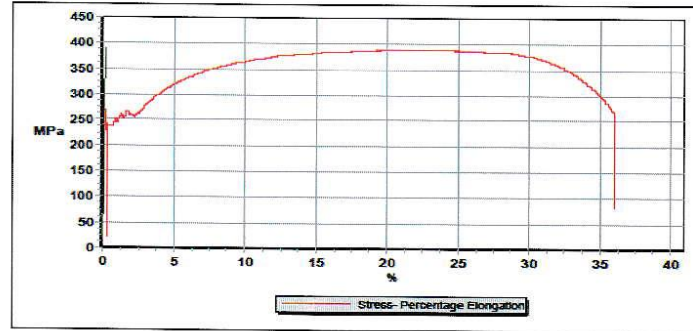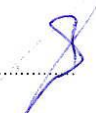
results CVUT Pha -KO 64 exA:

	ReH [MPa]	[MPa]	[MPa]	[%]	Z* [%]	E [GPa]
S1-1	268	240	388	40,8	69,4	205,826

Written by:..............................

K LAZ-m Martin Bambas

Checked and approved by: ....

VL Ing. L. Procházka, Ph.D.

Supplement No.2
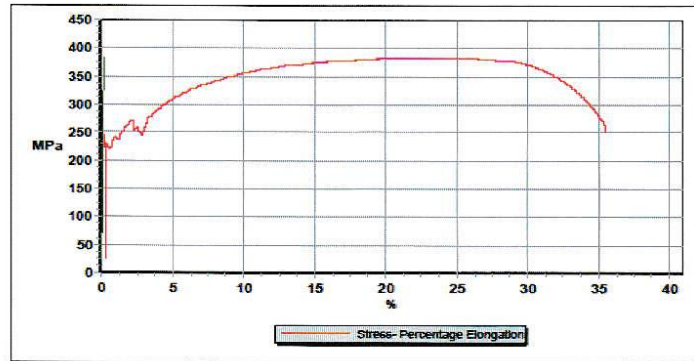
results ČVUT Pha -KO 64 exA:

	ReH [MPa]	[MPa]	[MPa]	[%]	Z* [%]	E [GPa]
S1-2	244	229	382	38,3	68,8	206,782

Written by: ....

K LAZ-m Martin Bambas

Checked and approved by: ....

VL Ing. L. Procházka, Ph.D.

174
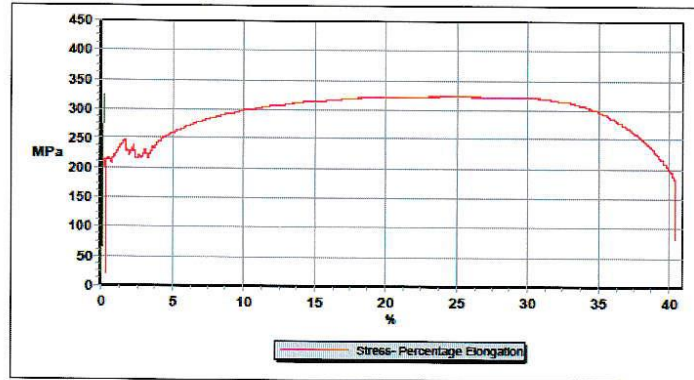
Supplement No.3

results CVUT Pha -KO 64 exA:

	ReH [MPa]	[MPa]	[MPa]	[%]	Z* [%]	E [GPa]
S1-5	220	212	322	44,0	79,8	207,201

Written by: ....
K LAZ-m Martin Bambas

Checked and approved by: ....
VL Ing. L. Procházka, Ph.D.

175
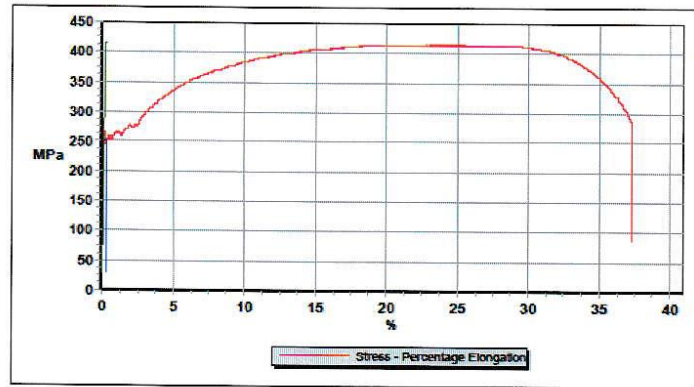
Supplement No.4

results ČVUT Pha – KO 65 exA:

	ReH [kN/m]	[MPa]	[MPa]	[%]	Z⁺ [%]	E [GPa]
S1-6	267	253	414	40,0	67,6	208,567

Written by: ....   Checked and approved by: ....

K LAZ-m Martin Bambas   VL Ing. L. Procházka, Ph.D.
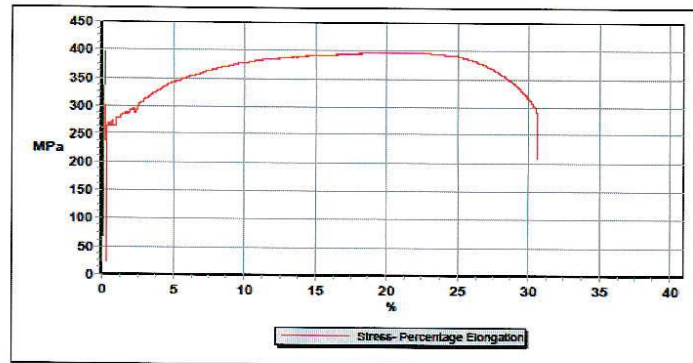
176
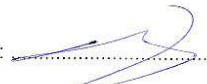
Supplement No.5

results ČVUT Pha -KO 64 exA:

	ReH [MPa]	[MPa]	[MPa]	[%]	Z* [%]	E [GPa]
S2-1	299	261	396	32,0	65,6	208,568

Written by: ....
K LAZ-m Martin Bambas

Checked and approved by: ....
VL Ing. L. Procházka, Ph.D.

177
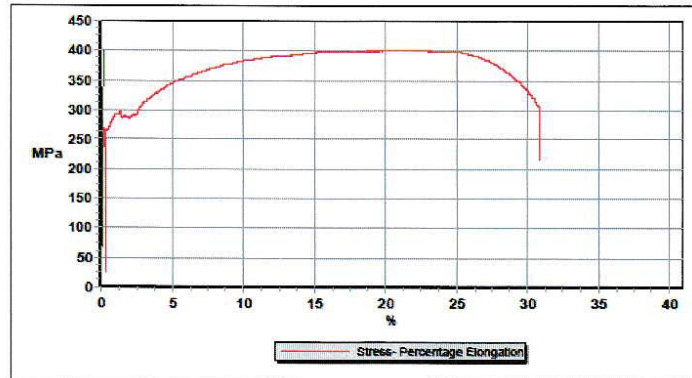
Supplement No.6

results CVUT Pha -KO 64 exA:

	ReH [MPa]	[MPa]	[MPa]	[%]	Z² [%]	E [GPa]
S2-2	267	265	400	31,8	63,8	207,388

Written by: ....
K LAZ-m Martin Bambas

Checked and approved by: ....
VL Ing. L. Procházka, Ph.D.

178
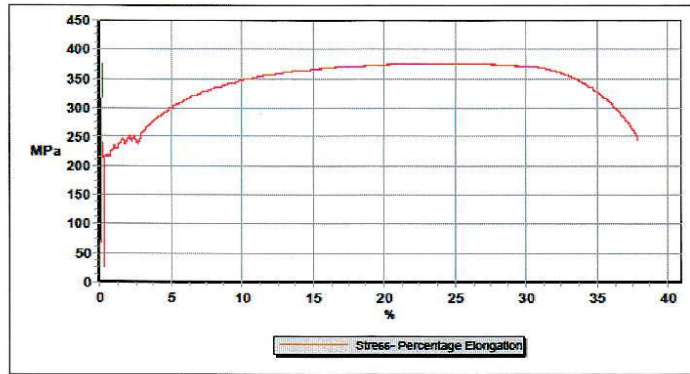
Supplement No.7

results ČVUT Pha -KO 64 exA:

	ReH [MPa]	[MPa]	[MPa]	[%]	Z* [%]	E [GPa]
S2-3	241	216	375	40,8	68,5	207,986

Written by: ....
K LAZ-m Martin Bambas

Checked and approved by: ....
VL Ing. L. Procházka, Ph.D.

Supplement No.8
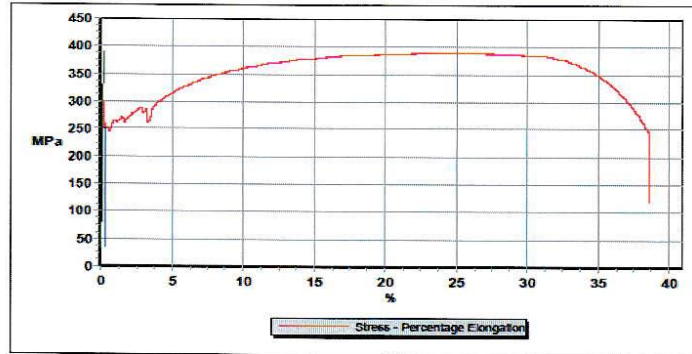
results ČVUT Pha - KO 65 exA:

	ReH [kN/m]	[MPa]	[MPa]	[%]	Z* [%]	E [GPa]
S2-4	299	252	388	41,7	73,0	209,809

Written by: ....

K LAZ-m Martin Bambas

Checked and approved by: ....

VL Ing. L. Procházka, Ph.D.

180

11.5.2. Microstructure test

CZ FERMET s.r.o.
LABORATORY CZ FERMET

Buštěhradská 283, Kladno 272 03

Test Certificate
No.141/2016/LAZ-g

Customer :   České vysoké učení technické v Praze

Address :   Fakulta stavební Thákurova 7
                166 29 PRAHA 6

Order No :   1113460040

MICROSTRUCTURE TEST

Specimen No. :   **S1-1, S1-5**

Pages :   4
Supplements :   2

Results are related only to the samples under the test
This protocol is not allowed to be reproduced incomplete without Laboratory CZ FERMET agreement.

Kladno, 3.6.2016

Microstructure Test:

Customer	Received	Order No.	Heat No.	Product	Size
ČVÚT PRAHA	2.6.2016	1113460040	---	L100x100x12	120x20x12
Specimen No.	Steel Grade	Test			Tested
S1-1	---	Microstructure test.			3.6.2016

Test	
Preparing specimen	Mechanically grinding and polishing
Etching	Nital 5%
Result	**Ferrite + pearlite + tertiary cementite (Fig.1,2).**

Magnification	Microscope	Tested by	Distribution List
100x,500x	NEOPHOT 32	Ing.M.Barinková	1 x LAZg

Microstructure Test:

Customer	Received	Order No.	Heat No.	Product	Size
ČVÚT PRAHA	2.6.2016	1113460040	---	L100x100x12	120x20x12
Specimen No.	Steel Grade	Test			Tested
S1-5	---	Microstructure test.			3.6.2016

Test	
Preparing specimen	Mechanically grinding and polishing
Etching	Nital 5%
Result	**Ferrite + tertiary cementite (Fig.3,4).**

Magnification	Microscope	Tested by	Distribution List
100x,500x	NEOPHOT 32	Ing.M.Barinková	1 x LAZg

Written by: ....

and liable for technical accuracy
VK LAZ-g Ing.M.Barinková

Checked and approved by: ....

Ing.L.Procházka,Ph.D
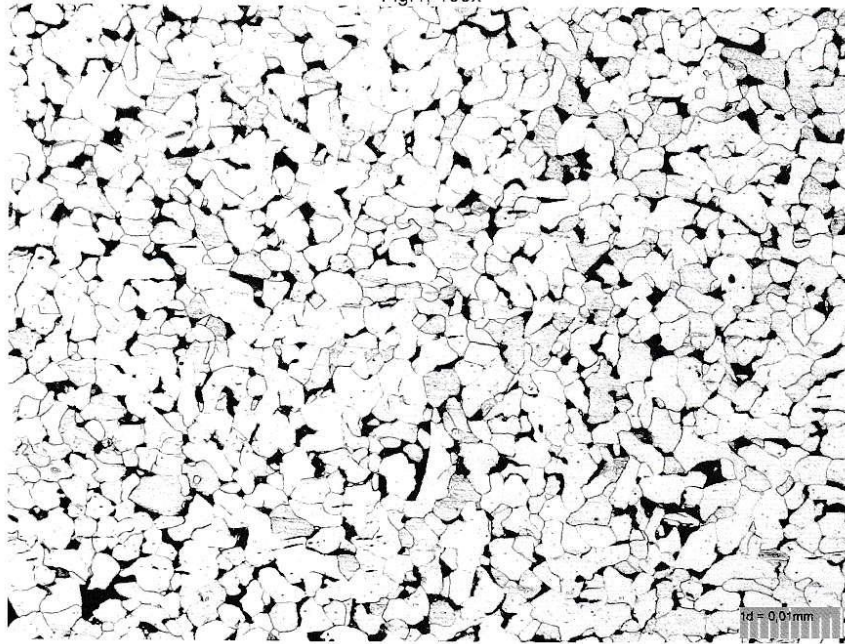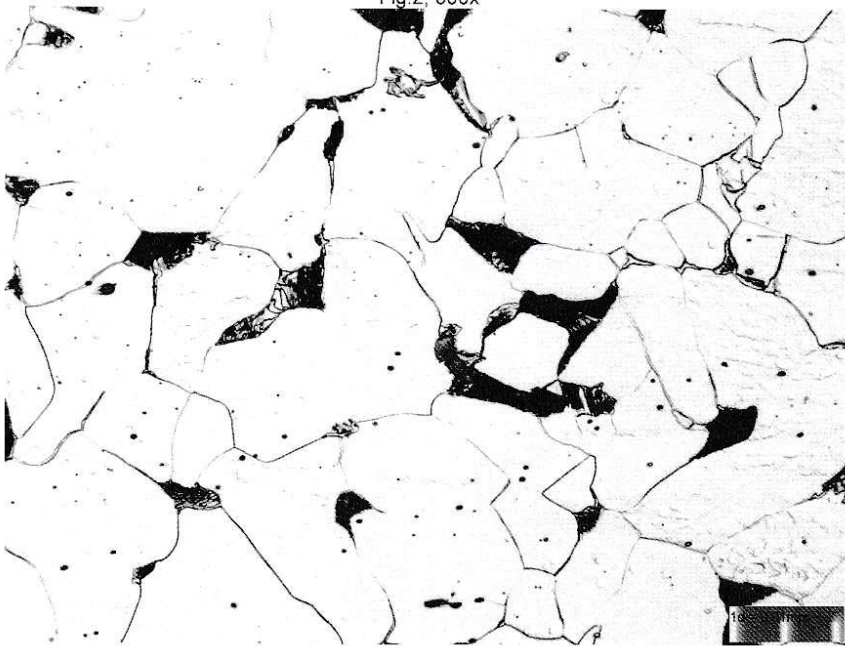VL

Fig.1, 100x

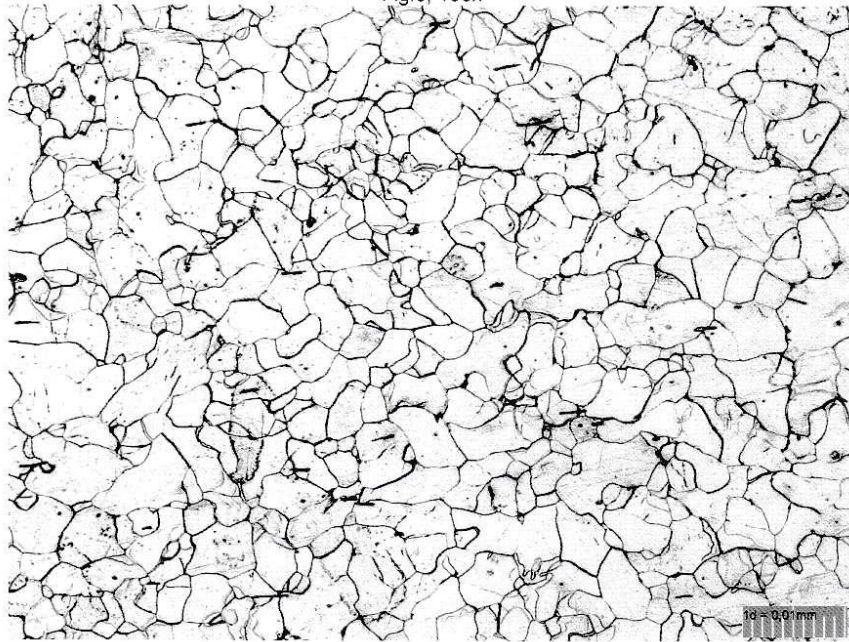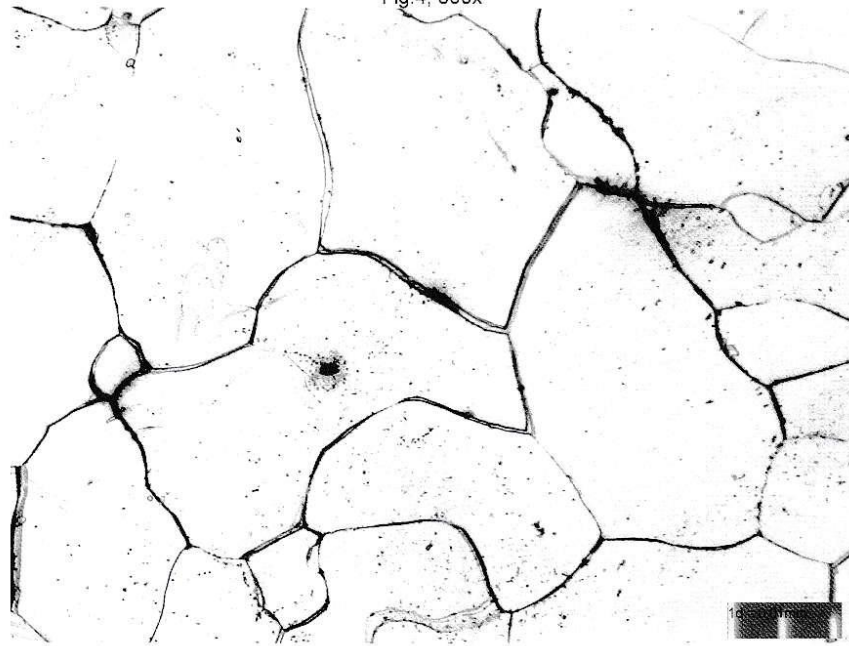Fig.2, 500x

Fig.3, 100x

Fig.4, 500x

11.5.3.   Chemical analysis

CZ FERMET s.r.o.
LABORATORY CZ FERMET
Buštěhradská 277, Kladno 272 03

page1/1

Test Certificate
No.98/2016/LAZ-c

Chemical analysis

Customer :   České vysoké učení technické v Praze Fakulta stavební
Address :   Thákurova 7
             166 29 Praha 6

Received :   2.6.2016
Tested :   2.6.2016
Apparatus :   QUANTRON Magellan
Testing Method   optical emission spectrometric method
Pages :   1
Supplements :   0

Order	Specimen	Steel	Heat	Product
1113460040	S1-1	- - - -	- - - -	120x20x12

Element	[%]	Element	[%]
C	0,17	Cu	0,02
Si	0,00	Nb	<0,002
Mn	0,30	Ti	0,004
P	0,032	V	<0,001
S	0,030	W	<0,005
Cr	0,01	Pb	0,000
Mo	<0,01	Sn	<0,001
Ni	0,02	As	0,025
Al	0,002	Sb	<0,001
Co	0,014	B	0,0015

Results are related only to the samples under the test.
This certificate is prohibited to reproduce incomplete without Laboratory CZ FERMET agreement.

Kladno: Written by: Checked and approved by:
2.6.2016   Žofie Zíková   T.Štefanová
                 K   K

185

CZ FERMET s.r.o.
LABORATORY CZ FERMET
Buštěhradská 277, Kladno 272 03

page1/1

Test Certificate
No.99/2016/LAZ-c

Chemical analysis

Customer :   České vysoké učení technické v Praze Fakulta stavební
Address :   Thákurova 7
               166 29 Praha 6

Received :   2.6.2016
Tested :   2.6.2016
Apparatus :   QUANTRON Magellan
Testing Method   optical emission spectrometric method
Pages :   1
Supplements :   0

Order	Specimen	Steel	Heat	Product
1113460040	S1-5	- - - -	- - - -	120x20x14

Element	[%]	Element	[%]
C	0,03	Cu	0,04
Si	0,000	Nb	<0,002
Mn	0,19	Ti	0,004
P	0,029	V	0,001
S	0,023	W	<0,005
Cr	0,01	Pb	0,000
Mo	<0,01	Sn	0,002
Ni	0,02	As	0,047
Al	0,001	Sb	<0,001
Co	0,015	B	0,0014

Results are related only to the samples under the test.
This certificate is prohibited to reproduce incomplete without Laboratory CZ FERMET agreement.

Kladno: Written by: Checked and approved by:
2.6.2016   Žofie Zíková   T.Štefanová
                 K   K